



Efficient Manufacture of Emulsion Intermediates in Cavity-design Mixers

Thesis submitted in accordance with the
requirements of the University of Liverpool for
the degree of Doctor in Philosophy
by

Ryan Burger

Ultra Mixing and Processing Facility
Department of Chemistry
The University of Liverpool

Submitted: November 2015

Abstract

Efficient Manufacture of Emulsion Intermediates in Cavity-design Mixers

by Ryan Burger

Emulsions are ubiquitous across the process industries and are often utilised in applications where controlled delivery of a key ingredient (e.g. an oil or water soluble compound) is an important consideration. Their functional properties e.g. the rate of absorption or coverage of a surface is generally determined by the size and size distribution of dispersed domains or microstructure. Control over the formulation, process route and type of equipment all influence the resulting microstructure.

The focus of this thesis is the development of process strategies for the efficient manufacture of emulsions in novel cavity-design mixers utilising the Controlled Deformation Dynamic Mixer (CDDM). The CDDM comprises a cylindrical rotor-stator design with opposing surfaces with embedded cavities. The novel design allows flexible operation and optimisation across the spectrum of process space, defined by dispersive and/or distributive mixers.

The process strategies are empirically demonstrated across several oil/surfactant types and the impact of emulsion composition, mixer geometry and process methods are studied. The resulting emulsions are assessed via light scattering measurement of the droplet domain sizes and interfacial areas. The link between microstructure and product viscosity is discussed.

An important output of this work was the development of an efficiency parameter that equates the surface creation to the amount of surfactant used during processing. The parameter provides a useful analytical tool for evaluating the process strategies and is used to provide insights into how the implementation of the in-line emulsification of high internal phase emulsion strategies could provide commercial opportunities via emulsifier raw materials saving and development of small footprint processes.

Dedications

I would like to dedicate this thesis to the many who have suffered loss as a result of the conflict in Syria.

Acknowledgements

I would like to sincerely thank my supervisor, Dr Mike Egan, for his ceaseless patience, guidance and supervision, in particular for the many early morning discussions on the aspects of the PhD. I would also like to thank my secondary supervisor, Professor Adam Kowalski for his useful input on research studies.

I want to express my sincere gratitude for the interest and invaluable input of my industrial supervisor, Dr Neil Irving, Unilever R&D, Port Sunlight, who on many occasions offered his extensive knowledge and experience to many aspects of the research study.

I would like to thank the ESPRC and Unilever for providing the financial support for the research studies, without which the project would not have been possible.

I would like to thank the UMPF team, particularly Richard Feetham, Isaac Pirisola and Dan Harvey, for their assistance throughout the project. I would also like to extend my thanks to the process science group at Unilever R&D, Port Sunlight, particularly Geraint Roberts for extending his experience on rheometry and to the team at the Centre for Material Discovery, University of Liverpool, for providing access to experimental apparatus.

Finally, I would like to thank Marie Pilton, my mum, dad, and family and for their unconditional support and encouragement during the studies.

Declaration

The work described in this dissertation was performed at the Department of Chemistry, University of Liverpool, between September 2010 and August 2014. I declare that this work is my original work and that no portion of the work referred to in this thesis has been submitted in support of an application for another degree or qualification of this or any other university or institute of learning.

Table of Contents

Abstract	i
Dedications.....	ii
Acknowledgements	iii
Declaration	iv
Table of Contents	v
List of Figures and Tables.....	xi
Glossary, Abbreviations and Nomenclature	xxvi
Chapter 1: Introduction	1
1.1 Emulsions	1
1.2 Emulsification	3
1.3 The Ultra Mixing and Processing Facility	5
1.4 Scope of Research	6
1.5 Thesis.....	7
Chapter 2: Literature Review	10
2.1 Emulsion Principles.....	10
2.1.1 Emulsion Types and Structure	11
2.1.2 Surfactants	14
2.2 Emulsion Formation	18
2.2.1 Mechanical Emulsification	18
2.2.2 Spontaneous Emulsification	20
2.3 Emulsion Characterisation	24
2.3.1 Domain Size and Distribution.....	24

2.3.2	Emulsion Rheology.....	29
2.4	Emulsion Destabilisation.....	40
2.5	Droplet Break-up by Mechanical Emulsification.....	43
2.5.1	Droplet Break-up in Laminar Flow	46
2.5.2	Droplet Break-up in Turbulent Flow	55
2.6	Rotor-stator Cavity-design Mixers.....	63
2.6.1	Cavity Transfer Mixer	65
2.6.2	Fluid Division Mixer	69
2.6.3	Controlled Deformation Dynamic Mixer	70
2.7	Conclusions of Literature Review.....	75
Chapter 3: Hypotheses and Experimental Strategies for Efficient Emulsion Manufacture		77
3.1	Key Literature Disclosures.....	77
3.1.1	Emulsion Formation	77
3.1.2	Emulsification.....	77
3.1.3	Droplet Break-up Mechanisms	78
3.1.4	Cavity-design Mixers.....	78
3.2	Hypotheses	79
3.2.1	Delivery of Shear	79
3.2.2	In-line Emulsification	79
3.2.3	Emulsification Efficiency	80
3.2.4	Viscosity Matching.....	82
3.2.5	Surface Stabilisation	82
3.2.6	HIPE Manufacture	82
3.3	Emulsion Manufacturing Strategies	83
3.3.1	Mixing Regime	83

3.3.2	Number of Cavity Stages	83
3.3.3	In-line Emulsification	83
3.3.4	Viscosity Matching Strategies	83
3.3.5	Surface Stabilisation Strategies	84
3.3.6	HIPE Manufacturing Strategies	84
Chapter 4:	Experimental Methods	85
4.1	Materials	85
4.2	Experimental Methods – Domain Size Analysis.....	87
4.2.1	Laser Diffraction – Malvern™ Mastersizer 2000.....	89
4.2.2	General Protocol for Sample Measurement via Laser Diffraction	90
4.2.3	Method for Sample Measurement – SFSO/Pluronic	91
4.2.4	Method for Sample Measurement – PJ/SLES	92
4.2.5	Method for Sample Measurement - SFSO/NS	93
4.3	Experimental Methods – Emulsion Viscosity	94
4.3.1	Emulsion Viscosity – Brookfield DV-II+ Viscometer	94
4.3.2	Method for Sample Viscosity Measurement	95
4.4	Experimental Methods – Data and Error Analysis.....	96
4.5	Emulsification Apparatus - Overhead Mixers.....	98
4.5.1	Coarse Pre-mix Formation.....	98
4.6	Emulsification Apparatus - CDDM.....	99
4.6.1	Bench-scale CDDM System	101
4.6.2	Laboratory-scale CDDM System.....	105
4.7	Emulsification Apparatus - FDM	110
4.8	Emulsification Apparatus - Formax™ Platform	111
Chapter 5:	Manufacturing Strategies for Emulsion Systems, Stabilised by Non-ionic Surfactants.....	116

5.1	Summary	116
5.2	Materials and Methods	116
5.2.1	Materials	116
5.2.2	Emulsification Equipment - Laboratory-scale CDDM.....	117
5.2.3	Emulsification Equipment - Bench-scale CDDM	117
5.3	Results and Discussion	118
5.3.1	Mixing Regimes.....	118
5.3.2	Number of Cavity Stages	124
5.3.3	In-line Emulsification Studies	129
5.3.4	Application of In-line and Cavity Stage Strategies	136
5.3.5	Extension of Strategies to Emulsions Stabilised with NS	137
5.4	Conclusions and Further Work.....	144
5.4.1	Mixing Regimes.....	144
5.4.2	Number of Cavity Stages	145
5.4.3	In-line Emulsification	145
Chapter 6: Manufacturing Strategies for Emulsion Systems, stabilised by Synthetic Surfactants.....		147
6.1	Summary	147
6.2	Materials and Methods	147
6.2.1	Materials	147
6.2.2	Experimental Methods - Overhead Mixer Studies	148
6.2.3	Experimental Methods - Formax™ Studies	148
6.2.4	Experimental Methods - FDM Studies	149
6.2.5	Experimental Methods - Laboratory-scale CDDM Studies.....	150
6.3	Results and Discussion - Viscosity Matching Strategies	151
6.3.1	Formax™ Studies	151

6.3.2	FDM Studies	158
6.3.3	CDDM Studies.....	161
6.3.4	Efficiency Analysis - Viscosity Matching Strategy (Set O:S Ratio) .	162
6.4	Results and Discussion - Surface Stabilisation Strategies.....	164
6.4.1	FDM Studies	164
6.4.2	CDDM Studies.....	171
6.4.3	Efficiency Analysis – Surface Stabilisation Strategies.....	175
6.4.4	Further Discussion of Results	176
6.5	Results and Discussion - HIPE strategy	178
6.5.1	FDM Studies	178
6.5.2	CDDM Studies.....	181
6.5.3	Efficiency Analysis – HIPE Strategy.....	186
6.5.4	Further Discussion of Results	187
6.6	Conclusions and Further Work.....	190
6.6.1	Viscosity Matching Strategies	190
6.6.2	Surface Stabilisation Strategies	191
6.6.3	HIPE Strategy	191
Chapter 7: Key Outcomes and Opportunities		193
7.1	Development of New Experimental Tool	193
7.2	Emulsification Efficiency Function.....	194
7.3	In-line Emulsification.....	194
7.4	HIPE Processing.....	194
7.5	Efficient Emulsification via Viscoelasticity?	195
7.6	Commercial Significance	195
Appendix		196
AX1:	Bibliography	196

AX2:	Chapter 4 Supporting Information.....	215
AX3:	Chapter 5 Supporting Information.....	222
AX4:	Chapter 6 Supporting Information.....	233

List of Figures and Tables

List of Figures:

Figure #	Description	Page #
1.1	Schematic describing models for deformation, break-up and stabilisation of droplets under shear (adapted from Karbstein and Schubert, 1995).	4
1.2	Schematic describing approach to research study, through optimisation of Equipment-Process-Formulation parameters for efficient emulsion manufacture.	7
2.1	Schematic displaying surfactant orientation at the droplet interface of an O/W emulsion.	12
2.2	Image describing surfactant structures a) cross-section of spheroidal micelle b) spheroidal micelles positioned in a cubic arrangement c) cylindrical rod-shaped micelles in a hexagonal arrangement and d) lamellar micelles (adapted from Rosen, 2004).	16
2.3	Schematic describing the creation of a homogeneous emulsion via a combination of distributive and dispersive mixing (adapted from Todd, 2004).	18
2.4	Schematic describing the spontaneous emulsification process.	20
2.5	Diagram presenting the surfactant curvature transition in Phase Inversion Temperature (Adapted from Leal-Calderon et al., 2007).	21
2.6	Schematic displaying the phase diagram of Winsor II SOW system (adapted from Salager, 2005).	22
2.7	Schematic displaying the phase diagram of Winsor III SOW system (adapted from Salager, 2005).	24

Figure #	Description	Page #
2.8	Schematic of a typical laser diffraction instrument (adapted from Kippax, 2005b).	27
2.9	Image of a typical light scattering predicted by Mie scattering model (adapted from Technical document 2).	28
2.10	Representation of a unidirectional shearing flow on a fluid (Adapted from Gupta, 2001).	30
2.11	Flow curve describing typical relationships between shear stress and shear rate for a) Newtonian and non-Newtonian fluids and b) power-law fluids (Adapted from Brown et al., 2004).	31
2.12	Image describing approach for fluid rheometry measurement using a) a Couette rotational rheometer and b) a capillary rheometer.	32
2.13	Schematic describing basic models for linear viscoelasticity, a) the Kelvin-Voigt model, considering the shear stress components relating to viscosity and elasticity and; b) the Maxwell model, considering the shear rate components relating to viscosity and elasticity.	33
2.14	Image describing transition of emulsion interaction and rheological properties with increasing dispersed phase concentration. For incompressible spheres, ϕ represents phase volume, ϕ_g represents the hard sphere glass transition volume fraction and ϕ_{CPH} represents the closed packing hexagonal volume fraction limit of mono-disperse spheres (adapted from Mason, 1999).	35
2.15	Schematic of a model describing the pressure exerted on droplets in HIPEs (adapted from Princen, 1986).	39
2.16	Image outlining mechanisms of emulsion destabilisation.	41

Figure #	Description	Page #
2.17	Schematic outlining the key attractive and repulsive forces acting on neighbouring droplets (adapted from Kaszuba et al., 2010).	42
2.18	Schematic describing the deformation of droplets subject to varying flow regimes.	45
2.19	Schematic describing fluid distribution through chaotic mixing of fluid 1 and fluid 2 in laminar flow, involving the periodic cutting and twisting of fluid portions (adapted from Harnby et al., 1997).	46
2.20	Schematic of experimental setup by Taylor (1934), investigating deformation and rupture of a suspended droplet in a) an axisymmetric hyperbolic extensional shear field and b) a simple shear field (adapted from Taylor, 1934).	47
2.21	Schematic showing the key dimensions for analysis of capillary instability of droplet (adapted from Rumscheidt and Mason, 1962).	49
2.22	Schematic of the Grace curve (Grace, 1982), correlating the critical capillary number against viscosity ratio between dispersed and continuous phases.	51
2.23	Schematic describing kinetic energy transfer in turbulent flow (adapted from Harnby et al., 1997).	56
2.24	Schematic describing droplet break-up mechanisms for a) inertial turbulence b) viscous turbulence c) microstructure-induced instability (adapted from Tcholakova et al., 2011).	58
2.25	Schematic of mixing apparatus comprising of overlapping grooved rings (adapted from Renk, 1981).	65
2.26	Schematic of Gale's Cavity Transfer Mixer Geometry a) Longitudinal View b) Cross-sectional View c) Cavity arrangement (adapted from Gale, 1983).	67

Figure #	Description	Page #
2.27	Schematics of the FDM a) outlining the fluid movement through the mixer b) displaying movement of fluid in the cavities (extracted from Maelstrom Advanced Process Technologies (APT) – accessed 27/08/2014).	69
2.28	Schematic displaying the CDDM apparatus a) design at full overlap b) design at 0mm position c) design of overlapping lands position.	73
3.1	Efficiency graph describing emulsion formation by effective methods (small droplet diameter; “direction a,”) and emulsion formation via efficient methods (low surfactant use; “direction b,”).	81
4.1	Schematic outlining molecular structure of a) SLES (1EO) and b) Pluronic F68.	86
4.2	Schematic of the Mastersizer 2000 laser diffraction Instrument (Malvern Instruments Ltd, Malvern, comprising of dispersion unit (1), optical bench (2), sample cell enclosure (3), diluent fluid entry (4) and fluid exit (5). The laser source within the optical bench assembly at (6) and the “backscatter,‟ and “wide-angle,‟ detectors are located at (7).	89
4.3	Schematic describing the equipment setup for the Brookfield DV-II Pro Extra Viscometer, consisting of an operating panel (1), a moving arm (2), a helipath stand (3), a shipping cap (4), a spindle holder (5), a T-bar spindle (6) and a CPU (7).	95
4.4	Schematic of the CDDM geometries nomenclature, where (a) a positive displacement refers to axial distances between lands that are not confronting; (b) a zero displacement which describes the point where landed sections are at the point of meeting and; (c) a negative displacement refers to axial displacements where land sections overlap.	100

Figure #	Description	Page #
4.5	Image showing the Bench-scale CDDM System and ancillary equipment, consisting of 2 litre and 5 litre vessels at “1,” and “2,” PCPs at “3,” and “4,” a gear pump at “5,” pressure gauges at “6,” “7,” and “8,” the CDDM mixer at “9,” and cooling water feed at “10.”	102
4.6	Bench-scale CDDM System comprising material entry point at “9A,” a material exit point at “9B,” rotor shaft at “9C,” mixer bearings at “9D,” water flush at “9E,” and a heater jacket at “9F.”	103
4.7	Image of the Bench-scale CDDM System Assembly and Downstream Ancillary Equipment. The numbers are explained in the text.	105
4.8	Image displaying the CDDM Laboratory system, comprising of 5 feed streams to the central mixer assembly, consisting of a motor, mixing housing and CDDM.	106
4.9	The control room featuring a HMI at “1,” a monitoring PC at “2,” and video feeds of mixer facility at “3.”	106
4.10	Image of major components of the inlet feeds for the CDDM Laboratory System including the feed hopper at “1,” check valve at “2,” dosing pump at “3,” CDDM mixer assembly at “4,” and motor at “5”.	108
4.11	Image displaying parts of the FDM geometry a) mixer assembly b) mixer inlet c) dismantled assembly of rotor and stator components d) outlet from mixer head with upper stator housing.	111
4.12	Schematic of the Formax™ Platform at (0, 0) coordinates, showing positions of the robotic arm at “1,” the 100ml mixing vessel at “2,” the gravimetric dispensing units at “3,” the CPU at “4,” the location of raw material for transfer at “5,” and the 60 ml dispersion cartridge at “6.”	113

Figure #	Description	Page #
4.13	The automated transfer of “pre-mix b,” to respective vessels. a) Initial position of equipment position; b) transfer of robotic arm to zero co-ordinate; c) collection of the gravimetric dispensing unit; d) collection of heated dispersion cartridge; e) collection of “pre-mix b,” and; f) delivery of “pre-mix b,” to nominated vessel.	114
5.1	Graph describing mean droplet diameter (d_{43}) with mixer position, for SFSO/Pluronic emulsions comprising SFSO fractions of 50wt.% and 70wt.% and SFSO/Pluronic mass ratios of 10 to 1, post-processed at various conditions on the Laboratory-scale CDDM at several mixer geometries. The lines of fit indicate the trajectory of the results.	119
5.2	Graph of power input (P) against throughput (Q) for SFSO/Pluronic emulsions, consisting of a 70wt.% SFSO, post-processed in the Laboratory-scale CDDM at various mixer geometries, at rotational speeds (N) of a) 0 RPM b) 5000 RPM and c) 10000 RPM. The lines of fit indicate the trajectory of the results.	121
5.3	Graph describing specific energy (E_m) against rotational speed (N) per unit throughput (Q) for SFSO/Pluronic emulsions, comprising a 70wt.% oil fraction, processed at various Q , N and mixer geometries. The lines of fit indicate the trajectory of the results.	123
5.4	Graph describing specific surface area (A_d) against specific energy (E_m) for SFSO/Pluronic emulsions, comprising a 70wt. % oil fraction, processed at various conditions on the Laboratory-scale CDDM at +0.25mm, +0.75mm, +1.75mm and +2.75 mm mixer geometries. The line of fit indicates the trajectory of the results.	123

Figure #	Description	Page #
5.5	Graph describing the effect of Rotational Speed (N) on mean droplet diameter (d_{43}), for SFSO/Pluronic emulsions, post-processed at various conditions on the Bench-scale CDDM at -0.25mm and 0mm mixer geometries. The lines of fit indicate the trajectory of the results.	125
5.6	Graph describing the effect of Q on mean droplet diameter (d_{43}) for SFSO/Pluronic emulsions, comprising 65vol.% SFSO and 23.3wt.% Pluronic solution, post-processed at N of 6000 RPM at various Q on the Bench-scale CDDM and at 0mm and +1.35mm mixer geometries. The lines of fit indicate the trajectory of the results.	126
5.7	Graph showing the effect of number of passes on mean droplet diameter (d_{43}) for emulsions comprising 65vol.% SFSO, 11.7wt.% and 23.3wt.% Pluronic solution, processed in the Bench-scale CDDM at N of 6000 RPM and a Q of 18+/-1.8 kg/hr at +1.35mm and 0mm mixer positions. The lines of fit indicate the trajectory of the results.	127
5.8	Graph showing the effect of number of passes on specific surface area (A_d) for emulsions comprising 65 vol.% SFSO, 11.7wt.% and 23.3wt.% Pluronic solution, processed in the Bench-scale CDDM at N of 6000 RPM and a Q of 18+/-1.8 kg/hr, at +1.35mm and 0mm mixer positions.	128
5.9	Graph describing the droplet size distribution for emulsions formed at their phase limit by in-line emulsification on the Bench-scale CDDM, comprising SFSO and 23.3wt.% Pluronic solution, processed at N of 6000 RPM and a Q of 36+/-3.6 kg/hr, at 0mm, +1mm and +1.35mm mixer geometries.	130
5.10	Graph describing mean droplet diameter (d_{43}) against SFSO fraction for emulsions, comprising SFSO and 23.3wt.% Pluronic solution, formed by in-line emulsification on the Bench-scale CDDM via a +1.35mm mixer geometry, at various N and Q . The lines of fit indicate the trajectory of the results.	131

Figure #	Description	Page #
5.11	Graph describing mean droplet diameter (d_{43}) against volume fraction for emulsions, comprising SFSO and 11.7wt.% Pluronic solution, formed by in-line emulsification on the Bench-scale CDDM via a +1.35mm mixer geometry, at various N and Q . The lines of fit indicate the trajectory of the results.	132
5.12	Image displaying emulsions, comprising 70vol.% SFSO stabilised with 11.7wt.% Pluronic solutions, formed by in-line emulsification on the Bench-scale CDDM via a +1.35mm mixer geometry at Q of 18+/-1.8 kg/hr and various N .	133
5.13	Graph describing the specific surface area (A_d) of emulsions, comprising SFSO, 11.7 wt.% and 23.3 wt. Pluronic solutions, formed on the Bench-scale CDDM by in-line emulsification or by post-processing of coarse pre-mixes, processed at 6000 RPM at 18+/-1.8 kg/hr, at a +1.35mm mixer position. The lines of fit indicate the trajectory of the results.	134
5.14	Graph showing the effect of oil fraction on mean droplet diameter (d_{43}) for emulsions comprising SFSO and 23.3wt.% Pluronic solution, concentrated in-line by blending with an SFSO and post-processed in-line via the Bench-scale CDDM, at N of 6000 RPM and Q of 18+/-1.8 kg/hr, in a +1.35mm position. The lines of fit indicate the trajectory of the results.	135
5.15	Image describing experiments on mid-point dilution compared with multiple-pass experiments, for a 65vol.% SFSO emulsions comprising a 23.3wt.% Pluronic solution, processed at N of 6000 RPM and at Q of 16 kg/hr and 18 kg/hr, at a 0mm CDDM geometry.	138
5.16	Graph describing the effect of oil fraction on the mean droplet diameter (d_{43}) of emulsions, comprising SFSO and 34.4wt.% NS solution, processed on the Bench-scale CDDM in a 0mm geometry, at similar Q and N of 10800 RPM, 13200 RPM and 15000 RPM. The lines of fit indicate the trajectory of the results.	139

Figure #	Description	Page #
5.17	Graph describing the effect of oil fraction on specific surface area, A_d of emulsions, comprising SFSO and 34.4wt.% NS solution, processed on the Bench-scale CDDM in a 0mm geometry, at similar Q and at N of 10800 RPM, 13200 RPM and 15000 RPM. The lines of fit indicate the trajectory of the results.	140
5.18	Graph describing the effect of SFSO fraction on viscosity of emulsions, of emulsions, comprising SFSO and 34.4wt.% NS solution of differing mean droplet diameters (d_{43}). The lines of fit indicate the trajectory of the results.	141
5.19	Graph describing the effect of pass number on mean droplet diameter (d_{43}) comprising an SFSO fraction of 67.5wt% and 34.4wt.% NS solution, for processed on the Bench-scale CDDM at 10800 RPM in 0mm and +1.35mm mixer geometries. The lines of fit indicate the trajectory of the results.	142
5.20	Graph describing the effect of pass number on specific surface area, A_d , for processed emulsions comprising a 67.5wt% SFSO and 34.4wt.% NS solution, processed on the Bench-scale CDDM at 10800 RPM in 0mm and +1.35mm mixer geometries. The lines of fit indicate the trajectory of the results.	142
5.21	Application of in-line emulsification process strategies for emulsions, comprising SFSO and 34.4wt.% NS Solution, processed on the Bench-scale CDDM at a +1.35mm mixer geometry. Stage 1 incorporates direct formation of emulsions, whereas Stage 2 blends SFSO with a coarse emulsion pre-mix. Circled data points at 1) may indicate a partially destabilised emulsion.	144
6.1	Schematic describing the concept of “split-stream,” emulsification, where emulsions comprising PJ stabilised with 25% SLES were brought together with streams comprising 70wt.% SLES (adapted from Technical document 7).	152

Figure #	Description	Page #
6.2	Images demonstrating split-stream emulsification approach on the bench, including a) Experimental setup b) Results of d_{32} vs. mixing time and c) Emulsion compositions, operating conditions and droplet size results.	155
6.3	Schematic describing the experimental methodology for “split-stream,” emulsification studies on the Formax™.	156
6.4	Droplet distributions of O/W dispersions, comprising PJ and SLES of varying quantities, processed on the Formax™ Platform as per methods described in Figure 6.3.	157
6.5	Droplet distributions of O/W dispersions, comprising PJ and SLES of varying quantities, processed on the Formax™ Platform as per methods described in Figure 6.3.	158
6.6	Graph describing the effect of mixing duration on mean droplet diameter (d_{43}) for dispersions, comprising PJ/SLES compositions of set O/S ratios, formed by melt emulsification, processed for varying mixer durations at 6000 RPM on the FDM apparatus. The lines of fit indicate the trajectory of the results.	160
6.7	Graph describing the impact of PJ fraction on droplet size distributions of emulsions, comprising PJ/SLES compositions of set PJ:SLES ratio (15:1 vs. 20:1), post-processed through the CDDM in a 0mm geometry at static and dynamic conditions at N of 10000 RPM and at Q of 243+/-18 kg/hr. The lines of fit indicate the trajectory of the results.	162
6.8	Efficiency Graph describing dispersions, comprising PJ/SLES compositions of set PJ:SLES mass ratio (8.33:1, 10:1, 15:1, 20:1), and processed on the Formax Platform (70°C), the FDM and Laboratory-scale CDDM at similar tip speeds and varying Q . The lines of fit indicate the trajectory of the results.	163

Figure #	Description	Page #
6.9	Graph describing the effect of mixing duration on mean droplet diameter (d_{43}) for dispersions comprising 74.6wt.% PJ and SLES solutions of varying concentration, formed by melt emulsification and processed for varying mixer durations, at N of 6000 RPM on the FDM apparatus. The lines of fit indicate the trajectory of the results.	166
6.10	Graph describing the change in mean droplet diameter (d_{43}) with mixing duration, for dispersions comprising 74.6wt.% PJ and SLES solutions of varying concentration, formed by melt emulsification and processed for varying mixer durations at 6000 RPM on the FDM apparatus. The lines of fit indicate the trajectory of the results.	166
6.11	Graph describing the change in specific surface area (A_d) with mixing duration, for dispersions comprising 74.6wt.% PJ and SLES solutions of varying concentration, formed by melt emulsification and processed for varying mixer durations, at N of 6000 RPM on the FDM apparatus. The lines of fit indicate the trajectory of the results.	167
6.12	Graph describing the change in efficiency function ($f(E)$) with SLES solution concentration, for dispersions comprising 74.6wt.% PJ and SLES solutions of varying concentration, formed by melt emulsification and processed for varying mixer durations, at N of 6000 RPM on the FDM apparatus. The lines of fit indicate the trajectory of the results.	168
6.13	Graph showing the change in mean droplet diameter (d_{43}) with mixing duration for emulsion, comprising PJ dispersed in 23.3wt.% SLES solution and PJ dispersed in a glycerol/SLES mix similar in viscosity to 23.3wt.% SLES solution. Emulsions were formed by melt emulsification, at 6000 RPM on the FDM. The lines of fit indicate the trajectory of the results.	170

Figure #	Description	Page #
6.14	Graph describing the impact of dispersed mass fraction on droplet size distribution of PJ/SLES emulsions, comprising PJ dispersed in SLES solutions of 12.5wt.% and 25.0wt.% concentration, post-processed through the CDDM in a 0mm geometry at static and dynamic conditions at Q of a) 55.7 \pm 7.0 kg/hr and 123 \pm 2 kg/hr and b) 51.9 \pm 4.9 kg/hr and 228 \pm 3 kg/hr.	172
6.15	Graph describing the impact of mixer speed on a) mean particle size (d_{43}) and b) specific surface area (A_d) for PJ/SLES emulsions comprising PJ dispersed in SLES solution and PJ dispersed in a SLES/Glycerol solution, at PJ:SLES mass ratios of 30:1, post-processed on the Laboratory-scale CDDM at a 0mm position at various mixer speeds, at low Q (59.4 \pm 4.0kg/hr) and high Q (254kg/hr). The lines of fit indicate the trajectory of the results.	173
6.16	Graph describing the impact of mixer speed on mean domain size (d_{43}) and specific surface area (A_d) of emulsions, comprising SFSO in 23.3wt.% Pluronic solution and PJ in 25.0wt.% dispersed in SLES solution, post-processed on the CDDM at a 0mm position at mixer speeds of 0, 5000 and 10000 RPM and Q of 210 \pm 16 kg/hr (SFSO/Pluronic) and 236 \pm 13 kg/hr (PJ/SLES). The lines of fit indicate the trajectory of the results.	174
6.17	Efficiency Graph describing dispersions, comprising PJ/SLES compositions of set PJ fraction and varying SLES concentration, processed on the FDM and Laboratory-scale CDDM at similar tip speeds and varying Q . The lines of fit indicate the trajectory of the results.	176
6.18	Image describing the kinetics for stabilisation of created interfaces, for surfactants held in aggregate form.	177

Figure #	Description	Page #
6.19	Graph describing the effect of mixing duration on mean droplet diameter (d_{43}) for dispersions, comprising various compositions of PJ dispersed in 25.0wt.% and 30.0wt.% SLES solutions, formed by melt emulsification, processed for varying mixer durations at N of 6000 RPM, on the FDM apparatus. The lines of fit indicate the trajectory of the results.	182
6.20	Graph describing the effect of PJ fraction on mean droplet diameter, (d_{43}) for dispersions, comprising various compositions of PJ dispersed in 25.0wt.% and 30.0wt.% SLES solutions, formed by melt emulsification, processed for varying mixer durations at 6000 RPM on the FDM apparatus. The lines of fit indicate the trajectory of the results.	183
6.21	Graph describing the effect of PJ fraction on specific surface area (A_d) for dispersions, comprising various compositions of PJ dispersed in 25.0wt.% and 30.0wt.% SLES solutions, formed by melt emulsification, processed for varying mixer durations at 6000 RPM on the FDM apparatus. The lines of fit indicate the trajectory of the results.	184
6.22	Graph describing the effect of dispersed mass fraction on droplet size distribution of PJ/SLES dispersions, comprising PJ and a 12.5 wt.% SLES solution, post-processed through the CDDM in a 0mm geometry at static and dynamic conditions at Q of a) 61.7+/-1.7 kg/hr and b) 254+/-8 kg/hr.	185
6.23	Graph describing the impact of dispersed mass fraction on droplet size distribution of PJ/SLES dispersions, comprising PJ and a 12.5wt.% SLES solution, post-processed through the CDDM in a 0mm geometry at static and dynamic conditions at Q of a) 62.5+/-0.9 kg/hr and b) 250+/-4 kg/hr.	186

Figure #	Description	Page #
6.24	Graph describing the effect of dispersed mass fraction on droplet size distribution of formed emulsions, comprising SF50 and 23.3wt.% Pluronic solution, post-processed through the CDDM in a 0mm geometry at static and dynamic conditions at Q of a) 55.0 \pm 3.5 kg/hr and b) 206 \pm 9 kg/hr.	187
6.25	Graph describing the impact of processing on droplet size distribution of emulsions, comprising 80wt.% and 85wt.% SF50 dispersed 23.3wt.% Pluronic solution, post-processed through the CDDM in a 0mm geometry at mixer speeds of 0, 5000 and 1000 RPM at Q of a) 196 \pm 2 kg/hr and b) 221 \pm 6 kg/hr.	188
6.26	Specific surface area against oil fraction for SF50/Pluronic emulsions and PJ/SLES dispersions processed at 210 \pm 16kg/hr at 10000 RPM at various mixer speeds in a 0mm CDDM mixer position. The lines of fit indicate the trajectory of the results.	189
6.27	Efficiency Graph describing dispersions, comprising PJ/SLES compositions of set SLES concentration (25.0wt.% and 30.0wt.% solution), and SF50/Pluronic compositions of set Pluronic concentration (23.3wt.%) processed on the FDM and Laboratory-scale CDDM at varying tip speeds and Q . The lines of fit indicate the trajectory of the results.	189
6.28	Model of domain spacing vs. domain volume fraction for various droplet diameters. Droplet spacing decreases with increasing phase volume and smaller droplet diameters.	191
6.29	Graph displaying efficiency versus water fraction for emulsions processed for 480 seconds at set SLES solution concentration (25.0% and 30.0% by weight), set PJ mass fraction and set PJ:SLES mass ratios (8.33 to 1).	192

Figure #	Description	Page #
6.31	Graph displaying efficiency vs water fraction for results described by Tcholakova et al. (2011), for emulsions formed via rotor-stator apparatus, comprising Hexadecane, Mineral Oil 25 and Mineral Oil 130 stabilised with 10wt.% Lutensol, and results described by Welch (2006) for emulsions formed via rotor-stator apparatus, comprising 100cst Silicone Oil and SLES at mass ratios of 15.6+/- 1.3 to 1. The lines of fit indicate the trajectory of the results.	193

List of Tables:

Table #	Description	Page #
2.1	Table describing emulsion types, size and thermodynamic stability (adapted from McClements, 2011).	12
2.2	Table describing the key domain size characteristics of emulsions.	26
4.1	Summary of error analysis functions applied to experimental studies.	98
4.2	Table describing the nominal operating limits for the Laboratory-scale CDDM and ancillary equipment.	110
4.3	Summary of key design criteria and operating limits of the FDM.	112
6.1	Table describing the apparent viscosities of PJ, SLES solutions and SLES/Water/Glycerol mixtures, measured at 65+/-1°C using the Rheostress Rheometer. Further information is provided on the viscosity ratio between dispersed and continuous phases, which decreases with increasing SLES solution concentration.	172
6.2	Table describing the apparent viscosities of 25.0wt.% SLES solution, measured at 65+/-1°C and Pluronic solutions, measured at 20+/-1°C. Further, results describing the apparent viscosity ratios of PJ/25.0wt.% SLES solutions, measured at 65+/-1°C and SF50/23.3wt.% Pluronic Solutions, measured at 20+/-1°C.	178

Glossary, Abbreviations and Nomenclature

Glossary of Terms:

Amphiphilic: defined as “a term used to describe a compound containing a large organic cation or anion which possesses a long unbranched hydrocarbon chain,” (IUPAC, 2014).

Critical Micelle Concentration: described as the “concentration separating the limit below which virtually no micelles are detected and the limit above which virtually all additional surfactant molecules form micelles,” (IUPAC, 2014).

Coalescence: defined as “the disappearance of the boundary between two particles (usually droplets or bubbles) in contact, or between one of these and a bulk phase followed by changes of shape leading to a reduction of the total surface area.”

Couette shear field: described by as “flow fields developed by rotation,” (Grace, 1982).

Deborah number: The ratio of a characteristic (relaxation) time of a material to a characteristic time of the relevant deformation process (Barnes and Hutton, 1989).

Dispersion: in agitation, referred to as “the break-up of drops,” (Leng and Calabrese, 2004).

Dispersive mixing: defined as the break-up of agglomerates or lumps to the desired grain size of solid particulates or the domain size (drops) of other immiscible fluids.

Distributive Mixing: defined as “providing spatial uniformity of all components.”

Emulsifier: defined as “a surfactant which when present in small amounts facilitates the formation of an emulsion, or enhances its colloidal stability by decreasing either or both of the rates of aggregation and coalescence,” (IUPAC, 2014).

Emulsion: defined as “A fluid colloidal system in which liquid droplets and/or liquid crystals are dispersed in a liquid,” (IUPAC, 2014).

Emulsification: described as “dispersing one fluid into another, non-miscible one, via creation of an interface,” (Leal-Calderon et al., 2007).

Extensional shear fields: described) as “shears that are irrotational,” (Grace, 1982).

High Internal Phase Emulsions: described as “emulsions comprising phase volume greater than 74%,” (Liu and Friberg, 2009).

Immiscible liquid-liquid systems: described as “two or more mutually insoluble liquids as separate phases,” (Leng and Calabrese, 2004).

Interface: defined as “the plane ideally marking the boundary between two phases,” (IUPAC, 2014).

Laminar flow: described as “flow without turbulence,” (Barnes and Hutton, 1989).

Micelles: defined as “surfactants in solution (that) are often association colloids, that is, they tend to form aggregates of colloidal dimensions, which exist in equilibrium with the molecules or ions from which they are formed” (IUPAC, 2014).

Mie Scattering: defined as “The scattering of electromagnetic radiation by spherical particles of any size, relative to the wavelength,” (IUPAC, 2014).

Newtonian fluid model: described as a “model characterised by a constant value for the quotient of the shear stress divided by the rate of shear in a simple shear flow and with zero normal stress differences.”

Non-Newtonian fluid: described as “any fluid whose behaviour is not characterised by the Navier-Stokes equations,” (Barnes and Hutton, 1989).

Phase: defined as “an entity of a material system which is uniform in chemical composition and physical state,” (IUPAC, 2014).

Reverse micelle: defined as micelles comprising “polar groups of the surfactants (that) are concentrated in the interior and the lipophilic groups extend towards and into the non-polar solvent,” (IUPAC, 2014).

Reynolds number: defined as the “product of a typical apparatus length and a typical fluid speed divided by the kinematic viscosity of the fluid, or the ratio of inertial forces to viscous forces,” (Barnes and Hutton, 1989).

Rheology: described as the “science of the deformation and flow of matter,” (Barnes and Hutton, 1989).

Shear rate: is described as “the velocity gradient in a flowing fluid.”

Shear strain: described as the “displacement of one surface with respect to another divided by the distance between them,” (IUPAC, 2014).

Shear stress is described as a “force acting tangentially to a surface divided by the area of the surface,” (IUPAC, 2014).

Shear thinning: defined as a viscosity is a univalued function of the rate of shear, a decrease of the viscosity with increasing rate of shear is called shear thinning, and an increase of the viscosity shear thickening (IUPAC, 2014).

Surfactant: defined as “A substance which lowers the surface tension of the medium in which it is dissolved, and/or the interfacial tension with other phases, and, accordingly, is positively adsorbed at the liquid/vapour and/or at other interfaces,” (IUPAC, 2014).

Surface tension: defined as “the work required to increase a surface area divided by that area. When two phases are studied it is often called interfacial tension,” (IUPAC, 2014).

Turbulence – described as “a condition of flow in which the velocity components show random variation,” (Barnes and Hutton, 1989).

Velocity gradient: described as “the derivative of the velocity of a fluid element with respect to a space coordinate,” (Barnes and Hutton, 1989).

Viscosity: described as “the measure this property, defined as the shear stress divided by the rate of shear in steady simple shear flows,” (Barnes and Hutton, 1989).

Abbreviations:

Abbreviation	Description
CDDM	Controlled Deformation Dynamic Mixer
CMC	Critical Micelle Concentration
CPH	Close Packed Hexagonal
CTM	Cavity Transfer Mixer
DLS	Dynamic Light Scattering
ESPRC	Engineering and Physical Sciences Research Council
FDM	Fluid Division Mixer
HIPE	High Internal Phase Emulsion
HLB	Hydrophilic Lipophilic Balance
HLD	Hydrophilic Lipophilic Deviation
HMI	Human Machine Interface

Abbreviation	Description
HSM	High Shear Mixer
IUPAC	International Union of Pure and Applied Chemistry
LALLS	Low-Angle Laser Light Scattering
NS	Natural surfactant
O	Oil
O/W	Oil-in-Water
o/W/O	oil-in-Water-in-Oil
PC	Personal Computer
PCP	Progressive Cavity Pumps
PLC	Program Logic Controller
PIT	Phase Inversion Temperature
PJ	Petroleum Jelly
RAPRA	Rubber and Plastics Research Association
S	Surfactant
SFISO	Sunflower Seed Oil
SEM	Scanning Electron Microscope
SLES	Sodium Lauryl Ether Sulphate
UMPF	Ultra Mixing and Processing Facility
W	Water
W/O	Water-in-Oil
w/O/W	water-in-Oil-in-Water

Nomenclature – Latin Symbols:

Symbol	Description	SI Unit
a	Viscosity ratio of dispersed to continuous phases	dimensionless
a^*	Ratio of elasticity to viscosity	s^{-1}
A	Interfacial Area	m^2
A_d	Specific surface area	$m^2 kg^{-1}$
A_h	Cross-sectional area of hydrophilic head-group	m^2
b	Constant relating to droplet viscosity	dimensionless
c	Solubility	$mol L^{-1}$
C	Concentration	$mol L^{-1}$
$C_1, C_2, C_3 \dots$	Constants	various

Symbol	Description	SI Unit
C_p	Specific Heat Capacity	$\text{J kg}^{-1} \text{K}^{-1}$
d	Droplet diameter	m
d_{32}	Sauter mean diameter	m
d_{32max}	Maximum stable Sauter mean diameter	m
d_{43}	De Brouckère mean diameter	m
d_{hmax}	Maximum stable mean diameter of a HIPE	m
d_{v10}	Domain diameter that 10 vol.% of sample population is below	m
d_{v50}	Domain diameter that 50 vol.% of sample population is below	m
d_{v90}	Domain diameter that 90 vol.% of sample population is below	m
d_{v95}	Domain diameter that 95 vol.% of sample population is below	m
D	Rotor diameter	m
E_m	Specific energy	kJ kg^{-1}
E_v	Volumetric energy density	J m^{-3}
EE	Experimental error	various
f	Mass fraction of phase in emulsion	dimensionless
$f(E)$	Efficiency function	$\text{m}^2 \text{kg}^{-1}$
f_k	Collision efficiency	$\text{s}^{-1} \text{m}^{-3}$
F	Force	N
g	Gravitational acceleration	m s^{-2}
G	Deformation rate	s^{-1}
G'	Storage modulus	N m^{-2}
h	Dimensionless function relating to growth factor in droplet instability	dimensionless
k	Collision efficiency	dimensionless
K	Constant relating to non-Newtonian behaviour	N s m^{-2}
l	Length of fracture layer	m
l_t	Length of hydrophobic tail	m
L	Length	m
M	Mass	m
M_{ds}	Mass ratio of dispersed phase to surfactant	dimensionless
n	Number of droplets/domains	dimensionless
n_{int}	Number of times fluid transferred between cavities	dimensionless
N	Mixer rotational speed	s^{-1}
$j(N_{Vi})$	Viscosity function	m s kg^{-1}
p	Pressure	N m^{-2}
Δp	Pressure drop	N m^{-2}

Symbol	Description	SI Unit
p^*	Packing parameter	J mol^{-1}
P	Power	W
P_0	Power number	dimensionless
q	Disturbance growth factor	dimensionless
Q	Throughput	kg hr^{-1}
u	Velocity	m s^{-1}
$u(l)$	Eddy characteristic velocity	m s^{-1}
ν	Kinematic viscosity	$\text{m}^2 \text{s}^{-1}$
r	Radius	m
R	Universal gas constant	$\text{J mol}^{-1} \text{K}^{-1}$
s	Entropy	J K^{-1}
SD	Standard deviation	various
SE	Standard error	various
t	time	s
$t(l)$	Eddy time-scale	s
T	Temperature	$^{\circ}\text{C}$
T_d	Torque	N m
V	Volume	m^3
V_{ds}	Volume ratio of dispersed phase to surfactant	dimensionless
V_h	Volume of hydrophobic tail group	m^3
V_{icav}	Volume of FDM cavity ‘i.’	m^3
V_m	Molar volume	mol m^{-3}

Nomenclature – Greek Symbols:

Symbol	Description	SI Unit
α	Disturbance amplitude	m
γ	Shear strain	dimensionless
$\dot{\gamma}$	Shear rate	s^{-1}
Γ	surface coverage	$\text{m}^2 \text{kg}^{-1}$
δ	Spacing	m
ε	Energy dissipation rate	$\text{m}^2 \text{s}^{-3}$
ζ	Zeta potential	V
θ	Angle	rad

Symbol	Description	SI Unit
λ	Wavelength	m
λ_k	Kolmogorov length scale	m
μ	Dynamic viscosity	N s m^{-2}
μ_r	Apparent viscosity	N s m^{-2}
ρ_{se}	Mass of surfactant per volume emulsion	kg m^{-3}
σ	Surface tension	N m^{-1}
τ	Shear stress	N m^{-2}
Π	Osmotic pressure	N m^{-2}
ρ	Density	kg m^{-3}
ρ_a	Surface area density	$\text{m}^2 \text{m}^{-3}$
$\bar{\tau}$	Constant shear stress	N m^{-2}
ϕ	Phase volume	$\text{m}^3 \text{m}^{-3}$
ϕ^*	Critical packing fraction	$\text{m}^3 \text{m}^{-3}$
ψ	Stern potential	V
ω	Angular velocity	rad s^{-1}

Nomenclature – Subscript Symbols:

Symbol	Description
0	Initial
1, 2, 3 ...	Distinction of terms of similar notation
<i>c</i>	Continuous phase
<i>ca</i>	Capillary
<i>cav</i>	Cavity
<i>CPH</i>	Close packed Hexagonal
<i>cr</i>	Critical
<i>d</i>	Dispersed phase
<i>dl</i>	Dilatational
<i>dr</i>	Droplet
<i>e</i>	Emulsion
<i>E</i>	Extensional
<i>f</i>	Final
<i>fl</i>	Fluid
<i>fm</i>	Film

Symbol	Description
<i>F</i>	Flow
<i>g</i>	Hard sphere glass transition
<i>G'</i>	Elastic
<i>hmax</i>	Maximum for HIPE
<i>H</i>	High
<i>HC</i>	High concentration
<i>in</i>	in
<i>L</i>	Low
<i>LC</i>	Low Concentration
<i>LS</i>	Losses.
<i>m</i>	Mass
<i>max</i>	Maximum
<i>NL</i>	Number-Length
<i>NS</i>	Number-Surface
<i>NV</i>	Number-Volume
<i>out</i>	Out
<i>row</i>	Cavity row
<i>R</i>	Rotational
<i>s</i>	Surfactant
<i>st</i>	Stokes
<i>T</i>	Total
<i>x, y, z</i>	x, y, z dimension

Nomenclature – Dimensionless Groups:

Symbol	Description
<i>Ca</i>	Capillary number
<i>We</i>	Weber number
<i>Re</i>	Reynolds number

Chapter 1: Introduction

1.1 Emulsions

Emulsions are an important class of colloids found in many formulated products.

Emulsions form part of a more general class of multiphase systems known as colloids, but are distinctly mixtures of immiscible liquids. In emulsions, one or more liquids (the “dispersed” or “drop” phase) are dispersed as discrete domains within a liquid continuum (the “continuous” or “matrix” phase) (Leng and Calabrese, 2004; Mason, 1999). The dispersed and continuous phases are separated by a boundary, known as the “interface”.

Emulsion material properties are linked to the volume fraction of the dispersed phase, and the size and size distribution of the dispersed phase domains. These can be altered to achieve a desired material property, for example a more effective active ingredient, a desired texture or flow property. Therefore, emulsions have been applied in products where the delivery and transport of key components is an important consideration; for example in the delivery of organic ingredients in foods, personal care creams, paints, pharmaceuticals and agrochemicals (Muschiolik, 2007; Tadros et al., 2004).

Two immiscible liquids, which are typically oil and water, can form different types of emulsions. For example, Oil-in-Water (O/W) emulsions consist of a dispersed oil phase within a water continuum. Likewise Water-in-Oil (W/O) emulsions consist of a dispersed water phase within an oil continuum. In some instances, multiple emulsions are formed; these consist of oil-in-Water-in-Oil (o/W/O) or water-in-Oil-in-Water (w/O/W) where the internal phase is represented by lower-case letters.

As liquids, emulsions do not exhibit a static internal structure. The droplets dispersed in the continuous phase are usually assumed to be statistically distributed.

Emulsions are typically unstable and are unlikely to form spontaneously. Their formation requires the input of energy and a chemical species known as surface active agents or “surfactants”, which may be synthetic or natural and may be in liquid or particulate form. Surfactants are “amphiphilic” and are soluble in both liquid phases, a property that allows them to kinetically stabilize the interface by lowering the droplet surface tension. However, emulsions do not always follow this rule; for example micro-emulsions are thermodynamically stable (Anton and Vandamme, 2009).

The type of emulsion formed (O/W or W/O) depends on the fraction of each liquid phase and the properties of surfactants. This generally follows Bancroft’s rule (Bancroft, 1913), where surfactants promote dispersion of the liquid phase that they have lower affinity to. For example, proteins dissolve better in water than in sunflower oil at ambient conditions, therefore they tend to form O/W-type emulsions (they promote the dispersion of oil droplets throughout a water continuous phase).

There are four types of instability in emulsions: flocculation, coalescence, creaming, and Ostwald ripening. Flocculation occurs when there are attractive forces between the droplets, so that they “bunch” to form flocs. Coalescence occurs when droplets collide and combine to form a larger droplet, so the average droplet size increases over time. The presence of surfactants on the droplet interface prevents coalescence by lowering the collision efficiency of droplets through increased repulsive interaction (Dukhin et. al., 2005). Emulsions may also undergo gravity-driven separation (creaming), whereby droplets rise to the top of the emulsion under the influence of buoyancy, or under the influence of the centripetal force induced when a centrifuge is used. Finally, Ostwald ripening is an effect describing the diffusion of small droplet to large droplets due to concentration gradients between them.

1.2 *Emulsification*

As noted in section 1.1, the properties of emulsions may be linked to the volume fraction of the dispersed phase, and the size and size distribution of the dispersed phase domains, formed during “emulsification”, the term used to describe the process whereby two or more immiscible liquids and typically a surfactant are converted into an emulsion.

Emulsification is generally achieved by processes that employ devices which deliver mechanical shear, which was established with the invention of the homogeniser by Gaulin (1904) for the treatment of milk to improve shelf-life. More recently, a number of other approaches have emerged, including methods employing ultrasound (Tal-Figiel, 2007), spontaneous emulsification (Mason, 2006), microfluidic devices (Shah et al., 2008) and the development of novel mixers that provide high levels of shear (Hall et al., 2011).

Emulsion formation is achieved by extending the interface between immiscible phases. Methods employing mechanical emulsification achieve this by shear-induced deformation of droplets and stabilisation of created surface by amphiphilic species. Deformation is achieved if the applied stress is higher than the droplet’s capillary (or Laplace) pressure, which describes the pressure difference between outer and inner curved surfaces on the droplet interface. As the interface is thin compared to the droplet size, the Young-Laplace equation is normally simplified to Equation 1.1, which indicates an increased pressure at larger surface tension and smaller droplet diameter.

$$P_{ca} = \frac{4\sigma}{d} \quad (1.1)$$

Where P_{ca} is the capillary pressure, σ is the surface tension and d is the droplet diameter. Droplet break-up requires sufficient levels of localised shear stress to be applied over a minimum breakage time to overcome droplet capillary pressure (Karbstein and Schubert, 1995). If critical deformation is achieved, the new surface

must be stabilised to prevent re-coalescence of the dispersed droplet (Karbstein and Schubert, 1995). Therefore, the means of stabilising the created interface receives due interest; where approaches to equipment and process design consider methods that promote ingredient distribution during processing (distributive mixing) and strategies that improve the availability of surfactants at the interface. These processes are described in Figure 1.1, which provides a model for slow and fast stabilisation rates on droplet formation. Stabilisation may be enhanced by the methods for combining ingredients. Furthermore, the properties of the surfactant determine surface stabilisation. Droplets are subject to deformation in the shear zone and breakage occurs when a critical deformation is reached. Fast stabilisation of a created interface leads to the formation of daughter droplets, whereas slow stabilisation leads to re-coalescence of the dispersed droplets.

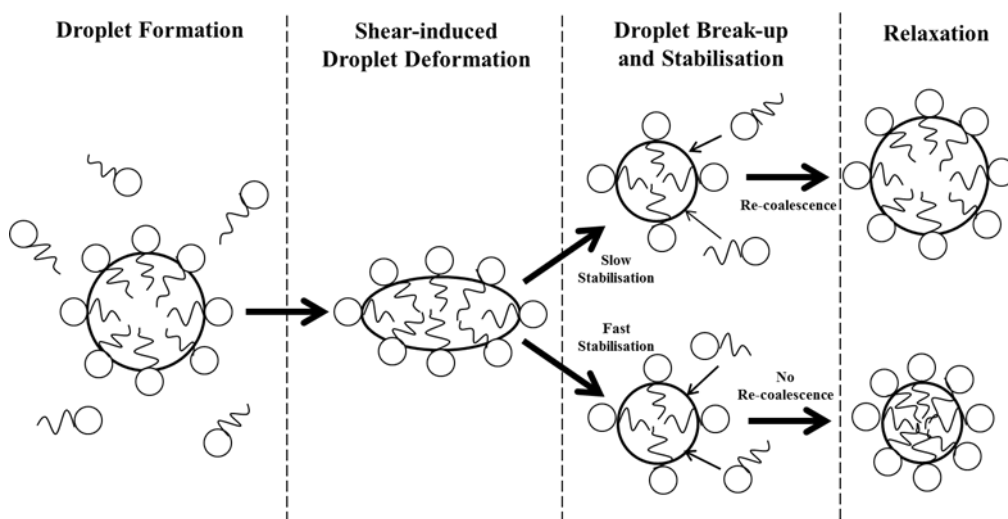


Figure 1.1: Schematic describing models for deformation, break-up and stabilisation of droplets under shear (adapted from Karbstein and Schubert, 1995).

The dispersed phase concentration is usually defined as a phase volume fraction, ϕ_d , which affects the rate of droplet dispersion (droplet break-up) or the rate of droplet coalescence (combining of droplets) (Leng and Calabrese, 2004).

A number of mixers have been applied to emulsification processes (Hall et al., 2011; Bongers et al., 2012; Piela et al., 2012), where considerations on the emulsion composition and the shear type delivered impact on equipment design. High Shear

Mixers (HSMs) of the rotor-stator type deliver shear to fluids positioned between confronting surfaces of near-proximity. The shear type is determined by the flow regime; Hyperbolic flows promote elongational shear by directing the bulk fluid between static and confronting surfaces. Couette flows promotes rotational shear by developing velocity gradients in fluids positioned between static and rotating surfaces (Grace, 1982).

1.3 The Ultra Mixing and Processing Facility

In 2002, the Department of Trade released a report summarising the current state of micro-technology and nano-technology in the United Kingdom (Taylor, 2002). While recognising that the UK had a strong academic background in nanotechnology and nanoscience, the report found that the contributions were predominantly from leading experts in the field rather than in academic centres and recognised the difficulty of collective research without strategic overview and coordination. The findings of the report resulted in a commitment by Lord Sainsbury, the Minister of Science and Innovation in 2004, to invest £90 million over 6 years into UK's research into nanotechnology, which was later increased to £200 million (House of Commons, 2004). One of the products of the initiative was the Ultra Mixing and Processing Facility (UMPF) at the University of Liverpool. The project, jointly funded by income from industry and research funding, included key partners such as Maelstrom APT Ltd, Nanocentral, Unilever and the University of Liverpool. Funding for the state-of-the-art facility amounted to £2.31 million, of which £780,000 was allocated to capital expenditure, £230,000 allocated toward refurbishment and £1.3 million to operating costs over the duration of the project.

The mixing capabilities offered within the facility, such as the Controlled Deformation Dynamic Mixer (CDDM; Maelstrom APT Ltd, Glossop, United Kingdom) and the Fluid Division Mixer (FDM; Maelstrom APT Ltd, Glossop, United Kingdom), which are used extensively in experimental studies outlined in Chapter 5 and Chapter 6.

1.4 Scope of Research

While the start (e.g. ingredient types, formulation limit), end (e.g. final composition, emulsion microstructure, product quality) and bounds of process design are set, there are often alternative routes for manufacture within those bounds. Determining the key objective for process design, such as improved product microstructure or efficient resource use, allows selection of one route over another. However, there is benefit in optimising emulsification strategies within the selected route.

There is scope for research on emulsification strategies which consider the impact of factors relating to equipment design, process methods and formulation on emulsion manufacture. Factors relating to equipment design may consider the practical means for manufacture, whereas process methods might consider the order or method of combining key ingredients and formulation might consider the impact of material composition on the mechanics which drive emulsion formation.

The approach outlined above is synonymous with the criteria against which claims are made in patents. This follows a general recognition that invention through process conception requires an approach that either introduces novel equipment design, process methods and formulations, or approaches that develop products with unique qualities. However, it is argued that the key elements of the product triangle, outlined in Figure 1.2, cannot be considered independently. A new process method may be limited by the formulation criteria, likewise a new equipment design may benefit from a particular process method or formulation characteristic. However, it may not be correct to consider criteria in isolation, as they may be linked.

The research project reported here was jointly funded by the Engineering and Physical Sciences Research Council (EPSRC) and Unilever, and is centred on emulsification in novel cavity-design rotor-stator mixers; namely, the FDM and the CDDM. The study forms part of a wider collaboration agreement between the UMPF (University of Liverpool), the Polymer Reaction Engineering Group (Technical University of Eindhoven) and the Centre for Process Design and Control (University of Massachusetts). Rotor-stator mixers consist of dynamic and static surfaces positioned in near proximity to one another, where either of the confronting surfaces

is altered geometrically. In a typical configuration, both the stationary and dynamic surfaces are encased in an external housing. The devices, which have demonstrated effective mixing, build on the highly successful cavity transfer mixing technology which emerged in the 1980s (Gale, 1982). Both the FDM and CDDM are designed with cavities embedded on the rotor and stator surfaces, which are opposing and normal to the direction of relative movement. A key design feature of the CDDM is the ability to alter axial position of confronting rotor and stator sections, which allows changes in the relative position of cavities on confronting surfaces. This alters the flow-path and consequently the degree of shear exerted on the fluid at specific positions along the length of the mixer, which may be optimised for processing a particular formulation.

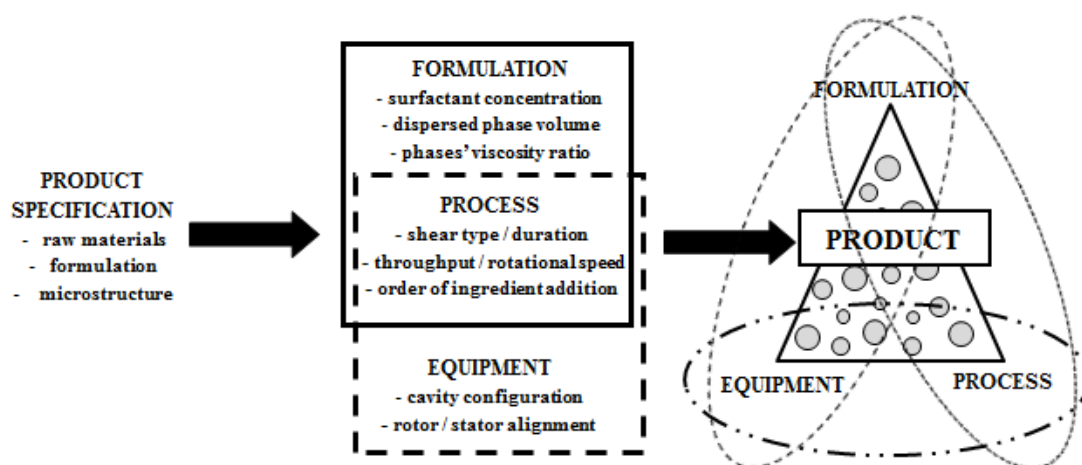


Figure 1.2: Schematic describing approach to research study, through optimisation of Equipment-Process-Formulation parameters for efficient emulsion manufacture.

1.5 Thesis

The present research study aimed to investigate methods for efficient emulsification in novel cavity-design rotor-stator mixers. The purpose of this research study was to optimise factors relating to formulation, process and equipment for the manufacture of emulsions in the FDM and CDDM, with the intention of delivering emulsion products and intermediates that possess distinct qualities. A summary of the thesis layout is outlined below:

Chapter 2 presents a literature review, comprising topics on emulsion principles, including emulsion types, emulsion structure and surfactants, approaches for emulsion formation, emulsion characterisation and emulsion destabilisation. Furthermore, previous research on droplet break-up in laminar and turbulent flow regimes and the development of rotor-stator cavity-design mixers are discussed.

Chapter 3 provides an analysis of existing literature and theory which was outlined Chapter 2. This chapter aims to identify key trends and gaps in the research area. These findings will be considered in the context of the current research study, where the scope and objectives of research study will be outlined.

Chapter 4 summarises the experimental techniques applied in studies reported in Chapter 5 and Chapter 6. The section includes a description of techniques used for material characterisation and the design and operation of mixing apparatus used in reported studies, including the Bench-scale CDDM, Laboratory-scale CDDM, FDM and Formax™ High-throughput Platform.

Chapter 5 reports on emulsification studies on model O/W systems, stabilised with non-ionic synthetic and natural surfactants, via the Laboratory-scale CDDM and Bench-scale CDDM. In addition, experimental studies investigating changes in equipment geometry and process methods on emulsion manufacture, with the aim of obtaining emulsions with desired product microstructures are outlined.

Chapter 6 reports on studies for melt emulsification of O/W wax compositions, stabilised by an anionic surfactant and processed on the Formax™, FDM and Laboratory-scale CDDM apparatus. These experiments investigate changes in formulation on emulsion manufacture, with the aim of identifying compositions that improve the efficiency of surfactant use. The findings were demonstrated for model O/W systems, stabilised with non-ionic synthetic and natural surfactants, via the Laboratory-scale CDDM.

Chapter 7 provides a discussion of key experimental findings described in Chapters 5 and Chapter 6 and potential further research on the subject area.

Finally, the Appendix provides supporting information for experimental techniques described in Chapter 4 and research studies described in Chapter 5 and Chapter 6.

Chapter 2: Literature Review

This chapter is presented in several sections and contains a review of theory on emulsion principles (section 2.1), including emulsion types, emulsion structure and surfactants, emulsion formation (section 2.2), emulsion characterisation (section 2.3) and emulsion destabilisation (section 2.4). Furthermore, droplet break-up by mechanical emulsification (section 2.5) and a review of reported studies on mixing rotor-stator cavity-design mixers (section 2.6) is reported. Details of references sourced may be obtained from the Bibliography of the Appendix.

2.1 *Emulsion Principles*

A brief introduction to emulsions was provided in Chapter 1. The following sections discuss the essential elements of emulsions pertinent to this research, in detail.

Emulsions typically comprise of a mixture of two or more immiscible, or partially miscible materials together with some form of stabilising material at the interface. Emulsions may be either liquid dispersed in one of the phases (commonly referred to as an emulsifier or surfactant) or consist of solid particles which migrate to the interface (e.g. mustard seed powder acting as a stabiliser in food dressings). Therefore, emulsions provide a useful means to combine several polar and non-polar materials together for use either as ingredients within products or as final products themselves.

Emulsions are found extensively in a wide range of industrial sectors, for example in foods, home and personal care products, cosmetics, paints, coatings and pharmaceuticals (Acosta, 2009; McClements, 2011; Hatanaka et al., 2008; Tal-Figiel, 2007; Sonnevile-Aubrun et al., 2004). The key elements driving process innovation include reduced production costs, improved shelf-life, enhanced

effectiveness, more desirable rheological properties and legislative restrictions on emulsion composition.

Therefore, it is argued that emulsion principles, including emulsion type, composition, microstructure and material properties, are key in determining their effectiveness as ingredients or products.

2.1.1 Emulsion Types and Structure

Emulsions are formed by extending the interfacial area between immiscible phases. Due to the large surface area created per unit volume of dispersed phase, emulsions typically require surface-active species, such as emulsifiers or surfactants, to stabilise the interface.

Winsor (1948) coined the term “amphiphiles,” in his description of surfactants, which highlights the molecule’s dual affinity to polar and non-polar phases. This property allows them to position at the O/W binary interface (Leal-Calderon et al., 2007; Dukhin et al., 2005) which lowers the interfacial surface tension, a measure of the droplet’s surface energy¹. Surfactants typically consist of an ionic head-group and a hydrophobic tail-group, which form the molecule’s affinity to the polar and non-polar phases, respectively. A schematic displaying surfactant orientation at the binary interface is provided in Figure 2.1. Furthermore, a detailed description of surfactant types and properties is provided in section 2.1.2.

1. For clarity, many authors identify the term “surface,” as a boundary between materials of different physical state and interface as the boundary between liquids. For simplicity, the terms “surface,” “interface,” and “interfacial surface area,” are used interchangeably throughout the current thesis to describe the boundary separating the dispersed and continuous phases.

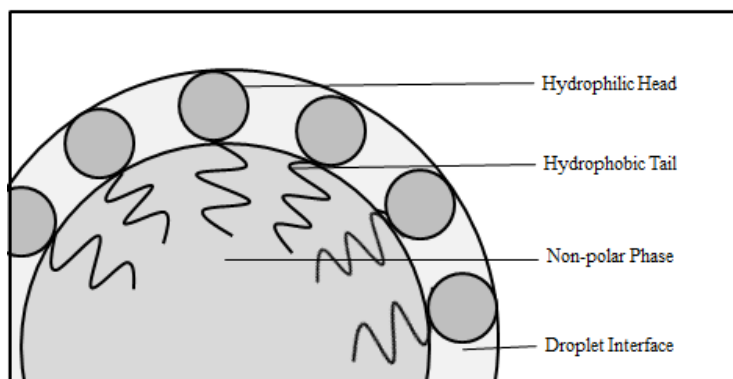


Figure 2.1: Schematic displaying surfactant orientation at the droplet interface of an O/W emulsion.

The typical size and thermodynamic stability of emulsion types are outlined in Table 2.1. Here, thermodynamic stability describes the emulsion's resistance to separation due to free energy minimisation. Macro-emulsions and nano-emulsions are meta-stable systems, which require the input of external energy, under specific conditions to emulsify (Leal-Calderon et al., 2007; Mason, 1999). They present thermodynamically unstable systems, where energy is typically delivered by applying inertial and/or viscous shear to the system. In comparison, micro-emulsions are thermodynamically stable and form spontaneously. These systems are only formed at specific temperatures and pressures, where components exhibit a lower free energy as a dispersion compared to a separated mixture (McClements, 2011). While micro-emulsions and nano-emulsions offer similar domain sizes, they vary in thermodynamic stability. Anton and Vandamme (2011) provide a thorough discussion on the difference between these emulsion forms.

Emulsion Type	Size range (μm)	Thermodynamic Stability
Macro-emulsion	0.1 to 100	Unstable
Nano-emulsion	0.01 to 0.1	Unstable
Micro-emulsion	0.002 to 0.05	Stable

Table 2.1: Table describing emulsion types, size and thermodynamic stability (adapted from McClements, 2011).

Nano-emulsions are formed by high-shear mixing, homogenisation and/or spontaneous emulsification processes (Mason et al., 2006; McClements, 2011). These emulsions comprise a very small droplet size, a property which allows manufacture of optically transparent or cloudy products (Graves and Mason, 2008; McClements, 2011) which offer desirable marketing attributes such as cleanliness, purity and freshness (Sonneville-Aubrun et al., 2004). For optical transparency, droplets must be sufficiently small to reduce the intensity of scattered light, which is proportional to the sixth power of the droplet diameter (Rayleigh, 1876). Recent studies have indicated that nano-emulsions improve the bioavailability of active ingredients (Acosta, 2009; Hatanaka et al., 2008; Talegaonkar et al., 2010), which considers the “fraction of a dose that is available at the site of action in the body,” (Tal-Figiel, 2007). Improved bioavailability is attributed to the small droplet size, which improves the rate of release of active substances through an increased interfacial area, enhanced ingredient penetration and transport through body barriers and membranes (Tadros et al., 2004; Tal-Figiel, 2007). Furthermore, a reduced droplet size improves active ingredient solubilisation, which may enhance ingredient absorption (McClements, 2011). The solubility of spherical particles in a liquid continuum is outlined in equation 2.1 below (Thomson, 1871; Kabalnov and Shchukin, 1992):

$$c_d = c_c \exp \left(\frac{4\sigma V_m}{RTd} \right) \quad (2.1)$$

Where c_d is the solubility of the droplet in the water phase, c_c is the bulk phase solubility of the oil, σ is the droplet interfacial tension, V_m is the molar volume of the dispersed phase, R is the universal gas constant, T is the absolute temperature and d is the droplet diameter. Equation 2.1 indicates that a reduction in droplet size exponentially increases the solubility of an oil droplet in a bulk aqueous phase.

Finally, nano-emulsions have improved stability compared to macro-emulsions, as Brownian forces dominate droplet movement, resisting emulsion destruction through gravity separation, droplet flocculation and droplet coalescence (Tadros et al., 2004. Tal-Figiel and Figiel, 2008).

In contrast, micro-emulsions comprise of a self-assembled collection of surfactant structures consisting of lamellar, hexagonal and micellar phases that configure to create a thermodynamically stable system (Mason et al., 2006; McClements, 2011). An equilibrium balance between components of the system exists; additionally, the oil and aqueous phases have relatively low immiscibility and the surfactant is soluble in both phases (Mason et al., 2006). Section 2.1.2 provides a more detailed description of surfactant structures.

In summary, the emulsion structure is central to their effectiveness as ingredients or products. Emulsions comprising of small droplet sizes can offer attractive properties including optical transparency, therefore improved solubility and bio-availability of suspended active ingredients. Efficient emulsification may consider methods for forming small droplet sizes, which exhibit large interfacial areas as a consequence.

2.1.2 Surfactants

There are vast numbers of leading texts describing surfactants (Leal-Calderon et al., 2007; Rosen, 2004; Dukhin et al., 2005), however a few key authors have contributed works which appear to be very important in shaping our knowledge on the subject, including:

- Bancroft (1913), who proposed that the phase in which the surfactant is constitutes the continuous phase.
- Griffin (1949), who developed a means of determining surfactant characteristics that provide the optimum droplet stability.
- Winsor (1948), who investigated the phase behaviour of surfactants in surfactant-oil-water (SOW) ternary systems.
- Shinoda and Saito (1969) and Shinoda and Kunieda (1973) who studied the phase equilibrium of surfactants with varying temperature.

Surfactants play a key role in emulsion formation, stability and physical properties (Tal-Figiel and Figiel, 2008); it is therefore essential that the key mechanisms governing their application are well understood. Their affinity to either the polar or non-polar phase is dependent on the charge of the hydrophilic group relative to the

size of the hydrophobic group. Surfactant types include those that possess an overall neutral charge in solution (non-ionic), a positive charge in solution (cationic), a negative charge in solution (anionic) or those that possess both positive and negative charges (zwitterionic).

In terms of emulsion systems, these molecules position on the O/W binary surface and reduce interfacial surface tension, as outlined in Figure 2.1. The amount of surfactant required to stabilise the surface may be determined from the critical micelle concentration (CMC), defined as the concentration at which free surfactant orientates to form structures that reduce the system's free energy. The CMC is determined by observing the change in surface tension with surfactant concentration and occurs when the surface tension does not change with increased concentration. The maximum stable droplet diameter of an emulsion system may be approximated from knowledge of the surfactant surface coverage, as outlined in Equation 2.2 (Tcholakova et al, 2004).

$$d_{32max} \approx \frac{6\phi_d}{1-\phi_d} \frac{\Gamma}{C_{S0}} \quad (2.2)$$

Where ϕ_d is the dispersed phase volume fraction, d_{32max} is the maximum stable sauter mean diameter, Γ is the surfactant surface coverage and C_{S0} is the initial surfactant concentration. A description of droplet size nomenclature is provided in section 2.3.1.

d_{32max} described in equation 2.2 refers to the Sauter mean droplet size above which larger droplets would disperse into smaller ones at a defined formulation. A number of surfactant structures (or phases) formed at concentrations above the CMC are displayed in Figure 2.2. The surfactant packing parameter, defined in Equation 2.3, provides an indication of surfactant orientation in formed structures (Mitchell and Ninham, 1981).

$$p^* = \frac{V_h}{A_h l_t} \quad (2.3)$$

Where p^* is the packing parameter, V_h is the volume of the hydrophilic head, A_h is the cross-sectional area of the hydrophilic head-group and l_t is the hydrophobic tail length. In aqueous fluids, surfactants in spheroidal micelles exhibit a p^* of 0 to 1/3 (Figure 2.2a and Figure 2.2b), a p^* of 1/3 to 1/2 in rod-shaped structures (Figure 2.2c) and a p^* of 1/2 to 1 in lamellar-shaped structures (Figure 2.2d). A surfactant-rich solution may comprise of many structures and may alter the solution's material properties (Rosen, 2004). For example, solutions containing rod-shaped structures can possess viscoelastic-type material properties and those lamellar phases can exhibit shear-thinning material properties (Rosen, 2004). According to Bancroft's theory (Bancroft, 1913), surfactant structures are prominent in the continuous phase of the emulsion. Emulsion flow properties are discussed in further detail in section 2.3.2.

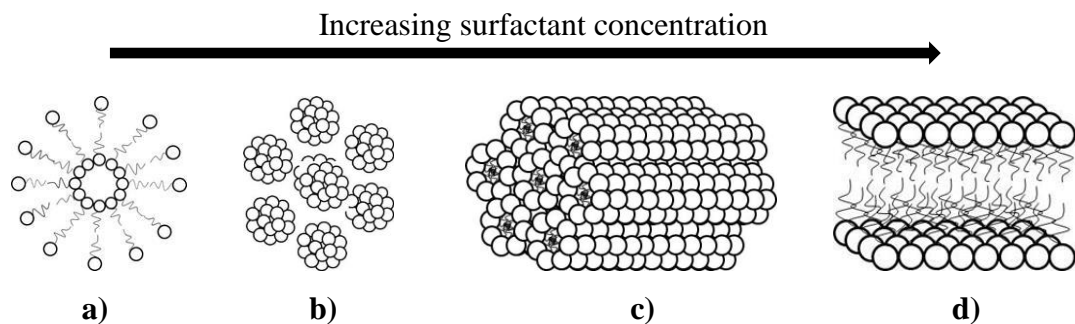


Figure 2.2: Image describing surfactant structures **a)** cross-section of spheroidal micelle **b)** spheroidal micelles positioned in a cubic arrangement **c)** cylindrical rod-shaped micelles in a hexagonal arrangement and **d)** lamellar micelles (adapted from Rosen, 2004).

The emulsification properties of surfactants are strongly influenced by their affinity to polar and non-polar phases of the particular mixture to be emulsified. Therefore, it is useful to be able to characterise this affinity via a simple metric. Griffin (1949) proposed the Hydrophilic-Lipophilic Balance (HLB) system as a straightforward means of classifying surfactants based on their polar state. The system provides an indication of a surfactant's phase behaviour and applies a numerical rating to indicate a surfactant's overall affinity to the non-polar phase (low HLB) or overall affinity to the polar phase (high HLB). The optimum HLB of a surfactant for a

particular system may be achieved through its maximum solubilisation of one immiscible phase in another at a selected composition (Shinoda and Saito, 1969). Furthermore, the use of hydrophilic and hydrophobic surfactant mixtures provides a means for obtaining a specific HLB. Griffin (1949) suggested Equation 2.4 to determine the overall HLB of a system containing two surfactants.

$$HLB_T = \frac{M_1HLB_1 + M_2HLB_2}{M_1 + M_2} \quad (2.4)$$

Where M_1 and M_2 are the masses of surfactant 1 and surfactant 2 respectively, HLB_T is the overall system HLB value and HLB_1 and HLB_2 are the HLB values of surfactants 1 and 2, respectively. By setting HLB_T to an optimum value, the optimum proportion of each surfactant may be determined. The effect of solubilisation of surfactant mixtures on a colloid surface was studied by Shinoda and Kunieda (1973). The authors suggested that the combined HLB of the surfactant phases are optimum at specific oil and water compositions, where the required amount of the lipophilic surfactant was determined the length of its hydrophobic chain due to its ability to absorb in the oil phase.

In terms of a set dispersed phase fraction, the micro-structure of a formed emulsion is affected by the type and concentration of the surfactant present. The structural of emulsions also affect the sensorial characteristics in food products, which are driven by consumer preferences regarding product texture and feel (Fischer and Windhab, 2010). Therefore, emulsion microstructure is a key consideration for the current thesis, where efficient emulsification may consider the criteria for surfactant selection which provides the optimum HLB for the target composition. Similarly, the amount of surfactant may be selected to form emulsion of a target droplet size or material behaviour. However, this is often limited to the formulation constraints set by the intended application; for example excess surfactant present in skin-care products can cause tissue irritation on application.

2.2 Emulsion Formation

This section details methods for emulsion formation, specifically approaches employing mechanical emulsification, described in section 2.2.1 and spontaneous emulsification, section 2.2.2. A review of theory on emulsion formation is important for identifying efficient emulsification strategies.

2.2.1 Mechanical Emulsification

Metastable emulsions may be formed by mechanical emulsification, where apparatus impose sufficiently high shear environments to overcome the droplet's resistance to deformation. Droplet breakage occurs on critical deformation, where the shear induced by the surrounding fluid exceeds the droplet's resistive surface and internal viscous forces (Leng and Calabrese, 2004). If a droplet does not reach critical deformation, it will not break and will attempt to return to its original shape due to interfacial tension (Leng and Calabrese, 2004). Emulsion formation by this method generally requires the slow addition of the dispersed phase to a surfactant rich continuous phase until the required volume fraction is reached. The pre-mix may then be post-processed to obtain a desired emulsion micro-structure.

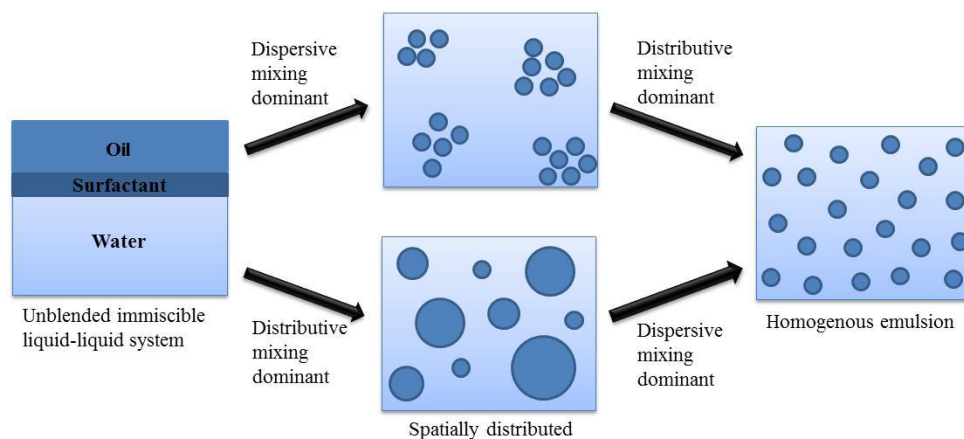


Figure 2.3: Schematic describing the creation of a homogeneous emulsion via a combination of distributive and dispersive mixing (adapted from Todd, 2004).

Numerous studies have investigated emulsification in novel apparatus, including methods incorporating ultra-sound (Tal-Figiel, 2007), microfluidic devices that form uniform droplet distributions (Shah et al., 2008) and high shear mixers that provide inertial or viscous shear to the system (Hall et al., 2011). In general, emulsification equipment aims to create and develop conditions that promote high shear environments for emulsification (dispersive mixing dominant) and the bulk transfer of one liquid phase within the other for homogenisation (distributive mixing dominant), as described in Figure 2.3.

Additionally, the property of the surrounding fluid, or continuum, directly affects the equipment's capability to transmit stress. This is exemplified by the Weber number (Equation 2.5) and Capillary number (Equation 2.6), which consider the impact on inertial and viscous shear stress relative to surface interfacial tension, or surface energy, respectively. The ratio of Equation 2.5 and Equation 2.6 leads to the Reynolds number (Re) outlined in Equation 2.7.

$$We = \frac{\rho_c u_{fl}^2 d}{\sigma} \quad (2.5)$$

$$Ca = \frac{\mu_c u_{fl}}{\sigma} \quad (2.6)$$

$$\frac{We}{Ca} = \frac{\rho_c u_{fl} d}{\mu_c} = Re \quad (2.7)$$

Where Ca is the capillary number, We is the Weber number, μ_c is continuous phase viscosity, ρ_c is the continuous phase density, u_{fl} is the fluid velocity, σ is the droplet interfacial tension and d is a characteristic diameter (e.g. droplet diameter). Therefore, the flow regime developed by the apparatus determines the droplet break-up mechanism. For emulsions comprising low viscosity continuums, droplet break-up is promoted by increased turbulent energy dissipation rates to the system (Leng and Calabrese, 2004). For emulsions comprising viscous continuums, droplet break-up is promoted by increased flow velocities, which promotes stress transfer in the said continuum (Leng and Calabrese, 2004).

2.2.2 Spontaneous Emulsification

The spontaneous emulsification approach is a low energy emulsification technique, which utilises the rapid transfer of a surfactant from the phase of lower miscibility to one of higher miscibility (Anton and Vandamme, 2009; McClements, 2011). Figure 2.4 shows a typical process for the formation of O/W type emulsions by this approach. As outlined in Figure 2.4, a pure polar phase is combined with a mixture containing a non-polar phase and a surfactant with an affinity to the polar phase. On blending the two mixtures at a set temperature, there is rapid transfer of the surfactant from the non-polar phase to the polar phase; this process induces rapid turbulence and droplet break-up to form a metastable emulsion, therefore is stable as an emulsion despite existing at a lower energy state as separate components.

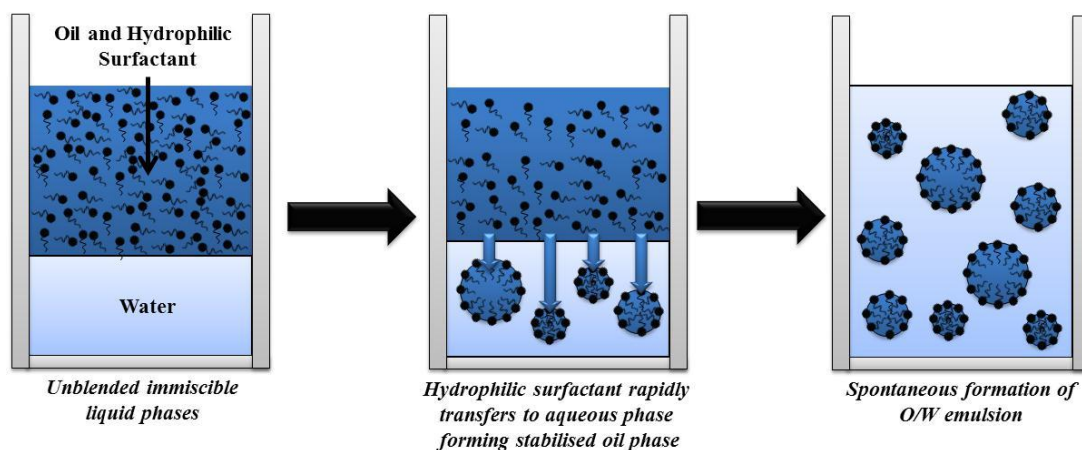


Figure 2.4: Schematic describing the spontaneous emulsification process.

One of the spontaneous mechanisms used to form emulsions is transitional phase inversion. This method manipulates the curvature of the surfactant at the O/W interface, which controls the surfactants affinity to a particular phase (Bancroft, 1913; Shinoda and Saito, 1969). Figure 2.5 shows the change in the curvature of a non-ionic surfactant with increasing temperature.

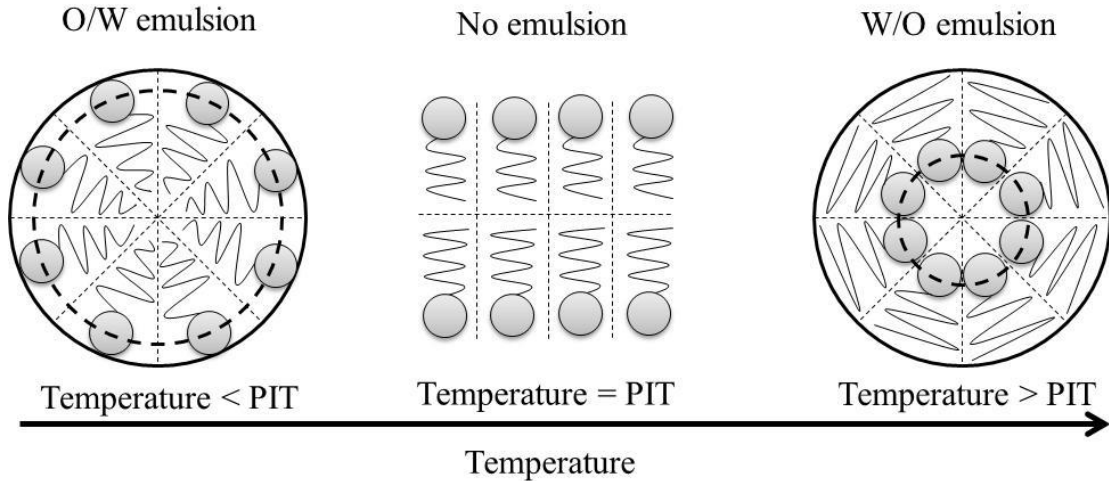


Figure 2.5: Diagram presenting the surfactant curvature transition in Phase Inversion Temperature (Adapted from Leal-Calderon et al., 2007).

At temperatures below the Phase Inversion Temperature (PIT), the surfactant structure will settle to lowest free energy (by reducing the surface area of its hydrophobic tail) and, with reference to Equation 2.3, favour an O/W type emulsion and orientate in a positive micellar arrangement where $p^* < 1$ (Leal-Calderon et al., 2007). With reference to Figure 2.5, an increase in temperature leads to excess free energy in the system and the surfactant orientation is altered to a larger surface area. Eventually the surfactant reaches a point where it has no curvature ($p^* = 1$) at this point no emulsion exists and the interfacial tension at the interface reaches a minimum (Aveyard et al., 1985). If the temperature of the system increases above the PIT, the surfactant switches from a positive to a negative curvature and therefore a W/O type emulsion or reverse micellar arrangement where $p^* > 1$ (Leal-Calderon et al., 2007).

A bi-continuous emulsion exists when the surfactant has a dual affinity to each phase (Liu and Friberg, 2009). Additionally, the surfactant head becomes less hydrated and therefore becomes more oil-soluble (Leal-Calderon et al., 2007). At PIT, the interfacial tension at the surface of the droplet is significantly reduced, which may favour the creation of nano-emulsions, if the transition between the oil dispersed and oil continuous phase is fast enough to prevent rapid coalescence (Leal-Calderon et al., 2007).

In terms of emulsion formation, several methods employing catastrophic phase inversion may be applied to emulsion formation. The methods are typically used in industrial processes involving a highly viscous oil dispersed phase such as an alkyd or an epoxy resin, which are difficult to disperse in simple shear regimes, due to the differences in viscosity between the oil and the aqueous phases (Grace, 1982; Salager et al., 2004; Watson and Mackley, 2002; Yang and Zhao, 2000). Liu and Friberg (2009) presented studies on the formation of a High Internal Phase Emulsion (HIPE) intermediates by the dilution of an intermediate multiple emulsion, which was inverted by adding water to a viscous silicone oil and a non-ionic surfactant. The dilution caused catastrophic phase inversion which resulted in the formation of an O/W HIPE with good stability. The structure and material properties HIPEs are described in more detail in section 2.3.2.

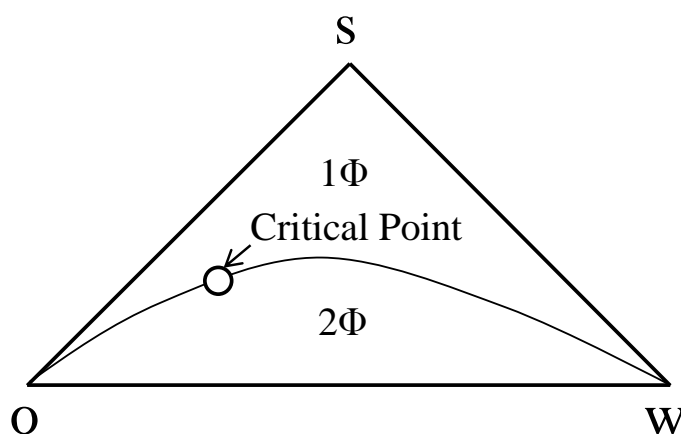


Figure 2.6: Schematic displaying the phase diagram of Winsor II SOW system (adapted from Salager, 2005).

As noted in section 2.1.1, micro-emulsions are thermodynamically stable systems whose orientation is dependent on surfactant characteristics. For these systems, the O/W or W/O emulsion structure depends on a number of variables that affect the equilibrium state, including formulation or field variables such as temperature, pressure and composition or extensive variables including component type and component proportions (e.g. phase volume, surfactant concentration and emulsification strategy) (Salager et al., 2004; Salager, 2005). A surfactant with a high HLB is predominantly present in the polar phase and will create a Winsor I type

system (Winsor, 1948) and tend to form O/W emulsions. However, a system with a surfactant with a low HLB will create a rich non-polar phase and a Winsor II type system (Figure 2.6) that tends to form a W/O emulsion (Bancroft, 1913; Salager, 2004; Shinoda and Saito, 1969; Salager, 2005; Winsor, 1948).

In a simple O/W micro-emulsion, in the presence of a non-ionic amphiphile and at surfactant concentrations greater than the CMC, swollen micelles are formed where the oil phase is held within the hydrophobic ends of the amphiphile (Anton and Vandamme, 2011). A critical point occurs when phases become miscible, and is normally positioned near the surfactant rich phase (Salager, 2005). A Winsor III type system (Winsor, 1948), described in Figure 2.7, is found when the surfactant has equal affinity to both polar and non-polar phases. In this case, a three-phase region is apparent where the polar, non-polar and micro-emulsion phases co-exist. Two critical points (x and y) exist in this instance, where the micro-emulsion phase forms a two phase system with either the pure polar or pure non-polar phase (Salager, 2005). The stability of micro-emulsions is sensitive to changes in temperature and composition. This poses difficulties in the applications of micro-emulsions in place of nano-emulsions as they may become unstable at the point of application (Anton and Vandamme, 2011; Kahlweit et al., 1996).

In terms of this present thesis, phase inversion offers a low energy approach for emulsion formation. However, the capability of the system to invert the internal and external phase is dependent on surfactant type and properties, which may be restricted when the emulsion composition is defined by the intended application. Therefore, phase inversion is not included in studies reported in this present thesis, however should be considered for further work. Additionally, while micro-emulsions present emulsion systems comprising small droplet sizes, it is clear that the micro-structure is linked to the temperature and pressure of the system. This may limit the suitability the manufactured emulsion in a target application, therefore these systems will be avoided as final products. However, strategies which benefit from processing of these systems will be investigated. Further, novel mixing technologies including the FDM and CDDM are central to studies described in this thesis. Therefore, efficient emulsification in these apparatus will consider mixing strategies that

promote droplet rupture and interfacial surface creation by deliver inertial and viscous shear regimes to the emulsion system.

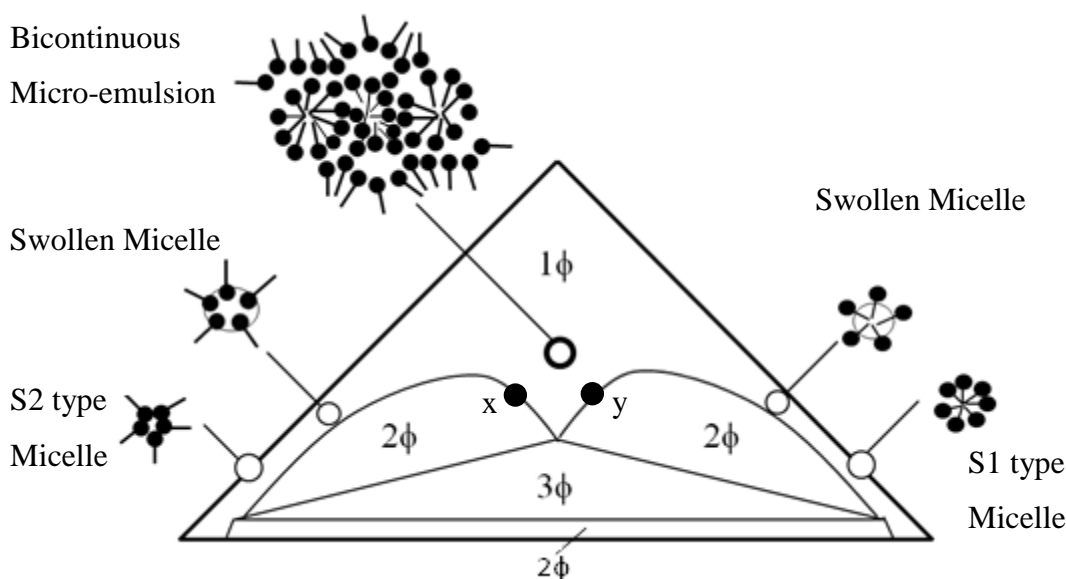


Figure 2.7: Schematic displaying the phase diagram of Winsor III SOW system (adapted from Salager, 2005).

2.3 Emulsion Characterisation

The theory and analysis of two essential emulsion characteristics, domain size and emulsion rheology, are described in this section.

2.3.1 Domain Size and Distribution

The term “domain,” is chosen to describe suspended ingredients in dispersions; however the type, state and physical properties of the domains studied in this current thesis vary per experiment. Typically, domains described in the current thesis will comprise of a liquid form, as a droplet, or a semi-solid form, such as a wax. Domain size and distribution is an important consideration for efficient emulsification. These characteristics affect the emulsion rheological characteristics and the effectiveness/solubility properties of dispersed active ingredients, allowing more effective transport of key ingredients through body tissue at the point of application (Tadros et al., 2004; Tal-Figiel, 2007). Additionally, increasing the interfacial

contact area between the active ingredient and affected tissue improves the rate of ingredient delivery.

Domain size analysis is used to describe the size distribution of domains in dispersions, where statistical analysis of the domain population is used to determine the system's average or mean domain size. This identifies a number of key characteristics, including mean domain sizes, specific surface area (A_d), describing the surface area per unit mass of dispersed phase, surface area density (ρ_d), describing the total surface area per volume of emulsion, domain size span present in a sample population and the maximum size which 10 vol.% (d_{v10}), 50 vol.% (d_{v50}) and 90 vol.% (d_{v90}) of a domain population is below.

Several key size characteristics are described in Table 2.2; here, d_i is the domain diameter, n_i is the number of domains of size d_i , n is the total number of domains in a sample population, ρ_d is the domain density and ϕ_d is the dispersed phase volume fraction. Mathematical descriptors defining mean diameters are typically presented in the form of Mugele and Evans (1951) D [p, q] nomenclature. For samples comprising domains of varying shape, an equivalent length may be derived by equating particles in terms of minimum or maximum lengths, surface areas, volumes or mass. The length selected is based on the characterisation technique used (Technical document 1).

Number-average means, D [n, 0], consider the mean length, surface area or volume of a measured sample. The number-average mean type selected should be representative of the information of interest. For example “number-surface area,” means, may be important as catalyst surface area affects the rate of reaction (Technical document 1), whereas “number-volume,” means, provide an indication of the mean distribution mass by extending the calculation to account for droplet density. This philosophy is relevant for all size characteristics described in this thesis, where an appropriate measure should be selected if a particular system's characteristics is being investigated (e.g. length, surface area or volume). The constraints of number-average means arise due to the number of particles or droplets present in a given sample population, in that particles counting for a given sample

volume may take a substantial length of time or may limit representative sample measurements (Technical document 1).

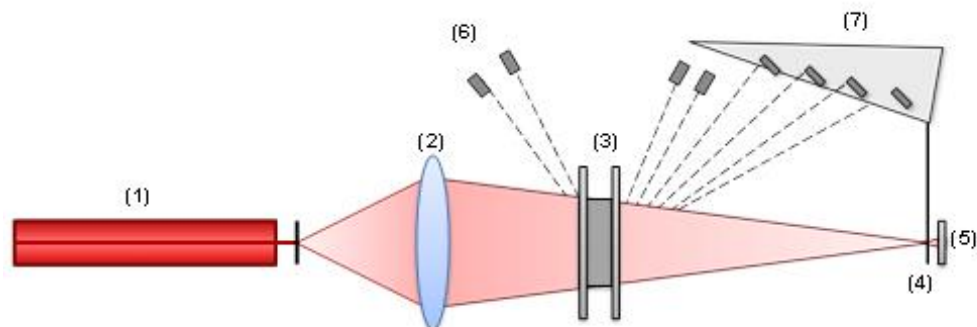
Table 2.2: Table describing the key domain size characteristics of emulsions.

Term	Nomenclature	Equation	Units
Number-length mean diameter:	D [1, 0] or d_{NL}	$\frac{\sum d_i}{n}$	m
Number-surface area mean diameter:	D [2, 0] or d_{NS}	$\sqrt{\frac{\sum d_i^2}{n}}$	m
Number-volume mean diameter:	D [3, 0] or d_{NV}	$\sqrt[3]{\frac{\sum d_i^3}{n}}$	m
Surface Area (Sauter) moment mean diameter:	D [3, 2] or d_{32}	$\frac{\sum n_i d_i^3}{\sum n_i d_i^2}$	m
Volume (De Brouckère) moment mean diameter:	D [4, 3] or d_{43}	$\frac{\sum n_i d_i^4}{\sum n_i d_i^3}$	m
Surface area density	ρ_a	$\frac{6\phi_{fl}}{d_{32}}$	$m^2 m^{-3}$
Specific surface area	A_d	$\frac{6}{d_{32}\rho_d}$	$m^2 kg^{-1}$
Span	-	$\frac{d_{v10} - d_{v50}}{d_{v90}}$	-

Furthermore, a moment mean, D [n, n-1] indicates “the centre of gravity of a frequency distribution with respect to an appropriate equivalent value,” (Technical document 1). Two types of moment means are often analysed, namely the surface area-weighted (Sauter) mean diameter and the volume-weighted (De Brouckère) mean diameter. These types of domain analysis eliminate the particle term, therefore reducing the processing time for measurement and providing more representative domain statistics for analysis. In some instances, applications benefit from dispersions comprising of a high interfacial surface area. For each experimental study performed, the physical states of ingredients are highlighted.

One method for analysing dispersions for domain size is laser diffraction, a non-destructive and non-intrusive technique that allows analysis of wet and dry samples

in the 0.02 to 2000 microns size range (Kippax, 2005b). It is often applied in the pharmaceutical industry, where applications include drug development and quality control (Kippax, 2005a). This method relies on measurement of the diffraction angle of scattering light, which is inversely related to the domain size (Technical document 1; Kippax, 2005 b). Figure 2.8 is a schematic of a typical laser diffraction instrument assembly. Light is sent from the light source at “(1),” and is directed toward lens at “(2),” which focuses the light toward the sample cell at “(3).” A He-Ne gas laser is normally selected to provide a light source, as this provides a stable, coherent light with a fixed wavelength of 620nm (Technical document 1). The diffracted and refracted light from the sample is measured by “backscatter,” and “wide-angled,” detection systems, located at “6,” and “7,” respectively, which determine the diffracted angle from the droplet (Technical document 1). The amount of sample measured is indicated by the obscuration detector at “5,” which collects focused light via an aperture at “4,” and determines the sample concentration.



Laser (1)	Provides a source of coherent, intense light of a fixed wavelength
Focusing Lens (2)	Used to diffract the light source towards the selected sample
Sample Cell (3)	Provides containment for the selected sample
Focal Plane Detector (4)	Detects light source along focal plain from the lens
Obscuration Detector (5)	Detects the level of obscuration observed through the selected sample
Backscatter Detection System (6)	Detects the amount of backscattered light from the selected sample
Wide Angle Detection System (7)	Detects the amount of wide-angled diffracted light from selected sample

Figure 2.8: Schematic of a typical laser diffraction instrument (adapted from Kippax, 2005b).

Collected scattering data is interpreted using an algorithm (Technical document 2), which incorporates one of two commonly used mathematical models (Kippax, 2005b). The Fraunhofer model assumes that all particles are opaque and that light is scattered at low refractive angles (Kippax, 2005b). The model assumes that light does not pass through the particle and is applicable in measurements where domains are greater than 50 μm in size. Mie Theory (Mie, 1908) accounts for light passing through the domains and is therefore a more suitable model for samples comprising domains below 50 μm .

Figure 2.9 describes the interaction of light with the domain according to Mie Theory. The model makes use of a general solution of the Maxwell Equations for the interaction of light within matter (Technical document 2). It predicts the primary scattering intensity of light from the particle surface and a second scattering behaviour caused by light refraction through the particle (Kippax, 2005b; Technical document 2).

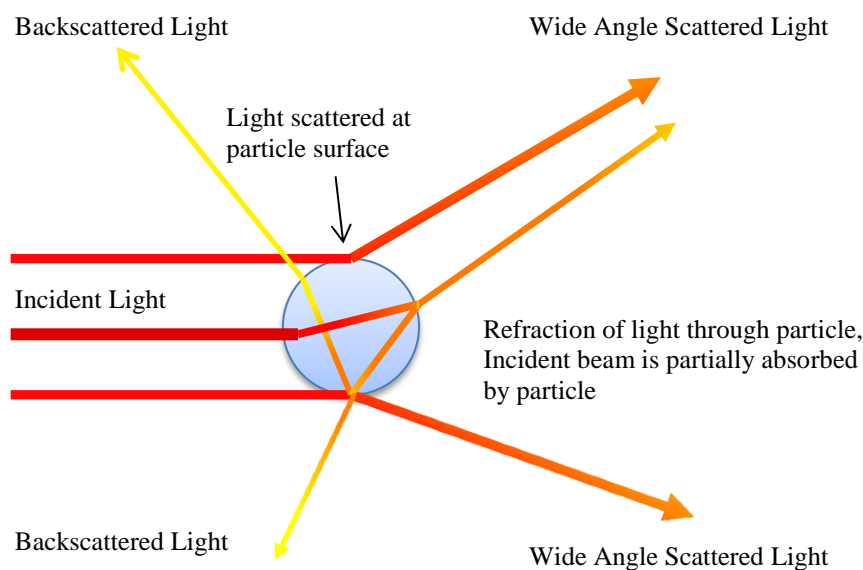


Figure 2.9: Image of a typical light scattering predicted by Mie scattering model (adapted from Technical document 2).

According to Mie theory (Mie, 1908), knowledge of the real and imaginary refractive index is important for determining the second scattering behaviour. This absorption coefficient is also dependent on the refractive index, which may be estimated (Technical document 2).

The results generated through laser diffraction calculate the frequency distribution by analysing the volume of the particles in the sample population, giving $D [4,3]$ or equivalent volume mean (Technical document 1). This is proportional to mass distribution if the density is assumed constant. Applying a reverse Fourier Transform, the selected model predicts a domain size distribution and generates a predicted scattering pattern. The predicted and actual scattering patterns are compared via an iterative calculation and the domain size distribution is modified until convergence between scattering patterns occurs (Technical document 2).

2.3.2 Emulsion Rheology

An understanding of the rheological behaviour of emulsions is essential in optimising material characteristics. Rheology is “the study of the relationships governing the deformation of a material when subjected to a force,” (Malkin et al., 1994). Furthermore, the type of deformation is dependent on the material state, for example applying a force to a gas or liquid will cause it to flow. However, applying the same force to a solid may cause it to deform elastically (Goodwin and Hughes, 2008). The flow properties of emulsions are also linked to inter-droplet interactions (Gupta, 2001). Therefore the study of dispersions/solutions as opposed to a bulk continuous phase is essential in determining the fluid’s rheological properties. In particular, the rheological properties of food products play a key role in product perception, including sensory perception, stability and nutritive characteristics (Fischer and Windhab, 2011).

Figure 2.10 presents a schematic of a fluid positioned between two parallel plates. The fluid is subjected to a unidirectional shear deformation when a force is applied to one of the plates. Furthermore, an equal and opposite internal resistive force is exerted by the fluid. The movement of this plate develops a velocity gradient

between parallel plates, du_x/dy , where u_x represents the velocity of the plate in the x dimension; this is equivalent to an applied shear rate, $\dot{\gamma}$. The shear stress, τ , applied by the plate on the fluid will be a function of the force, F , applied per plate surface area, A (Gupta, 2001).

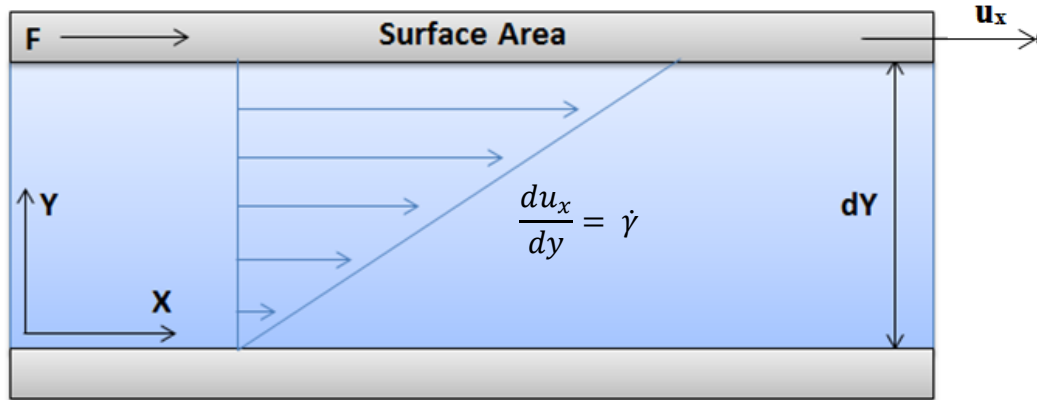


Figure 2.10: Representation of a unidirectional shearing flow on a fluid (Adapted from Gupta, 2001).

A similar model may be applied to a fluid exposed to extensional shear, which considers the velocity gradient developed between stationary plates, du_y/dy . The capillary rheometer, described below and displayed in Figure 2.12b, is an example of a device that determines fluid rheology through extensional shear. Both rotational and extensional shear methods are relevant in the CDDM apparatus, which comprises of several axial constrictions that promote extensional shear and confronting surfaces between which a rotational shear is developed. This is described in more detail in section 2.6.3.

The Newton-Stokes law, described in Equation 2.8, relates τ and $\dot{\gamma}$ to the fluid viscosity, μ_{fl} , which varies with temperature and pressure. This is analogous to Hooke's Law, which describes the relationship between stress and strain for Hookean solid materials (Goodwin and Hughes, 2008).

$$\tau = \mu_{fl}\dot{\gamma} \quad (2.8)$$

Fluids may be characterised as Newtonian or non-Newtonian, with typical flow curves of fluid types are outlined in Figure 2.11 a). Newtonian fluids are characterised as fluids whose viscosity is independent of shear rate and reduces to zero once shear has ceased (Brown et al., 2004), whereas non-Newtonian fluids do not obey Newton-stokes law and comprise fluids whose viscosity is shear rate dependent or those that possess a minimum viscosity at zero shear. In contrast, a power-law fluid, described in Figure 2.11 b), comprises three distinct flow properties, including regions of constant viscosity at low shear (low-shear limit region) and high shear (low-shear limit region), separated by a region of shear-thinning properties. For power-law fluids, the Newton-Stokes law may be applied by replacing μ_{fl} with an apparent viscosity, μ_{flr} , which is proportional to the linear section located at * in Figure 2.11 b).

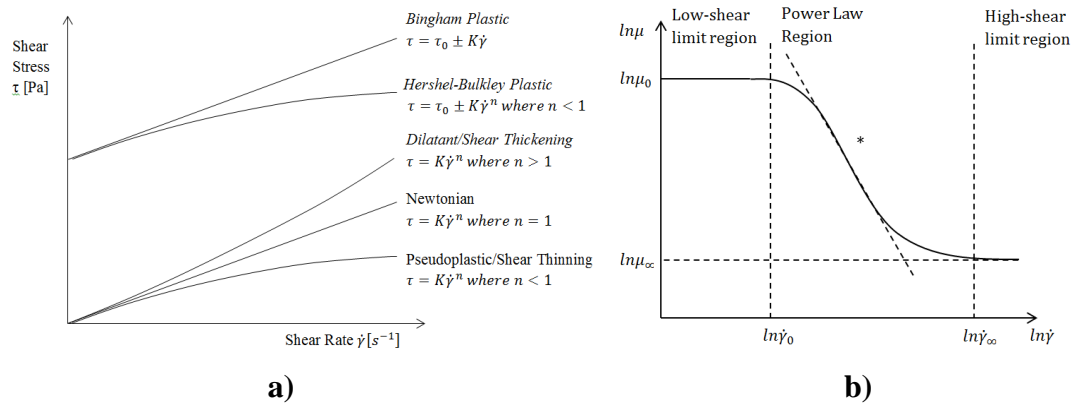


Figure 2.11: Flow curve describing typical relationships between shear stress and shear rate for **a)** Newtonian and non-Newtonian fluids and **b)** power-law fluids (Adapted from Brown et al., 2004).

In terms of rheological measurement, several methods are available. A rotational rheometer, for example the Couette rheometer (Figure 2.12 a), comprises of a moving spindle at a defined position, relative to a stationary surface, with a test sample held between said surfaces. Depending on the instrument type, the viscosity of the material is determined at an applied shear stress, by imposing a known torque to the spindle and measuring the resulting shear rate. Conversely, by applying a known shear rate and measuring the torque needed to rotate the spindle. These

approaches are used to construct flow curves, shown in (Figure 2.11 a) and b)) however, each test is typically restricted to a single test sample, which may alter in structure with applied shear.

Rotational rheometers are often restricted to measurement of viscosity at low shear rates. However, a capillary rheometer, displayed in Figure 2.12 b), may be applied if determining fluid viscosity at high shear rates is required. Here, material is forced at a series of flowrates through a capillary tube of radius r and length L . Measurement of the pressure drop is made along the capillary tube, where viscosity at the wall is determined by considering the shear stress and shear rate applied to the fluid at the capillary wall.

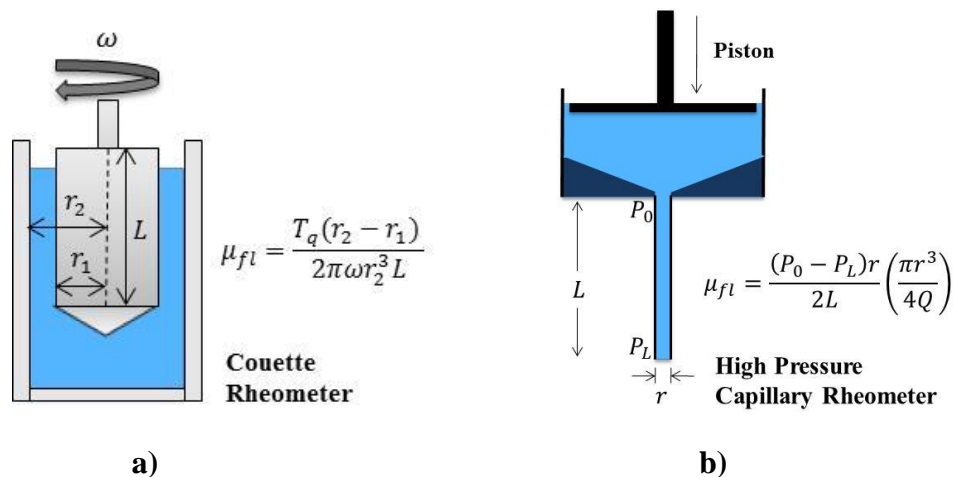


Figure 2.12: Image describing approach for fluid rheometry measurement using **a)** a Couette rotational rheometer and **b)** a capillary rheometer.

A viscometer offers another method for measuring viscosity, defined by Barnes and Hutton (1989) as “an instrument for the measurement of viscosity.” While the definition seems obvious, it highlights the point that viscometers are designed to determine a fluids apparent resistance to shear without obtaining the full rheology profile as determined by rheometers. Despite providing less information, viscometers offer a rapid means for determining material properties of different fluids. One class of viscometer involves a rotating spindle, which includes the Brookfield viscometer (Barnes and Hutton, 1989).

In some instances, fluids possess both Newtonian and Hookean characteristics with varying shear conditions (Barnes and Hutton, 1989). Examples include viscoelastic materials, described as “systems which exhibit a blend of viscous fluid-like behaviour and of elastic solid-like,” or viscoplastic behaviour described as a “non-Newtonian fluid behaviour characterized by the existence of a threshold stress,” (Krishnan et al., 2010). The extent of viscous or elastic fluid behaviour is dependent on the shear rate (Barnes and Hutton, 1989). Therefore, under certain conditions the material can store part of the shear energy applied to it. Basic models for viscoelasticity have been described by the Kelvin-Voigt model, considering components stress on the system (Figure 2.13a) and the Maxwell model (Figure 2.13b) considering components of shear rate on the system.

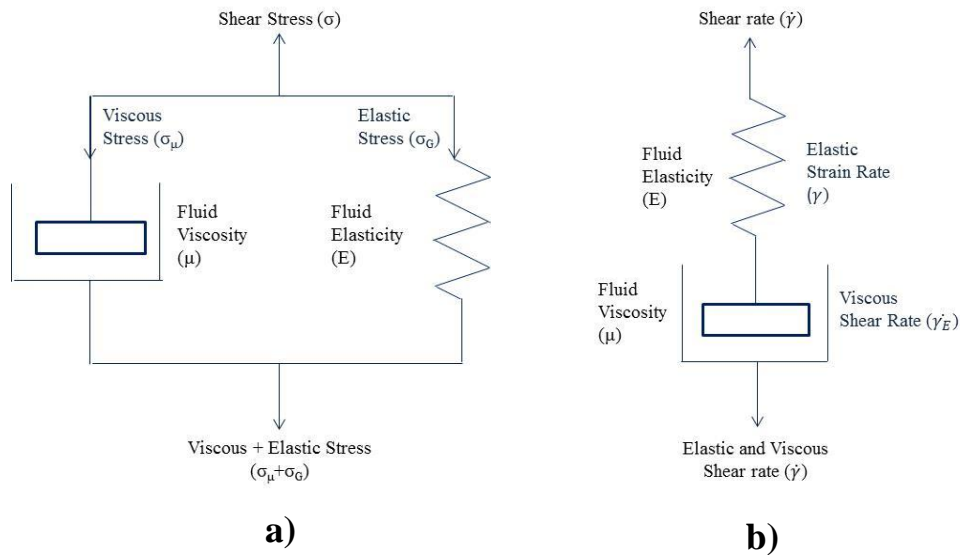


Figure 2.13: Schematic describing basic models for linear viscoelasticity, **a)** the Kelvin-Voigt model, considering the shear stress components relating to viscosity and elasticity and; **b)** the Maxwell model, considering the shear rate components relating to viscosity and elasticity.

For the Kelvin-Voigt Model, the total shear stress (τ) comprises the viscous (τ_μ) and elastic components ($\tau_{G'}$), which can be summarised by Equation 2.9:

$$\tau = \tau_\mu + \tau_{G'} \rightarrow \tau = \mu\dot{\gamma} + G'\gamma \quad (2.9)$$

Where $\dot{\gamma}$ is the shear rate, γ is the strain, μ is the viscosity and G' is the material's storage modulus. Solving Equation 2.9 for conditions of constant shear stress, applied at $t = 0$, leads to Equation 2.10.

$$G'\gamma/\bar{\tau} = 1 - \exp(-a^*t) \quad (2.10)$$

Where $\bar{\tau}$ is the constant shear stress applied, t is the time and a^* is the ratio of elasticity and the viscosity, describing the rate at which the elastic fluid returns to its original state. As time increases, the term exponentially decays reaching an asymptote at 1, which describes Hookean behaviour (Barnes and Hutton, 1989). The Maxwell equations also consider the viscous and elastic components, in this instance the shear rate and strain are considered in Equation 2.11.

$$\dot{\gamma} = \dot{\gamma}_E + \dot{\gamma}_G \rightarrow \dot{\gamma} = \dot{\sigma}/G + \sigma/\mu \quad (2.11)$$

Measurements for viscoelasticity can be performed by oscillatory shear methods (Barnes and Hutton, 1989; Krishnan et al., 2010), where the applied shear rate is oscillated during measurement. For an elastic Hookean solid, the phase difference between the applied strain and the resulting shear is zero. However, for Newtonian liquids the fluid stress lags the applied strain by phase difference of $\pi/2$. By measuring the phase difference of a viscoelastic fluid, the degree of viscoelasticity can be quantitatively determined (Krishnan et al., 2010).

Figure 2.14 outlines the interaction of said droplets with phase volume. The rheology of emulsions is, in part, a function of the degree of interaction between dispersed droplets. While little interaction is observed at fractions below 30vol.%, droplets interact frequently at fractions between 30vol.% to 74vol.% (Harnby et al., 1997). This corresponds to an increase in emulsion viscosity with increased phase volume. At fractions of 58vol.%, a “glass transition volume fraction,” (ϕ_g) is reached, signalling the point when droplets become “caged,” by neighbouring droplets (Mason, 1999). Finally, emulsions with volume fractions above 74vol.% exceed the

hexagonal close packing limit for mono-disperse systems. Therefore, droplets are compressed to accommodate the additional fraction.

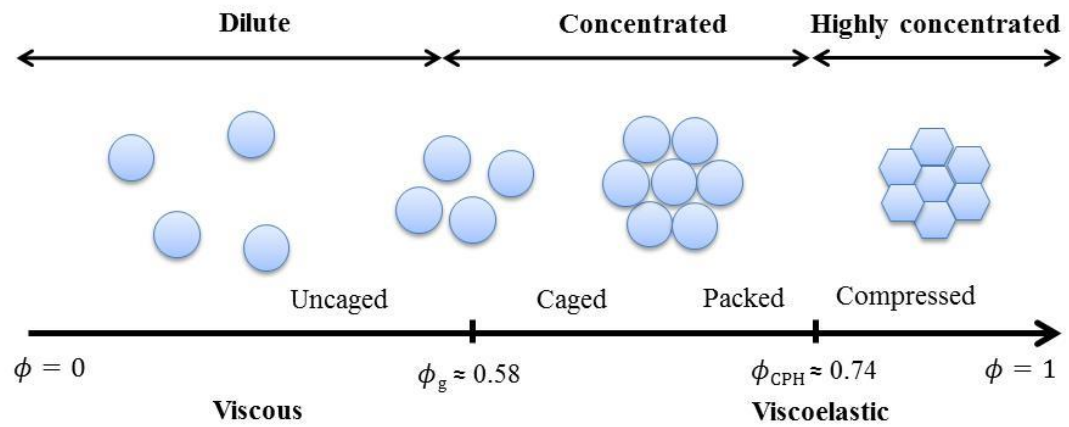


Figure 2.14: Image describing transition of emulsion interaction and rheological properties with increasing dispersed phase concentration. For incompressible spheres, ϕ represents phase volume, ϕ_g represents the hard sphere glass transition volume fraction and ϕ_{CPH} represents the closed packing hexagonal volume fraction limit of mono-disperse spheres (adapted from Mason, 1999).

In summary, for dilute emulsions, droplets are sufficiently isolated to minimise interaction and therefore these systems possess Newtonian behaviour (Derkach, 2009). However, droplets in “concentrated,” and “highly concentrated,” systems are positioned in near-proximity to one another. Therefore, droplet interaction strongly affects emulsion rheology and results in non-Newtonian fluid properties (Niedziedz et al., 2010; Derkach, 2009). Changes in emulsion composition, droplet structure and interfacial interactions affect rheological behaviour in these systems (Mason, 1999). Further, domain interaction is affected by domain size distribution (Mason, 1999).

Many of the models predicting dilute emulsion viscosity have developed from equations for solid spherical particles, suspended in a liquid continuum. Stokes Law (Equation 2.12) describes the movement of a solid particle through a liquid continuum of known viscosity.

$$u_{st} = \frac{d^2 g (\rho_c - \rho_d)}{18 \mu_c} \quad (2.12)$$

Here u_{st} is the Stokes velocity, d is the droplet diameter, g is the gravitational acceleration, ρ_c and ρ_d are the densities of the dispersed and continuous phases respectively and μ_c is the dynamic viscosity of the continuum. Einstein's law (Einstein, 1906), outlined in Equation 2.13 shows the dependence of dispersed phase concentration for a solid on dispersion viscosity.

$$\mu_e = \mu_c (1 + 2.5 \phi_d) \quad (2.13)$$

Where μ_e is the viscosity of the dilute emulsion, ϕ_d is the phase volume and μ_c is the viscosity of the continuum.

These expressions provide a suitable basis for describing the viscosity of dilute emulsions, as the domains are sufficiently isolated to neglect inter-droplet interaction. A notable extension of these expressions to dispersed liquids is an account of the viscosity of dispersed and continuous phases. This includes Hadamard-Rybczynski equation (Hadamard, 1911; Rybczynski, 1911) described in Equation 2.14, where $\Delta\rho$ is the difference in density of the sphere and continuum, r is the droplet radius and a is the ratio of the dispersed and continuous phase viscosities.

$$\mu = \frac{\Delta\rho g d^2 (1+a)}{6\mu_c (2+a)} \quad (2.14)$$

Further extensions for describing emulsion rheology consider the droplet's interfacial properties, which are fundamentally different from those of a solid-liquid interface (Derkach et al., 2009).

Taylor (1932) investigated the break-up mechanisms of isolated droplets by a surrounding fluid. This was an extension of the work of Einstein (1906), describing the rheology of a liquid containing suspended solid particles. Einstein's work has proved valid for dilute droplet dispersions where the droplets were very small or had high surface tensions, and therefore assumed spherical under shear. However, Taylor (1932) developed the Einstein equation to incorporate deformation of the droplet surface. Taylor (1932) proposed Equation 2.15, where μ_e is the emulsion viscosity, μ_c is the viscosity of the continuum, ϕ_d is the dispersed volume fraction and μ_d is the dispersed phase viscosity.

$$\mu_e = \mu_c + \frac{5}{3}\mu_c\phi_d \frac{\mu_d + 0.4\mu_c}{\mu_d + \mu_c} \quad (2.15)$$

For immiscible liquid systems, an interfacial layer exhibiting an interfacial rheology exists between phases, which can alter the emulsions apparent viscosity. Oldroyd (1955) presented Equation 2.16, which considers the impact of the droplet's interfacial viscosity on emulsion viscosity. Here, μ_r is the apparent viscosity, μ_d is the viscosity of the liquid in the droplet, μ_s is the surface shear viscosity and μ_{dl} is the dilatational viscosity, the latter describing the interfacial resistance of the droplet to 2D extensional shear (Derkach, 2009).

$$\mu_r = 1 + \frac{\phi_d \left(\mu_c + \frac{5}{2}\mu_d + \frac{2}{3}\mu_{dl} + \mu_r \right)}{\mu_c + \mu_d + \frac{2}{5}(\mu_{dl} + \mu_r)} \quad (2.16)$$

For emulsions comprising of higher dispersed phase volume fractions, inter-domain interactions affect rheological behaviour and therefore the assumptions made for dilute emulsions are not valid. This is observed for "concentrated emulsions," which have a lower phase volume limit when domains are sufficiently close in order to interact with one another, and an upper phase volume limit when droplets reach a critical packing fraction. This has been defined as the maximum concentration that an emulsion system can reach without droplet deformation. Maximum phase volumes of 0.71 to 0.75 may be observed for these systems, where the highest

fraction is affected by domain size and polydispersivity (Das and Ghosh, 1990). Pal (2001) presents two novel viscosity expressions where the maximum packing fraction of droplets in an emulsion is included, these equations are outlined in Equation 2.17 and Equation 2.18, where ϕ^* is the critical packing fraction of the emulsion.

$$\mu_r \left[\frac{2\mu_r + 5a}{2 + 5a} \right]^{\frac{1}{2}} = e^{\frac{5\phi\phi^*}{\phi^* - \phi}} \quad (2.17)$$

$$\mu_r \left[\frac{2\mu_r + 5a}{2 + 5a} \right]^{\frac{1}{2}} = \left[1 - \frac{\phi}{\phi^*} \right]^{-\frac{5\phi^*}{2}} \quad (2.18)$$

In HIPEs, the dispersed phase volume fraction exceeds the critical packing fraction of non-compressible spheres. HIPE formation is possible due to droplet deformation, a property which allows the material to flow which is not observed in similarly concentrated solids suspensions (Niedzwi edz et al., 2010). In these systems, droplets are compressed to form polyhedral shapes and therefore, an increased surface area to volume ratio. This results in a thermodynamic equilibrium between the external stress applied on the droplet surface and the increased droplet contact area. Princen (1986) provides a description of this thermodynamic equilibrium relationship, described in Equation 2.19 and Figure 2.15.

$$-\Pi dV = \sigma ds \quad (2.19)$$

A thermodynamic equilibrium is maintained by applying pressure to the system, described here as an osmotic pressure Π , equivalent to the stress induced on a droplet by surrounding droplets. As pressure increases, the work performed on the droplets is compensated for by increased interfacial area, resulting in domain deformation. The excess free energy in the system is present as a residual potential energy. Therefore, as materials HIPEs often exhibit a non-Newtonian, viscoelastic rheology.

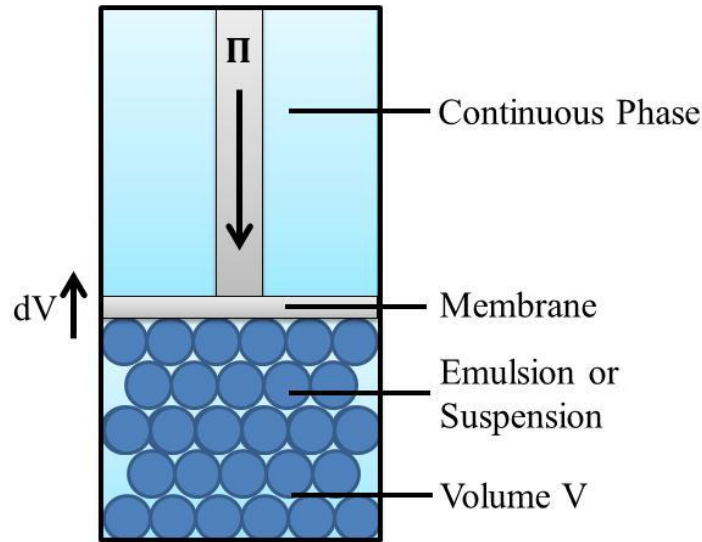


Figure 2.15: Schematic of a model describing the pressure exerted on droplets in HIPEs (adapted from Princen, 1986).

HIPE viscoelasticity was modelled by Princen and Kiss (1986), who developed and validated Equation 2.20 to model the static shear modulus of a paraffin O/W HIPEs.

$$G' = 1.769 \frac{2\sigma}{d_{32}} \phi^{\frac{1}{3}} (\phi - 0.712) \quad (2.20)$$

The storage modulus (G') of studied emulsions is inversely related to the sauter-mean droplet diameter (d_{32}) and proportional to the dispersed phase volume fraction (ϕ_d) and surface tension (σ).

$$\tau_0 = C_1 \frac{2\sigma \cos \theta_{fm}}{d} \phi^{\frac{1}{3}} \quad (2.21)$$

Further, Princen (1983) proposed Equation 2.21 for determining the yield stress (τ_0) of a monodisperse HIPE, where C_0 is a constant, d is the droplet diameter and θ_{fm} is the contact angle between films of adjacent droplets. Similarly, τ_0 is inversely proportional to d and proportional to σ and ϕ .

The literature indicates that emulsion flow behaviour is strongly affected by dispersed phase concentration and mean droplet diameter. Laser diffraction is an effective approach for characterising emulsions for droplet size, providing measurement of a representative sample and information on surface area and volume moment means. Within the present thesis, this technique will be applied to compare processes for efficient emulsification in FDM and CDDM apparatus. Emulsion material properties will be studied using viscometers and rotational rheometers. However, these instruments are unable to match the shear rates observed in the FDM and CDDM. This is a challenge for concentrated emulsion systems, which are non-Newtonian fluids whose rheology alters with shear intensity. Further work may investigate the flow regimes developed at high shear by utilising capillary rheometers.

2.4 Emulsion Destabilisation

Chapter 1, section 1.1 provides a brief description of key causes of emulsion destabilisation. It is essential that emulsion products are stable enough to be commercially viable (Leal-Calderon et al., 2007). Therefore, it is important that the circumstances that cause the phases to separate are understood. The key mechanisms for destabilisation are outlined in Figure 2.16. They are caused by the collision and interaction of droplets (flocculation and coalescence), through gravity driven separation (creaming) and through the mass transfer of the dispersed phase material through the continuous phase (Oswald ripening).

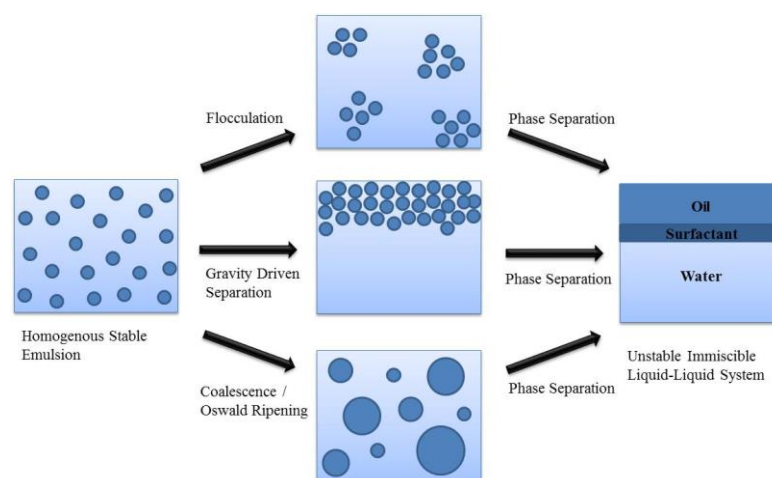


Figure 2.16: Image outlining mechanisms of emulsion destabilisation.

$$f_k = k u_{dr} d_{32}^2 \left(\frac{n}{V_e}\right)^2 \quad (2.22)$$

The collision efficiency, which is the probability that colliding droplets will form a permanent aggregate, is determined by the strength of their attractive and repulsive interactions (Dukhin et al., 2005). The key attractive and repulsive forces acting on an oil droplet stabilised in an aqueous continuum are outlined in Figure 2.17.

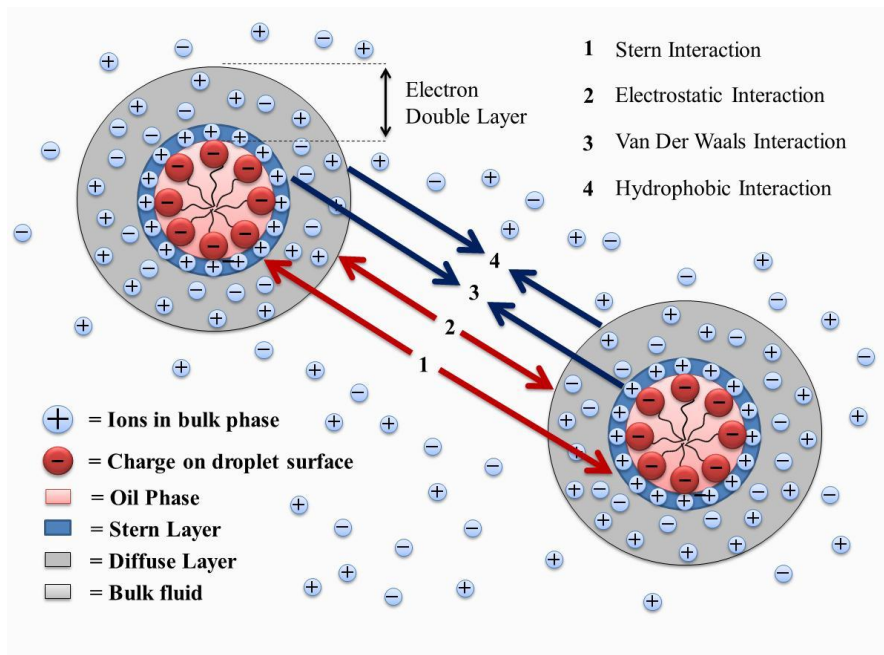


Figure 2.17: Schematic outlining the key attractive and repulsive forces acting on neighbouring droplets (adapted from Kaszuba et al., 2010).

There are a number of attractive forces that drive droplet aggregation, including van der Waal's interaction and hydrophobic interaction. The latter is the attraction of hydrophobic sections of the droplet interface due to the non-uniformity of the surfactant species (Dukhin et al., 2005). Droplets present in a polar continuous phase tend to carry an electric charge, which results in the formation of an electrical double layer (see Figure 2.17), comprising counterions situated near the droplet surface (Stern layer) and within close proximity (diffuse layer or Gouy layer) to the droplet (Kaszuba et al., 2010; Dukhin et al., 2005). The Stern layer may be further divided into the Inner Helmholtz layer (IHL) and Outer Helmholtz Layer (OHL). The ions in

the IHL are absorbed on the droplet surface through chemical affinity whereas the ions present in the OHL are held by electrostatic interaction with the surface (Delgado et al., 2007). The OHL extends between the IHL and the Stern Layer (Delgado et al., 2007), which is the boundary between the Stern Layer and diffuse layers (Dukhin et al., 2005). Counterions present in the diffuse layer will remain in close proximity with a droplet as it moves (Kaszuba et al., 2010). The tangential motion of fluid near a charged surface is known as electrokinetic phenomena (Delgado et al., 2007). The Stern Potential (ψ), which is the electric potential at the Stern Layer, is most relevant to droplet interaction when their diffuse layers overlap (Dukhin et al., 2005).

The Zeta potential (ζ) is the electric potential in the boundary between the diffuse layer and the bulk fluid. The counterion density in the electron double layer is higher than that in the bulk electrolyte solution (Grosse and Delgado, 2010). It may be said that, on the application of an electric field in an electrolyte continuous phase, the conductivity through the electrical double layer is higher than that of the bulk fluid.

Sedimentation stability describes the resistance of droplets in the emulsion to separation due to gravitational forces, which is evident even when small differences in density exist between the dispersed and the continuous phases (Mason, 1999; Dukhin et al., 2005). The parameters driving gravity separation are outlined in Stokes Law (Stokes, 1851), described in Equation 2.12. The equation defines the movement of a droplet through a continuous phase of varying density due to gravitational effects. Sedimentation stability is improved by reducing u_{st} , to a point where Brownian forces dominate droplet movement (McClements, 2011). Emulsions comprising small droplets and higher continuous phase viscosities reduce the Stokes velocity and therefore resist gravity-driven separation.

Oswald ripening is caused by the mass transport of the dispersed phase through the continuous phase due to concentration gradients between domains. This is a key cause of emulsion destruction for emulsions comprising small domain sizes. As described in Equation 2.1, the dispersed phase domains are highly soluble and therefore the rate of diffusion of said domains increases (McClements, 2011). The

solubility of the dispersed phase medium in the continuous phase is directly proportional to the rate of Oswald Ripening. Therefore, the selection of a less soluble dispersed phase improves emulsion stability. Furthermore, an increase in immiscibility between the dispersed and the continuous phase reduces the rate of Oswald ripening, as this inhibits the transfer of material between the droplets (McClements, 2011).

Finally, formulation induced instability occurs when the phase volume of either the polar or non-polar phase exceeds the maximum limit that may be stabilised when the system Hydrophilic Lipophilic Deviation (HLD) is altered. The HLD is similar to HLB, however attempts to account for all the formulation variables, including ionic charge and pH (Leal-Calderon et al., 2007; Salager et al., 2004). Changes to the HLD may be achieved through the addition of either a polar or non-polar phase or adding a concentrated, miscible solution to the external phase (Salager et al., 2004). Formulation induced phase inversion also occurs due to changes in dispersed phase morphology. Salager et al. (2004) notes the following:

- “slowly adding the dispersed phase may delay phase inversion, which may occur once a significant change in droplet diameter occurs.”
- “the slow addition of a dispersed phase can delay phase inversion until a significant change in morphology is presented for example a change in droplet size.”

2.5 Droplet Break-up by Mechanical Emulsification

The mechanisms describing droplet break-up by mechanical emulsification are central to research on emulsification. There have been a number of key studies which have provided a foundation for studies on mechanical emulsification, including:

- Lord Rayleigh (1879) investigated the effects of fluid dynamics on the break-up process. In these studies, Lord Rayleigh quantitatively determined the surface tension of a fluid jet by determining the velocity, cross-section and the length of waves formed on a jet.
 - Reynolds (1885) studied the effects of inertial /viscous forces on fluid behaviour.
-

- Taylor (1934) reported the impact of the surrounding continuum viscosity and droplet viscosity on critical capillary number, and later Grace (1982) on the effect of viscosity ratio on critical capillary number under simple shear.
- Kolmogorov (1941a, 1941b) proposed that eddy behaviour in turbulent flow be considered statistically and later Kolmogorov (1949) and Hinze (1955), who proposed theories for determining the maximum stable droplet size obtained in turbulent flow regimes.

A brief description of emulsification by mixing is provided in section 2.2.1. This approach aims to develop mixing environments which impose shear on the processed fluid and promote droplet rupture. It is important to gain an understanding of droplet break-up mechanisms for developing strategies for efficient emulsification.

The type and intensity of shear imposed on the system is dependent on the flow regime developed by the mixing apparatus, where the modes of droplet break-up are shear-type dependent. For fluids subject to simple shear, the only stress generated is shear stress. Additionally, when different types of deformation applied (e.g. uniaxial, extensional and simple shear flow) the measured viscosities are proportional to one another (Brown et al., 2004). The mechanisms for droplets deformation under various flow regimes are described by Hinze (1955) and summarised in Figure 2.18 and the text below (bullet points):

- *Lenticular deformation*: the extension of a droplet along multiple axes, causing the droplet to flatten and form an oblate ellipsoid.
- *Cigar-shaped deformation*: The extension of the droplet about a central axis, causing the droplet to elongate to form prolate ellipsoid.
- *Bulgy deformation*: Local deformation of the droplet surface, where sections of the droplet are drawn away in multiple direction – caused by irregular flow patterns

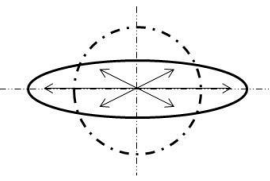
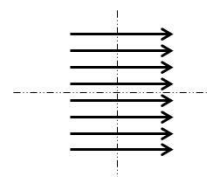
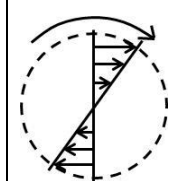
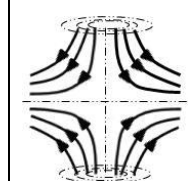
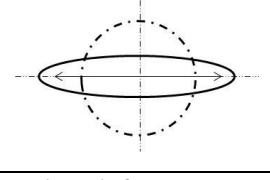
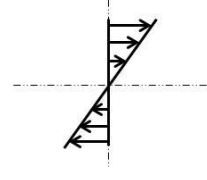
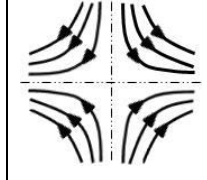
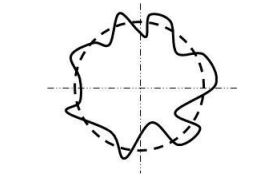
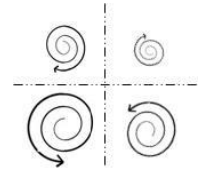
<i>Deformation Type</i>	<i>Flow Regime Imposing Deformation</i>		
<i>Lenticular deformation:</i> 	<i>Parallel flow:</i> 	<i>Rotating Flow:</i> 	<i>Axisymmetric Hyperbolic Flow:</i> 
<i>Cigar-shaped deformation:</i> 	<i>Couette flow:</i> 	<i>Plane Hyperbolic Flow:</i> 	
<i>Bulgy deformation:</i> 	<i>Irregular Flow:</i> 		

Figure 2.18: Schematic describing the deformation of droplets subject to varying flow regimes.

In terms of laminar and turbulent flows, both regimes dissipate energy through viscous heating. However, as laminar and turbulent flows offer varying degrees of inertia, the process for energy transfer is different. Droplet break-up in each environment is a function of the shear developed by the molecular viscosity and the localised velocity fluctuations in the flow and is described as energy dissipation rate per unit volume.

Janssen et al. (1994) proposes that research regarding droplet breakup can be divided into either break-up mechanisms of single drops subject to shear environments or correlations involving a droplet population. This is exemplified by many of the early studies on the subject, which have investigated emulsification in the absence of

inertia or systems with sufficient levels of surfactant to prevent droplet coalescence. To extend this thought, the types of emulsion systems studied have generally increased in complexity with time as authors attempt to gain insight into emulsification in real fluids. A review of studies on droplet break-up in laminar and turbulent flow regimes are provided in section 2.5.1 and section 2.5.2, respectively. The aim of the review on droplet break-up mechanisms is to provide insight on the mechanisms that for break-up that could be observed in cavity-design mixers.

2.5.1 Droplet Break-up in Laminar Flow

Laminar flows are ordered and exhibit limited inertia; as a result they are subject to viscous shear from molecular viscosity and are inherently difficult to mix. Laminar flows typically involve fluids of high viscosity, where implementing methods that develop turbulent conditions requires significant energy input. Therefore, dispersion and spatial distribution of fluid is achieved by imposing velocity gradients in directions away from the bulk flow direction. An effective approach for promoting distributive mixing utilises chaotic fluid flow, which involves the periodic cutting and twisting of fluid portion leading to distribution (Harnby et al., 1997). This concept is described in Figure 2.19.

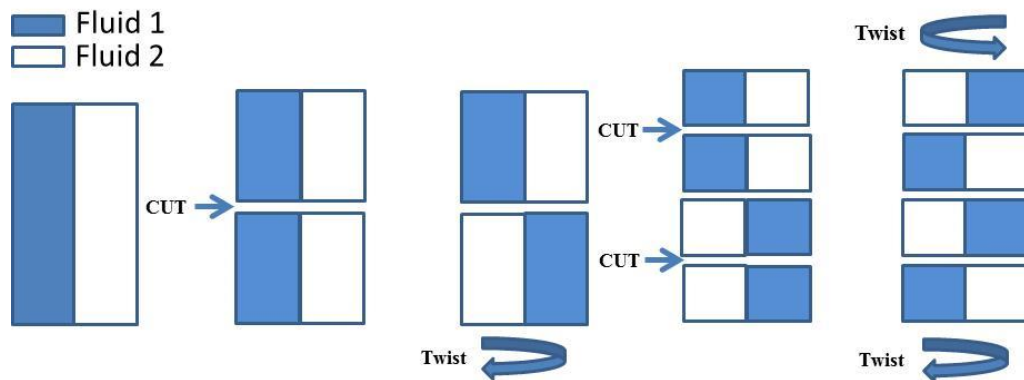


Figure 2.19: Schematic describing fluid distribution through chaotic mixing of fluid 1 and fluid 2 in laminar flow, involving the periodic cutting and twisting of fluid portions (adapted from Harnby et al., 1997).

Many studies investigating droplet break-up in laminar flow are founded on the classical studies by Taylor (1934), who analysed the deformation and break-up of droplets exposed to axisymmetric hyperbolic extensional flows and simple shear flows. A schematic of the apparatus used by Taylor (1934) for studies on droplet break-up by extensional flow and simple shear flow is outlined in Figure 2.20 a) and Figure 2.20 b).

Figure 2.20a) comprises of four cylindrical rollers rotated concurrently with one another by a pulley and bevel wheel mechanism. Whereas, Figure 2.20b) utilises facing surfaces of two rotating pulleys, driven in opposite directions to one another. In both apparatus, an oil droplet was added via the sample inlet, containing an aqueous Newtonian fluid of 5000-15000cP viscosity and positioned as described in Figure 2.20 a) and Figure 2.20 b). Once the droplet was in position, the speed of the rotating surfaces was varied and the ratio of the droplet length and diameter analysed by photography. The oil droplet composition was chosen to achieve droplet viscosities which were lower, equal and higher than the continuum.

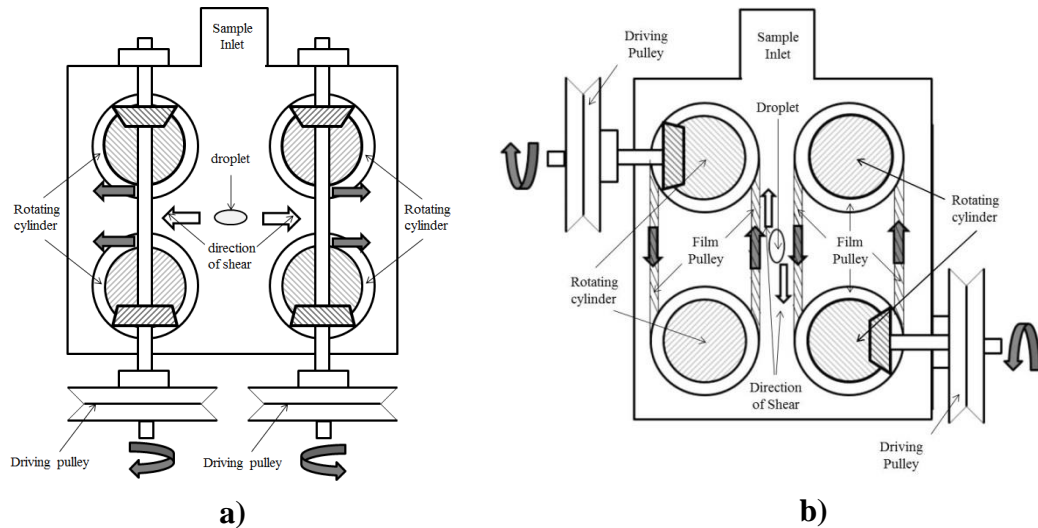


Figure 2.20 Schematic of experimental setup by Taylor (1934), investigating deformation and rupture of a suspended droplet in **a)** an axisymmetric hyperbolic extensional shear field and **b)** a simple shear field (adapted from Taylor, 1934).

Taylor (1934) observed a number of key findings from the experiments, including:

- Droplet break-up occurs at critical ratios of the viscous shear imposed by the fluid and the droplet surface tension, which corresponds to a critical capillary number (see Equation 2.6).
- Deformation of the droplet is affected by the viscosity ratio of the oil droplets and the surrounding fluid.
- Droplet deformation by extensional shear stretches the droplet to a threadlike form, which reaches a critical point and subsequently ruptures the droplet and forms many smaller droplets (1/100 of the size of the original droplet). Taylor (1934) attributed this finding to a Rayleigh-type instability and a laminar flow.
- The critical capillary number was lowest for droplets of similar viscosity ratios ($\mu_d/\mu_c = 0.9$).
- At $\mu_d/\mu_c = 20$, droplet break-up was achieved for extensional shear but not achieved for simple shear flows, regardless of the roller speed applied.
- At low viscosity ratios ($\mu_d/\mu_c = 0.0003$), droplets exposed to both simple and extensional shear flows experienced significant elongation but did break.

The studies by Taylor (1934) provided key insights on droplet break-up mechanisms in laminar flow and a basis for further study. Tomotika (1935) reported mathematical support to Taylor's findings, for systems comprising a cylindrical thread in a viscous continuum, in the absence of inertial forces and under the influence of interfacial tension. Tomotika (1935) determined that the maximum instability of threads comprising very low and very high μ_d/μ_c required a very large varicosity wavelength compared to the thread radius. These findings concurred with the observations of Taylor (1934) and provided a reasonable prediction of daughter droplet spacing for $\mu_d/\mu_c = 0.91$. Furthermore, maximum instability was found to occur at a specific wavelength, and when the wavelength was very large compared to the cylinder radius.

While the development of an axisymmetric extensional shear field provides an effective means for lenticular droplet deformation, it is unlikely that this type of flow will be developed in the novel cavity-design mixers used in this research study. However, the work provides some useful insight on the break-up mechanisms of droplets subject to extensional shear in axial positioned constrictions in the CDDM. This is described in more detail in section 2.6.3.

Rumscheidt and Mason (1962) offered quantitative support to the results of Taylor (1932) and Tomotika (1935) through a series of experiments comprising of oil droplets suspended in an aqueous continuum in a 4-roller apparatus. The droplets were subject to extensional shear and stretched until critical deformation was approached and analysed for disturbance amplitude and wavelength. With reference to Figure 2.21, the growth in disturbance amplitude may be considered by Equation 2.23:

$$\alpha = \alpha_0 \exp(qt) \quad (2.23)$$

Where t is the time from the original amplitude measurement, α_0 it the amplitude at $t=0$ and q is the growth factor. The growth factor, which accounts for the rate of growth in disturbance amplitude, may be modelled as per Equation 2.24.

$$q = \frac{\sigma}{2\mu_2 r} (1 - x^2) h(x, a) \quad (2.24)$$

Where σ is the surface tension, μ_2 is the viscosity of the continuum, r is the cylindrical thread radius, h is a function considering x , a dimensionless parameter relating to $2\pi r/\lambda$ and a is the viscosity ratio of the suspended fluid (μ_1), and μ_2 .

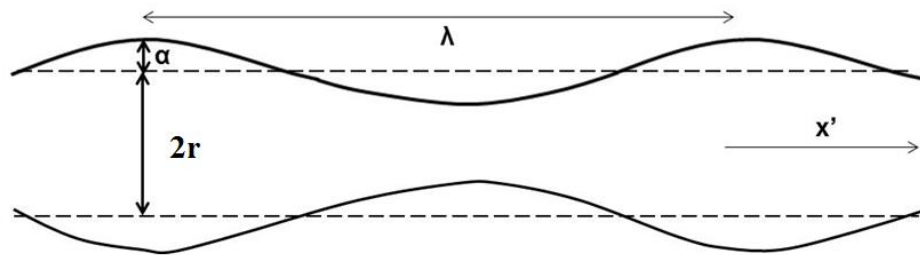


Figure 2.21: Schematic showing the key dimensions for analysis of capillary instability of droplet (adapted from Rumscheidt and Mason, 1962).

Rumscheidt and Mason (1962) confirmed that the disturbance amplitude increased exponentially with time and analysis of the growth factor. These findings provided

good agreement with analysis by Tomotika (1935), however systems comprising viscoelastic oils and surfactants indicated some deviation to the theory, in that variations were found for final droplet diameter and droplet spacing. These findings were attributed to a non-uniform distribution of surfactant at the interface. Furthermore, while systems comprising of low impurity levels gave little variation in λ . Systems with surfactant present were found to vary in final droplet diameter and droplet spacing at the point of breakage. Consequently, the results of these experiments indicate that deviations in interfacial viscosity and surfactant concentrations cause variations in formed droplet diameters.

Subsequently studies on droplet break-up in laminar aimed to analyse break-up in systems of increased complexity and sophistication. Hinch and Acrivos (1980) analysed the break-up mechanism of droplets subject to shear fields of varying rate. They found that applying an instantaneous shear propagated droplet rupture. Applying a quasi-static shear allowed for stable droplet deformation, just below the critical capillary number.

Grace (1982) investigated droplet break-up in laminar flow subject to rotational and extensional shear fields. An adapted figure (from Grace, 1982) described the critical capillary number against the viscosity ratio of dispersed to continuous phases is displayed in Figure 2.22. This graph provides support to the observations of Taylor (1934), Tomotika (1935) and Rumscheidt and Mason (1962) and shows that extensional shear fields cause droplet break-up at significantly lower critical capillary numbers than found in simple shear fields, a minimum critical capillary number observed between 0.1 and 1 and an asymptote in critical capillary number at μ_d/μ_c of around 5.

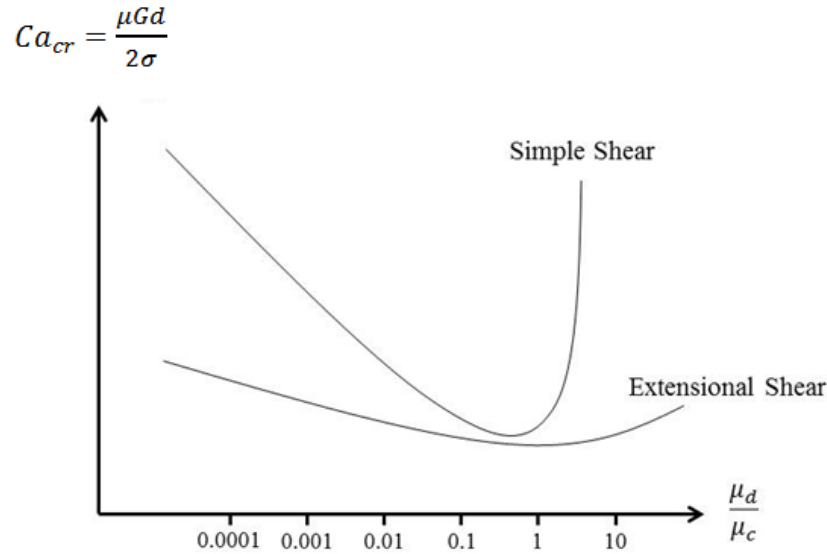


Figure 2.22: Schematic of the Grace curve (Grace, 1982), correlating the critical capillary number against viscosity ratio between dispersed and continuous phases.

Bentley and Leal (1986a, 1986b) developed a computerised control system for a 4-roller apparatus, where images of droplets were digitised and roller speeds were automatically adjusted to impose droplet deformation rates and flows regimes. Automation of the experimental apparatus provided quantitative data which supported the observations reported by other authors deformation as described by other authors (e.g. Taylor, 1934; Rumscheidt and Mason, 1961; Hinch and Acrivos, 1980; Grace, 1982). The aforementioned works describe the fundamental theories of droplet break-up in laminar flow, which occur by an extension to a critical point, where the viscous energy overcomes the droplets surface energy.

Janssen et al. (1994) investigated droplet break-up for W/O emulsion systems in surfactant-poor and surfactant-rich systems, subject to simple shear. Within this study, shear was applied instantaneously or raised in a quasi-steady state to just above the critical capillary number. The authors observed a maximum in critical capillary number at intermediate surfactant concentrations, which aligned to an increase in measured interfacial tension. These findings were independent to the method of applied shear and were attributed to the development of an interfacial

viscoelasticity at the droplet interface, caused by a deviation in equilibrium adsorption from adsorption/desorption of the surfactant species at the interface.

While the break-up mechanisms for dilute emulsions have been comprehensively studied, little is known about droplet rupture in concentrated emulsions. Jansen et al. (2001) extended the studies of Grace (1982) to formulations with dispersed phase volume fractions of up to 70vol.%, using a rotating couette cell connected to an optical system. The results indicate that the traditional Grace curve for simple shear was not followed for emulsions with dispersed volume fractions above 30vol.%. However, the author showed that emulsions followed the Grace curve when a scaling parameter was applied to account for the impact of emulsion viscosity. The modified expressions are outlined in Equation 2.25 and Equation 2.26, where Ca_{cr}^* is the modified capillary number, Ca_{cr} is the critical capillary number, μ_r^* is the modified viscosity ratio of dispersed and continuous phases, μ_r is the viscosity ratio of dispersed and continuous phases, μ_e is the emulsion viscosity, μ_c is the continuous phase viscosity, μ_d is the dispersed phase viscosity.

$$Ca_{cr}^* = \frac{\mu_e}{\mu_c} Ca_{cr} \quad (2.25)$$

$$\mu_r^* = \mu_r / \frac{\mu_e}{\mu_c} = \frac{\mu_d}{\mu_e} \quad (2.26)$$

A key finding of studies by Jansen et al. (2001) was the complex break-up mechanism that results, in part, from increased interaction between droplets. Golemanov et al. (2008) proposed the use of a dimensionless critical shear stress, analogous to the critical capillary number, to predict droplet disruption in highly concentrated emulsions and foams. These emulsions were found to exhibit very low critical stress values, which the authors proposed as a “structure-induced critical instability,” of a central drop by surrounding droplets.

Several authors have extended the complexity of the systems analysed to comprise a non-Newtonian continuous phase. Mason and Bibette (1996, 1997) performed a series of experiments on droplet rupture of viscous oils in a viscoelastic, shear

thinning continuum, subject to simple shear. Polydisperse pre-mixes comprising concentrated dispersed phase volume fractions and a surfactant-rich continuous phase were subject to simple shear through controlled oscillations of facing glass surfaces. The applied shear resulted in the formation of mono-disperse emulsions, whose droplet radius decreased with shear rate despite a reduced apparent emulsion viscosity. The region for monodisperse emulsion formation increased for volume fractions above 64 vol.%, the point of random close packing for monodisperse spheres.

Mason and Bibette (1996, 1997) observed that the critically capillary number was not sufficient to predict the point of droplet rupture and highlighted the material's elastic properties as the key cause, where a critical strain amplitude may be required for break-up. Further studies by Mabillet et al. (2000) indicated the significance of shear gap on the likelihood of disruption quality. This was attributed to the proportion of droplets in the fracture zone, where the fluid undergoes plastic flow and is surrounded by elastic material. The thickness of fracture layer (l) increases with emulsion viscosity (μ_e) and the stress (τ_x) applied to the fracture segment by the surrounding the elastically deformed fluid, moving with velocity u_{fl} as described in Equation 2.27.

$$l \approx \frac{\mu_e u_{fl}}{\tau_x} \quad (2.27)$$

Mabillet et al. (2000) proposed Equation 2.28 for predicting the final droplet diameter of the studied emulsion system, where r is the droplet radius, μ_r is the effective emulsion viscosity, $\dot{\gamma}$ is the shear rate and C_2 is a constant, equal to 0.9.

$$d \approx \frac{C_2 \sigma}{\mu_r \dot{\gamma}} \quad (2.28)$$

While the mechanisms for droplet break-up were not clearly identified, the authors attributed the mono-disperse droplet formation to a Rayleigh-type instability, where

the droplet is sufficiently stretched such that the material's elasticity exceeds the droplets Laplace pressure, inducing a capillary instability.

Mabille et al. (2003) later confirmed capillary instability as the mechanism for droplet rupture through photographic analysis of the emulsion system. The authors determined that the final droplet diameter of the formed emulsion was strongly dependent on the applied stress amplitude and that the resulting span was instigated by the viscosity ratio between internal and external phases. Further, the impact of each shear step on the resulting droplet diameter was found to depend on the droplet diameter of the pre-mix, where an emulsion system comprising droplets below a critical diameter did not emulsify from the initial shear step.

The findings were expanded by Welch et al. (2006), who applied the observations of Mason and Bibette (1996, 1997) to an emulsification of HIPE pre-mixes, formed in a concentrated surfactant solution, in rotor-stator apparatus. The formed emulsions were mono-disperse and comprised droplet diameters below 0.50 μm . The authors attributed the effective droplet break-up to the viscous, shear thinning properties of the continuous phase, causing capillary instability.

In summary, analysis of studies described above has indicated that the mechanism for droplet break-up in laminar flow changes with increased emulsion system complexity. Droplet deformation in laminar flow is achieved by imposing a viscous shear on the system. However, material properties including the dispersed to continuous phase viscosity ratios, dispersed phase volume fraction and component viscoelasticity impact on the droplet break-up mechanism. Emulsification in viscoelastic media, described by Mason and Bibette (1996, 1997) appears to provide an effective strategy for efficient emulsification in the FDM and CDDM apparatus, where fluids will likely be subject to varying shear rates, as it travels through the mixer's complex geometry. As commented by Golemanov et al. (2008), "droplet break-up in concentrated emulsions, with $\phi > 74\%$, is far from clear," and there is scope for study in the subject.

2.5.2 Droplet Break-up in Turbulent Flow

Turbulence is described by Kresta and Brodkey (2004) as “a state of fluid motion where the velocity fluctuates in time”. In comparison to laminar conditions, where the flow fields are ordered, turbulent systems comprise inertial forces which develop a non-linear flow field in the form of “eddies,” described by Pope (2000) as “a turbulent motion, localised within a region of size l , that is at least moderately coherent over this region.”. Eddies of size l have a corresponding characteristic velocity $u(l)$ and time-scale $t(l) = l/u(l)$. They vary in size, kinetic energy and the amount of viscous shear exerted by the fluids molecular viscosity, which is negligible in comparison to inertial forces in fully turbulent flow (Kresta and Brodkey, 2004). Dispersion and distribution of fluid within the bulk is promoted through eddy diffusion, where large eddies promote bulk mixing in the apparatus (distributive mixing) and smaller eddies promote dispersion (dispersed mixing) (Harnby et al., 1997). The largest eddies contain the highest levels of kinetic energy, which is transferred to progressively smaller eddies. This energy transfer continues until the inertial forces developed by the eddy are equivalent to the viscous forces developed. The eddy size at which this is achieved is known as the Kolmogorov microscale. However, eddies enter a viscous subrange below the Kolmogorov microscale, where energy is dissipated by molecular viscosity. This concept is outlined in Figure 2.23.

Fluids in near proximity to the mixer’s moving surface typically experience the highest mixing rates (Harnby et al., 1997), therefore the smallest eddy characteristic lengths. Predictions of droplet break-up in turbulent flow have typically involved droplet populations being exposed to an isotropic turbulence, which is described a state of flow where fluid velocities about the x, y and z dimensions are equal Pope (2000). According to Kolmogorov (1941a), this assumption is appropriate for highly turbulent systems and correlates the mean fluctuating velocity of an eddy of particular size to the rate of energy dissipation delivered per unit mass of fluid. As described by Taylor (1935), the rate of energy dissipation of a fluid at any instant depends only on the viscosity, μ , and on the instantaneous distribution of velocity.

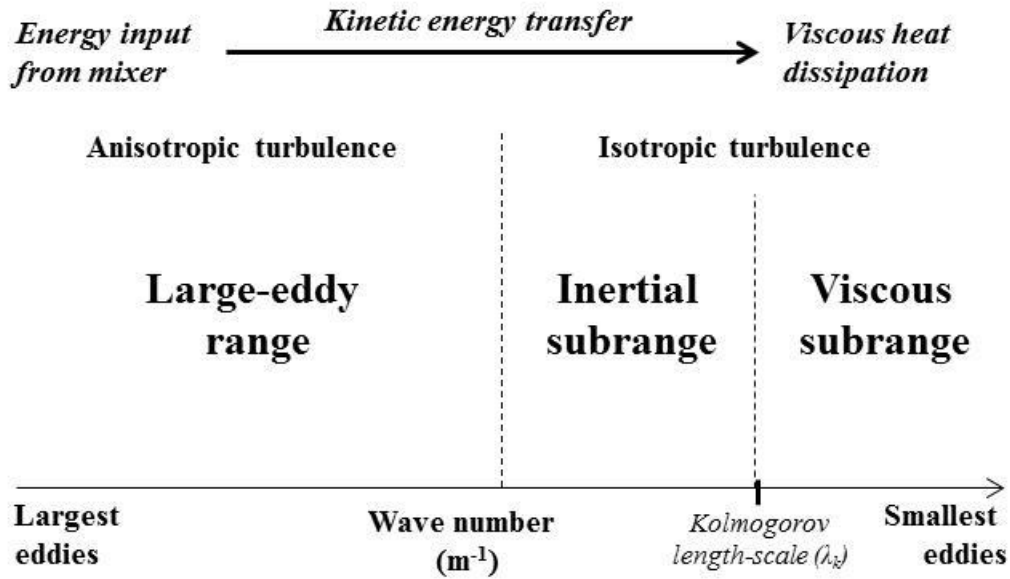


Figure 2.23: Schematic describing kinetic energy transfer in turbulent flow (adapted from Harnby et al., 1997).

Kolmogorov (1949), proposed that λ_k is a function of continuous phase kinematic viscosity, ν_c , and energy dissipation rate, ε , as per Equation 2.29.

$$\lambda_k = \nu_c^{3/4} \varepsilon^{-1/4} \quad (2.29)$$

To relate energy density to mean square velocity fluctuations, $\overline{u^2}$, in isotropic turbulence of equivalent size to the droplet diameter, d . Batchelor (1951) provides Equation 2.30, with C_3 being ~ 2 .

$$\overline{u^2} = C_3 \varepsilon^{2/3} d^{2/3} \quad (2.30)$$

Hinze (1955) applied the theories of Kolmogorov (1941a, 1941b, 1949) and the findings of Batchelor (1951) to mechanisms for droplet break-up in turbulent flow. Hinze (1955) proposed that local fluctuations in velocity had a far greater impact on droplet rupture in turbulent flow regimes, compared to viscous shear. The author proposed that the droplet's viscous and surface resistance to critical deformation would be overcome on reaching a critical Weber number, proposed Equation 2.31.

$$We_{cr} = C_4[1 + j(N_{Vi})], \text{ where } N_{Vi} = \frac{\mu_d}{\sqrt{\rho_d \sigma D}} \quad (2.31)$$

Where We_{cr} is the critical Weber number, C_4 is a constant, N_{Vi} is a viscosity function, μ_d is the dispersed phase viscosity, ρ_d is the dispersed phase density, σ is the droplet surface tension, d is the droplet diameter and $\varphi(N_{Vi})$ is a function relating to the viscosity term which reduces to zero when μ_d approaches 0, where inviscid fluids align to C_4 . Hinze (1955) further proposed that the maximum droplet size of systems subject turbulence would correlate to the size of formed eddies. With reference to Equation 2.5, We_{cr} in these systems may be considered by Equation 2.32:

$$We_{cr} = \frac{\rho_c \overline{u^2} d_{max}}{\sigma} \quad (2.32)$$

Where ρ_c is the continuous phase density, $\overline{u^2}$ is the mean-square velocity fluctuation caused by eddies and d_{max} is the maximum droplet diameter. In terms of highly inertial systems exhibiting isotropic turbulence, $\overline{u^2}$ correlates to a local energy density (ε) as per Equation 2.30. Hinze (1955) incorporating Equation 2.30, Equation 2.31 and Equation 2.32 and assumed N_{Vi} as negligible. Equation 2.33 was proposed for determining the maximum stable droplet size of the system.

$$d_{max} \approx C_5 \left(\frac{\rho_c}{\sigma} \right)^{-3/5} \varepsilon^{-2/5} \quad (2.33)$$

With reference to equation 2.2, d_{max} refers to the droplet size above which larger droplets would disperse into smaller ones under described conditions. Equation 2.33 correlated well with experimental data reported by Clay (1940), with constant C_5 determined as 0.725 for the analysed data and d_{max} assumed as the droplet size for 95% of the sample population (d_{v95}). Deviations from the expression were attributed to statistical variations in turbulent velocity fluctuations. Furthermore, Hinze (1955) noted that a departure from isotropic flow would lead to spatial variations in energy input /dissipation and that the model would only be valid for non-coalescing

systems. The maximum stable diameter of droplets subject to viscous turbulent flow can be approximated by Equation 2.34 (Kolmogorov, 1949; Hinze, 1955; Vankova et al., 2007), where C_6 is a constant and μ_c is the continuous phase viscosity.

$$d_{max} \approx C_6 \left(\frac{1}{\varepsilon \mu_c \rho_c} \right)^{-1/2} \sigma \quad (2.34)$$

Subsequent studies extended analysis of turbulent break-up in varying mixing apparatus and emulsion formulations. Shinnar (1961) extended the work of Hinze (1955) to consider droplet break-up in shear environments comprising eddies above and below the Kolmogorov length scale, λ_k . With reference to Figure 2.23, Shinnar (1961) proposed that droplet break-up in inertial shear forms diameters greater than λ_k are subject to break-up through inertia, likewise droplets smaller than by viscous shear for droplets smaller than λ_k . Shinnar (1961) proposed Equation 2.35 and Equation 2.36 for predicting the Sauter-mean droplet diameter (d_{32}) for turbulent droplet break-up in these conditions, with surface tension (σ), continuous phase density (ρ_c), continuous phase viscosity (μ_c) and energy dissipation rate (ε).

$$d_{32} \approx \sigma^{1/3} \rho_c^{-2/3} \mu_c^{1/3} \varepsilon^{-1/3} \quad (2.35)$$

$$d_{32} \approx \sigma \rho_c^{-1/2} \mu_c^{-1/2} \varepsilon^{-1/2} \quad (2.36)$$

Davies (1985) investigated emulsification in a type of rotor-stator apparatus (i.e. colloid mill). The reported findings supported the view of Hinze (1955), in that velocity fluctuations formed by turbulence were the primary cause for inducing break-up, as opposed to shear intensity, droplet stretching and surfactant. Davies (1985) highlighted the significance of droplet viscosity in predicting final droplet diameter.

Many other authors have contributed to developing the fundamental theories of turbulent droplet break-up in emulsification apparatus including Chen and Middleman (1967), McManamey (1979), Calabrese, Chang and Dang (1986a), Wang and Calabrese (1986b) and Calabrese, Wang and Bryner (1986c). More recent

research on emulsification in turbulent flow include studies by Tcholakova et al. (2004), who investigated droplet break-up in O/W for low concentration surfactant solutions subject to turbulent shear in a high pressure homogeniser. The maximum droplet sizes observed correlated well with the Kolmogorov-Hinze theory. Tcholakova et al. (2004) observed that within the “surfactant-rich,” regime (>0.1wt.% Brij 58 solution), droplet break-up was dominated by interfacial tension and power density, however in the “surfactant-poor,” regime (<0.1wt.% Brij 58 solution), droplet break-up was strongly dependent on surfactant concentration.

Additionally, Vankova et al. (2007) performed a series of studies on the formulation properties and energy input on final d_{32} and d_{v95} values of O/W emulsions processed through a custom built homogeniser. The authors validated expressions for maximum droplet diameters in inertial turbulent regimes (Equation 2.33) and viscous turbulent regimes (Equation 2.34). They observed a transition from inertial turbulent to viscous turbulent break-up with increasing dispersed phase fractions. At high dispersed phase mass fractions, it was found that the droplet size significantly reduced with increasing phase volume, which was more prominent for high viscosity droplets. For low dispersed phase mass fractions, experiments correlated well with break-up models proposed by Davies (1985).

Tcholakova et al. (2011) developed the work by Vankova et al. (2007) with emulsification studies in an IKA™ Magic Lab rotor-stator homogeniser (IKA®-Werke GmbH & Co. KG, Germany). Coarse pre-mixes, which varied in dispersed phase viscosity and phase volume, were passed multiple times through the mixer at different mixer speeds. The formed emulsions were analysed by optical microscopy, where results indicated a sharp reduction in maximum droplet size at oil fractions greater than 50 vol.%. Additionally, formed emulsions comprising of viscous dispersed phase viscosities were significantly lower droplet diameter compared to other systems comprising lower dispersed phase viscosities. Consequently, Tcholakova et al. (2011) proposed a number of break-up models for droplet break-up, outlined in Figure 2.24.

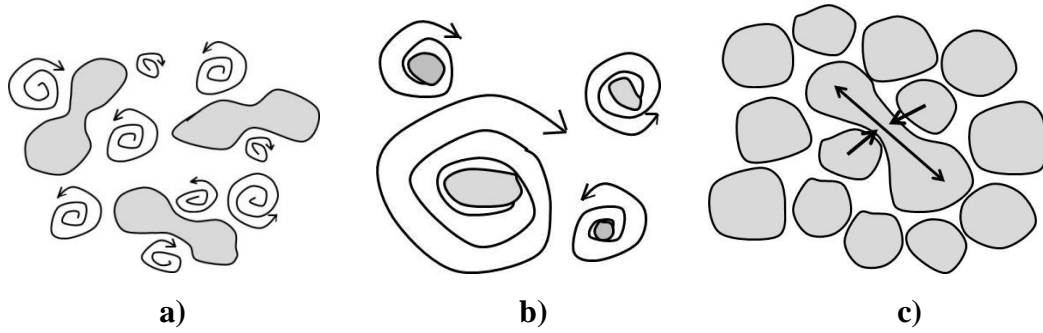


Figure 2.24: Schematic describing droplet break-up mechanisms for a) inertial turbulence b) viscous turbulence c) microstructure-induced instability (adapted from Tcholakova et al., 2011).

Additionally, Tcholakova et al. (2011) found that the formed emulsions exhibited a narrow droplet size distribution as found by other authors (Welch et al. 2006, Vankova et al., 2007). The effect of rotor speed was investigated for systems consisting of varying dispersed phase volume fractions. Whilst the final droplet diameters of processed emulsion systems comprising low volume fractions (below 50vol %) varied significantly with rotor speed, the effect was less significant in concentrated systems (greater than 50vol.%). The authors hypothesised that the break-up mechanisms had either resulted from complex emulsification in rotor-stator devices or by structure-induced capillary instability (as proposed by Mason and Bibette, 1996; 1997). Further results indicated that the effects of surface tension were minimal at high volume fractions. The authors confirmed that the viscous regime did not suitably model droplet break-up at volume fractions above 0.75 and found that a laminar flow of fluids existed. However, they proposed Equation 2.37 for the predication of the maximum stable droplet diameter where d_{hmax} is the maximum stable droplet diameter of the HIPE, $\dot{\gamma}$ is the shear rate, μ_d is the oil viscosity, μ_e is the emulsion viscosity and C_7 is a constant.

$$d_{hmax} = C_7 \dot{\gamma}^{-1/2} \left(\frac{\mu_d}{\mu_e} \right)^{1/6} \quad (2.37)$$

Equations which provide a prediction of maximum stable droplet diameter in turbulent flow provide a basis for scale-up of mixing apparatus, which is a key consideration in industrial applications. For emulsification, the aim of scale-up is to obtain a large-scale equipment design which mimics the performance of small-scale mixers. For this, emulsification equipment design must consider several variables including the required throughput of processed emulsion, the emulsion's composition, emulsion material properties, the mechanical limitations of the equipment (e.g. rotational speed), the mode of mixer operation and mechanical design (Atiemo-Obeng and Calabrese, 2004).

One key consideration for scale-up is power input by the mixer in turbulent flow regimes, which has been the focus of study of several authors. Kowalski (2009) developed an expression for determining turbulent power draw (P) in rotor stator devices (see Equation 2.39), where the function P_R corresponds to power requirement for rotation, P_F corresponds to power requirement for flow and P_{LS} relates to power losses through equipment operation. k_0 , k_1 and P_{LS} are determined by data fitting. In turbulent flow conditions, P_R is determined from the power number, P_0 , rotational speed N , and rotor diameter D , provided in Equation 2.40 (Kowalski, 2009). Kowalski (2009) analysed the results predicted by the expression against power measurements for calcite and soda ash slurries and found that the measured power correlated well with predicted values.

$$P = P_R + P_F + P_{LS} \quad (2.39)$$

$$P_R = P_0 \rho N^3 D^5 \quad (2.40)$$

Furthermore, Cooke et al. (2008) applied Equation 2.39 to determine power numbers for an in-line silverson rotor-stator apparatus, by considering operation modes in the presence and absence of flow. P_0 was determined as constant for all rotor speeds tested and measured power draw correlated well with predicted values. Cooke et al., (2012) expanded this work by determining P_0 for laminar and turbulent flow regimes, within in-line rotor-stator mixers, which comprised of varying geometries. Power input was determined from torque and calorimetry measurements, where the

results showed a good agreement between predicted power and measured power. However corrections for bearing losses against measured power were necessary.

The approach applied to scale-up of emulsification processes include fixing process and design so that small-scale and large-scale devices exhibit similar power numbers (see equation 2.3.9), rotor tip speeds and shear rates. However, for rotor-stator mixers, variations in performance are sometimes observed due to the mixer's complex geometry (Atiemo-Obeng and Calabrese, 2004). Therefore, a number of authors have correlated the maximum droplet diameter to energy or power input per mass/volume emulsion in rotor-stator mixers.

Karbstein and Schubert (1995) performed a series of continuous emulsification studies on systems subject to turbulent flow regimes in colloid mills and high pressure homogenisers. They demonstrated that the d_{32} correlated well with the volumetric energy density (E_v) applied to the system. This process is described within Equation 2.38, where b and C_8 are constants, the latter relating to the dispersed phase viscosity. The expression is valid for systems experiencing low residence times (10^{-2} to 10^{-3} seconds) in the high shear environment, where Karbstein and Schubert (1995) emphasised the importance of stabilisation of formed interface in preventing droplet re-coalescence.

$$d_{32} \approx C_8 E_v^{-b} \approx C_8 \left(\frac{P}{V} \right)^{-b} \quad (2.38)$$

Davies (1987) correlated the maximum stable droplet diameter to local power draw for dilute emulsion systems, processed in several emulsification devices. Analysis was limited to fluid processed in the high intensity shear region, where the lowest diameters were observed in devices that delivered the highest levels local power draw. For rotor-stator devices, mixers delivered between 10^3 - 10^5 W/kg, resulting in a typical size range of 0.5-100 μ m (Atiemo-Obeng and Calabrese, 2004).

Overall, the literature shows that emulsification in turbulent regimes is a function of the local energy dissipation to the emulsion system, where droplet size prediction

assumes a system with isotropic turbulence. As the FDM and CDDM exhibit complex geometries, this ideal state may not be valid in all parts of the flow field in but may exist in certain sections. Certainly, the droplet break-up mechanisms described will likely be observed in the FDM and CDDM apparatus, which are able to impose high levels of inertia on processed emulsions. Therefore, analysis of created surface against power input may provide an insight on approaches for efficient emulsification. Furthermore, while investigations on scale-up of the FDM and CDDM apparatus would be insightful in this current thesis, limitations in equipment design prevented the validity of study on this subject. However, investigations on equipment scale-up should be considered in further work.

2.6 Rotor-stator Cavity-design Mixers

This section provides a brief review on the invention and reported studies on mixing in cavity design apparatus, including the FDM and CDDM.

Cavity-design mixers emerged from a need to effectively mix viscous materials without compromising on quality control and spoil material through localised viscous heating, a problem which earlier solutions to viscous dissipation had failed to solve (Marshall, 1947). As described in section 2.5.1, laminar flow regimes are ordered and are inherently difficult to mix. As a result, several inventions have emerged with the aim of promoting homogenous mixing of viscous fluids, such as the development of methods for improving the quality of soap products through uniform working of ingredients. Albert (1950) filed an invention for a process for creating a floating soap product, where the quality of the manufactured soap is dependent on the uniformity of distribution of air within the product alongside providing sufficient time for the soap to solidify such that the air may be held.

An early invention to rectify inefficient mixing was proposed by Beck (1957), who submitted a patent for the process and apparatus for homogenising and extruding plastersizable materials. The mixer consisted of an axial passage formed between two facing surfaces which have ribs imbedded circumferentially. The design requires that the internal component of the extruder is rotated relative to the stator housing,

whereby the presence of the ribs located on the confronting faces promoted the circumferential movement of bulk fluid. Beck (1957) claimed this process disrupted the continuity of flow through the mixer by creating a tortuous flow path, which promoted fluid homogenisation.

A further invention Renk (1981) proposed an apparatus for blending of plasticisable synthetic resins and additives. The design of the mixer, presented in Figure 2.25, consists of several rows of inner and outer grooved rings which are attached by fitting keys to the internal rotor and external stator surfaces. The geometry is such that the rotor and stator surfaces oppose one another and the outer groove rings (consisting of circumferentially offset helical spur teeth) are axially offset in that they overlap. The geometry is designed such that the bulk fluid is driven between the opposing surfaces. Therefore, the fluid is directed radially and axially from the inner grooved ring of the rotor to those on the stator. The rotor (mounted to the motor shaft by a threaded screw), facilitates the movement of fluid between the grooves as it rotates within the mixer housing.

Renk (1981) claimed that the mixer design not only provided a more effective means of distributing additives uniformly, but also allowed for easy removal of the rotor due to the absence of mixing assemblies or disc assemblies found in other extruder type mixers. This is essential from a practical point of view as it ensures safe and efficient mixing operations particularly with plasticizers. Additionally, Renk (1981) proposed that the axial positioning of outer grooved rings (which are not opposing) mitigates the risk of jamming at land sections during thermal expansion, which might occur during mixing operations involving viscous heating.

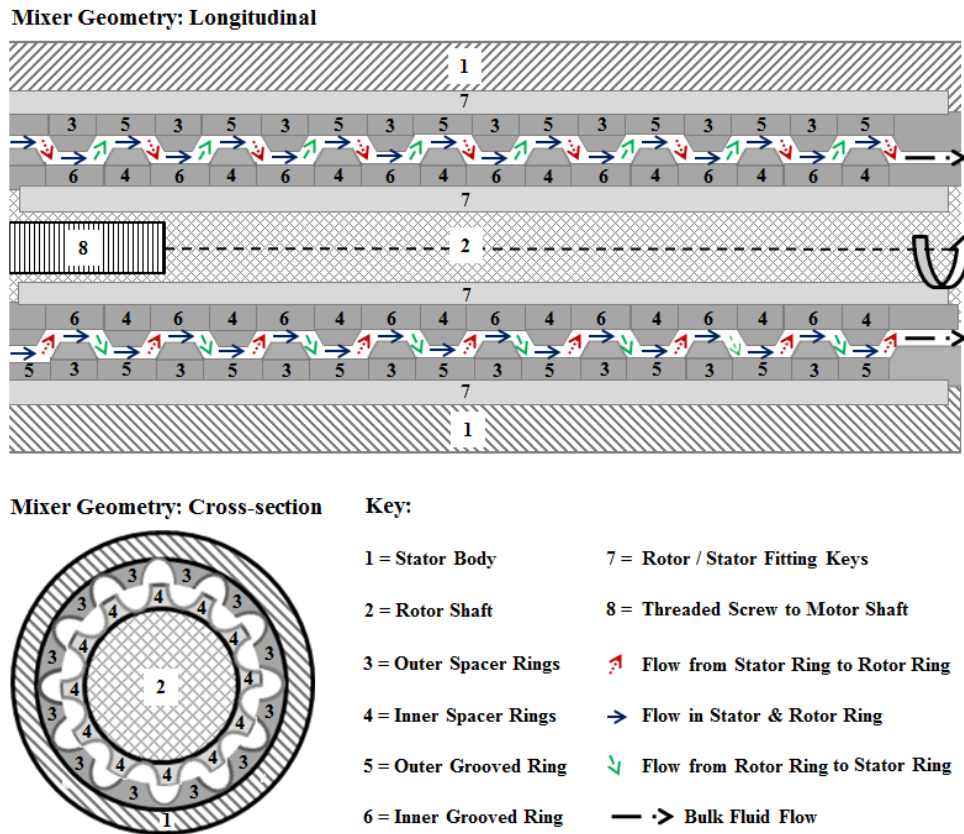


Figure 2.25: Schematic of mixing apparatus comprising of overlapping grooved rings (adapted from Renk, 1981).

2.6.1 Cavity Transfer Mixer

A substantial improvement to the method for blending viscous materials was proposed by Gale (1983), who filed an invention for a Cavity Transfer Mixer (CTM) that mitigated the effects of localised heating and scale-up for the mixing of viscous materials. Particularly, at a fixed length to diameter ratio of extruder, an increase in unit output from the extruder per revolution is proportional to the cube of the rotor shaft diameter; however at constant tip speed, a unit increase in shaft diameter corresponds only to a square increase in the surface area of opposing faces (Gale, 1983).

In order to increase the capacity of the mixer, Gale (1983) suggested that the available volume should be extended along the third dimension. However, for cavity or grooved designs, this would require deeper chambers on the rotor and stator

surfaces, where material could stagnate and cause materials to spoil during the processing of molten plastics, rubbers and polymer blends (Beck, 1957; Gale, 1983). The apparatus design evolved from observations by Spencer and Wiley (1951), who identified theoretically that the mixing efficiency of a fluid subject to a simple shear could be improved by periodically turning of the fluid. The quality of mixing of two liquids may be determined by analysing the created surface area between said liquids. Hindmarch and Gale (1982) propose that for unidirectional simple shear, the extension of interface is may be determined, as per Equation 2.41.

$$\frac{A}{A_0} = \gamma \cos \theta_{fl} \quad (2.41)$$

Where A is the formed interfacial area, A_0 is the original area, γ is the shear strain and θ_{fl} is the angle of the fluid to the shear strain. As proposed by Hindmarch and Gale (1982), the orientation of a fluid striation when exposed to subsequent shear sections affects how the fluid is extended, where maximum efficiency is achieved when $\cos \theta_{fl}$ is equal to unity. The efficiency further improves with the number of shearing stages.

With reference to Figure 2.26 a), the CTM describes the design of a mixer comprising of a rotor at “5,” housed within a stator body, with several rows of cavities embedded in the rotor and stator surfaces at “3,” and “6,” respectively. Here, material enters the mixer at “2,” and is forced between the rotor and stator surfaces, promoting interflow between the rotor and the stator cavities, which are positioned parallel and are circumferentially offset from one other. Additionally, the opposing cavities of the rotor and stator at “4,” and “7,” are axially offset by half of the axial spacing of cavity centres on the opposing surface (Gale, 1983). An adapted cross-sectional view of the mixer is presented in Figure 2.26 b).

Gale (1983) claimed that arranging the cavities as described in Figure 2.26 leads to an increased surface coverage of cavities up to 60%, promoting the flow of fluid between them, resulting in effective mixing. Furthermore, it was claimed that this offset arrangement leads to more effective mixing for the same pressure drop by

maximising the mixing surface area available for a given volumetric increase in flow (outlined in Figure 2.26 c)). Gale (1983) also noted that it was desirable to keep cavities in a hemispherical shape, as it benefited from a streamlined transfer of fluid from one cavity to another, thus preventing fluid stagnation and promoting ease of cleaning (Gale, 1983).

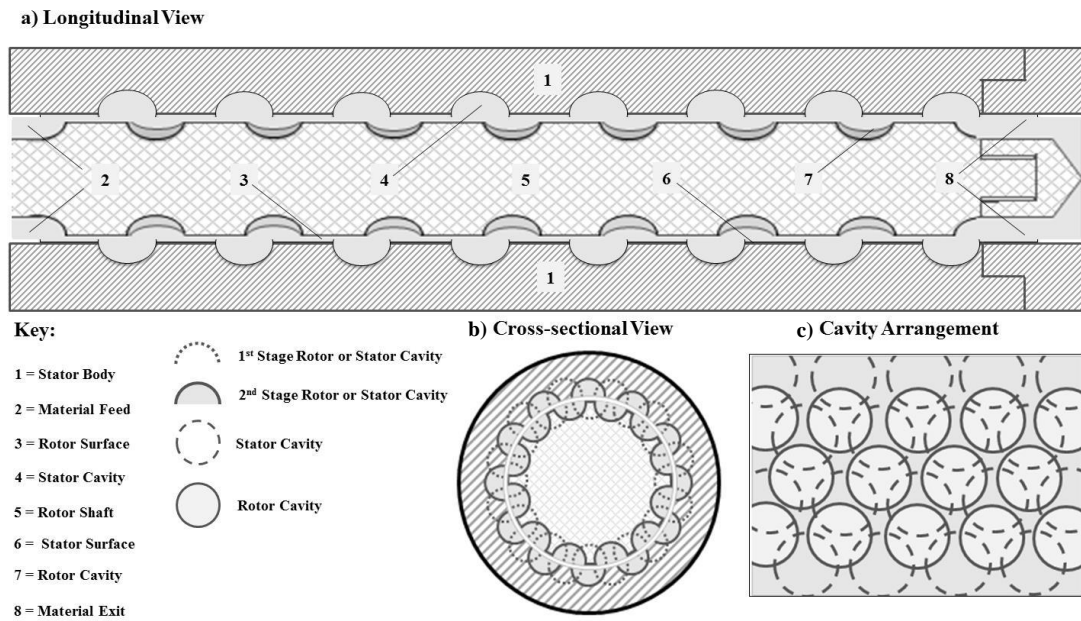


Figure 2.26: Schematic of Gale's Cavity Transfer Mixer Geometry **a)** Longitudinal View **b)** Cross-sectional View **c)** Cavity arrangement (adapted from Gale, 1983).

Further claims in the invention include axially offsetting cavity rows on the rotor and stator surfaces, which promotes efficient mixing by implementing a cutting, twisting and folding action at right angles to the direction of flow, such that in certain positions three cavities may overlap. This was demonstrated in a series of experiments on the proposed mixer design and an existing cavity design, where the thickness of PVC striations against mixer length stage was compared to the original striation thickness. A thinner striation thickness is an indication of more efficient mixing; and it was found that the new design reduced the striation thickness quicker than the existing mixer (Gale, 1983).

The CTM was initially designed to be positioned between existing extruders and the extrusion die, particularly for the polymer, plastics and rubber industries (Hindmarch and Gale, 1982; Hindmarch, 1987; Harnby et al., 1997). For example, Huddleston (1988) employed a CTM for incorporating crosslinking agents and tackifier ingredients in the manufacture of rubber based adhesives. Additionally, the device has been extensively used in other applications such as processing in personal care and food products. In particular, applications in the processing of detergent bars and soaps which included a means of uniformly distributing volatile ingredients such as a perfumes (Clark et al., 1986a), a method for distributing gases through the mix to reduce soap density (Clark et al., 1986b), the creation of transparent soap by imposing sufficient shear at uniform temperature (Clark et al., 1986c), a method that is claimed to improve the lather properties (Clarke et al. 1986d) and to reduce the grittiness of the soap on use (Clarke et al., 1986e).

The CTM has also found use as a low shear mixer for the blending of molten fat-based confectionary ingredients with water (Sanders, 2001). Further, the mixer has been applied in processes used to create spreads with improved properties (Wesdorp and Struik, 1988), spreads with low-fat content (Cain and De Wit, 1994) and the manufacture “no butter fat,” spreads of similar quality to spreads comprising butter fat (Bodor et al., 1999).

In addition to research in the field, a number of academic studies have also been performed on CTMs. Hindmarch and Gale (1982) demonstrated the effectiveness of the CTM by analysing the temperature profiles and quality of extrudate in black and white chloroprene compounds blended using the CTM and a screw extruder. The authors observed little variation in temperature for blends mixed through the CTM. However, hot and cold sections were found for screw extruder blends. Further analysis of Scanning Electron Microscope (SEM) images indicated excellent uniformity of chloroprenes in extrudates formed by the CTM.

Furthermore, Hindmarch and Gale (1983) performed a series of experiments to analyse the flow of a thickened liquid silicone polymer through an acrylic model CTM. The fluid was injected with a coloured polymer marker of similar composition

to the polymer, where the striation movement through the apparatus was analysed. The authors noted a repetitive mixing action on striations which involved a turning action at a 90° angle to the shear direction, the cutting of striation into segments which were then displaced perpendicular to the original shear direction. The original striation was dispersed throughout the fluid volume, to a point where formed striations could not distinguished separately. Further, the authors demonstrated the effectiveness of the CTM as a post-mixing unit, by improving the blend quality of several poorly dispersed polymers.

Wang and Manas-zloczower (1994) developed a finite element simulation to analyse fluid flow patterns in the CTM for processing of a polyvinylchloride. The authors achieved a good agreement between simulation and experimental data provided by Rubber and Plastics Research Association (RAPRA) and observed high elongational shear rates and the potential application of the CTM as a dispersive mixer.

2.6.2 Fluid Division Mixer

Brown (2001) presented a patent for a type of cavity-design mixer known as the Fluid Division Mixer (FDM). This apparatus was used during studies described in the present Thesis and it comprises of a rotor-stator type design of semi-hemispherical cavities embedded on each surface (see Figure 2.27).

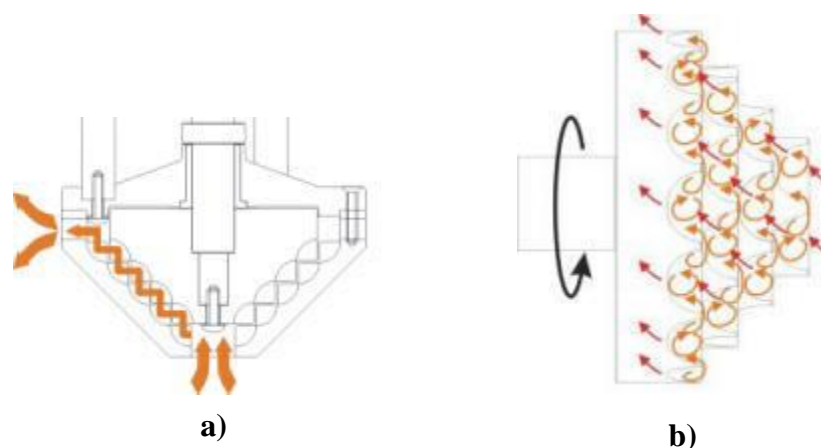


Figure 2.27: Schematics of the FDM **a)** outlining the fluid movement through the mixer **b)** displaying movement of fluid in the cavities (extracted from Maelstrom Advanced Process Technologies (APT) – accessed 27/08/2014).

As seen in Figure 2.27, rotation of the conically shaped mixer causes fluid to be drawn between the rotor and stator surfaces and allows axial and radial movement of flow through the mixer geometry; this is an issue in cylindrical CTMs which do not effectively promote movement of bulk flow into cavities. The FDM design promotes an inner-cavity transfer of material, creating vortices within the cavities which collide to promote hydraulic shear. The overlapping of cavities allows for effective transfer of material between them and the design promotes division of flow along separate streams on entering the mixing enclosure (Brown, 2001).

Thus far, relatively few studies have been published on the FDM. Piela et al. (2012) performed power consumption studies employing FDM apparatus of varying mixer head size to process W/O emulsions. The power consumption was compared to a model considering the cavity-cavity interaction of fluid transferred. The results indicated a good correlation between the model and measured power consumption. Equation 2.42 describes the model used for power use per cavity row.

$$P_{row} = \frac{1}{2} \rho_{fl} V_{icav} n_{int} (\pi DN)^2 \quad (2.42)$$

Where P_{row} is the power consumption per row, ρ_{fl} is the fluid density, V_{icav} is the cavity volume at row i , n_{int} is the number of mass transfer times between cavities, D is the rotor diameter and N is the mixer rotational. n_{int} is inferred from the mixer's rotational speed and geometry and assumes fluid transfer from rotor to stator cavities (or vice versa).

2.6.3 Controlled Deformation Dynamic Mixer

The CTM, described in section 2.6.1, has proven an effective distributive mixer and has found applications in the blending of polymer melts and rubber adhesives, as well as in the processing of detergent bars and soaps. Further, it has been applied as a low shear mixer in the production of food products, such as the manufacture of edible fats such as spreads and confectionary. The CTM's effectiveness as a distributive mixer has been attributed to its unique geometry, which is claimed to

induce a cutting, twisting and folding action on the processed fluid, causing it to turn at 90° to the bulk flow (Hindmarch, 1987). Additionally, it is claimed that the offset arrangement of cavities allows for a larger surface coverage which allows for effective scale-up of the device (Gale, 1983). However, application of the mixing apparatus to emulsion systems is limited. While the device produces an effective low shear emulsion, the processing of emulsions requires generation of sufficient levels of shear for droplet dispersion.

Consequently, a patent disclosure by Akay et al. (1996) described a method and novel cavity-transfer type mixing apparatus for the manufacture of liquid compositions, including detergents, personal care products, cosmetics and food products (Akay et al., 1996). In the patent disclosure, Akay et al. (1996) identifies several limitations within mixing in conventional devices. Firstly, they propose that the handling of liquid compositions to those of low concentration is limited due to concentrated systems being viscous, shear thinning, difficult to homogenise and disperse in conventional mixing processes. Secondly, they suggest that for conventional methods, compositions requiring a molten active ingredient do not allow for a uniform distribution of temperature. The process involves the formation of a concentrated paste containing an active ingredient, which is heated, diluted and subsequently post-processed. Therefore, the authors proposed the CDDM, a novel mixer for the post-processing step. It is suggested that this apparatus is capable of mixing viscous fluids and promoting dispersive mixing by inducing extensional and rotational shear to the system.

The CDDM disclosed by Akay et al. (1996) comprises of six rows of eight cavities embedded on the rotor and stator, each of which are elliptically shaped. The CDDM is similar in design to the CTM, comprising of a cylindrical rotor positioned within a hollow cylindrical stator. The rotor and stator surfaces have cavities embedded in each surface, which are opposing and positioned perpendicular to the direction of bulk fluid flow. Further, the design involves at least a five-fold increase in surface area (Akay et al., 1996). In the CDDM, processed fluids are subject to competing shear types and the mechanisms for break-up in the CDDM are non-trivial. However, the highest shear rates are likely found at positions of confronting surfaces of near-

proximity, which is supported by derived equations Equation 2.43 and Equation 2.44, describing nominal shear rates by rotation and extension for concentric cylinders.

$$\dot{\gamma}_R = \frac{u_R}{\delta} = \frac{\pi D_1 N}{D_2 - D_1} \quad (2.43)$$

$$\dot{\gamma}_E = \frac{u_f}{\delta} = \frac{Q}{4\pi(D_2 + D_1)(D_2 - D_1)^2} \quad (2.44)$$

Where $\dot{\gamma}_R$ is the rotational shear rate, $\dot{\gamma}_E$ is the extensional shear rate, δ is the annular gap between concentric cylinders. u_R is the velocity of the rotating surface, u_f is the velocity of flow through the annular gap, N is the mixer rotational speed, Q is the throughput and D_2 and D_1 are the outer and inner cylinder diameters, respectively.

The intensity and duration of extensional shear increases at larger velocity gradients between bulk flow and parallel surfaces (higher throughput), as well as number and length of constricted sections positioned along the axial direction. Similarly, the intensity and duration of rotational shear is greater with increased velocity gradient between confronting surfaces (faster mixer speed), longer residence times through the mixer (lower throughput) and the number and length of constrictions in the circumferential direction. Therefore, for a set mixer configuration, fluids processed at high throughputs experience more extensional shear and lower rotational shear. In contrast, fluids processed at low throughputs experience less extensional shear and more rotational shear.

One of the key design features of the CDDM is the flexibility to alter the relative axial displacement of the rotor and stator cavities, which is outlined in Figure 2.28. With reference to Figures 2.28 a), the overlapping cavities are analogous to the design of the CTM, where fluid is transferred between cavities positioned on the rotor and stator sections. In this configuration, the clearance gap between the opposing land sections is at a maximum. Therefore, the relative amount of extensional shear to which the fluid is subjected is low. In contrast, Figure 2.28 b) and Figure 2.28 c) represent axial positions where the land sections of the rotor and

stator sections overlap. These regions present positions with the lowest radial clearance (as per Equation 2.44) and present the highest levels of extensional shear.

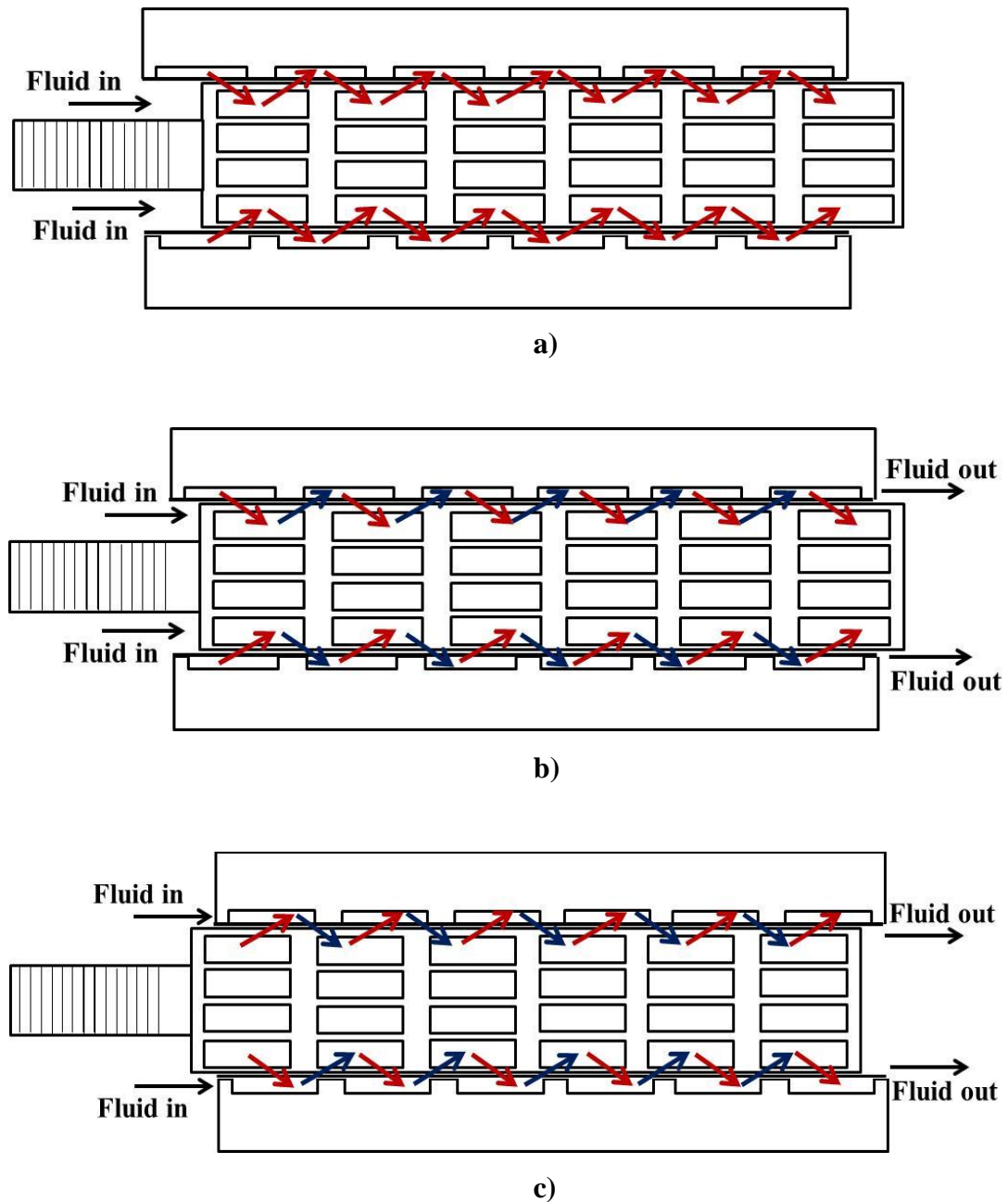


Figure 2.28: Schematic displaying the CDDM apparatus **a)** design at full overlap **b)** design at 0mm position **c)** design of overlapping lands position.

There is little academic literature describing emulsification in the CDDM, however there are a number of inventions disclosed in patent literature. A number of authors

describe the practical issues with the CDDM design, primarily as a rotor-stator mixer (Brown et al., 2010a; Brown et al., 2010b; Rivera et al., 2012). These limitations include difficulties for geometries with small radial gaps and significant overlaps in the land section, in that confronting surfaces may collide due to differences in the thermal expansion of the rotor and stator surfaces. Further, the presence of overlapping land sections requires the generation of high stresses and therefore large torques, which are energy intensive. These limitations can be mitigated by increasing the radial gap between the land sections and between the rotor and stator, by reducing the amount of overlap of land sections on each surface or by limiting the use of extensional and rotational shear.

Rivera et al. (2012) disclosed an invention for the use of a mixer of CDDM design, which limits the total overlap of cavities to between +600 μm and -3000 μm . The authors argued that, whilst reducing the radial gap significantly promoted droplet break-up, altering relative overlap of the cavities did not. This was evident for experiments on the post-processing of a dilute emulsion, consisting of a 5wt.% Sunflower Oil dispersed phase and a continuous phase comprised of a 0.105wt.% Pluronic F68 solution (Rivera et al., 2012). The results showed that the smallest droplets were achieved at the shortest overlap of 2.7mm and at similar pressure drops. The overall throughput of material was 1.9 times greater at the 2.7mm overlap than the 4mm overlap. Furthermore, the authors found that for the same emulsion system processed at a throughput of 40ml/s through lands with an 80 micron overlap, operation of the mixer in static mode produced droplets of equivalent size to emulsions achieved at 25000RPM. Rivera et al. (2012) also demonstrated that the mixer could be used to post-process a highly concentrated and viscous emulsion, consisting of a 10000cst Silicone Oil dispersed phase and a 15wt.% Sodium Lauryl Ether Sulphate (SLES) solution continuous phase. At a flowrate of 19.11ml/s, a reduction in d_{32} from 2.47 μm to 0.87 μm was observed at low pressure drops of 20.52 barG.

Further improvements to the CDDM design have been proposed, including a design which incorporates a “cage,” between the rotor and the stator surfaces (Brown et al.,

2010a), and a design which seeks to mitigate the issues of thermal expansion with close confronting surfaces (Brown et al., 2010b).

Several inventions disclose methods for emulsification using the CDDM. Bongers et al. (2012) propose a method for encapsulating a molten ingredient within the lipophilic phase of an O/W emulsion, where the preferred apparatus considered are the CDDM and the CTM. Studies presented by Bongers et al. (2012) include the encapsulation of Phytosterol blend within a Myritol® lipophilic phase, which occupied 65-70wt.% of dispersion, which was then emulsified using 25wt.% Tween® 20 solution.

The CDDM has also been applied to a method for manufacture of edible spreads (Bongers et al., 2012), which consisted of a molten fat, an oil blend and an aqueous phase. The authors found the method and apparatus successfully created a good quality spread product, with a d_{33} values between 1.5 and 1.8 microns with good spreadability and no free water.

Egan et al. (2013) disclosed a method for the post-processing of structured liquids using a CDDM, which was operated in static mode at 300 L/h. The formulations, which varied in water content, were observed to build in viscosity with each pass.

2.7 Conclusions of Literature Review

In summary, the current section provides a review of theory on emulsion types, emulsion structure, surfactants, mechanical and spontaneous emulsification, emulsion domain size characterisation and emulsion destabilisation. Strategies for efficient emulsification may consider approaches that enhance emulsion effectiveness by creating emulsions with small domains or desirable material properties. Additionally, the current section presents a review of droplet break-up mechanisms in laminar and turbulent flow regimes and details previous experimental studies performed on the FDM and CDDM apparatus. These present novel mixers comprising of complex cavity-design geometries, where droplets in processed emulsions would likely experience varied levels of shear type, intensity and duration.

Further analysis of the literature review is outlined in Chapter 3, which details the key literature disclosures identified in Chapter 2 and presents several hypotheses on strategies for efficient emulsification, which were investigated in studies reported in Chapter 5 and Chapter 6.

Chapter 3: Hypotheses and Experimental Strategies for Efficient Emulsion Manufacture

This chapter aims to briefly summarise the literature discussed in Chapter 2, in terms of emulsion formation (section 3.1.1), emulsification (section 3.1.2), droplet break-up mechanisms (section 3.1.3) and cavity-design mixers (section 3.1.4). Key hypotheses are then drawn from the summarised literature and strategies which are argued to promote efficient emulsion manufacture are proposed for experimental studies outlined in Chapter 5 and Chapter 6.

3.1 Key Literature Disclosures

3.1.1 Emulsion Formation

All emulsions require the creation of interfacial surface between immiscible phases, and many require chemical stabilisation of said interface by the addition of surfactants. In the presence of shear, the formation of O/W emulsions is achieved by introducing quantities of ingredients directly, by adding oil to a surfactant-rich aqueous phase or by diluting the oil with a surfactant-rich aqueous phase (Liu and Friberg, 2009). Spontaneous emulsification processes offer a low energy approach for emulsion formation, however are limited by the properties of the surfactant, which should favour formation.

3.1.2 Emulsification

Mechanical emulsification requires the deformation and dispersion of domains through stress and the stabilisation of formed surface by amphiphilic species. Failure

to stabilise the surface leads to re-coalescence of the dispersed droplet. Deformation is achieved by delivering sufficient stress to overcome the droplet's capillary pressure, which is proportional to interfacial surface tension (σ) and inversely proportional to droplet diameter (d) (Karbstein and Schubert, 1995). Dispersion is affected by the shear type, shear intensity and shear duration delivered to the system.

3.1.3 Droplet Break-up Mechanisms

For emulsions comprising dilute dispersed phases (<50vol.%), turbulent droplet break-up is dominated by inertial mixing regimes and is improved with increased mixing intensity (Tcholakova et al., 2011). The critical Weber number indicates droplet break-up by inertial regimes, which is proportional to ρ_c , u_c^2 and d (Hinze, 1955). For emulsions of semi-concentrated dispersed phases (50vol.% to 70vol.%), turbulent droplet break-up is dominated by viscous mixing regimes and is improved with increased continuous phase viscosity (Tcholakova et al., 2011). The critical capillary number indicates break-up by laminar flows, which is proportional to μ_c and u_c (Taylor, 1934). Under simple shear conditions, stress transfer is ineffective for dispersed phase to continuous phase viscosity ratios >5. For emulsions of highly-concentrated dispersed phase fractions (>74vol.%), droplet break-up is dominated by microstructure-induced destabilisation (Tcholakova et al., 2011). The critical capillary number may be modified to describe break-up in these regimes, where the continuous phase viscosity, μ_c , is replaced with the emulsion, μ_e (Jansen et al., 2001). Furthermore, studies by Mason and Bibette (1996, 1997) and Welch et al. (2006) indicate benefits in processing of emulsions comprising concentrated surfactant phases.

3.1.4 Cavity-design Mixers

The FDM and CDDM are mixers of the rotor-stator type, with confronting static and dynamic surfaces comprising of cavities on each surface (Brown, 2001; Akay et al., 1996). The cavities are profiled to impose radial flow within the bulk flow. The axial position of confronting cavities may be altered to change the flow path of material through the mixer. The FDM delivers extensional shear by radially discharging

material at high velocity at the mixer outlet, and rotational shear by developing velocity gradients between confronting surfaces. The shear intensity is determined by rotational speed and shear duration by total mixing time. The CDDM delivers extensional shear in static and dynamic modes at axially positioned constrictions in the flow path and rotational shear in dynamic mode at circumferentially positioned constrictions in the flow path. The shear intensity is determined by rotational speed and shear duration by the residence time of material in high shear regions.

3.2 Hypotheses

3.2.1 Delivery of Shear

It is hypothesised that emulsification is improved by increasing the exposure time of emulsions to the shear zone. During emulsification, dominant mechanisms for droplet break-up are dependent on the formulation, where low dispersed phase fractions favour inertial regimes and high dispersed phase concentrations favour viscous regimes. Additionally, surface creation depends on the type of shear and therefore, the mixing regime induced during processing. For a given formulation, it is proposed that the CDDM geometry and the number of axially displaced nips may be altered to deliver a desired mixing regime, shear type, intensity and duration.

3.2.2 In-line Emulsification

It is hypothesised that O/W emulsion formation is analogous to infinite size droplet dispersion during emulsification, where the addition of oil is equivalent to the formation of surface during droplet disruption. For surface stabilisation, the introduced oil must be stabilised to prevent the system destabilising through rapid re-coalescence. Formation is determined by the properties of the formulation, such as component amounts and surfactant type. Further, processing promotes stabilisation of surface by controlling the amount of shear delivered to the system. Introducing the oil phase in aliquots limits the surface formed in each step and prevents destabilisation by phase inversion (Salager et al., 2004). Therefore, allowing more

effective stabilisation of surface at each step and the formation of concentrated emulsions.

3.2.3 Emulsification Efficiency

It is hypothesised that the efficiency with which surfactant is used during emulsification provides a measure of the efficiency of the process. In part, emulsification efficiency may be compared by determining the amount of surface stabilised in emulsions processed at equivalent conditions. However, the amount of surfactant used to stabilise said surface is a key consideration. Therefore, an expression was developed to evaluate emulsification efficiency with consideration to surfactant use. The efficiency function, $f(E)$, is described in Equation 3.1 and Equation 3.2.

$$f(E) = \frac{\text{Interfacial area per volume emulsion}(\rho_a)}{\text{Mass of surfactant per volume emulsion}(\rho_{se})}$$

$$(1) \quad \rho_a = \frac{6\phi_d \sum n_i d_i^2}{\sum n_i d_i^3} \rightarrow \rho_a = \frac{6V_d}{V_e d_{32}}$$

$$(2) \quad \rho_{se} = \frac{(1 - f_d)\rho_e V_e C_s}{V_e} \rightarrow \rho_{se} = (1 - f_d)\rho_e C_s$$

$$(3) \quad f(E) = \frac{6V_d}{\rho_e V_e d_{32} (1 - f_d) C_s} \rightarrow \frac{6M_d}{(1 - f_d) M_e C_s d_{32} \rho_d}$$

$$(4) \quad M_{ds} = \frac{M_d}{(1 - f_d) M_e C_s} \quad \therefore \quad f(E) = \frac{6M_{ds}}{d_{32} \rho_d}$$

$$f(E) = \frac{6M_{ds}}{d_{32} \rho_d} \tag{3.1}$$

Where ϕ_d is the dispersed phase volume fraction, n_i is the number of domains of domain diameter d_i , d_{32} is the Sauter mean diameter, M_d is the mass of dispersed phase, V_d is the volume of dispersed phase, V_e is the volume of emulsion, M_e is the mass of emulsion, M_{ds} is the mass ratio of dispersed and surfactant phases, f_d is the mass fraction of dispersed phase, ρ_e is the emulsion density, ρ_d is the dispersed phase density and C_s is the surfactant concentration by mass. The final expression derived in step 4 may be altered to consider a volumetric-based function:

$$(5) \quad f(E) = \frac{6M_{ds}}{d_{32}\rho_d} \rightarrow \frac{6V_d}{d_{32}V_s\rho_s} \rightarrow \frac{6V_{ds}}{d_{32}\rho_s}$$

$$f(E) = \frac{6V_{ds}}{d_{32}\rho_s} \quad (3.2)$$

Where V_d is the volume of dispersed phase, V_{ds} is the volume ratio of dispersed and surfactant phases and ρ_s is the surfactant density. Equation 3.1 was used in these studies, as Equation 3.2 requires knowledge of the surfactant density.

Further, Figure 3.1 presents the efficiency graph. More effective emulsions (direction “a,”) at set M_{ds} requires an increase in efficiency along the set ratio contour, requiring a larger domain size surface area. More efficient surfactant use (direction “b,”) at set d_{32} requires an increase in mass of oil stabilised per mass surfactant (i.e. an increase in O:S mass ratio).

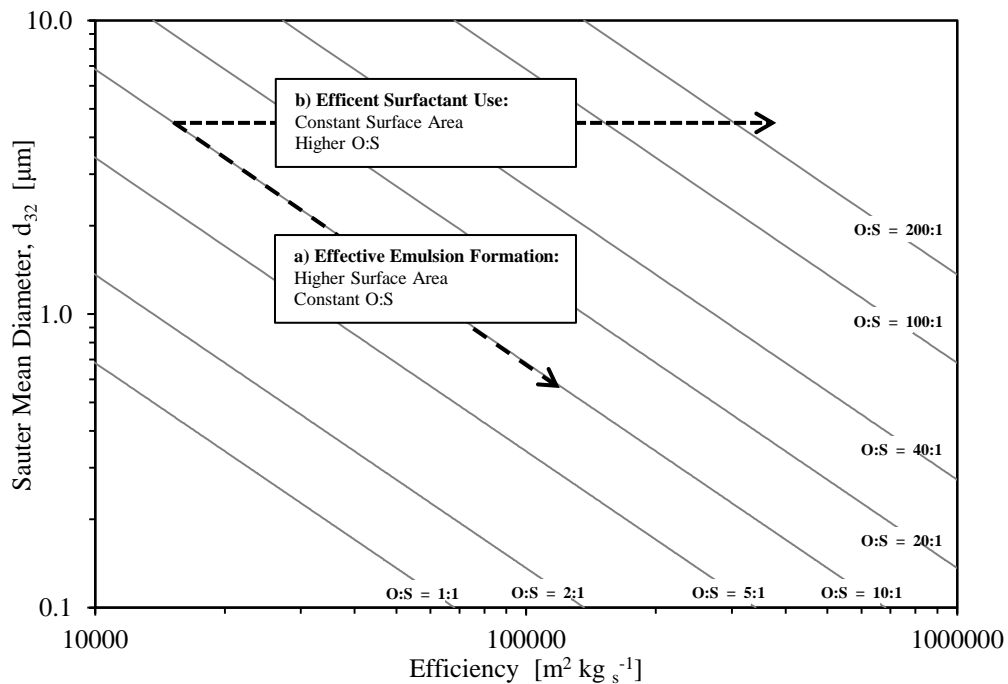


Figure 3.1: Efficiency graph describing emulsion formation by effective methods (small droplet diameter; “direction a,”) and emulsion formation via efficient methods (low surfactant use; “direction b,”).

3.2.4 Viscosity Matching

It is hypothesised that the ability of the system to transfer stress results from the type of shear delivered to the system. For rotor-stator mixers, shear is applied by developing velocity gradients between the rotating and stationary surfaces. This is analogous to simple shear and is ineffective for mixing regimes where processed emulsions comprise dispersed phase to continuous phase viscosity ratios greater than 5. Simple shear may be delivered by increasing the viscosity of the continuous phase, which may be achieved by raising the concentration of certain surfactant systems. Further, by “viscosity-matching,” the dispersed phase and continuous phase viscosities, the critical capillary number is reduced and therefore efficiency is improved.

3.2.5 Surface Stabilisation

It is hypothesised that during O/W emulsion manufacture, the efficiency of surface stabilisation is a function of the availability of surfactant at those surfaces. For some systems, the viscosity of the continuous phase increases with surfactant concentration. For surfactant concentrations above the CMC, surface formation is determined by the energy density applied to the system. At a given oil fraction, the concentration of surfactant may be optimised to promote more efficient surface stabilisation.

3.2.6 HIPE Manufacture

It is hypothesised that the processing of highly concentrated emulsions promotes stress transfer in simple shear due to the close proximity of surrounding droplets and hence droplet dispersion. Additionally, raising the oil fraction increases the amount of available surface to stabilise, promoting efficient surfactant use during emulsification. The emulsification efficiency may be improved by processing emulsions of high dispersed phase concentrations.

3.3 Emulsion Manufacturing Strategies

3.3.1 Mixing Regime

Considering hypotheses described in section 3.2.1, strategies that alter the fluid's exposure to a type of shear, therefore droplet break-up mechanisms may be implemented by CDDM emulsion manufacture by altering the mixer geometry. Chapter 5 (section 5.3.1) reports investigations regarding this proposed strategy.

3.3.2 Number of Cavity Stages

Considering hypotheses described in section 3.2.1, strategies that deliver shear during emulsification improve droplet break-up by increasing the exposure time of emulsions to the high-shear region. This may be implemented in the CDDM by altering the number of cavities, therefore axially displaced constrictions, along the material flow path. Chapter 5 (section 5.3.2) reports investigations regarding this proposed strategy.

3.3.3 In-line Emulsification

Considering hypotheses described in section 3.2.2, methods that incorporate in-line emulsion manufacture versus batch formation promote “process intensification,” a term used here to identify a process route that provides a similar throughput output of processed emulsion of similar characteristics, however with a reduced the number of processing steps or smaller mixer volume. This may be achieved via in-line blending of ingredient streams in the CDDM apparatus. Chapter 5 (section 5.3.3) reports investigations regarding this proposed strategy.

3.3.4 Viscosity Matching Strategies

Considering hypotheses described in section 3.2.4, methods for viscosity-matching of dispersed and continuous phases offer improved droplet break-up by reducing the critical capillary number. This may be improved by the viscosity of the continuous

phase by forming concentrated surfactant. Chapter 6 (section 6.3) reports investigations regarding this proposed strategy.

3.3.5 Surface Stabilisation Strategies

Considering hypotheses described in section 3.2.5, surface stabilisation may alter with changes in surfactant concentration. Surfactant use may be optimised to achieve efficient stabilisation of formed surface during emulsification. Studies described in Chapter 6 (section 6.4) reports investigations regarding this proposed strategy.

3.3.6 HIPE Manufacturing Strategies

As described in section 3.2.6, HIPE manufacture may improve droplet dispersion by improving stress transfer in simple shear and promote efficient surfactant use by increasing the availability of surface for stabilisation. Studies described in Chapter 6 (section 6.5) reports investigations regarding this proposed strategy.

Chapter 4: Experimental Methods

Before proceeding to studies reported in Chapters 5 and 6, it is advantageous to present an overview of the experimental methods used. Particular attention is given to the modes and methods for emulsion characterisation, including domain size measurements, material characterisation, approaches applied for error analysis and the emulsification apparatus applied in experimental studies. The purpose of this section is to provide a description of the methods employed during experimental studies and to describe the design characteristics and assembly of the mixers.

4.1 *Materials*

A number of model O/W emulsions were used during study. For experiments reported in Chapter 5, Sunflower Seed Oil (SFSO; Tesco, United Kingdom) was used as the dispersed phase ingredient. For studies described in Chapter 6, SFSO and Petrolatum were used as the dispersed phase ingredients. Petroleum Jelly (PJ; also known as Petrolatum or Paraffin Jelly) is a semi-translucent, semi-solid hydrocarbon mix obtained predominantly from the methane series of petroleum (Morrison, 1996). PJ has emollient properties that promote effective moisturising and is often found in skin-care products (Morrison, 1996).

For studies reported in Chapter 6, PJ droplets were stabilised with Sodium Lauryl Ether Sulphate (SLES; Cognis, Germany) which is a synthetic anionic surfactant of molecular weight ~332g/mol. The SLES molecular structure (displayed in Figure 4.1 a)) comprises of a sodium cation, a sulphate head-group and a hydrocarbon tail-group consisting of one or more ethoxylated groups, which increases the molecule's hydrophilicity. SLES has an HLB of 42 and is an effective surfactant commonly used in personal care products.

SFSO is a non-volatile, naturally sourced organic oil comprising of oleic acids. It is often applied in food products as an edible oil (McClements, 2009) and in cosmetic products as an emollient (Rele and Mohile, 2003; Asztalos et al., 2013). For studies reported in Chapter 5, the material was stabilised with a synthetic non-ionic surfactant, Pluronic F68 (Carbosynth Ltd, Compton, UK) which is a triblock graft copolymer comprising of an ethylene oxide-propylene oxide-ethylene oxide block arrangement, as displayed in Figure 4.1 b). Pluronic F68, which has a molecular weight ~8400 g/mol, a CMC at 0.00048M at 37°C and an HLB of 29 (Hait and Moulik, 2001), is an effective surfactant often applied in many pharmaceutical applications (Kabanov, 2002). Further studies reported in Chapter 5 involve the stabilisation of SFSO droplets using an edible, naturally sourced surfactant mixture (NS), consisting of proteins, phospholipids and lecithins.

For clarification, synthetic surfactants are amphiphilic species that have been formed by chemical reaction. Natural surfactants are amphiphilic species that are naturally occurring, requiring no further chemical modification. SLES was chosen as the stabilising ingredient for PJ, which is prevalent in non-food grade applications. Pluronic and natural surfactant were used to stabilise SFSO, as it has application in both food-grade and non-food grade products.

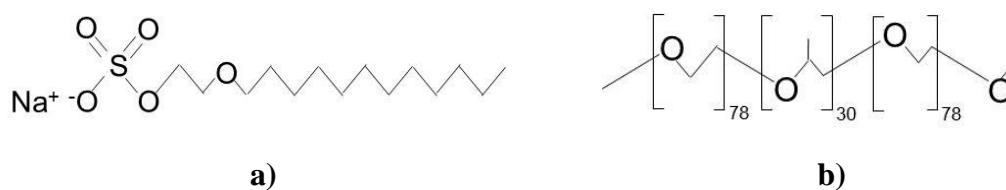


Figure 4.1: Schematic outlining molecular structure of **a)** SLES (1EO) and **b)** Pluronic F68.

4.2 Experimental Methods – Domain Size Analysis

The analysis of the emulsion domain size forms an essential part of investigations on formulation, process and equipment on emulsification. The domain size distribution affects emulsion quality, through improved emulsion effectiveness with small domains and tailored microstructures for a desired material texture and thickness. To determine the effect of emulsification strategy on product microstructure for manufactured emulsions, it is essential that we understand the method for domain size characterisation and the key domain size data, while limiting subjective data through measurement error that could distort our findings.

Considerations for Domain Size Measurement

The inconsistencies observed in domain sizing techniques are a consequence of an inappropriate method for domain size measurement, sample material characteristics, inappropriate sampling conditions, operator error and sampling repeatability (Kippax, 2005a). The most appropriate domain sizing technique for a specific sample must be selected when performing domain size analysis. The information of interest (length, surface area or volume) is a key consideration as the size measurements vary with type of analysis used. For example, microscopy may size a number of domains based on maximum or minimum length, leading to a number mean result (Rawle, 1993). This may not be suitable if a volume-based mean is required.

The sample material properties may determine the method for domain size measurement, for example, the validity of the results by image analysis software in microscopy measurements may not account for non-spherical domains and therefore this may not be a suitable technique. Further, the precision of measurements made depends on the difference in refractive index between the dispersed phase and the continuous phase, as this determines how well resolved the domain boundary is (Kippax, 2005a). Chromophores, such as pigments, present in the internal structure may absorb light during laser diffraction experiments, which may deem it an unsuitable method (Technical document 2).

Several common operator errors can cause discrepancies when analysing the domain size distribution of a select sample. The methods used when creating an emulsion should be rigorously critiqued to prevent the ingress of impurities into the sample. This includes the use of distilled, deionised or purified water in place of tap water; due to the presence of significant amounts of bacteria and particulates the results achieved may have an adverse effect on domain sizing. In addition, the mixing equipment used must be cleaned thoroughly to prevent the ingress of impurities during the mixing process. The sampling procedure used should also consider any possible risks of impurity ingress (Kippax, 2005a). The reliability of results should be improved through repeated experiments whilst maintaining experimental consistency. Dispersion, coalescence and agglomeration may occur after emulsion formation and should be considered (Leng and Calabrese, 2004; Kippax, 2005a). Further, the dispersion may occur when measuring the domain size distribution; this is the case in laser diffraction sample measurements, where samples may be subject to shear by methods where particulates are entrained in an air stream or where dispersions are added to a diluent of similar properties to the continuous phase (Kippax, 2005a).

Finally, consideration should be given to whether a measurement is representative of a sample; for example the number of domains examined by microscopy may be substantially less than for laser diffraction, therefore less representative of the sample population (Rawle, 1993). Furthermore, the chosen point of sample collection may consider whether the collected sample is representative of the process.

For experimental studies reported in Chapters 5 and 6, light scattering was the selected method for determining the domain size of analysed dispersions. The technique is well-established and is extensively used to characterise the domain size distributions of pharmaceutical, petrochemical and food products. The Mastersizer 2000 (Malvern Instruments Ltd, Malvern) was used for experimental studies. While many light scattering methods are available commercially, this instrument was selected due to equipment availability. The instrument uses laser diffraction or Low-Angle Laser Light Scattering (LALLS; Technical document 1) to determine the size of domains by interpreting measured scattering data, which is outlined in section

4.2.1. Additionally, the general protocol used to determine the domain size of processed dispersions is outlined in section 4.2.2. Furthermore, protocols for determining domain size of specific materials are provided in section 4.2.3, section 4.2.4 and section 4.2.5.

4.2.1 Laser Diffraction – Malvern™ Mastersizer 2000

The internal assembly of the laser diffraction instrument (described in Chapter 2, section 2.3.1) is similar in design to the Mastersizer 2000 (Malvern Instruments Ltd, Malvern), displayed in Figure 4.2. An emulsion sample is added to a diluent circulation stream of a similar composition to the sample continuous phase via a dispersion unit at “1,” which enters the optical bench assembly at “2,” via PVC tubing at “4.”

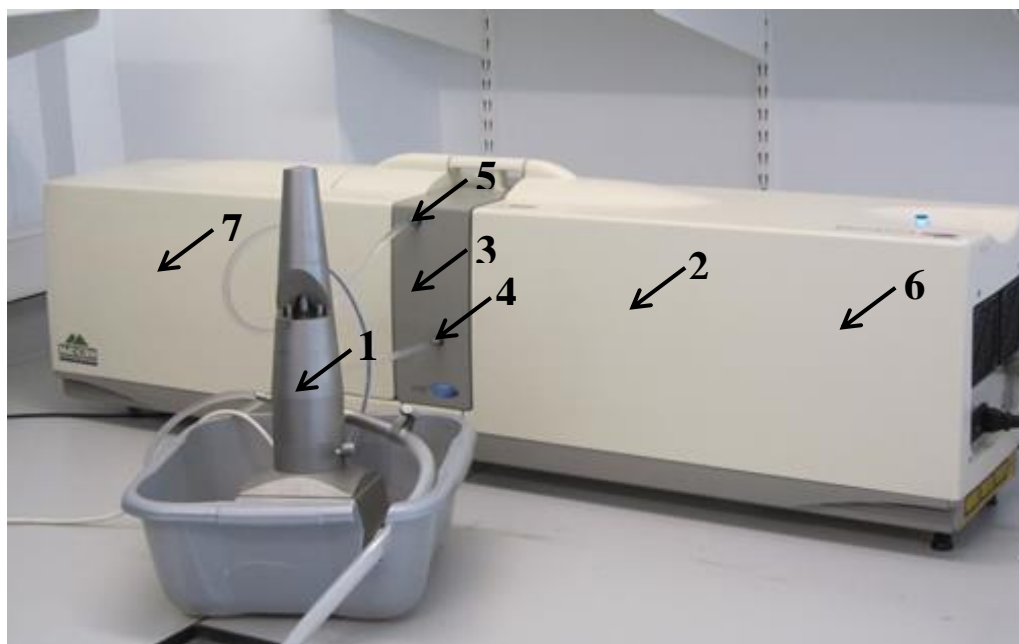


Figure 4.2: Schematic of the Mastersizer 2000 laser diffraction Instrument (Malvern Instruments Ltd, Malvern, comprising of dispersion unit (1), optical bench (2), sample cell enclosure (3), diluent fluid entry (4) and fluid exit (5). The laser source within the optical bench assembly at (6) and the “backscatter,” and “wide-angle,” detectors are located at (7).

The diluent and sample entering the optical bench assembly is directed toward the sample cell, encased within the sample cell enclosure at “3.” The light source, located at “6,” comprises of a He-Ne laser which provides a red light source of wavelength 633nm and a solid-state laser which provides a blue light source of wavelength 466nm. The latter light source improves the detection sensitivity of small droplets within the measured sample (Kippax, 2005b). Light is directed via a lens towards the sample cell; scattered light is detected by back-scattering and wide-angle detectors at “7.” The instrument is connected to a computer, where the operator is able to input commands via a software package that provides options to alter SOPs, input sample details, perform measurements and analyse the results of measurement.

4.2.2 General Protocol for Sample Measurement via Laser Diffraction

A general SOP was used for domain size measurements on the Mastersizer 2000. The material specific SOP instructions were created using the “Malvern Application 5.6,” software, installed on a Central Processing Unit (CPU) connected to the instrument. The SOP was adapted to include the optical properties of each material analysed for domain size. Details of the general protocol applied during domain size measurement are outlined in the Appendix (section AX2.1).

The general method for domain size measurements was performed as follows:

1. The instrument was turned on and left for 15 minutes, such that a steady temperature was reached.
2. The operator opened the “Malvern Application Software v5.6,” on the connected CPU and loaded the material-specific SOP.
3. The contents of the dispersion unit were emptied and replaced with clean distilled water. The detected laser strength was determined; if this was found to be below 78%, the dispersion unit contents were emptied and replaced with clean distilled water. If the laser strength remained below 78%, the sample cell was removed and cleaned using lens paper and surfactant

solution. The sample cell was rinsed with distilled water and re-installed in the optical bed.

4. On measurement, the operator followed the instructions provided on the Malvern Application Software, including the input of sample details. The sample, held in a 60ml polypropylene container with a lid, was turned over to promote sample uniformity. When instructed, the operator added a sample via a polypropylene pipette into the diluent stream and the measurement commenced. Care was taken to limit the obscuration to a maximum of 13%, to prevent the effects of inter-domain scattering.

The above protocol was tested using glass bead standards (Whitehouse Scientific Ltd, Chester, UK) of known particle size Results described in the Appendix (section AX2.2; table a)), indicate that measured samples were 5.376% higher in d_{50} compared to the listed size of the standards, which comprised a particle size range of 1 to 10 μm . Additionally, results described in table b) indicate that measured samples were 4.750% higher in d_{32} compared to the listed standard size, which comprised a mono-disperse size range of 0.2 μm .

4.2.3 Method for Sample Measurement – SFSO/Pluronic

Chapter 5 and Chapter 6 report experiments on the emulsification of SFSO/Pluronic compositions. The specific protocol for domain size measurement is described below:

Sample Preparation

The concentration of surfactant used during study was sufficiently high to prevent drop-drop coalescence on dilution. An aliquot of the sample was carefully extracted from the processed emulsion using a spatula and was diluted immediately in distilled water in a 60ml polypropylene container to an oil fraction below 2wt.%. The contents were gently stirred with a spatula to promote uniformity of the ingredients.

Sample Measurement

The SOP (described in section 4.2.2 and Appendix, section AX2.1) was altered for material characteristics and calculation model. The optical properties of the dispersed phase were selected from literature. A real refractive index (RI) of 1.47 (Asztalos et al., 2013) and an imaginary RI of 0.001 was selected for domains and a real RI of 1.33 was selected for the diluent. The calculation model settings were set to a general purpose Mie model, with a normal sensitivity and a spherical domain shape. Samples were measured for droplet size characteristics using a Malvern Mastersizer 2000 (Malvern Instruments Ltd, Malvern), as per the general method described in section 4.2.2.

4.2.4 Method for Sample Measurement – PJ/SLES

Chapter 6 describes experiments for emulsification of PJ/SLES compositions. The specific protocol for domain size measurement is described below:

Sample Preparation

In all experiments performed, the levels of surfactant present in the formulation were sufficiently high to prevent the droplet coalescence or emulsion destabilising on dilution. An aliquot of hot processed PJ/SLES emulsion (>60°C) was extracted by a spatula and immediately diluted in hot distilled water in a 60ml polypropylene container, to dispersed phase concentrations below 2wt.%. The contents were gently stirred with a spatula to promote uniformity of ingredients. Dilution in hot distilled water was essential in preventing freezing of the dispersion on dilution, however diluted samples were left to cool to ambient temperatures prior to measurement.

Sample Measurement

The SOP (described in section 4.2.2 and Appendix, section AX2.1) was altered for material characteristics and calculation model. Rowe et al. (2006) and Vishnupad et al. (1990) provide a RI range for PJ of 1.46 and 1.47 at 60°C, where the range in this RI is due to the mixture of hydrocarbons present. The optimal optical properties of the domains were determined by methods described in Technical document 2, by minimising the residual error between the predicted data and the measured data on the Mastersizer 2000 instrument. A selection of PJ/SLES dispersions were analysed;

the results are outlined in the Appendix, section AX2.3. Mean optical settings of measured samples were determined as 1.49 for the real RI and 0.003 for the imaginary RI; these results were higher than optical properties which were quoted by Vishnupad et al. (1990). As measurements were performed at ambient conditions, the RI of PJ may have been higher in a semi-solid state compared to a liquid state. Further, the optimal imaginary RI was found to be higher than was suggested for emulsions; again this was attributed to measurements made to domains in a semi-solid, translucent state. For individual samples considered, a difference of 5% was found for domain sizes determined at mean optical settings and optimal optical settings, for which the lowest residual error was found.

The calculation model settings were set to a general purpose Mie model, with a normal sensitivity and a non-spherical domain shape. Samples were measured for droplet size characteristics using a Malvern Mastersizer 2000 (Malvern Instruments Ltd, Malvern), as per the general method described in section 4.2.2.

4.2.5 Method for Sample Measurement - SFSO/NS

Chapter 5 describes experiments for emulsification of SFSO/NS compositions. The specific protocol for domain size measurement is described below:

Sample Preparation

An aliquot of the sample was carefully extracted from processed dispersions using a spatula and was diluted immediately in a 1wt.% SLES solution in a 60ml polypropylene container, to prevent the droplets coalescing or destabilising on dilution. The contents were gently stirred with a spatula to promote sample uniformity.

Sample Measurement

The SOP (described in section 4.2.2 and Appendix, section AX2.1) was altered for material characteristics and calculation model. The optical properties of the domains and diluent for measurement were selected from literature. A real RI of 1.47 (Asztalos et al., 2013) and an imaginary RI of 0.001 was selected for domains and a

real RI of 1.33 was selected for the diluent. The calculation model settings were set to a general purpose Mie model, with a normal sensitivity and a spherical domain shape. Samples were measured for droplet size characteristics using a Malvern Mastersizer 2000 (Malvern Instruments Ltd, Malvern), as per the general method described in section 4.2.2.

4.3 Experimental Methods – Emulsion Viscosity

For experiments described in Chapter 5, section 5.3.5, the viscosities of formed emulsions were studied to analyse emulsion microstructure. The methods used to characterise these emulsions are described below:

4.3.1 Emulsion Viscosity – Brookfield DV-II+ Viscometer

The equipment setup and experimental methods used for viscosity measurement are described here. Figure 4.3 describes the equipment setup of the Brookfield DV-II+ Pro Programmable Viscometer (Brookfield Instruments, Brookfield Engineering Laboratories, Inc., Massachusetts), which was used to determine the viscosity of processed emulsions.

The instrument setup comprises a main operating panel at “1,” and a moving arm at “2,” that oscillates between two extents of the Helipath Stand at “3,” as determined by the user. The use of the Helipath allows the spindle to pass axially through the sample, which ensures that the position measured in the sample changes with time. This is particularly useful for analysing structured materials that deform plastically with an applied shear, as a change in axial position ensures a “fresh,” sample is tested. The spindle assembly comprises of a shipping cap (4), spindle holder (5) and T-bar spindle (6) which provide the shear necessary for the viscosity measurement of the sample in the sample container, which must be large enough to prevent measurement error due to wall effects. Spindle connections are constructed from 300 series Stainless Steel (Technical document 3) and vary in geometry, including those of the vane, disk, cylinder and T-bar type. These connections can be chosen to measure samples of differing viscosities, sample sizes and measurement types. For the Brookfield viscometers which utilise the helipath stand, it is normal to use a T-

bar spindle geometry (Technical document 3). The user can operate the instrument in manual mode, via the operating panel, or in external mode via a CPU (7), which has been installed with Rheocalc32 software (described in Technical document 4). The program allows the operator to create a measurement protocol for analysis, including selected spindle speeds and total measurement time. It also provides information on measured torque, monitor apparent viscosity and temperature during measurement.



Figure 4.3: Schematic describing the equipment setup for the Brookfield DV-II Pro Extra Viscometer, consisting of an operating panel (1), a moving arm (2), a helipath stand (3), a shipping cap (4), a spindle holder (5), a T-bar spindle (6) and a CPU (7).

4.3.2 Method for Sample Viscosity Measurement

For experiments described in Chapter 5, processed dispersions were measured for apparent viscosity using a Brookfield DV-II+ Pro Programmable Viscometer (Brookfield Instruments, Brookfield Engineering Laboratories, Inc., Massachusetts). A T-D type spindle, which provided the required range of measured viscosities, was

installed and programmed to a set rotational speed of 10 RPM. Measurements were performed at temperatures of 20 \pm 1°C. The height of the moving arm was altered to position the spindle above the emulsion sample container, which was allowed to descend into the emulsion prior to measurement. Due to the shear-sensitive nature of the processed emulsions, measurements were limited to one descent and an average viscosity was taken \pm 20 seconds between the top and bottom of the sample.

The method was tested against silicone oil standards of known viscosity at 25 \pm 1°C. The results of measurements on 10000cSt samples (provided in Appendix, section AX2.4) were determined as 11.19% above the listed viscosity. Additionally, the results of 60000cSt sample measurements (provided in Appendix, section AX2.5) indicated that measured samples were only 0.992% higher than the listed standard viscosity. This suggested that the SFSSO/NS emulsions measured using this protocol may be higher than actual values. However, measurements were more accurate at higher sample viscosities.

4.4 Experimental Methods – Data and Error Analysis

The approaches for error analysis applied in the studies are described here. Table 4.1 lists the names and equations for the calculation of key statistical functions applied in the analysis of experimental results, described in Chapter 5 and Chapter 6.

For experiments where repeat samples are obtained at a particular x-variable, such as mixing duration, a mean result has been listed and error bars applied to indicate the standard error of results from the said mean. Additionally, individual results obtained at alternative x-variables are generally considered to be separate to other results. However, a line of fit may be applied to indicate the trajectory of the results. Occasionally, results obtained at similar formulation or process conditions are grouped for analysis. In these instances, the mean and range of the common variable that results have been grouped under is made clear. For clarity, the extent of the listed range equates to the maximum and minimum values of common variables, observed for grouped results.

Finally, it was necessary in some instances to apply error bars to results by determining the experimental error from measurement. This is made clear for relevant results, where the experimental error is indicated by error bars and considered by the accumulation of errors, as determined by Equation 4.1. Typically experimental errors include axial and radial variations in coarse pre-mix droplet diameter and variations in measured domain sizes of sample emulsions.

Table 4.1: Summary of error analysis functions applied to experimental studies.

Mean (\bar{x})	$\bar{x} = \frac{\sum x}{n_x}$
Standard deviation (SD)	$SD = \sqrt{\frac{\sum(x-\bar{x})^2}{n_x}}$
Percent standard deviation (% SD)	$\% SD = \frac{SD}{\bar{x}} \times 100$
Standard error (SE)	$SE = \frac{SD}{\sqrt{n_x}}$
Percent standard error (% SE)	$\% SE = \frac{SE}{\bar{x}} \times 100$

$$EE = \sqrt{EE_1^2 + EE_2^2 + \dots} \quad (4.1)$$

The above analysis has been applied to determine errors in sample measurement. The results of ten repeat measurements on a processed SFSO/NS sample, performed as per methods described in section 4.2.2 and 4.2.5, is provided in Appendix, section AX2.6, Table a). For sample d_{32} , a %SD of 8.395% and a %SE of 2.665% was determined. Similarly, for sample d_{43} an %SD of 3.059 and %SE of 0.967% was determined. Additionally, the results of ten repeat measurements on a processed PJ/SLES sample, performed as per methods described in section 4.2.2 and 4.2.4, is provided in Appendix, section AX2.6, Table b). For sample d_{32} , a %SD of 1.571% and %SE of 0.497% was determined. Similarly, for sample d_{43} , a %SD of 9.446% and %SE of 2.987% was determined. Furthermore, the results of three repeat

measurements on a processed SFSO/Pluronic emulsions, performed as per methods described in section 4.2.2 and 4.2.2, is provided in Appendix, section AX2.6, Table c). Similarly, for sample d₄₃, a %SD of 0.466% and %SE of 0.008% was determined. Finally, the results of repeat viscosity measurements for a processed SFSO/NS sample is provided in Appendix, section AX2.7. For 10 measurements performed as per the method described in section 4.3.2, a % SD of 8.848 and a % SE of 2.798% was determined.

4.5 Emulsification Apparatus - Overhead Mixers

Overhead Mixers were used to prepare pre-mixes for experimental studies reported in Chapter 5 and Chapter 6. This was the preferred approach for emulsification studies on the Bench-scale CDDM and Laboratory-scale CDDM, as it allowed processing of emulsions with accurate compositions and high dispersed phase concentrations. Images and the key design characteristics of the overhead mixers used during experimental studies are summarised in the Appendix, section AX2.8, with information sourced from Technical document 5 and Technical document 6. The equipment allows for installation of mixer attachments of varying design, which could be selected and attached by a “chuck and key,” to meet the requirements of a desired mixing approach. Overhead mixer attachments were selected on an ad-hoc basis, where selected mixer head designs were considered against criteria such as batch size, fluid viscosity and the responsiveness of the formulation to shear. For this reason, the geometry and size of the mixer head was a consideration which affected the amount of shear delivered to a system and allowed effective distribution of fluid. The types and design criteria of mixer heads used during these studies are described in the Appendix, section AX2.9.

4.5.1 Coarse Pre-mix Formation

Emulsification experiments described in Chapters 5 and 6 utilised coarse pre-mixes comprising SFSO/Pluronic, SFSO/NS and PJ/SLES compositions. Pre-mixes were formed using an IKA™ overhead mixer (IKA-Werke GmbH & Co. KG, Staufen, Germany) installed with a 4-blade paddle attachment. For SFSO/Pluronic and SFSO/NS compositions, emulsions were formed by a “concentrating-up,” approach,

where quantities of SFISO were weighed out using a mass balance of accuracy $\pm 0.01\text{g}$ and a desired amount of Pluronic/NS solution of desired concentration was added to a mixing vessel. Subsequently, aliquots of SFISO were added slowly to the vessel at mixer speeds of between 0 and 1000 RPM. Care was taken to limit the rate of oil addition, such that the oil was uniformly distributed within the pre-mix. Further, pre-mix was periodically hand-mixed to improve distribution of the ingredients. For PJ/SLES compositions, the required quantities of each ingredient were weighed out using a mass balance with an accuracy of $\pm 0.01\text{g}$ and added to a heating vessel. The contents were covered and raised to a temperature above 65°C . On reaching temperatures above 65°C , the ingredients were blended using an IKA overhead mixer (IKA-Werke GmbH & Co. KG, Staufen, Germany) with a propeller-type attachment at mixer speeds of 1000 RPM. The pre-mix was periodically hand-mixed to improve axial and radial distribution of the ingredients.

On addition of coarse pre-mixes to the Bench-scale and Laboratory-scale CDDM feed vessels, pre-mixes were overturned to promote chemical uniformity. While this was not measured, variations in chemical uniformity would result in changes in droplet size during processing. Therefore, an indication of consistency is provided by size characteristics of emulsions measured via laser diffraction techniques (described in section 4.2.2, section 4.2.3, section 4.2.4 and section 4.2.5). The uniformity of coarse pre-mix droplet size with axial and radial position in the preparation container is provided in the Appendix, for compositions comprising SFISO/Pluronic (Appendix, section AX2.10, Appendix, section AX2.11), SFISO/NS (Appendix, section AX2.11) and PJ/SLES (Appendix, section AX2.12 and section AX2.13).

4.6 Emulsification Apparatus - CDDM

As described in section 2.6.3, the key benefit of CDDM technology is the flexibility to alter the axial position of the stator relative to the rotor; this allows optimisation of emulsification processes by controlling the degree and duration of extensional shear delivered to the fluid. The CDDM geometry was altered for studies reported in Chapter 5 and Chapter 6.

Figure 4.4 provides guidance on described geometries:

- Geometries described with a positive axial displacement (Figure 4.4a) relate to positions where axially displaced lands are not overlapping.
- Geometries described with a zero axial displacement (Figure 4.4b) relate to positions where axially displaced lands are at the point of overlapping.
- Geometries described with a zero axial displacement (Figure 4.4c) relate to positions where axially displaced lands are overlapping.

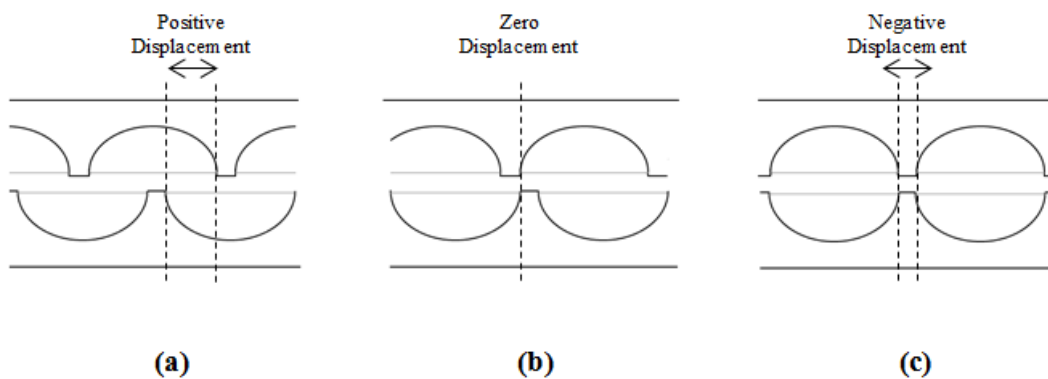


Figure 4.4: Schematic of the CDDM geometries nomenclature, where **(a)** a positive displacement refers to axial distances between lands that are not confronting; **(b)** a zero displacement which describes the point where landed sections are at the point of meeting and; **(c)** a negative displacement refers to axial displacements where land sections overlap.

The value of axial displacement is indicative of the spacing between axially displaced lands on the rotor and stator surfaces. For instance, a mixer comprising a +1.35mm geometry represents a distance of 1.35mm between axially displaced lands on the rotor and stator surfaces, which are not confronting. The axial position was displaced using metal shims, whose thickness was measured to an accuracy of +/- 0.1mm.

The basis for this research study centres on emulsification in cavity-design mixers and many of the studies performed in this thesis involve the CDDM technology. This section provides an overview of design and operation of the Bench-scale CDDM and Laboratory-scale CDDM systems used during the studies (described in Chapter 5 and Chapter 6).

4.6.1 Bench-scale CDDM System

The CDDM Bench-scale System (displayed in Figure 4.5 and Figure 4.6) was applied to process coarse pre-mixes in experiments reported in Chapter 5. Details of equipment assembly and methods for emulsification studies are outlined here.

With reference to Figure 4.5, raw materials and coarse pre-mix emulsions were provided to Progressive Cavity Pumps (PCP; Mono Pumps Ltd, Manchester, UK) located at “3,” and “4,” each driven by 0.55kW motors (WEG Electric Motors Ltd, Redditch, UK) via 2 litre and 5 litre vessels at “1,” and “2,” which were connected by “quick release couplings.” For experiments described in Chapter 5 (section 5.3.2, section 5.3.3, section 5.3.4 and section 5.3.5), the PCP speeds were calibrated against flowrates of feed materials. This was necessary as effective control of the streams ratio was required for study. The method for calibration involved disconnecting the pipework between the PCP and the gear pump and determining the mass of material discharged from the PCP over a measured time. On commencing experiments, the PCP and gear pump (typically set to 10% of the total capacity) were switched on, which allowed material to pass through the ancillary equipment toward the mixer assembly. The gear pump speed setting was optimised such that the pressure upstream of the gear pump was 0 barG. This was important for the in-line emulsification studies, as it allowed effective proportioning of stream flowrates from each PCP. Once a steady flow had developed and the mixer had been “ramped up,” to the required speed, the emulsion sample was collected in a 180ml polypropylene container and the output flowrate was determined by measuring the mass of sample collected at the outlet over a given time period. The gear pump at “5,” has two objectives. Firstly, the speed is set via a potentiometer such that the feed pipework upstream of the gear pump has a net pressure of zero; this is to prevent the cavity pumps delivering fluid against a head of pressure (indicated by pressure gauges “6,” and “7,”) ensuring that each pump delivers raw material at a target ratio.

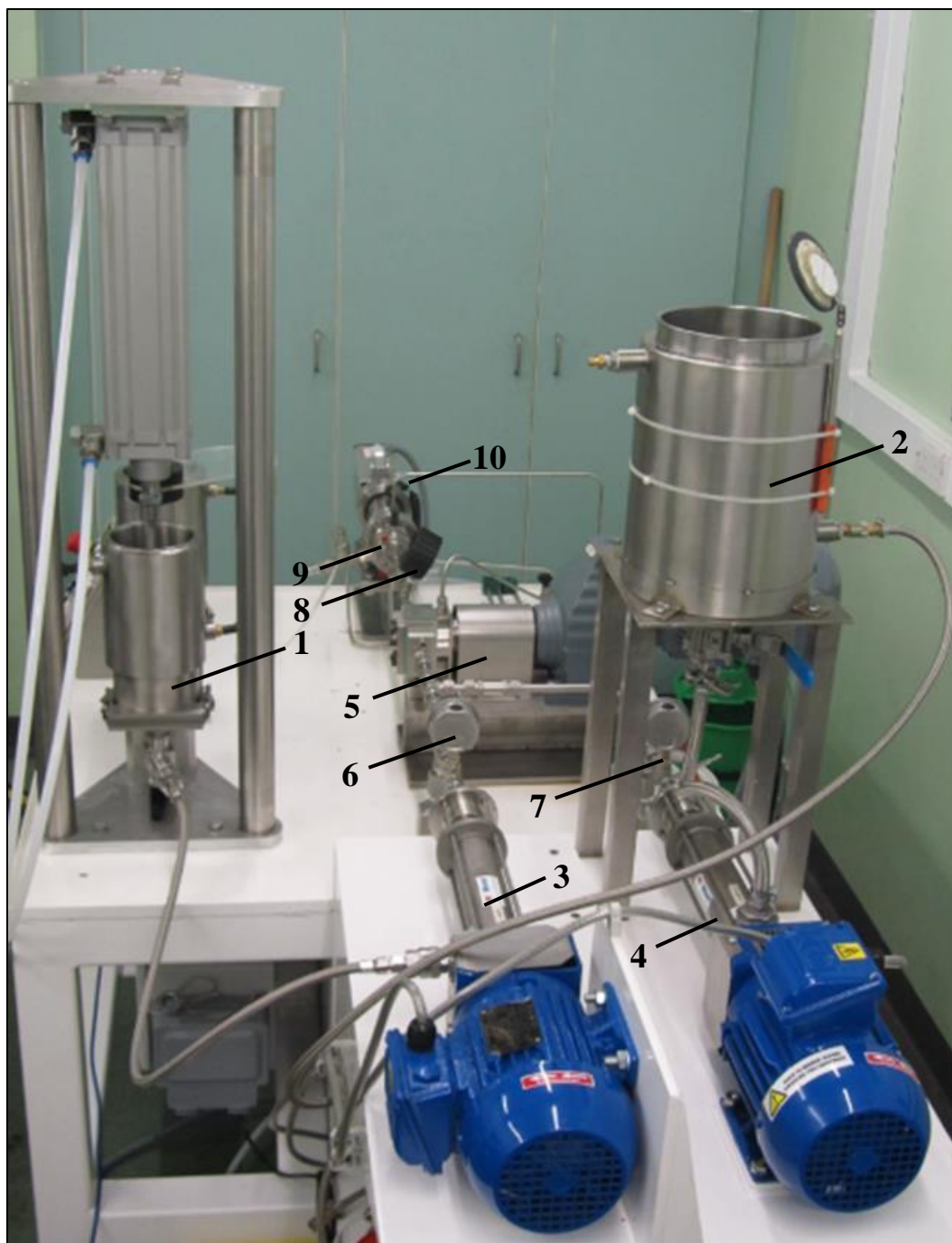


Figure 4.5: Image showing the Bench-scale CDDM System and ancillary equipment, consisting of 2 litre and 5 litre vessels at “1,” and “2,” PCPs at “3,” and “4,” a gear pump at “5,” pressure gauges at “6,” “7,” and “8,” the CDDM mixer at “9,” and cooling water feed at “10.”

Secondly, the gear pump should provide sufficient flow to overcome the resistance of the remaining pipework and mixer components. The speed of the gear pump is set via an ABB™ ACS355 inverter drive (ABB Group, Zurich, Switzerland) which

restricts the supply of current to between 0 and 100%. A pressure transmitter and the CDDM are located at “8,” and “9,” respectively. The pump and mixer sections are cooled using a mains-water cooling feed at “10.” On exiting the PCP, the material feeds merge and are directed to a gear pump with a 2.2kW motor (SEW-EURODRIVE Ltd, Normanton, UK). A non-return valve is located on each feed stream to prevent back-flow of material to the PCP. The output volumetric flowrate of raw material delivered by each PCP was controlled by ABB™ ACS355 inverter drives (ABB Group, Zurich, Switzerland), which restricted the supply of current to between 4-20 amps.

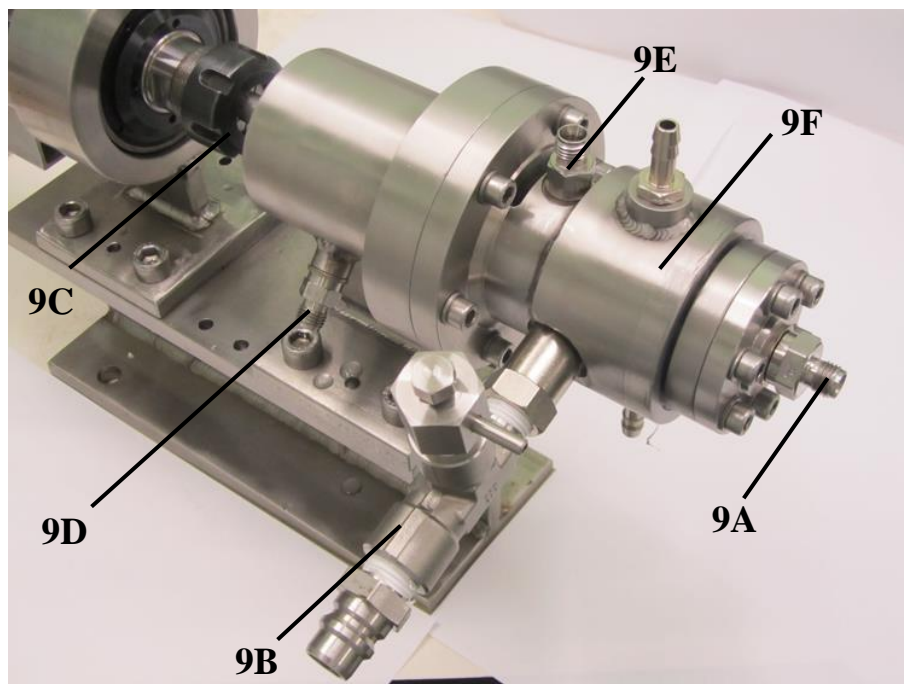


Figure 4.6: Bench-scale CDDM System comprising material entry point at “9A,” a material exit point at “9B,” rotor shaft at “9C,” mixer bearings at “9D,” water flush at “9E,” and a heater jacket at “9F.”

Figure 4.6 presents a disconnected CDDM assembly. Material supplied from the gear pump enters the mixer at “9A,” which sits along the direction of flow, and exits in a direction perpendicular to the mixer at “9B.” The axial position of the mixer can be altered by introducing “shims,” which alter the position of the stator relative to the rotor. The rotor is secured to a rotor shaft at “9C,” where the speed of rotation is

controlled by an inverter drive which restricts the current supplied to the motor. Cooling water is supplied to prevent overheating of the motor bearings at “9D,” and a water flush is supplied at “9E,” to flush the material that may enter the mixer seal. A heating or cooling jacket is located at “9F.” Table 4.1 provides the nominal operating limits for the Bench-scale CDDM apparatus.

Table 4.1: Summary of the operating limits for the Bench-scale CDDM apparatus.

Equipment Operating Limits	
Throughput range (litres/hr) :	5 to 50
Viscosity range (cP) :	1 to 100000
Maximum operating pressure (Bar) :	200
Maximum operating temperature (°C) :	120
Rotational Speed Range (RPM) :	0 to 15000

Figure 4.7 presents the CDDM assembly and downstream ancillary equipment. The CDDM is located at “1,” and the motor located at “2.” Material exits the mixer and is fed to a 2 litre storage vessel at “3.” Both the 2 litre feed vessel and the sample collection vessel are connected on a swivel and are interchangeable. Therefore, the arrangement can be easily manipulated such that material collected in the storage vessel may be positioned in place of the feed vessel.

This facility enables the collected sample to be re-processed through the apparatus. The control panel at “4,” comprises of three “ten-turn,” potentiometers at “5,” that are positioned here to control the pump speeds and an inverter display interface at “6,” which allows control of the mixer speed. Operations performed on the Bench-scale CDDM were recorded by a data-acquisition system comprising of hardware from Measurement Computing 1608B and TracerDAQ Pro software (Measurement Computing, Norton, USA). Mixer and pump speed were recorded during each experiment across the Bench-scale CDDM, which were measured and checked using tachometers.



Figure 4.7: Image of the Bench-scale CDDM System Assembly and Downstream Ancillary Equipment. The numbers are explained in the text.

In summary, the Bench-scale CDDM system is a versatile experimental device that allows the processing of a wide range of fluids and provides effective means of testing formulation, process and equipment specific parameters for emulsification.

4.6.2 Laboratory-scale CDDM System

The Laboratory-Scale CDDM system has been extensively applied during the research studies described in Chapter 5 and Chapter 6. The equipment layout for the system is displayed in Figure 4.8. The equipment setup is comprised of five material feed streams that deliver material independently to the centrally located CDDM. Four of the streams use medium size piston pumps that deliver maximum throughputs of up to 72 litres/hour and one of the streams delivers throughputs of up to 288 litres/hr.



Figure 4.8: Image displaying the CDDM Laboratory system, comprising of 5 feed streams to the central mixer assembly, consisting of a motor, mixing housing and CDDM.



Figure 4.9: The control room featuring a HMI at “1,” a monitoring PC at “2,” and video feeds of mixer facility at “3.”

The system is operated from a central control room, described in Figure 4.9, which includes a Human Machine Interface (HMI) connected to a Program Logic Controller (PLC), where the user is able to select operating conditions. A connected monitoring Personal Computer (PC) provides live information and data-logging of processing variables such as displaced volume, material throughput, mixer speed and heating control, which may be viewed and recorded. Additionally, two monitoring screens provide a live feed of the facility in operation.

With reference to Figure 4.10, details of equipment assembly and methods for equipment operation are described below:

1. Raw materials, in the form of coarse emulsion pre-mixes, were loaded into a 10 litre hopper at “1,” which was pressurised to ensure effective feeding of material into the system. The preparation of course pre-mixes prepared for study are described in section 4.5.2.
2. The mixer operations were controlled via a PLC interface, which allowed the operator to set the required throughput and mixer speed for study.
3. On commencing experiments, material was drawn from the feed hopper to a piston pump at “3,” via a check valve at “2,” (Harwood Engineering Inc., Walpole). The amount of material drawn into the piston pump (i.e. the shot volume), was set by the operator at the HMI.
4. Material was discharged from the piston through a high pressure pipeline at an input volumetric throughput. This was achieved by controlling the axial displacement of the cylindrical zirconia ram. On discharge, the check valve at “3,” prevented fluid from re-entering the feed vessels. Three pumps provided the hydraulic fluid needed to ensure sufficient pressure was generated to deliver the required throughput.
5. 600-700ml of coarse emulsion pre-mix was discharged from the piston pump and directed towards the mixer assembly at “4,” which encased the CDDM. The mixer was initiated once the piston pump began dispensing fluid, and 140 ml of emulsion was allowed to pass prior to sample collection, to ensure that the mixer had reached a steady speed. The throughput from each measurement was determined from the average rate of axial displacement of the piston pump during shot delivery.

6. The coarse pre-mix was driven toward the mixer assembly, which comprised of a bottom section secured to the ground and encased the CDDM stator. The top section included the motor at “5,” (Dynomax Inc., Wheeling, USA) to which the CDDM rotor was attached. The top section was set down on the top of the base section, such that the rotor was positioned within the stator. Each section was separated by “shims,” the thickness of which was adjusted to alter the relative position of the stator and rotor. Fluid entered at the top of the mixer at right-angles to the mixer position. It was then driven between the rotor and stator and directed toward the outlet at the mixer base. The rotor was attached to the motor drive shaft, which was capable of generating mixer speeds up to 20000 RPM. Cooling water was supplied to the motor bearings to prevent any overheating. Samples were collected at the mixer output using a 180ml polypropylene sample container.

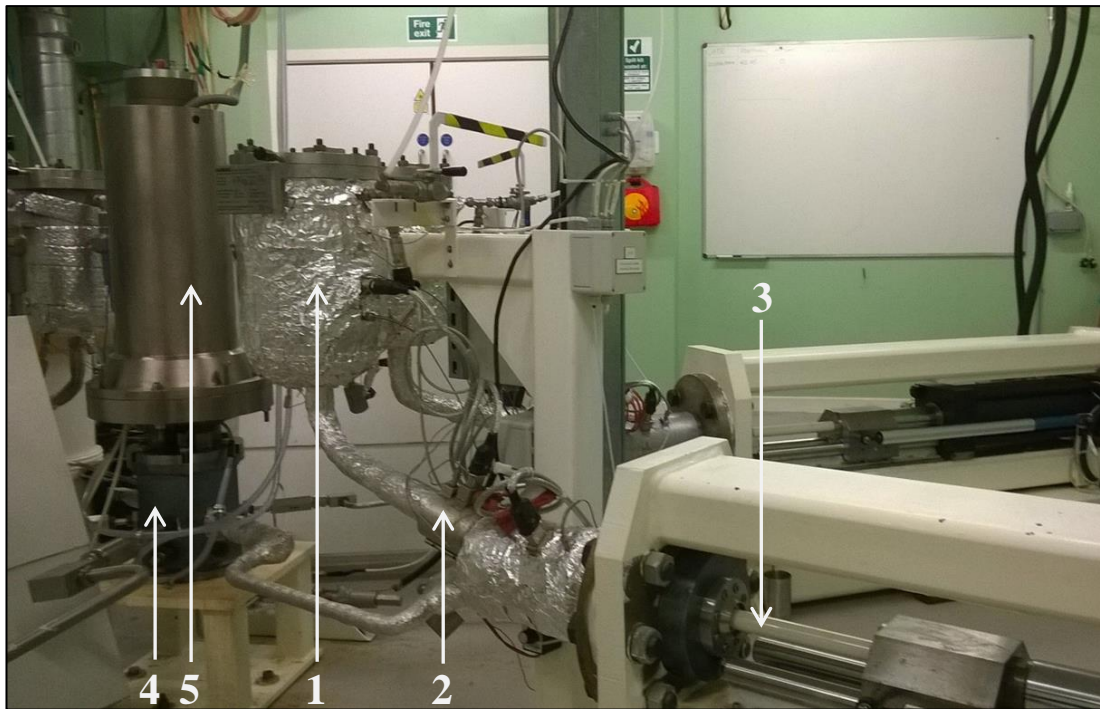


Figure 4.10: Image of major components of the inlet feeds for the CDDM Laboratory System including the feed hopper at “1,” check valve at “2,” dosing pump at “3,” CDDM mixer assembly at “4,” and motor at “5”.

Table 4.2: Table describing the nominal operating limits for the Laboratory-scale CDDM and ancillary equipment.

Equipment Operating Limits	
Throughput range – medium scale piston pump (litres/hr)	0 to 72
Throughput range – large scale piston pump (litres/hr)	0 to 288
Maximum operating pressure (Bar)	350 barG
Maximum operating temperature (°C)	200 °C
Mixer Speed Range (RPM) maximum / minimum	0 - 20000
Motor Maximum Torque (Nm)	34

Details of the nominal operating limits for the Laboratory-scale CDDM is provided in Table 4.2. Both the Laboratory-scale CDDM and the Bench-scale CDDM are similar in design. However, the Laboratory-scale CDDM comprises of rotor diameters, rotor-stator radial clearances, cavity lengths and depths which are twice the size of the Bench-scale CDDM dimensions. There are a number of notable differences between the two apparatus. Firstly, the means by which fluid enters and exits the mixer is different. For the Laboratory-scale CDDM, fluid enters at a direction perpendicular to the axial dimension of the mixer. Therefore, a long cavity section is employed to facilitate the blending of inlet streams. Whereas, fluid entering the Bench-scale CDDM enters along the axial dimension and exits radially from the mixer. Furthermore, the means by which material is delivered to the mixing assemblies differs between systems. For the Laboratory-scale CDDM, the use of piston pumps allows for delivery of fluids of high viscosity. However, the Bench-scale CDDM system relies on the suction power of the PCPs to draw material. Both machines require material specific calibration and adjustments in settings for processed materials whose microstructure may change during mixing. However, the Bench-scale CDDM design provides a better consistency in flow and can more readily achieve steady state conditions. It is noted that each system will favour certain experimental objectives. Therefore, the use of each should be considered on an ad-hoc basis.

4.7 Emulsification Apparatus - FDM

The FDM (described in section 2.6.2) is a high shear cavity-design mixer comprising of an internal rotor and external stator. Table 4.3 summarises the design characteristics and operating parameters associated with FDM and Figure 4.11 outlines the mixer's assembly. Figure 4.11 a) shows the mixer head stator at "1," which was held in position by two supporting rods at "2." The rotor section was secured to a rotor shaft at "3," and attached to an overhead motor at "4," (ABB motors). The motor electric supply was provided via an inverter, which controlled the motor speed by limiting the input of current to between 0-100%. A water feed connected to the mains supply was fed to a cooling jacket around the bearing housing, in order to limit any heat rising from friction on the bearings.

Table 4.3: Summary of key design criteria and operating limits of the FDM.

Design Criteria (Cavity Rows)	Cavity Row 1	Cavity Row 2	Cavity Row 3	Cavity Row 4
Number of Cavities on Rotor/Stator	14/14	11 / 11	8 / 8	5 / 5
Cavity Row Height (mm +/- 1) of Rotor/Stator	5/5	5/5	5/5	5/5
Mean Cavity Diameter (mm +/-1) of Rotor/Stator	10/10	10/10	10/10	10/10
Maximum Row Diameter (mm +/-1) of Rotor/Stator	61/49	51/39	40/30	30/20
Minimum Row Diameter (mm +/-1) of Rotor/Stator	50/39	40/30	30/20	20/9

The mixing operation was performed as follows. With reference to Figure 4.11 b), the bulk fluid was drawn into the base of the mixer head (conical in shape) and entered the internal mixer geometry (see Figure 4.11 c)). The rotor and the stator surfaces both comprised of five rows of overlapping cavities that were semi-hemispherical in shape and aligned perpendicular to the direction of bulk flow. The rate at which fluid was drawn through the mixer, indicative of the level of shear, was

determined by the rotor speed. The fluid was discharged radially from the mixer head, between the top of the mixer configuration and the upper stator housing. It is argued that this action provides elements of dispersive mixing to the exiting fluid.

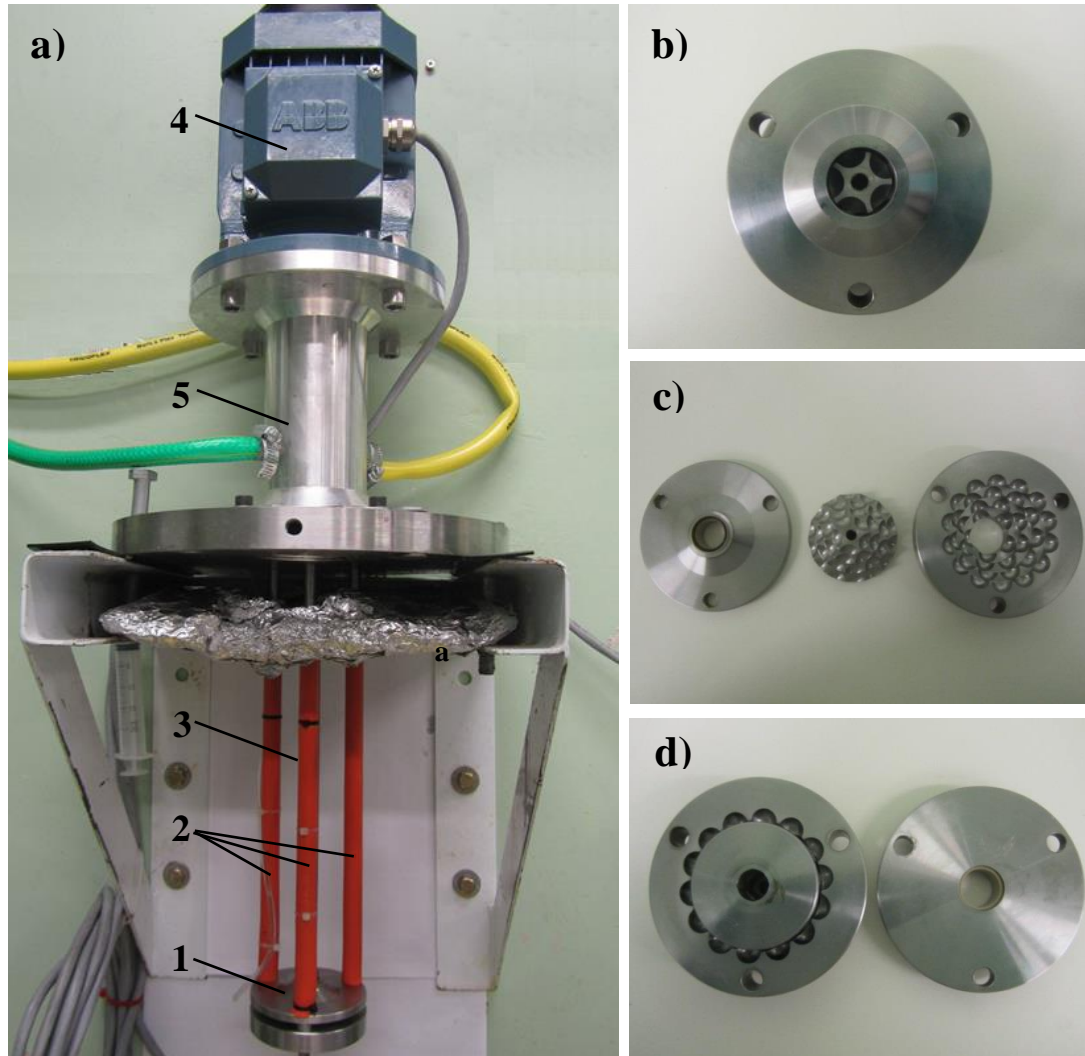


Figure 4.11: Image displaying parts of the FDM geometry **a)** mixer assembly **b)** mixer inlet **c)** dismantled assembly of rotor and stator components **d)** outlet from mixer head with upper stator housing.

4.8 Emulsification Apparatus - Formax™ Platform

The Formax™ (Chemspeed Technologies AG, Augst, Switzerland) is a high throughput robotic platform capable of performing 12 mixing operations simultaneously. The device is able to provide accurate temperature control to mixing

operations through: 1) the automated hot transfer and accurate addition of a material into each mixing vessel using the robotic arm and heater dispersion cylinders; 2) the automated execution of experimental operations at stated times based on a programmed set of instructions and; 3) a variable speed mixing control. Figure 4.12 provides a schematic of the Formax™ Platform, positioned at (0, 0) coordinates. It comprises of:

- A robotic arm located at “1,” was used to perform operations, such as collection of the dispensing unit and heated dispersion cartridges and ingredient transport.
- 100ml reactor vessels located at “2,” were installed with impellers of dissolver-disk design or rotor-stator, where the latter comprises a four-bladed impeller within a toothed stator. A gear motor at the base of the vessel provided the torque necessary for mixing operations. Further, close-fitting rotating baffles were installed to promote distribution of the ingredients. The vessels are designed with heating and cooling capabilities with a sensitivity of 0.385 ohms/°C.
- Standard and “high-viscosity,” gravimetric dispensing units with a bolt-on mass balance, located at “3,” were connected to the robotic arm for controlled collection and the delivery of quantities of ingredients to mixing vessels.
- A CPU located at “4,” allowed for instructions on equipment operation and experimental protocols to be programmed by the operator.
- The location of raw materials at “5,” for collection by the robotic arm and transfer to the mixing vessel, located at “2.”
- Heated dispersion cartridges were located at “6,” with options to select a standard nominal bore needle for low viscosity fluid transfer or a higher nominal bore needle for viscous fluid transfer.

At the time of study, the device was located in the Centre for Materials Discovery (Department of Chemistry, University of Liverpool, Liverpool) and was accessed with permission. For experimental studies described in Chapter 6, section 6.3.1, the Formax™ was applied with the aim of determining the formulation-process rules for emulsification of PJ/SLES compositions, through the controlled addition of one coarse pre-mix to another.

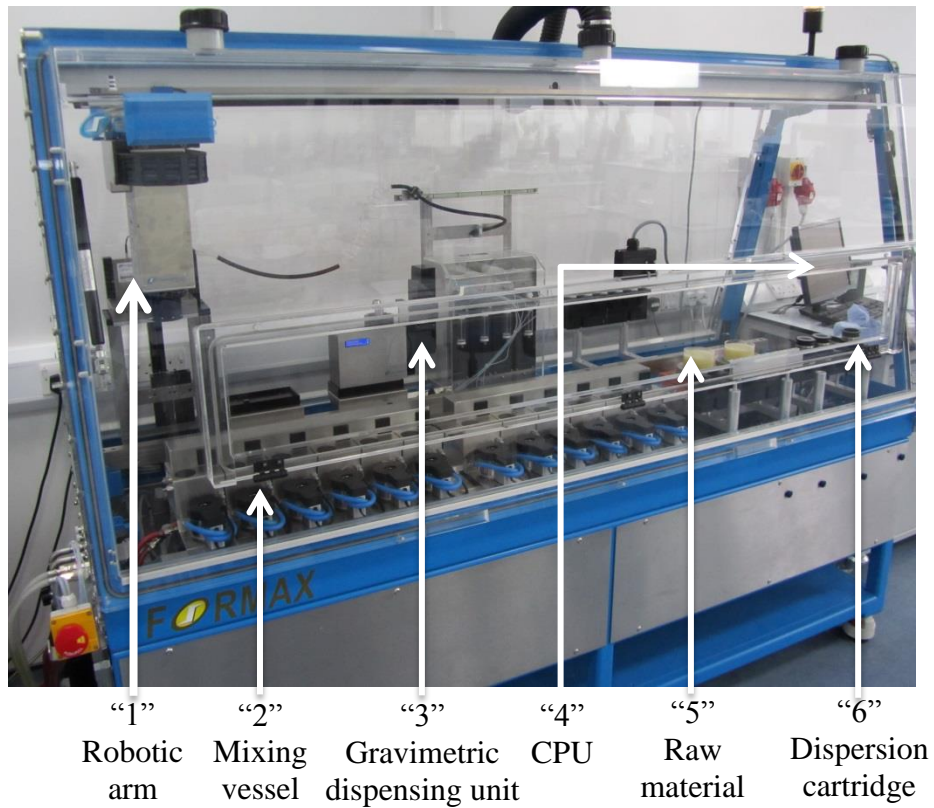


Figure 4.12: Schematic of the Formax™ Platform at (0, 0) coordinates, showing positions of the robotic arm at “1,” the 100ml mixing vessel at “2,” the gravimetric dispensing units at “3,” the CPU at “4,” the location of raw material for transfer at “5,” and the 60 ml dispersion cartridge at “6.”

Figure 4.13 shows the experimental procedure used during studies reported in Chapter 6, section 6.3.1 and provides further insight on the Formax™ operation. From its initial position at Figure 4.13 a), the robotic arm moved toward the (0, 0) coordinate position (as described in Figure 4.13 b)), which provided a reference point for its navigation to other locations within the equipment.

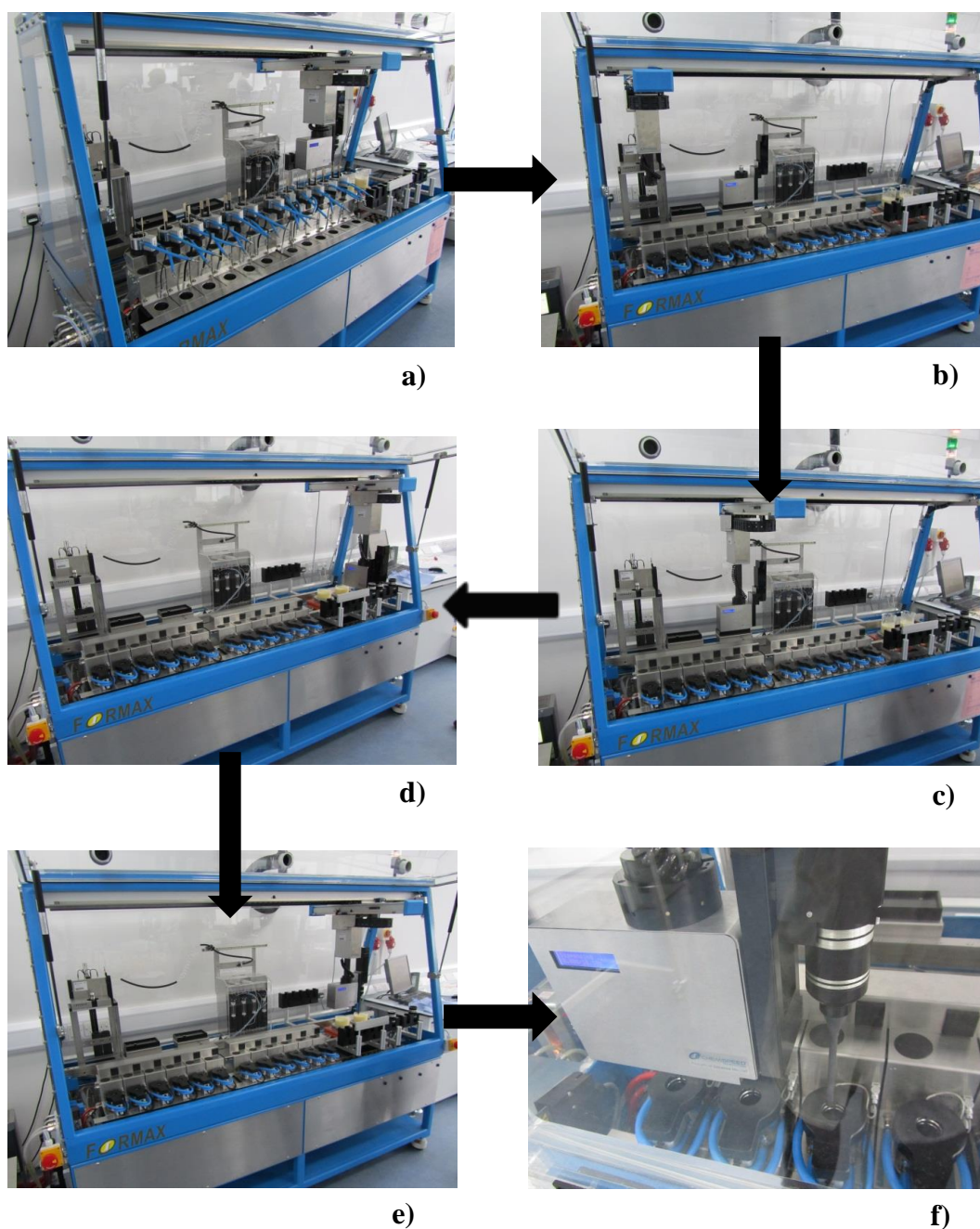


Figure 4.13: The automated transfer of “pre-mix b,” to respective vessels. **a)** Initial position of equipment position; **b)** transfer of robotic arm to zero co-ordinate; **c)** collection of the gravimetric dispensing unit; **d)** collection of heated dispersion cartridge; **e)** collection of “pre-mix b,” and; **f)** delivery of “pre-mix b,” to nominated vessel.

As per the programmed instructions, the robotic arm collected the bolt-on mass balance (Figure 4.13 c)) and proceeded to collect a heated dispersion cartridge (Figure 4.13 d)), where the temperature of each heater cartridge corresponded to the temperature of the “pre-mix b,” container. This was to prevent freezing of the material within the cartridge. The robotic arm with the attached mass balance and heated dispersion cartridge was then positioned above one of the “pre-mix b,” containers, where a sufficient amount of the pre-mix was extracted (Figure 4.13 e). The required aliquot of material was then delivered to the mixing vessel. Following the combining of pre-mixes, mixing was implemented for a further 30 minutes at the set temperature.

Chapter 5: Manufacturing Strategies for Emulsion Systems, Stabilised by Non-ionic Surfactants

5.1 Summary

This chapter reports investigations of process-equipment strategies for efficient emulsion manufacture on the Controlled Deformation Dynamic Mixer (CDDM). Strategies incorporated methods for developing of mixing regimes, increased shear duration and in-line emulsion formation for emulsification of a model O/W system, comprising Sunflower Oil (SFSO) stabilised by a fast-absorbing synthetic surfactant non-ionic triblock copolymer (Pluronic F68). The applied strategies were found to improve emulsification efficiency.

These process-equipment strategies were extended to another model O/W emulsion, comprising SFSO stabilised by a slow-absorbing protein and phospholipid based natural surfactant (NS). The applied strategies again improved emulsification efficiency but were less effective in comparison to emulsification of SFSO/Pluronic systems.

5.2 Materials and Methods

5.2.1 Materials

For the majority of experimental studies described in the current chapter, a model emulsion system comprising of SFSO and a synthetic non-ionic surfactant Pluronic (Carbosynth Ltd, Compton, UK) was used. A number of experimental studies for O/W SFSO/Pluronic emulsions were extended to O/W emulsions comprising SFSO/NS, where the surfactant comprised of a mix of phospholipids, lecithin and

proteins. The experiments aimed to validate the findings of emulsification strategies for emulsions stabilised with fast-absorbing surfactants (Pluronic) with emulsions stabilised with slow-absorbing (NS) surfactants. The properties of each are described and methods for preparing Pluronic and NS solutions are described in Chapter 4 (section 4.1).

5.2.2 Emulsification Equipment - Laboratory-scale CDDM

Several experiments, described in section 5.3.1, were performed on SFSO/Pluronic compositions, processed on the Laboratory-scale CDDM (Maelstrom APT Ltd, Glossop, United Kingdom) at target Q, N and mixer geometries. The studies involved the post-processing of coarse emulsion pre-mixes, prepared by methods described in Chapter 4 (section 4.5.1) and processed on the Laboratory-scale CDDM, as described in Chapter 4 (section 4.6.2). This approach was used to improve the accuracy of formulation studies, as compositions could be combined offline in accurate quantities instead of relying on the correct ratio of syringe pump delivery rates. Collected samples were analysed for domain size characteristics using the Malvern Mastersizer 2000, applying the protocol for measurement described in Chapter 4 (section 4.2.2 and section 4.2.3).

5.2.3 Emulsification Equipment - Bench-scale CDDM

A number of experimental studies, described in section 5.3.2, section 5.3.3, section 5.3.4 and section 5.3.5 of this chapter were performed on SFSO/Pluronic compositions and SFSO/NS compositions, processed on the Bench-scale CDDM. Depending on the study performed, raw materials and/or coarse emulsion pre-mixes were loaded into the feed vessels for processing. The methods for coarse pre-mix formation of SFSO/Pluronic and SFSO/NS compositions are outlined in Chapter 4 (section 4.2.1). Flow calibration studies were performed “in-line emulsification,” studies, where the pump speed settings were correlated against Progressive Cavity Pump (PCP) discharge rate for specific materials. Operation of the equipment was as described in Chapter 4 (section 4.6.1) and collected samples were analysed for domain size characteristics using the Malvern Mastersizer 2000. The protocol for

measurement is described in the Chapter 4 (section 4.2.2, section 4.2.3 and section 4.2.5).

5.3 Results and Discussion

5.3.1 Mixing Regimes

This section reports investigations of the process strategies which develop mixing regimes that promote extensional and rotational shear in the CDDM. As described in Chapter 3, materials processed in the CDDM apparatus are subject to competing shear types, where the intensity of shear is determined by material throughput (Q), mixer rotational speed (N) and the number of axially and circumferentially positioned constrictions within the mixer geometry.

Experiments were performed as described in Chapter 4 (section 4.6.2) and section 5.2.2, on post-processing of SFSO/Pluronic systems comprising 50wt.% and 70wt.% SFSO dispersed in 10wt.% and 23.3wt% Pluronic solutions.

The formulations were selected to describe concentrated and semi-concentrated emulsion systems, further the Pluronic solution concentrations were selected to maintain a SFSO:Pluronic mass ratio of 10:1. The experiments investigated mixer geometries of +0.25mm, +0.75mm, +1.75mm and +2.75mm. Chapter 4 (section 4.6) provides an outline of nomenclature used to describe mixer position. Geometries were chosen at intermediate points between “half-cavity” and zero displacement positions and were sufficiently distanced to identify mixing regimes of low extensional shear (full overlap) and high extensional shear (approaching displaced lands).

A full data-set for studies reported here may be found in Appendix (section AX 3.1). Formed emulsions were analysed for droplet size distribution, as per methods described in Chapter 4 (section 4.2.2 and section 4.2.3). It is noted that the works of Welch et al. (2006) and Tcholakova et al. (2011) indicated benefits in processing

concentrated emulsions in rotor-stator systems were attributed to the interaction of surrounding droplets in microstructure-induced break-up mechanisms.

Figure 5.1 describes the change in mean droplet diameter (d_{43}) with mixer geometry. Results generally indicate improved droplet break-up with decreasing axial displacement of confronting lands, however, 50wt.% SFSO results show little change in d_{43} with mixer geometry, which were substantially higher compared to emulsions comprising 70wt.% SFSO; this indicates improved break-up in concentrated systems. Comparing results of similar throughputs, the change in droplet diameter is more apparent for N of 5000 RPM, while little change is observed at 10000 RPM. This suggests that the impact of extensional shear is more influential at low N while rotational shear dominates at high N . The final d_{43} of emulsions post-processed at similar throughputs are smaller at higher N , as expected.

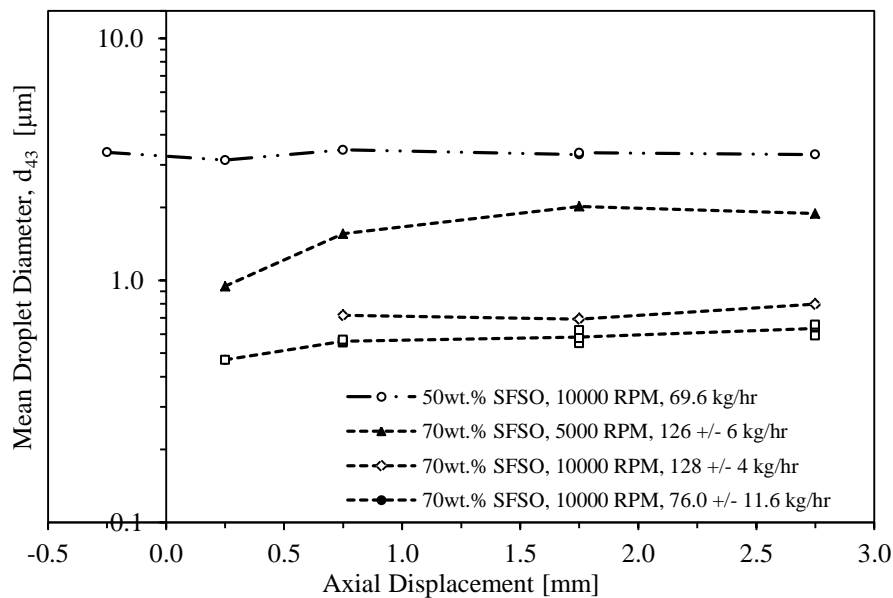


Figure 5.1: Graph describing mean droplet diameter (d_{43}) with mixer position, for SFSO/Pluronic emulsions comprising SFSO fractions of 50wt.% and 70wt.% and SFSO/Pluronic mass ratios of 10 to 1, post-processed at various conditions on the Laboratory-scale CDDM at several mixer geometries. The lines of fit indicate the trajectory of the results.

In order to analyse power input during emulsification, calorimetry studies were performed for processed emulsions at various mixer geometries. Power measurements were determined from Equation 5.1.

$$P = Q_e C_p (T_{out} - T_{in}) \quad (5.1)$$

Where P is the total power input to the emulsions, Q_e is the emulsion mass flowrate, C_p is the Specific Heat Capacity of the emulsion, T_{in} is the emulsion temperature at the mixer inlet and T_{out} is the emulsion temperature at the mixer outlet. The measurements are qualitative, as the equipment design does not allow development of steady state flows at set temperature and the accuracies of measurement are limited by heat losses from the system. Analysis was restricted to 70wt.% SFSO emulsion compositions which, when processed, resulted in higher levels of viscous heating compared to emulsions comprising lower phase volumes; this negated temperature losses in the system. Temperature measurements were collected at the vessel hopper and the mixer outlet, measured to an accuracy of $\pm 0.1^\circ\text{C}$. The feed lines to the mixer were lagged with fibreglass insulation to limit heat losses from the system and the mixer assembly comprised a separate seal to the mixer housing, therefore losses through seal cooling water were limited. Unfortunately, the pressure drop across the mixer during processing could not be determined, as the pressure sensor was externally mounted. This would have allowed the power from extension to be determined, by considering the product of Q and the pressure drop, Δp . Further work should consider a mixer design with a surface-mounted pressure sensor. The emulsion C_p (described in Appendix, section AX3.2) was estimated at 20°C as $2.79 \text{ kJ Kg}^{-1} \text{ K}^{-1}$, assuming a dispersed phase C_p of $2.193 \text{ kJ Kg}^{-1} \text{ K}^{-1}$ (Fasina and Colley, 2008) for SFSO at 20°C and C_p of $4.183 \text{ kJ Kg}^{-1} \text{ K}^{-1}$ for distilled water at 20°C .

Figure 5.2 describes P vs. Q for 70wt.% SFSO/Pluronic emulsions, post-processed at varying mixer geometries and mixer speeds of 0 RPM (Figure 5.2 a)), 5000 RPM (Figure 5.2 b)) and 10000 RPM (Figure 5.2 c)). Interestingly, the results indicate that, for all mixer positions, P converges at similar intercepts when $Q = 0 \text{ kg/hr}$, which could be considered as the rotational power in the absence of flow, P_R .

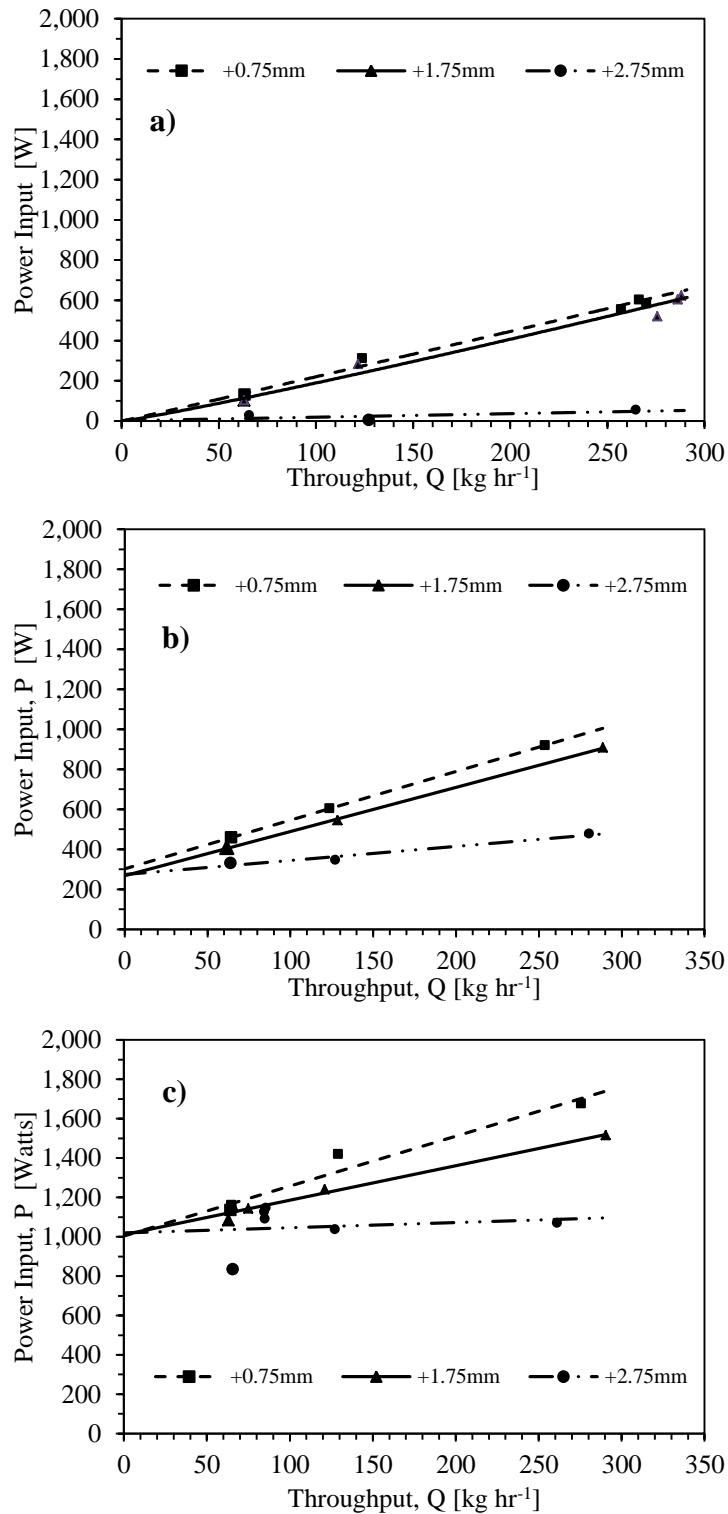


Figure 5.2: Graph of power input (P) against throughput (Q) for SFSO/Pluronic emulsions, consisting of a 70wt.% SFSO, post-processed in the Laboratory-scale CDDM at various mixer geometries, at rotational speeds (N) of **a)** 0 RPM **b)** 5000 RPM and **c)** 10000 RPM. The lines of fit indicate the trajectory of the results.

The lowest P is observed for experiments described in Figure 5.2a), whereby the mixer is static and does not contribute to the total P delivered to the emulsion system. Comparing P_R between intercepts at N of 0 RPM (3.15 +/- 2.05 W), 5000 RPM (281 +/- 15 W) and 10000 RPM (1011 +/- 7 W), in the absence of flow, P_R is approximately related to $N^{3.5}$. Considering the Equation 2.40, P_R is related to N^3 in the absence of flow; the difference in relationship may be due to the inaccuracies of calorimetric studies, it is proposed that P_R might follow an N^3 relationship in the absence of flow, however further studies are required for validation.

The Specific Energy (E_m) was considered against N per unit Q , to provide a measure of shear delivered with respect to N and Q . E_m was determined from calorimetry experiments, calculated as per with Equation 5.2.

$$E_m = C_p(T_{out} - T_{in}) \quad (5.2)$$

Where C_p is the specific heat capacity and T_{in} is the emulsion temperature at the mixer inlet and T_{out} is the emulsion temperature at the mixer outlet. The results of experiments are provided in Figure 5.3, which indicate a proportional correlation between E_m and N per unit Q . Additionally, the intercept values increase with decreasing axial displacements between confronting lands sections. This may suggest an increase in E_m delivered through extension, which appears negligible for mixer geometries approaching full cavity overlap. Once again, the results were limited by the quality of calorimetry measurements performed.

Finally, the Specific Surface Area (A_d) (described in Chapter 2, Table 2.2) of post-processed emulsions were plotted against E_m for SF50/Pluronic emulsions, post-processed at various conditions at +0.25mm, +0.75mm, +1.75mm and +2.75mm mixer geometries. The correlation is described in Figure 5.4 and shows a diminishing increase in A_d with E_m . With consideration to Equation 1.1, the stress required to deform droplets increases with increased capillary pressure (P_c). With reference to Equation 2.38, the d_{32} is inversely related to E_v , therefore this may support results indicating a diminishing A_d with E_m .

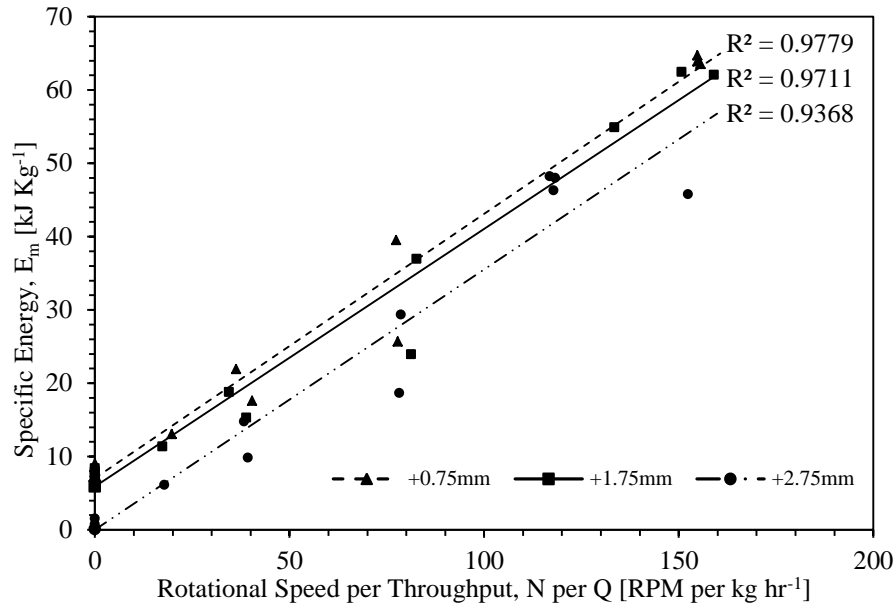


Figure 5.3: Graph describing specific energy (E_m) against rotational speed (N) per unit throughput (Q) for SFSO/Pluronic emulsions, comprising a 70wt.% oil fraction, processed at various Q , N and mixer geometries. The lines of fit indicate the trajectory of the results.

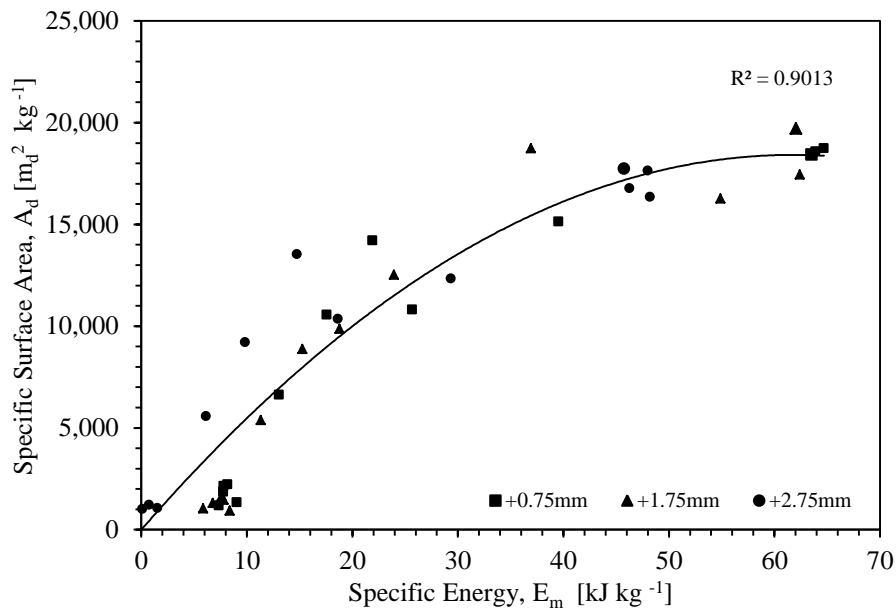


Figure 5.4: Graph describing specific surface area (A_d) against specific energy (E_m) for SFSO/Pluronic emulsions, comprising a 70wt. % oil fraction, processed at various conditions on the Laboratory-scale CDDM at +0.25mm, +0.75mm, +1.75mm and +2.75 mm mixer geometries. The line of fit indicates the trajectory of the results.

5.3.2 Number of Cavity Stages

This section reports investigations for strategies of increased shear duration and intensity by cavity stage number.

Studies on the effect of cavity stage number compared emulsions which were post-processed once (single-pass studies) and multiple times (multiple-pass studies) through the CDDM apparatus. Investigations were performed on the Bench-scale CDDM apparatus, described in Chapter 4 (section 4.6.1) and section 5.2.2. This CDDM system was selected over the Laboratory-scale CDDM as it provides a more convenient means of collecting processed emulsion and re-introducing the formed emulsions for subsequent passes. The apparatus comprises a 5-stage cavity design; therefore a single pass corresponds to processing in 5 cavity stages. Processed emulsions were analysed for droplet size distribution, as per methods described in Chapter 4 (section 4.2.2 and section 4.2.3).

Single-pass studies were performed on the Bench-scale CDDM system to determine the impact of post-processing and mixer geometry for SFSO/Pluronic emulsions. A full data-set for studies reported here may be found in Appendix (section AX3.3). Results describing the effects of N on d_{43} are described in Figure 5.5 and indicate more effective droplet break-up for emulsions comprising higher SFSO fractions (65.0vol.% vs. 79.5vol.%) and reduced axial displacement between confronting lands on the rotor and stator surfaces. With respect to the oil fraction, results support the findings of section 5.3.1, however in these instances emulsions were dispersed in 11.7wt.% Pluronic solution, therefore the SFSO:Pluronic mass ratio increased from 14.21:1 at 65.0vol.% to 30:1 at 79.5vol% oil fractions, indicating more efficient surfactant use. Further, at set oil fractions of 65vol.%, emulsions comprising of 23.3wt.% Pluronic surfactant solution concentrations resulted in significantly lower d_{43} than observed in emulsions processed comprising an 11.7wt.% Pluronic solution. This supports results described in section 5.3.1, which indicated more efficient break-up for emulsions comprising SFSO:Pluronic mass ratios of 10:1, stabilised with 23.3wt.% Pluronic solutions versus emulsions stabilised with 10wt.% Pluronic solutions.

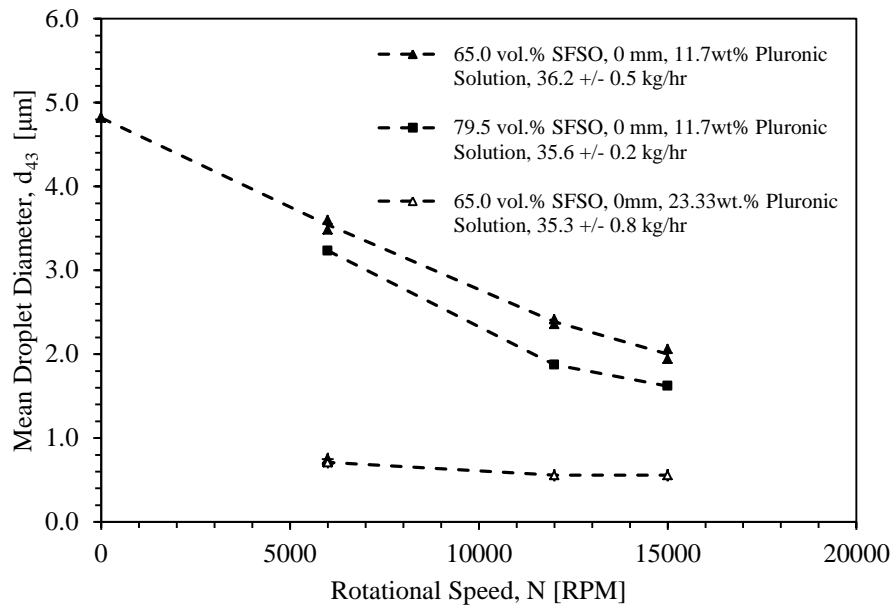


Figure 5.5: Graph describing the effect of Rotational Speed (N) on mean droplet diameter (d_{43}), for SFSO/Pluronic emulsions, post-processed at various conditions on the Bench-scale CDDM at -0.25mm and 0mm mixer geometries. The lines of fit indicate the trajectory of the results.

Results displayed in Figure 5.6 indicate that emulsions post-processed at the +1.35mm CDDM position profit from low coarse pre-mix droplet diameters, though some results indicate benefits in post-processing of emulsions comprising large coarse pre-mix diameters at low Q . Additionally, emulsions with the lowest d_{43} values are formed at low Q . In contrast, emulsions processed at the 0mm position observed the lowest d_{43} values at high Q . This indicates a transition in the dominant shear type from rotational to extensional, where the latter is promoted by nearer land axial displacements. The standard deviation for results described in Figure 5.5 and Figure 5.6 was determined as a SD% of 2.05%, which considered the variation droplet size in measurement error (see Appendix, section AX2.6) and the coarse pre-mix size variation (see Appendix, section AX2.11).

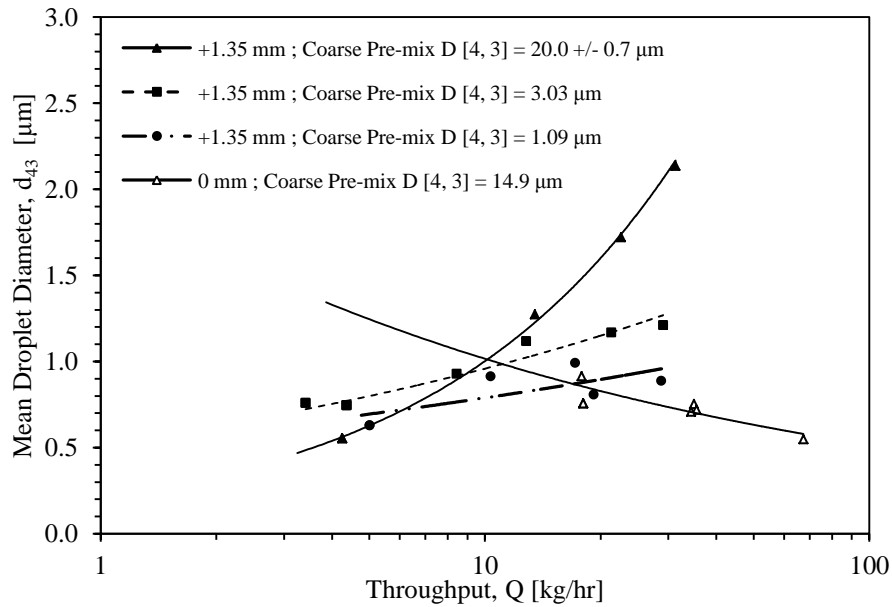


Figure 5.6: Graph describing the effect of Q on mean droplet diameter (d_{43}) for SFSSO/Pluronic emulsions, comprising 65.0vol.% SFSSO and 23.3wt.% Pluronic solution, post-processed at N of 6000 RPM at various Q on the Bench-scale CDDM and at 0mm and +1.35mm mixer geometries. The lines of fit indicate the trajectory of the results.

Studies were performed to investigate strategies that incorporate multiple-passes for emulsification. It is known that in many emulsification operations, for example studies on high pressure homogenisers (Raikar et al., 2011), have indicated reduction in droplet size with number of passes. For continuous emulsification, the maximum Sauter mean droplet diameter can be approximated from E_v , as described in Equation 2.38 (Karbstein and Schubert, 1995). The expression is valid for systems experiencing low residence times (10^{-2} to 10^{-3} seconds) in the high shear environment. While the final droplet diameter is related to the E_v applied to the system, the highest stable droplet diameter depends on the maximum surface coverage of surfactant at the interface, as described in Equation 2.2 (Tcholokova et al., 2004).

The Bench-scale CDDM apparatus used in these studies incorporates a 5 stage cavity design, where the flow is significantly restricted at axial positions of near-proximity lands, positioned on rotor and stator surface. It is of interest to determine the extent

to which the droplet size can be reduced through multiple passes, as a means for improved stress transfer to the system. Coarse emulsion pre-mixes of varying compositions were prepared using an overhead mixer with a 4-blade paddle connected by methods described in Chapter 4 (section 4.5.1). The pre-mixes were added to feed hoppers and processed in the Bench-scale CDDM system at 0mm and +1.35mm mixer geometries, at Q of 18+/-1.8 kg/hr and at N of 6000 RPM. The equipment design limited the formulations studies, as the method for feeding the mixing apparatus were restricted by material viscosity. Emulsions formed at higher oil fractions formed viscous emulsion intermediates which could not be processed through the system for subsequent passes. Formed emulsions were analysed for droplet size distribution, as per methods described in Chapter 4 (section 4.2.2 and section 4.2.3). A full dataset of results are provided in Appendix, section AX3.4.

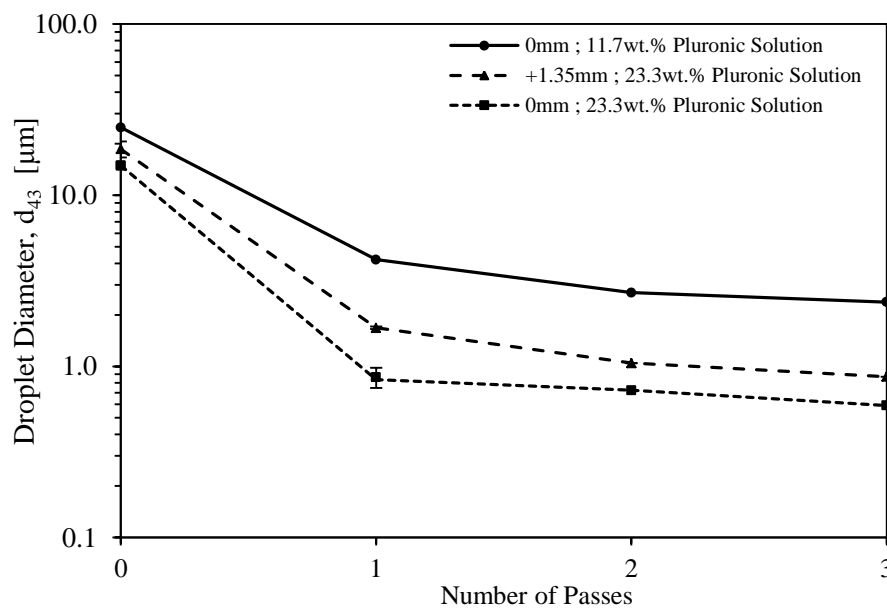


Figure 5.7: Graph showing the effect of number of passes on mean droplet diameter (d_{43}) for emulsions comprising 65.0vol.% SFSO, 11.7wt.% and 23.3wt.% Pluronic solution, processed in the Bench-scale CDDM at N of 6000 RPM and a Q of 18+/-1.8 kg/hr at +1.35mm and 0mm mixer positions. The lines of fit indicate the trajectory of the results.

The results of experiments are described in Figure 5.7 and Figure 5.8. As expected, the d_{43} decreases with increasing number of passes. Additionally, the lowest droplet diameter is observed for the 0mm mixer geometry. While Figure 5.7 indicates a diminishing reduction in d_{43} with pass number, analysis of Figure 5.8 shows a substantial increase in A_d with pass number, which provides information on the surface area created per mass dispersed phase. Analysis of A_d is distinctly different to analysis of d_{43} , as it is determined from the Sauter mean droplet diameter (d_{32}) and therefore considers a “surface-area,” based mean, as opposed to a “volume,” based mean. Chapter 2 (section 2.3.1) provides a description of the key size terms analysed in this current thesis.

Diminishing diameters may indicate depletion of surfactant available to stabilise the free surface. This result is extenuated by reduced axial displacements (0mm vs. +1.35mm positions). Furthermore, results indicate that emulsions formed with 23.3wt.% Pluronic solutions form more than double A_d compared to 11.7wt.% Pluronic solutions, indicating more efficient surfactant use. Similar results were observed for experiments described in section 5.3.1.

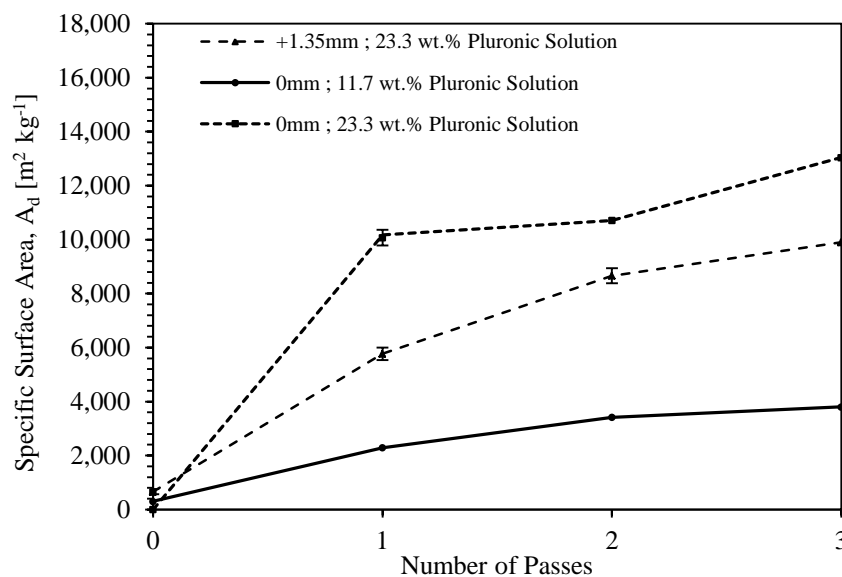


Figure 5.8: Graph showing the effect of number of passes on specific surface area (A_d) for emulsions comprising 65.0vol.% SFSO, 11.7wt.% and 23.3wt.% Pluronic solution, processed in the Bench-scale CDDM at N of 6000 RPM and a Q of 18+/- 1.8 kg/hr, at +1.35mm and 0mm mixer positions.

Finally, as described in Chapter 3, increases in cavity stage number improve stress transfer to emulsions by increasing the shear duration of extensional and rotational shear types, by increasing the number of constrictions between cavity lands positioned radially and circumferentially.

5.3.3 In-line Emulsification Studies

This section reports investigations for strategies for concentrated emulsion formation via CDDM processing.

The results of studies described in section 5.3.1 and 5.3.2 indicate improved emulsification for post-processing of concentrated emulsions results. Therefore, the method for forming concentrated emulsions requires due consideration. The approach for direct emulsification involved blending streams of raw ingredients at the required ratios in the Bench-scale CDDM system; the approach is outlined in Chapter 4, section 4.6.1. The PCPs were calibrated against material discharge rate, to combine the streams at the correct ratio while Q through the mixer remained consistent. Formed emulsions were analysed for droplet size distribution, as per methods described in Chapter 4 (section 4.2.2 and section 4.2.3.) A full dataset of results are provided in the Appendix (section AX3.5).

Figure 5.9 describes the effect of mixer position on droplet size distribution for the emulsions comprising of SF50/23.3wt.% Pluronic solution. These emulsions are formed directly and represent at the maximum phase limit achieved. Results indicate that the highest SF50 fraction is achieved at the +1.35mm mixer geometry, though the smallest droplet diameter and most uniform droplet size distribution is found in the 0mm mixer geometry. The results may indicate a limit in the maximum in amount of surface that may be stabilised, where emulsions formed at the greatest overlap (+1.35mm position) exhibit larger d_{43} values compared to materials formed at +1mm and 0mm positions.

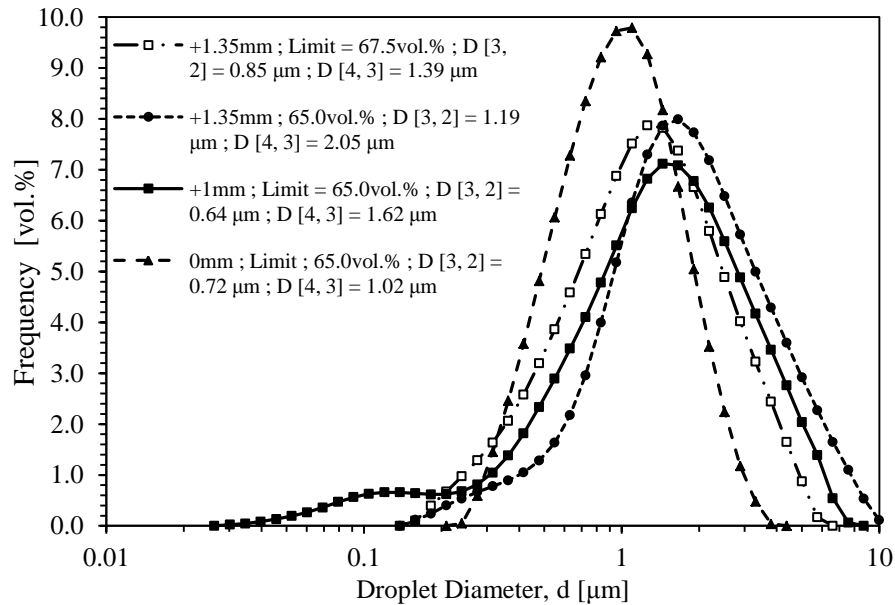


Figure 5.9: Graph describing the droplet size distribution for emulsions formed at their phase limit by in-line emulsification on the Bench-scale CDDM, comprising SF50 and 23.3wt.% Pluronic solution, processed at N of 6000 RPM and a Q of 36 \pm 3.6 kg/hr, at 0mm, +1mm and +1.35mm mixer geometries.

Figure 5.10 describes SF50/Pluronic emulsions, formed in the Bench-scale CDDM at a +1.35mm mixer geometry. The highest phase limit was achieved for emulsions formed at 6000 RPM, 18 \pm 1.8 kg/hr. Interestingly, emulsions below 30vol.% did not form, which may indicate a minimum energy requirement to form the emulsion. Additionally, materials processed at mixer speeds above 6000 RPM failed to form. An argument for this may consider excess shear on the system limits, where the rate of droplet disruption creates too great a surface to stabilise. Failure to stabilise excessive may lead to rapid re-coalescence and consequently emulsion destabilisation.

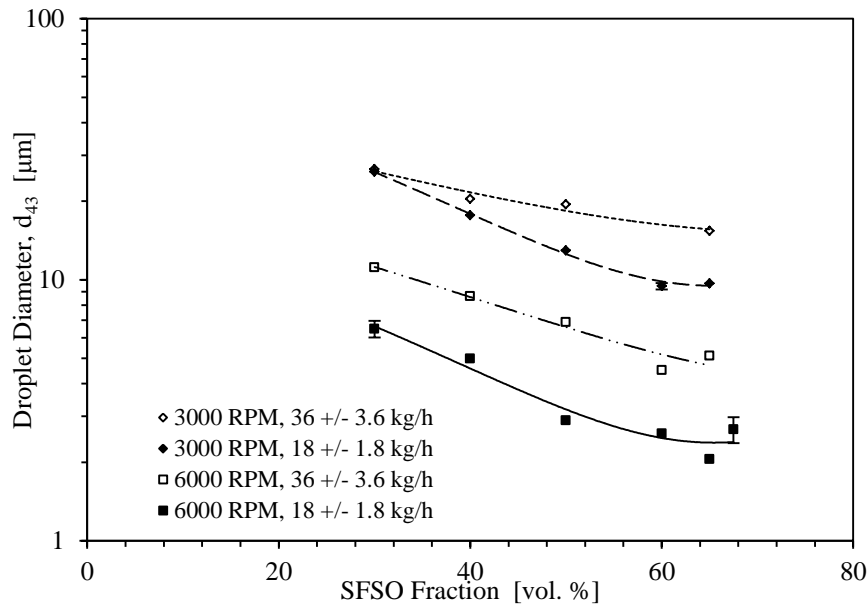


Figure 5.10: Graph describing mean droplet diameter (d_{43}) against SFSO fraction for emulsions, comprising SFSO and 23.3wt.% Pluronic solution, formed by in-line emulsification on the Bench-scale CDDM via a +1.35mm mixer geometry, at various N and Q . The lines of fit indicate the trajectory of the results.

Figure 5.11 shows the change in d_{43} with oil fraction for emulsions, comprising SFSO and 11.7wt.% Pluronic solution, formed by in-line emulsification on the Bench-scale CDDM via a +1.35mm mixer geometry. The limit of emulsion formation was found at around 67.5wt%. Further, emulsions with the lowest d_{43} were formed at low Q (18+/-1.8 kg/hr vs. 36+/-3.6 kg/hr) and high N (3000 vs. 6000 vs. 8400 vs. 9600). Comparing results described in Figure 5.10, emulsions formed with an 11.7wt.% Pluronic solution generally exhibited maximum phase volumes (~67.5vol.%) compared with compositions comprising 23.3wt.% Pluronic solution (~65.0vol.%). This suggests that the amount of interfacial surface may affect the maximum surface limit, where lower mean diameters prevent formation of emulsions of higher SFSO volume fraction.

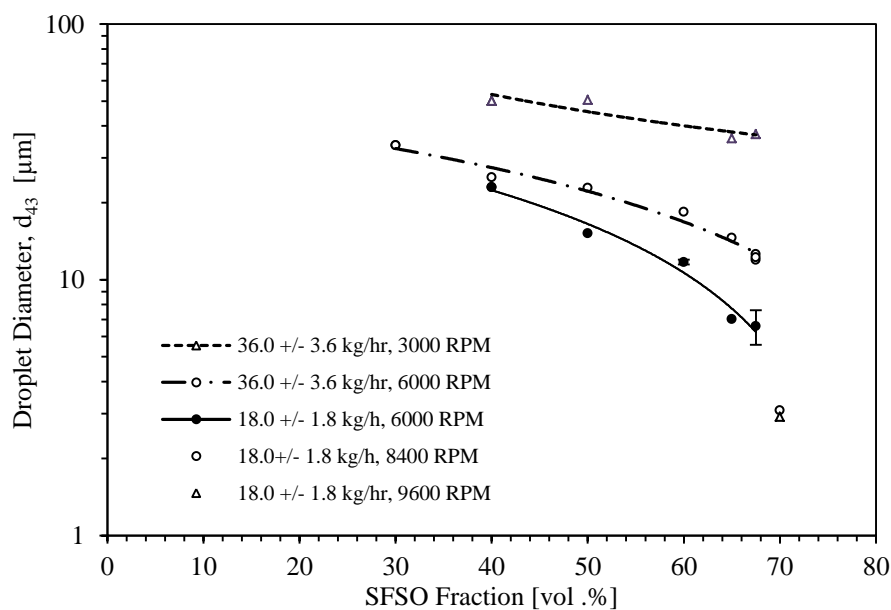


Figure 5.11: Graph describing mean droplet diameter (d_{43}) against volume fraction for emulsions, comprising SFSO and 11.7wt.% Pluronic solution, formed by in-line emulsification on the Bench-scale CDDM via a +1.35mm mixer geometry, at various N and Q . The lines of fit indicate the trajectory of the results.

The results indicate that at low flowrates, stable emulsion formation can be achieved with additional rotation. Figure 5.12 indicates that an increase in rotor speed leads to the formation of stable emulsions and provides evidence to support this statement. Applying excessive shear to the system may lead to the formation of excessive interfacial surface which cannot be stabilised, leading to rapid re-coalescence and emulsion destabilisation. However, in some instances an increased mixer speed appears to increase the maximum emulsion phase limit. This may be due to an improved stabilisation of the interface by allowing increase transfer of material within the mixer cavities. While this provides additional shear, it may improve distribution of the emulsion ingredients. Finally, standard deviation is listed as error bars for results described in Figure 5.9, Figure 5.10 and Figure 5.11 were determined with consideration to repeat results (see Appendix, section 2.6, table c) and measurement analysis (see Appendix, section 2.11, table a).

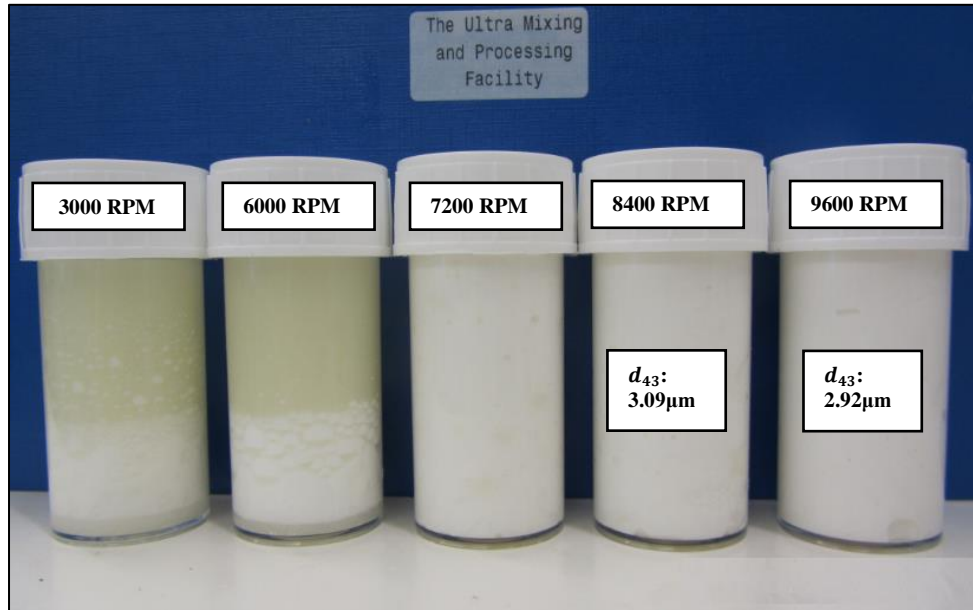


Figure 5.12: Image displaying emulsions, comprising 70vol.% SFISO stabilised with 11.7wt.% Pluronic solutions, formed by in-line emulsification on the Bench-scale CDDM via a +1.35mm mixer geometry at Q of 18+/-1.8 kg/hr and various N .

Figure 5.13 compares A_d for emulsions, comprising SFISO and 23.3wt.% Pluronic and 11.7wt.% Pluronic, formed by in-line emulsification and post-processing of coarse pre-mixes. Interestingly, for results describing in-line formation, emulsions stabilised with 23.3wt.% Pluronic solution exhibited more than double the A_d compared with emulsions formed with 11.7wt.% Pluronic solution, indicating more efficient surfactant use. Further, the results show that emulsions formed in-line are similar in size to post-processed emulsion pre-mixes of equivalent oil volume fraction. This suggests that emulsions of a similar size can be formed from direct emulsification as with a post-processed pre-mix, therefore offers opportunities for reduced manufacturing stage number. However, the maximum stable phase volume limits of emulsions formed in-line were lower than emulsions formed as coarse pre-mixes.

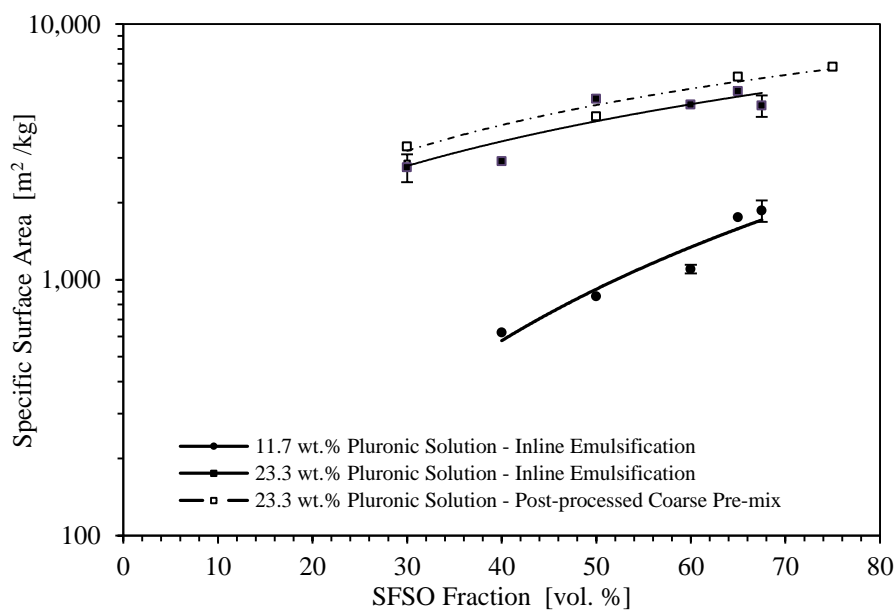


Figure 5.13: Graph describing the specific surface area (A_d) of emulsions, comprising SFSO, 11.7 wt.% and 23.3 wt. Pluronic solutions, formed on the Bench-scale CDDM by in-line emulsification or by post-processing of coarse pre-mixes, processed at 6000 RPM at 18+/-1.8 kg/hr, at a +1.35mm mixer position. The lines of fit indicate the trajectory of the results.

Subsequent studies investigated methods for increasing the phase limit of formed emulsions. The approach involved concentrating-up a coarse emulsion by in-line blending Sunflower Oil stream via the Bench-scale CDDM system. The approach is analogous to “concentrating up” methods described in literature, where emulsions are formed by the slow addition of oil to a low phase volume pre-mix (Liu and Friberg, 2009). Formation involves the slow addition of the oil to a surfactant rich composition, which prevents destabilisation of the system.

Once again, the equipment was operated as described in Chapter 4 (section 4.6.1). The PCPs were calibrated against material discharge rate, to combine the streams at the correct ratio while ensuring that material throughputs through the mixer remained consistent. For simplicity, the pre-mixes were formed on the bench using a 4-blade paddle mixer, by methods described in Chapter 4 (section 4.5.1). In this instance, a 75vol.% coarse pre-mix, comprising SFSO and 23.3% Pluronic solution,

was the formed to a desired size. Subsequently, portions of the pre-mix were diluted to 30vol.%, 50vol.%, 65vol.% and 75vol.% with a 23.3wt.% Pluronic solution using a low speed (500 RPM) overhead stirrer with 4 blade connection. This ensured that the droplet size distribution did not change substantially during study. As described in the Appendix (section AX2.10), emulsions were similar in droplet size distribution and indicated good uniformity throughout the pre-mix containers. The formed coarse pre-mix emulsions were processed at Q of 18+/-1.8 kg/hr and N of 6000 RPM. A full dataset of results are provided in Appendix, AX3.6.

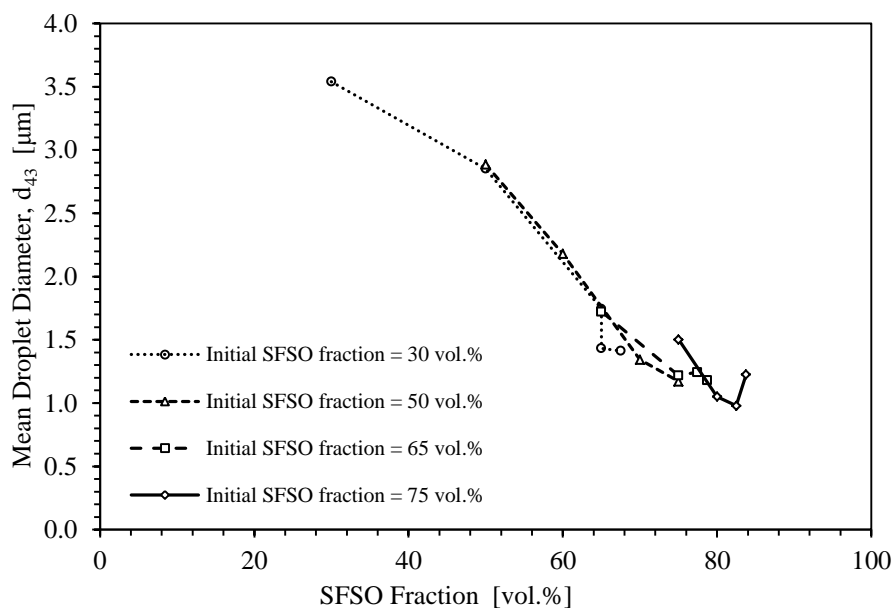


Figure 5.14: Graph showing the effect of oil fraction on mean droplet diameter (d_{43}) for emulsions comprising SFSO and 23.3wt.% Pluronic solution, concentrated in-line by blending with an SFSO and post-processed in-line via the Bench-scale CDDM, at N of 6000 RPM and Q of 18+/-1.8 kg/hr, in a +1.35mm position. The lines of fit indicate the trajectory of the results.

The results of experiments are outlined in Figure 5.14. Firstly, results indicate that the phase volume limits generally increased with higher SFSO fraction present in the coarse pre-mix (30vol.% to 70vol.%; 50vol.% to 75vol.%; 65vol.% to 78.7vol.%; 75vol.% to 83.75 vol.%). Additionally, the largest increase in SFSO is observed for emulsions with larger initial d_{43} . This again indicates a limit with respect to surface

creation, where excessive surface may not be stabilised, leading to rapid coalescence and consequently emulsion destabilisation. Additionally, results indicate similar final d_{43} for emulsions of different initial oil fractions concentrated to similar final oil fractions. Finally, this process method may be applied to in-line formation of concentrated emulsions via the Bench-scale CDDM.

5.3.4 Application of In-line and Cavity Stage Strategies

This section reports on investigations of a process strategy incorporating concentrated emulsion formation via in-line emulsification and cavity number, aimed at more efficient emulsification.

The process strategies incorporating in-line emulsification and multiple pass, described in section 5.3.3 and section 5.3.5, indicated improved emulsification efficiency by increasing the dispersed SFSO fraction and reduced d_{43} at set surfactant concentration. A process strategy, utilising in-line emulsification and multiple-pass methods was compared on a 1kg basis against course emulsion pre-mixes, comprising SFSO and 23.3wt.% Pluronic solution, and processed at similar conditions at a +0mm position on the Bench-scale CDDM. The processes are described in Figure 5.15. Process 1 involved the formation of a 65vol% SFSO emulsion, formed in-line via the Bench-scale CDDM at Q of 18.1 kg/hr at N between 3000-6000 RPM. The formed emulsions were subsequently blended with SFSO in-line via the Bench-scale CDDM, at Q of 17.2 kg/hr at N of 6000 RPM, whereby the formed emulsion comprised an SFSO fraction of 75vol%. Subsequently, the emulsion was diluted offline using an overhead mixer with 4-blade paddle connection at low N (500 RPM). For process 2, an emulsion comprising 65vol.% SFSO and 23.3wt.% Pluronic solution was prepared using an overhead mixer with 4-blade paddle connection, as per methods described in Chapter 4 (section 4.5.1). A full dataset of results are provided in the Appendix (section AX3.7).

Formed emulsions were analysed for droplet size distribution, as per methods described in Chapter 4 (section 4.2.2 and section 4.2.3). The formed emulsion was

subsequently processed multiple times through the Bench-scale CDDM system at Q of 17.3 kg/hr and N of 6000 RPM. An initial basis of 1kg was chosen to simply show differences in processed emulsion at each stage. Results described at each stage of Figure 5.15, describes the properties of emulsions formed in each step. With reference to Figure 5.15, results described at “Pass 2” indicate similar d_{43} and A_d for emulsions formed, however the SF50:Pluronic mass ratio for Process 1 is substantially higher than emulsions formed in Process 2 (11.43:1 vs 7.11:1), indicating more efficient surfactant use. Additionally, the quantity of material produced as per Process 1 was 37.8% higher than material formed in Process 2, which required more process stages. Therefore, comparing results of Process 2, “Pass 2” with the dilution stage of Process 1, which have comparable processing, number of stages and composition, the amount of material formed comprised 60% more processed material. Process 1 therefore indicates improved efficiency compared with Process 2.

5.3.5 Extension of Strategies to Emulsions Stabilised with NS

The experiments described in section 5.3.2, section 5.3.3 and section 5.3.4 for SF50/Pluronic emulsions were extended to SF50/NS compositions. This surfactant comprises a mixture of naturally sourced surfactants, comprising high density lipoproteins, low density phospholipids and lecithin. Due to the size and structure of these molecules, this mix is considered as slow-absorbing. This allows comparison of a fast-absorbing synthetic surfactant with a slow-absorbing natural surfactant. The intention of these studies are to determine if the findings of experiments described in section 5.3.2, section 5.3.3 and section 5.3.4 may be extended to a slow-absorbing surfactant mixture. Emulsions pre-mixes were formed as per methods described in Chapter 4 (section 4.5.1). A full dataset of results are provided in the Appendix (section AX3.8). Formed emulsions were analysed for droplet size distribution, as per methods described in Chapter 4 (section 4.2.2 and section 4.2.5). Additional data describing the modification of emulsion microstructure with dilution and the effect of NS is provided in the Appendix (section AX3.9).

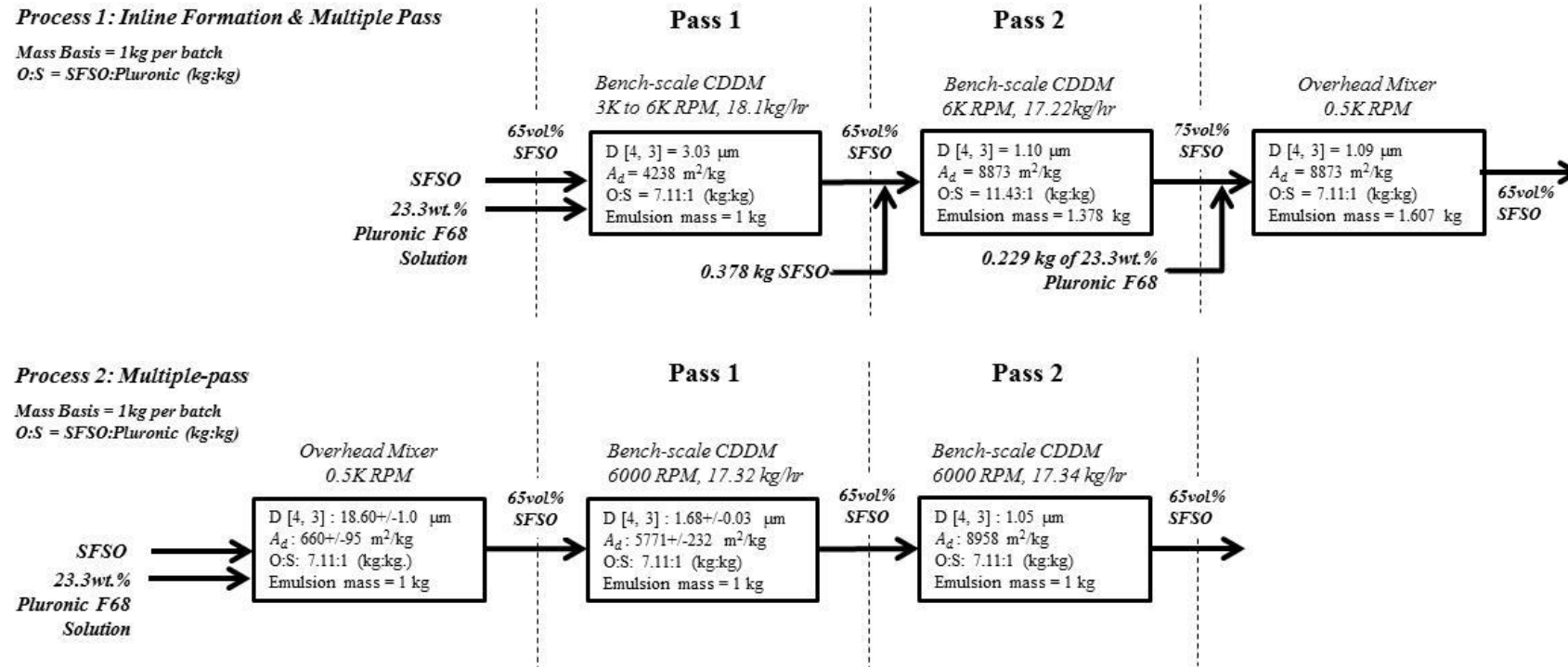


Figure 5.15: Image describing experiments on mid-point dilution compared with multiple-pass experiments, for a 65vol.% SFSO emulsions comprising a 23.3wt.% Pluronic solution, processed at N of 6000 RPM and at Q of 16 kg/hr and 18 kg/hr, at a 0mm CDDM geometry.

Number of Cavity Stages - Single Pass Studies

Single pass studies were performed on SFSO/NS emulsions, whereby coarse pre-mixes were formed by methods described in Section 4.5.1. Figure 5.16 displays the effect of SFSO fraction of d_{43} , for emulsions, comprising SFSO and 34.4wt.% NS solution, post-processed in the Bench-scale CDDM at a 0mm mixer geometry at similar Q and N of 10800 RPM, 13200 RPM and 15000 RPM. While little difference in d_{43} is observed between results of 10800 RPM vs. 13200 RPM, results of 10800 RPM vs. 15000 RPM indicate emulsions comprising higher SFSO fractions and processed at higher mixer speeds comprised of lower d_{43} .

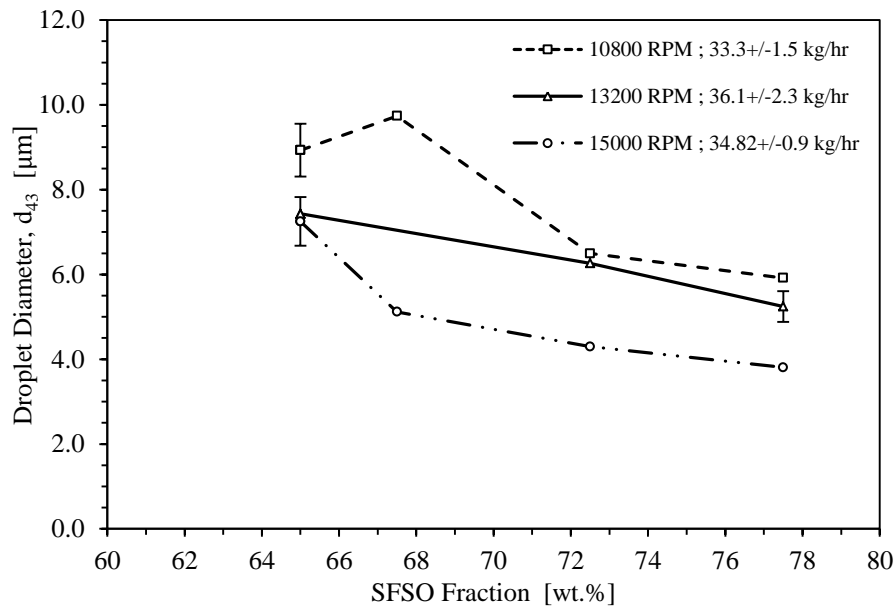


Figure 5.16: Graph describing the effect of SFSO fraction on the mean droplet diameter (d_{43}) of emulsions, comprising SFSO and 34.4wt.% NS solution, processed on the Bench-scale CDDM in a 0mm geometry, at similar Q and N of 10800 RPM, 13200 RPM and 15000 RPM. The lines of fit indicate the trajectory of the results.

Figure 5.17 displays the effect of SFSO fraction on A_d , for emulsions, comprising SFSO and 34.4wt.% NS solution, post-processed in the Bench-scale CDDM at a 0mm mixer geometry at similar Q and N of 10800 RPM, 13200 RPM and 15000 RPM. Results indicate that emulsions comprising higher SFSO fractions and processed at higher mixer speeds comprise a higher A_d .

These results are in agreement with results described in section 5.3.2, indicating that the findings extended to emulsification of a slow-absorbing natural surfactant. However, absorption was less efficient, indicated by significantly higher d_{43} and significantly lower A_d .

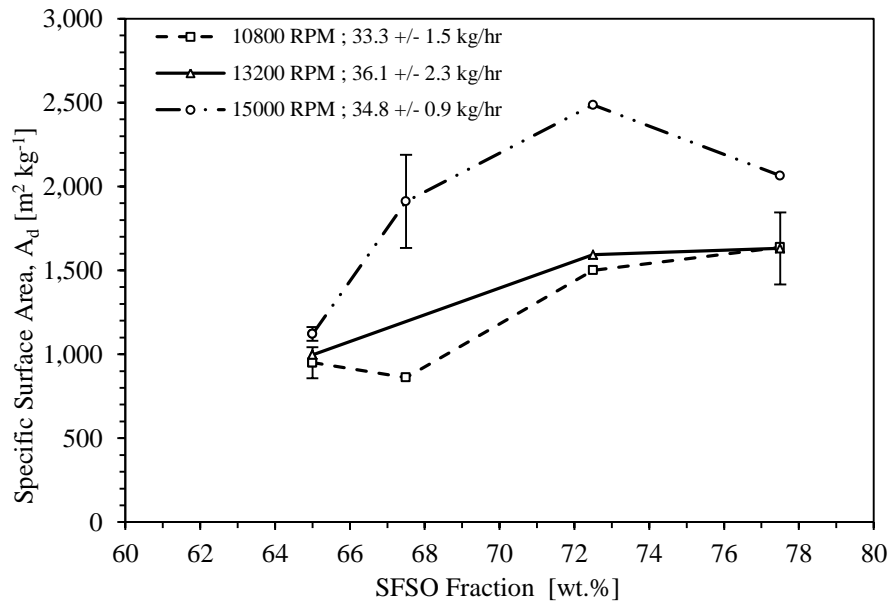


Figure 5.17: Graph describing the effect of SFSO fraction on specific surface area, A_d of emulsions, comprising SFSO and 34.4wt.% NS solution, processed on the Bench-scale CDDM in a 0mm geometry, at similar Q and at N of 10800 RPM, 13200 RPM and 15000 RPM. The lines of fit indicate the trajectory of the results.

Further, Figure 5.18 displays experimental results of apparent viscosity of emulsions, comprising SFSO and 34.4wt.% NS compositions of differing d_{43} values, post-processed on the Bench-scale CDDM in a 0mm mixer geometry. In addition to d_{43} , the emulsion's apparent viscosity provides an indication of emulsion efficiency, for applications where material consistency is a key consideration. These measurements provide insight on product microstructure. The emulsion's apparent viscosity was measured 1 hour post-processing as per methods described in Chapter 4 (section 4.3.2). The droplet size results of processed SFSO/NS emulsions, comprising of varying phase volume, were grouped under a d_{43} size range and analysed against measured emulsion viscosity. These results are displayed in Figure 5.18 and indicate

that the SFISO fraction strongly influences emulsion viscosity, which is further enhanced with reduced d_{43} .

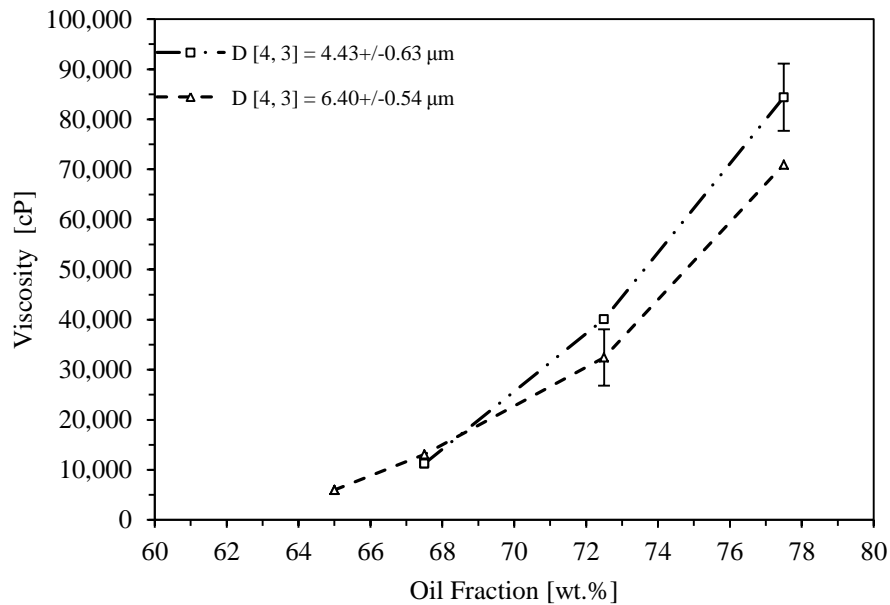


Figure 5.18: Graph describing the effect of SFISO fraction on viscosity of emulsions, of emulsions, comprising SFISO and 34.4wt.% NS solution of differing mean droplet diameters (d_{43}). The lines of fit indicate the trajectory of the results.

Number of Cavity-stages - Multiple-Pass Studies

Multiple-pass studies were performed for emulsions comprising 67.5wt.% SFISO and a 34.4wt.% NS solution, processed on the Bench-scale CDDM at 0mm and +1.35mm mixer geometries, at N of 10800 RPM and Q between 30.1 kg/hr and 35.2 kg/hr. The results of experiments are described in Figure 5.19 and Figure 5.20, which indicate little changes in d_{43} and A_d for emulsions processed more than once and contrary to results described in Figure 5.7 and Figure 5.8.

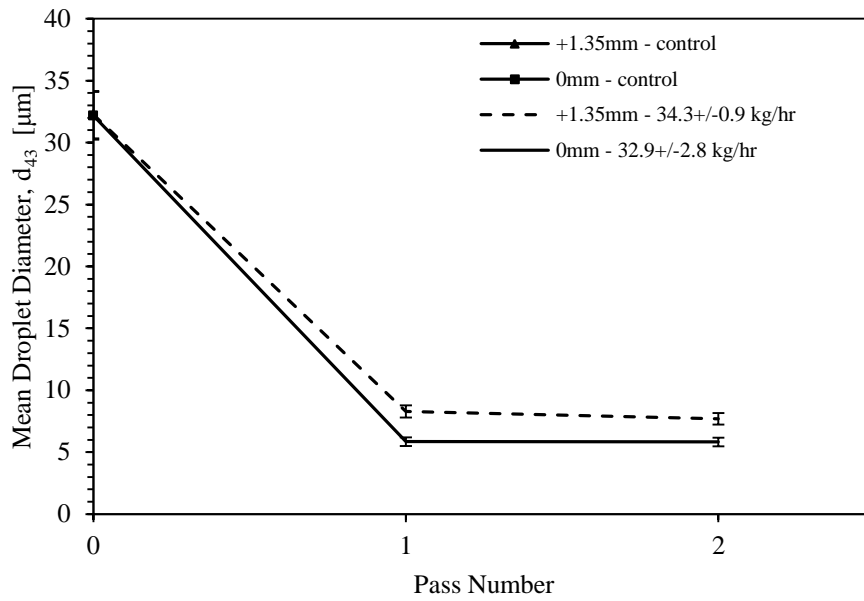


Figure 5.19: Graph describing the effect of pass number on mean droplet diameter (d_{43}) comprising an SFSO fraction of 67.5wt% and 34.4wt.% NS solution, for processed on the Bench-scale CDDM at 10800 RPM in 0mm and +1.35mm mixer geometries. The lines of fit indicate the trajectory of the results.

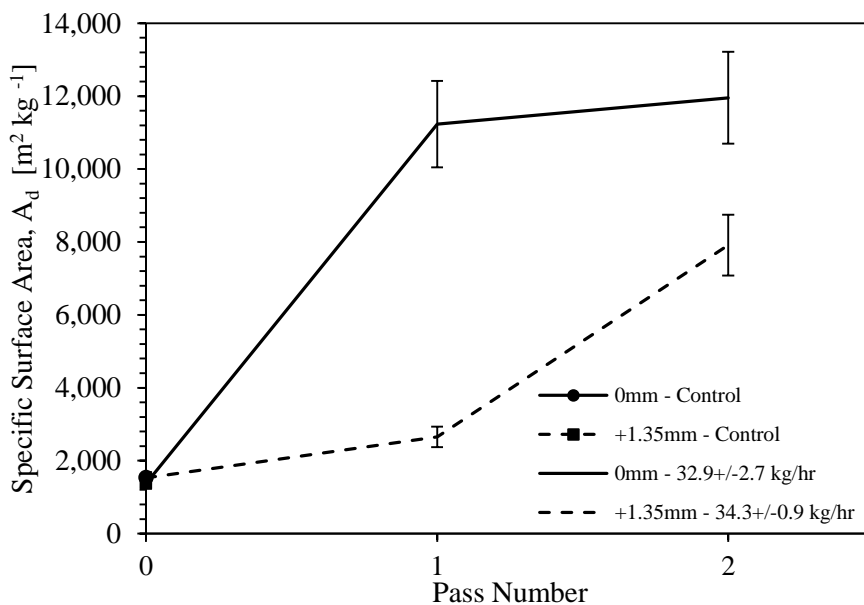


Figure 5.20: Graph describing the effect of pass number on specific surface area, A_d , for processed emulsions comprising a 67.5wt% SFSO and 34.4wt.% NS solution, processed on the Bench-scale CDDM at 10800 RPM in 0mm and +1.35mm mixer geometries. The lines of fit indicate the trajectory of the results.

No effect with pass number may be due to less efficient stabilisation of surface with the NS surfactant. However, the results do indicate an increase in A_d with pass number, for emulsions processed at a +1.35mm mixer geometry. The standard deviation for provide in error bars listed Figure 5.19 and Figure 5.20 were determined from measurement errors (see Appendix, section AX2.6, table b) and variations in size results observed in analysis of course emulsion pre-mixes (see Appendix, section AX2.11, table b).

In-line Emulsification Studies

The studies outlined in section 5.3.3 indicated methods for forming concentrated emulsions by in-line emulsification. These studies were extended to SFSO/NS emulsions, to determine whether the method could be extended for slow-absorbing natural surfactants. Figure 5.21 displays the results of in-line formation of SFSO/NS emulsions, formed firstly by in-line emulsification of SFSO and 34.4wt.% NS solution on the Bench-scale CDDM in a +1.35mm mixer geometry, and the subsequently by raising the SFSO fraction by blending the formed emulsion with SFSO via the Bench-scale CDDM in a +1.35mm position. The emulsion viscosity, which was measured 1 hour post-processing as per methods described in Chapter 4 (section 4.3.2), was used as a measure for evaluating emulsification efficiency.

For the emulsion formation step, it was noted that emulsions did not form at SFSO fractions above or below 57.2wt.%, however at oil fractions of 57.2wt.%, consistent emulsions formed at mixer speeds up to and including 15000 RPM. A large batch of material, comprising a 57.2wt.% SFSO dispersed phase and 34.4wt.% NS solution was formed N of 10800 RPM and Q of 29.6 kg/hr and. The formed material was re-introduced to the Bench-scale CDDM and blended in-line with SFSO, in a +1.35mm mixer geometry at various N and Q . The results indicate that SFSO/NS emulsions comprising a concentrated SFSO fraction could be formed via in-line blending with the formed emulsion. The best results were observed for the highest mixer speeds, where the results indicate similar viscosities to the benchmark emulsions at SFSO fractions of 72.5wt%.

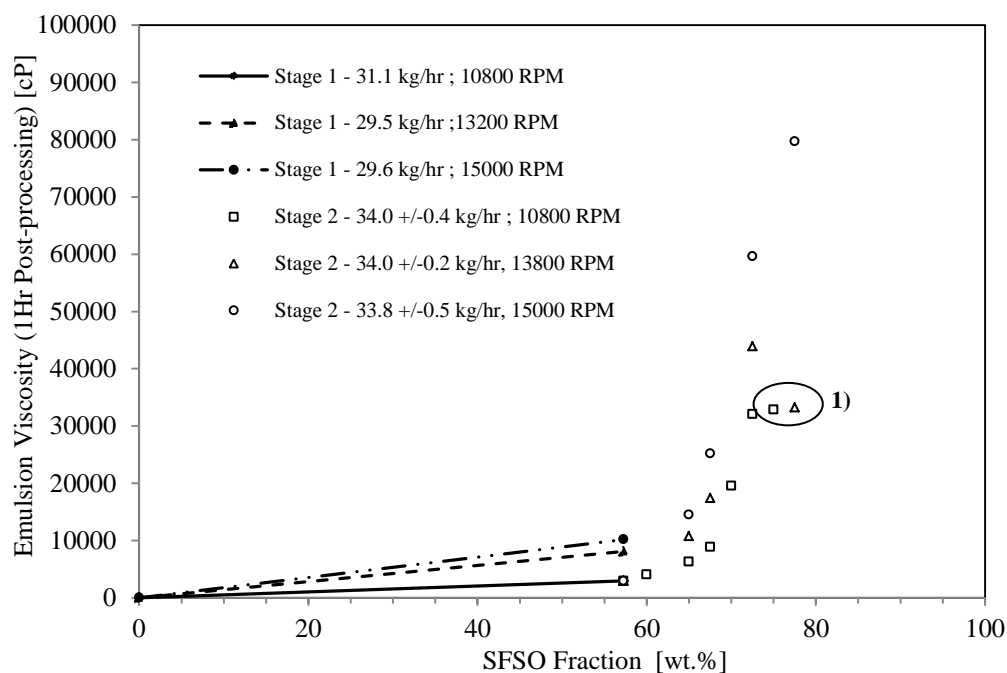


Figure 5.21: Application of in-line emulsification process strategies for emulsions, comprising SFSO and 34.4wt.% NS Solution, processed on the Bench-scale CDDM at a +1.35mm mixer geometry. Stage 1 incorporates direct formation of emulsions, whereas Stage 2 blends SFSO with a coarse emulsion pre-mix. Circled data points at 1) may indicate a partially destabilised emulsion.

5.4 Conclusions and Further Work

5.4.1 Mixing Regimes

- A strategy for developing mixing regimes was investigated for a model O/W system (section 5.3.1), stabilised with a synthetic non-ionic surfactant. Efficient emulsification was achieved by optimising the mixer geometry and processing conditions within the limits of equipment design and operation for a particular formulation.
- One of the limitations of study was the approach used to measure energy use.

Best efforts were applied to limit heat loss from the system, by insulating vessels and pipework between the coarse emulsion and mixer assembly, however these calorimetry measurements can only be considered as a

qualitative measurement of the total energy use in studies. While mixer power measurement was recorded, difficulty arises in accounting for power loss through noise, vibration and heating of seal bearings and fluid during operation. A limited equipment design prevented pressure measurement across the mixer assembly, therefore this approach could not account for the relative power input from rotation and extension. Experiments may be improved by installing torque-meter to account for power from rotation and a surface mounted pressure sensor prior to the mixer inlet to account for power from extension. This may validate findings for total energy input to system and provide insight on emulsification efficiency for alternate mixing regimes.

5.4.2 Number of Cavity Stages

- Strategies exploiting cavity stage number were investigated for efficient manufacture of model O/W emulsions systems stabilised with both synthetic (section 5.3.2) and a natural surfactants (section 5.3.5). The strategy demonstrated improved efficiency with increasing cavity stage number, extenuated by reducing the axial displacement of cavities.
- The studies may have been improved by comparing emulsification via multiple pass methods to emulsification in mixer designs with an equal number of cavity stages. The results of experiments may have found improved emulsification for mixer designs of increased cavity number over multiple-pass methods, as the former approach prevents relaxation of the emulsion system between cavity stages.

5.4.3 In-line Emulsification

- Methods for in-line emulsification via CDDM apparatus were studied for model O/W systems, stabilised with synthetic (section 5.3.3 and 5.3.4) and natural surfactants (section 5.3.4). The approached allowed direct manufacture of emulsions and the formation of concentrated emulsions by

blending coarse pre-mixes with additional oil. The strategy indicated a reduced number of processing stages by forming emulsions of equivalent specific surface areas to emulsions formed directly.

- While the approach was tested for non-ionic surfactants, further experiments may have considered effects of surfactant hydrophilicity on emulsion formation, for example, matching the surfactant HLB to the optimum oil HLB.

Chapter 6: Manufacturing Strategies for Emulsion Systems, stabilised by Synthetic Surfactants

6.1 Summary

This chapter reports on investigations of strategies for efficient emulsion manufacture of an O/W system, comprising Petroleum Jelly (PJ) stabilised with an anionic surfactant Sodium Lauryl Ether Sulphate (SLES), processed in the Fluid Division Mixer (FDM) and Controlled Deformation Dynamic Mixer (CDDM). Strategies involved approaches incorporating viscosity matching, surface stabilisation and HIPEs and were evaluated as per the efficiency function described in Chapter 3. Results indicated the efficiency of emulsions improved comprised of high dispersed phase fractions and concentrated surfactant solutions. Interestingly, emulsions with low surfactant concentrations were highly efficient.

6.2 Materials and Methods

6.2.1 Materials

The majority of studies reported within the current chapter consider model O/W emulsions comprising of PJ and SLES. Later studies reported in the current chapter considered a model O/W system comprising Sunflower Seed Oil (SFSO), stabilised with a non-ionic surfactant, Pluronic F68.

6.2.2 Experimental Methods - Overhead Mixer Studies

IKA™ overhead mixers (IKA®-Werke GmbH & Co. KG, Staufen, Germany) were used in experimental studies described in section 6.3.1. The design and operation limits of the apparatus are described in detail in the Appendix (section AX2.8 and section AX2.9). With reference to Figure 6.2, the following method was used for experimental studies:

A 150g mix, comprising of PJ and 70% SLES was weighed out in a 250ml beaker using a mass balance of 0.01g accuracy. PJ comprised of 87.5wt.% of the total mix and the PJ:SLES mass ratio was maintained at 10:1. A separate 150 g mix, comprising of Petrolatum and 25% SLES was weighed out in a 600 ml beaker using a mass balance of 0.01g accuracy, Here, PJ comprised 71.4wt% of the total mix, with the mass ratio maintained at 10:1. The contents of the 250ml beaker and 600ml beakers were heated to above 60°C in Silicone Oil baths. Once a temperature above 60°C was reached in both vessels, the contents of the 250 ml beaker was mixed using an overhead mixer (described in section 4.5) at 1000 RPM using a 5-blade toothed impeller. The contents of the 600ml beaker were mixed using an overhead mixer with a 3-Blade Propeller attachment, at 1000 RPM. The vessel contents were mixed for a period of 30 minutes. Subsequently, the contents of the 250ml beaker were added to the contents of the 600ml beaker and the combined contents were mixed for a further 55 minutes. Samples were collected periodically during the experiment and were diluted in hot distilled water and mixed for one minute using the IKA™ homogeniser, operating at 500 RPM, in order to promote emulsion dispersion in the hot distilled water.

6.2.3 Experimental Methods - Formax™ Studies

For experimental studies described in section 6.3.1, PJ/SLES compositions were emulsified using the Formax™ Platform (Chemspeed Technologies AG, Augst, Switzerland). During these studies, the equipment (termed Formax™) was operated as per methods described in Chapter 4, section 4.8. The measurement protocol used

was outlined in Chapter 4, sections 4.2 and 4.4. With reference to Figure 4.13 and Figure 6.3, the experiments described in section 6.3.1 were performed as follows:

Quantities of PJ and SLES solution were added to mixing vessels, such that the mix comprised 71.4wt.% PJ and 25.0wt.% SLES. The total mass of material added to the mixing vessels varied between 25.0-50.0g, which were labelled “pre-mix A,” and are described in Figure 6.3. The mixing vessels were installed with a dissolver disk impeller, which was operated at 1000 RPM or 4000 RPM. The contents of each vessel was heated to a pre-determined temperature (50°C to 70°C), at which point the ingredients were mixed for a further 30 minutes. Separately, compositions comprising of 87.5wt.% PJ and 70wt.% SLES solution were labelled “pre-mix B,” and weighed out in crystallisation dishes using a mass balance of +/-0.01g accuracy. The contents of the crystallisation dishes were then heated via a heated plate to temperatures of 50°C and 70°C and were stirred using a stirrer bar. On completion of the 30 minute processing step for “pre-mix A,” quantities of “pre-mix B,” (10-25g) were added via the robotic arm, with connected mass balance and heated dispersion cartridge. The final mass of material in the mixing vessels was maintained at 50g. The experimental protocol was programed to allow transfer of ingredients from each of the “pre-mix B,” batches, such that the temperature of material in the mixing vessels did not change substantially during the addition of “pre-mix B”. The robotic arm, with the attached mass balance and heated dispersion cartridge was then positioned above one of the “pre-mix B,” containers, where a sufficient amount of the pre-mix was extracted (see Figure 4.13e). The required aliquot of material was then delivered to the mixing vessel. Following the combining of pre-mix compositions, mixing was implemented for a further 30 minutes at the set temperature (50°C and 70°C).

6.2.4 Experimental Methods - FDM Studies

For experimental studies described in section 6.3.2, batch emulsification of PJ/SLES compositions were studied using the FDM (Maelstrom APT Ltd, Glossop, United

Kingdom). The design and operation of the equipment is described in Chapter 4, section 4.7. A general method was applied for the batch operation of the FDM experimental studies. Pre-determined amounts PJ, 25wt.% SLES solution and in some instances 70wt.% SLES solution were added to a 2 litre mixing vessel at ambient conditions. The vessel and vessel contents (comprising of a total mass of 1kg) were covered using paraffin film and heated to a temperature of 65+/-1°C, using a water bath. On reaching the target temperature, the paraffin film was removed and the FDM mixer head assembly was immersed to a depth of around ¾ of the total vessel depth, to reduce entrainment of air during the experiment. A temperature probe was secured to one of the mixer assembly supporting rods to monitor temperature during the experimental studies. As the vessel ingredients cooled on contact with the mixer housing, the temperature was raised to 65.0+/-1°C using a water bath, at which point the experiment was initiated. A stopwatch was initiated once the mixer had reached full speed to record mixing duration. The mixer speed was set to the maximum of 100Hz (6000 RPM) to ensure that the material was drawn through the mixer housing effectively. Samples were collected during the experiment and diluted immediately in hot distilled water. As the mixer was high-shear, concentrated emulsions were more readily formed. As a result, emulsions were formed directly rather than by the split stream emulsification method described previously. However, a combination of 25wt.% SLES and 70wt.% SLES solutions were used in instances where the required weight ratio of oil to surfactant could not be achieved directly. This was implemented by separately heating mixes comprising PJ and 25wt.% SLES in the 2 litre mixing vessel and 70wt.% SLES in a separate container, to a temperature of 65°C. The 70wt.% SLES was added to the mixing vessel in the moments prior to commencing the experiment.

6.2.5 Experimental Methods - Laboratory-scale CDDM Studies

Emulsification studies on PJ/SLES systems and SFSO/Pluronic systems were performed on the Laboratory-scale CDDM System (Maelstrom APT Ltd, Glossop, United Kingdom). The experiments involved the post-processing of coarse pre-mixes; this approach improved the accuracy of formulation studies by combining ingredients offline in accurate amounts and allowed formation of concentrated

emulsions which could not be formed in-line. The operation of the Laboratory-scale CDDM was executed as per methods described Chapter 4, section 4.6.2. The methods for coarse pre-mix formation of SFSO/Pluronic and PJ/SLES compositions are outlined in Chapter 4, section 4.5.1.

6.3 Results and Discussion - Viscosity Matching Strategies

The following sections report investigations on “viscosity-matching,” for efficient manufacture of a model O/W system comprising of PJ dispersed in SLES solution and SFSO dispersed in Pluronic solution.

The strategy described in this section was initially proposed in Chapter 3 (section 3.3.4) and aims to improve emulsification efficiency by raising the dispersed phase fraction at a set dispersed phase to surfactant mass ratio. Further, experimental findings described in Chapter 5 (section 5.3.1) indicated opportunities for efficient emulsion manufacture for emulsions of high dispersed phase fractions (50wt.% vs. 70wt.%) at set SFSO:Pluronic mass ratio (10:1).

6.3.1 Formax™ Studies

Experimental findings described in Chapter 5 (section 5.3.1, section 5.3.2 and section 5.3.4) indicate benefits in processing emulsions comprising high dispersed phase fractions. With reference to the efficiency function described in Chapter 3 (section 3.2.3), the strategies were investigated as a means of improving surfactant use during emulsification. The experiments described here considered melt emulsification of PJ/SLES compositions, comprising set mass ratios of PJ:SLES of 10:1. Experimental studies were performed on the Formax™ (the operation of this equipment was described in Chapter 4, section 4.8). This approach allowed for study of the process rules for melt emulsification, which requires all ingredients to be brought to liquid form and subsequently emulsified via the mixing apparatus.

Experimental studies aimed to form and process concentrated PJ/SLES emulsions comprising PJ:SLES mass ratios of 10:1. A set ratio was chosen to maintain the relative quantities of PJ and SLES on stabilisation. Systems comprising of high dispersed phase fractions required highly concentrated surfactant solutions. Figure 6.1 describes the change in SLES solution viscosity with concentration. Results indicated a significant increase in viscosity between concentrations of 27% and 70%, which was attributed to the formation of micellar and hexagonal surfactant phases. For studies performed on the Formax™, the process for handling viscous intermediates was problematic in that forming the surfactant solution directly made it difficult to combine with PJ. To overcome this issue, an approach was developed where two separate pre-mix streams (described here as split-stream emulsification), of differing PJ fraction and equal PJ:SLES mass ratios, were combined in pre-determined quantities. The strategy was tested via overhead mixers, where the design and operational limits are described in Appendix, section AX2.8 and section AX2.9.

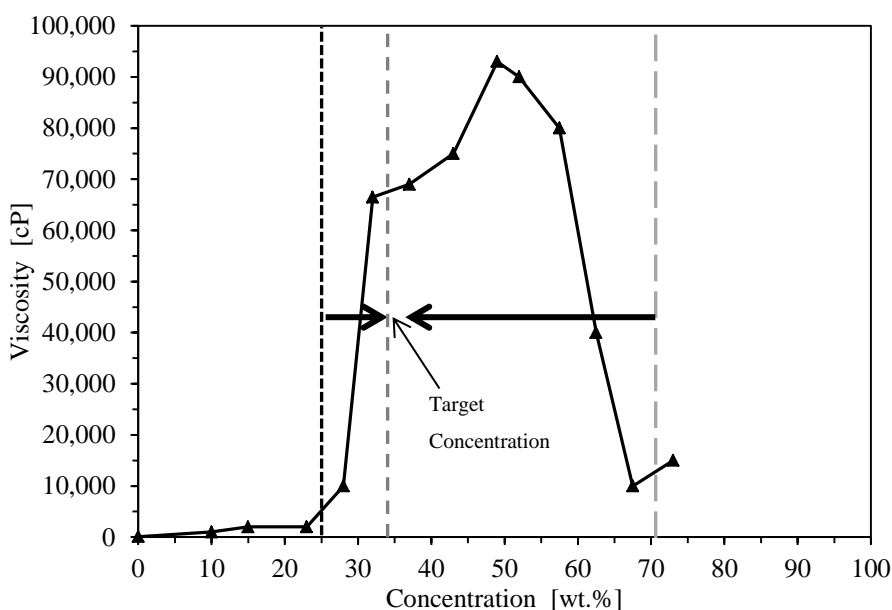


Figure 6.1: Schematic describing the concept of “split-stream,” emulsification, where emulsions comprising PJ stabilised with 25wt.% SLES were brought together with streams comprising 70wt.% SLES (adapted from Technical document 7).

Section 6.2.2 provides the methodology for the described experiments and Figure 6.2 provides a schematic of the equipment setup. Changes in composition and domain size diameter during the experimental study. Samples were collected periodically during the experiment and measured using methods (described in Chapter 4, section 4.2.2 and section 4.2.4). A full data-set for studies reported here may be found in the Appendix, section AX4.1. The approach, illustrated in Figure 6.2, enabled formation of concentrated emulsions while maintaining the PJ:SLES mass ratio, which prevented the formation of viscous SLES intermediate phases up until the coarse pre-mixes were combined.

A number of limitations were observed during these experiments. Firstly, the apparatus did not promote effective distribution of the viscous emulsion. Therefore, selecting a method that distributes the batch effectively may further promote stress transfer of the emulsion intermediate. Further, the experiment did not allow for accurate control of mixture temperature, which relied on heating separate oil baths to temperatures above 60°C.

The split-stream emulsification approach was applied in studies on the Formax™. Further, the purpose of the experiment was to provide process insights for melt emulsification of PJ/SLES compositions and to determine the impact of PJ fraction on emulsification efficiency. The Formax™ was useful as it provides systematic process control through metered addition of ingredients, accurate control of operating temperature and process conditions. The experimental methods used in studies are described in Section 6.2.3 and Figure 6.3.

Due to the limited availability of the equipment, the impeller type was not studied. Further work may consider the impact of using dissolver disks and rotor-stator type impellers on split-stream emulsification on the Formax™. Further, only one of the processes was repeated successfully due to technical difficulties on the apparatus. Again, access limitations prevented further repeats of experiments. The repeat dataset presented in Appendix, section AX4.2, shows the variation in droplet size

distribution for a 79.5wt.% PJ fraction, collected at different points of the mixing vessel. Further work should aim to repeat these processes to provide further information of the experiment reliability.

To negate the limitations observed in bench-top studies, the mixing vessels were installed with rotating baffle attachments to promote bulk mixing of the material. During experiments, the baffles rotated at the perimeter of the vessels at a speed of 50 RPM which prevented the material from stagnating at vessel walls. Further, heated dispersion cartridges were employed to prevent freezing of the material within the cartridge; collection and delivery of “pre-mix B,” by the Formax™ to the mixing vessels has been described in Chapter 4, Figure 4.13. Samples were collected after experiment and measured using methods described in Chapter 4, section 4.2.2 and section 4.2.4.

The results of experiments are summarised in Figure 6.4 and describe experiments performed at a set N of 4000 RPM and at a PJ:SLES mass ratio of 10:1, with varying final PJ fraction (71.4wt.% vs. 74.6wt.% vs. 77.3wt.%) and process temperature (60°C vs. 70°C). Furthermore, Figure 6.5 describes the effects of mixer speed (1000 RPM vs. 4000 RPM), final oil fraction (77.3wt.% vs. 79.5wt.%) and operating temperature (60°C vs. 70°C) on domain size distribution. The results indicate a general decrease in droplet diameter with increasing oil fraction, which supports findings described in Chapter 5 (section 5.3.1). This may be attributed to several changes in formulation; the first consideration is the spatial positioning of droplets. The majority of the emulsions formed from experiments may be described as highly concentrated, exhibiting dispersed phase volume fractions at or above the maximum packing fraction of monodisperse spheres (74.0vol.%). As per findings described by Tcholakova et al. (2011), this leads to droplet break-up mechanisms by microstructure instability. Furthermore, increased SLES solution concentration may have improved emulsification, where an increase in PJ fraction between 71.4-77.3wt.% corresponded to higher SLES solution concentrations between 25.0-34.0wt.%.

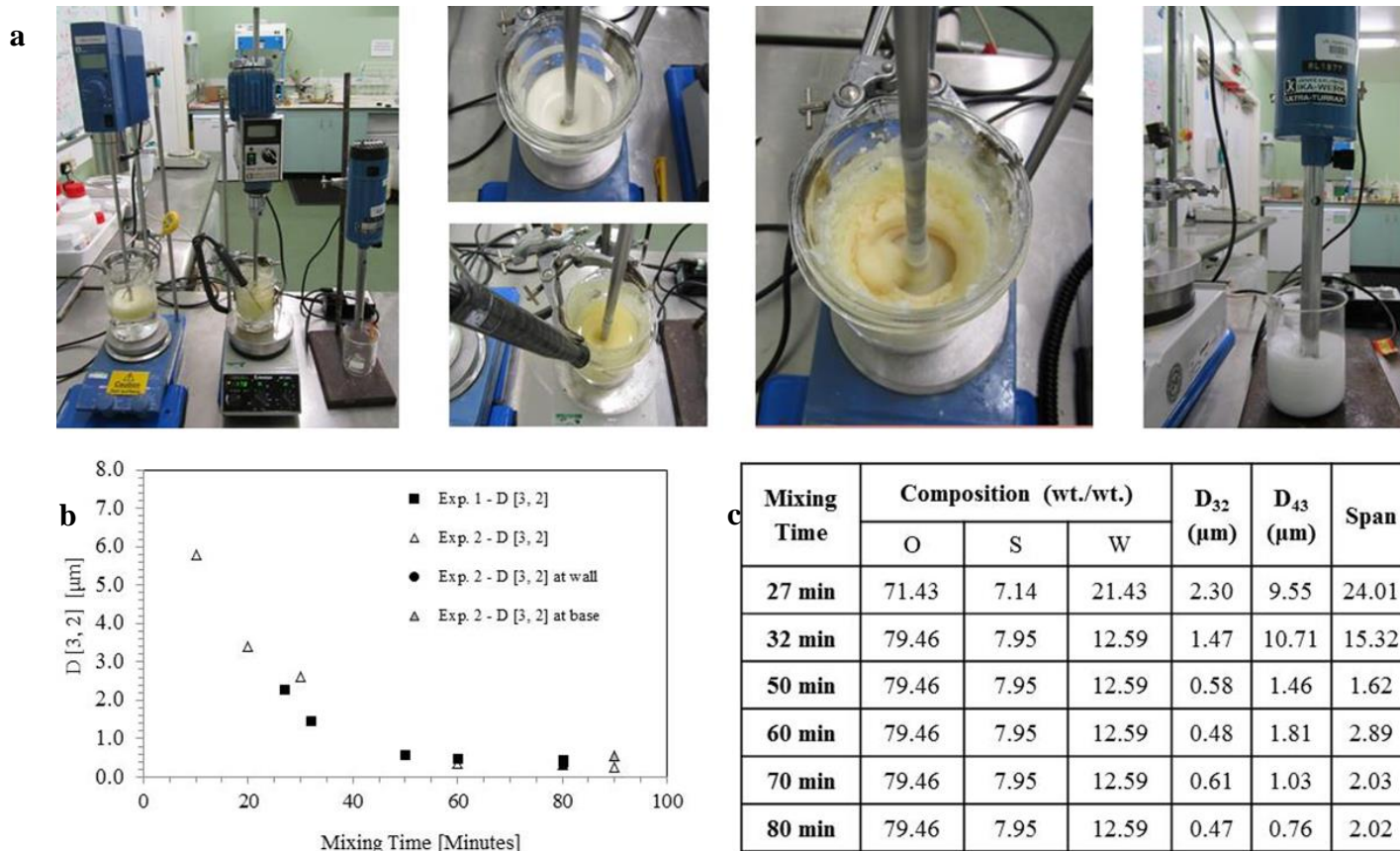
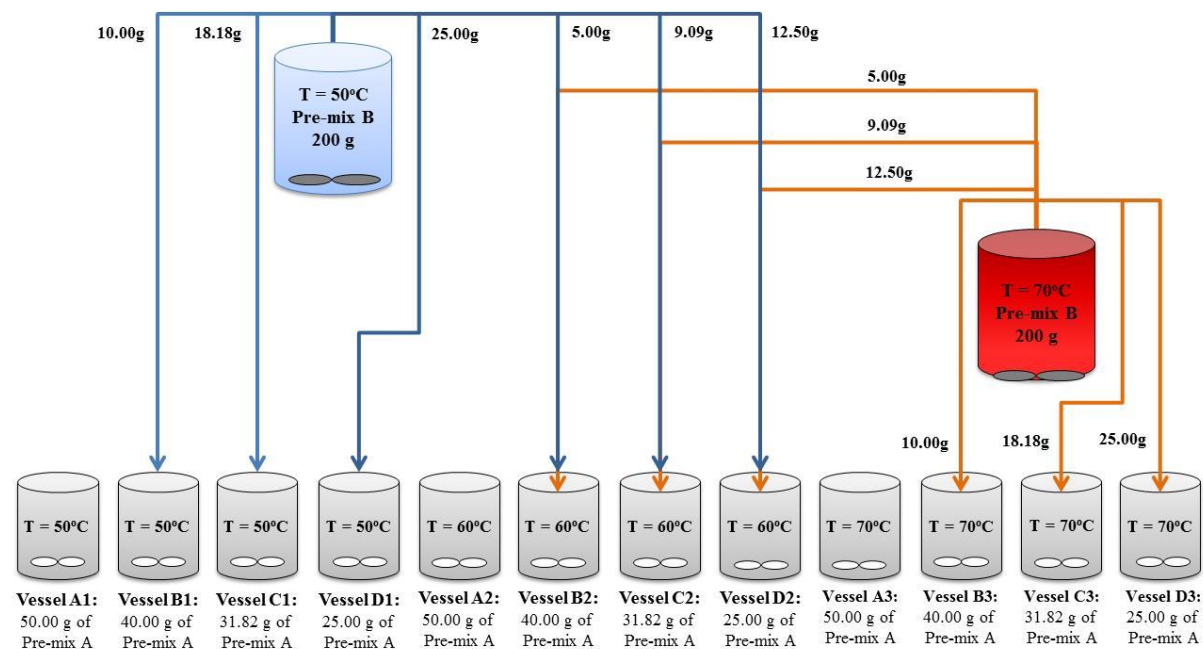


Figure 6.2: Images demonstrating split-stream emulsification approach on the bench, including a) Experimental setup b) Results of d_{32} vs. mixing time and c) Emulsion compositions, operating conditions and droplet size results.



Emulsion Compositions	PJ	SLES	Water	Design of Experiments	
Pre-Mix A Composition (wt. %):	71.43	7.14	21.43	Mixer Type:	Dissolver Disk
Pre-Mix B Composition (wt. %):	87.50	8.75	3.75	Mixer Speed (RPM):	1000, 4000
Final Composition of A1, A2, A3 (wt. %):	71.43	7.14	21.43	Final Emulsion Mass (g):	50.00
Final Composition of B1, B2, B3 (wt. %):	74.64	7.46	17.89	Operating Temperatures (°C)	50, 60, 70
Final Composition of C1, C2, C3 (wt. %):	77.27	7.73	15.00	Total Mixing Time (min)	30
Final Composition of D1, D2, D3 (wt. %):	79.47	7.95	12.95	Addition of Pre-mix A to Premix B (min):	60

Figure 6.3: Schematic describing the experimental methodology for "split-stream," emulsification studies on the Formax™.

While a portion of the surfactant was likely held at the O/W interface for surface stabilisation, the SLES solution concentration was indicative of the higher concentration, therefore increased viscosity of the continuous phase. The formed emulsions were considerably above the CMC of SLES, which occurs at around 0.3%. Therefore, it is suggested that an increase in concentration above the CMC may cause a change in micelle structure of the continuous phase altering the shear behaviour of the fluid. The droplet size reduced with increased mixer speed, which is expected as higher shear was delivered to the system. The strategy was tested via overhead mixers, whose design and operational limits are described in the Appendix, section AX2.8 and section AX2.9.

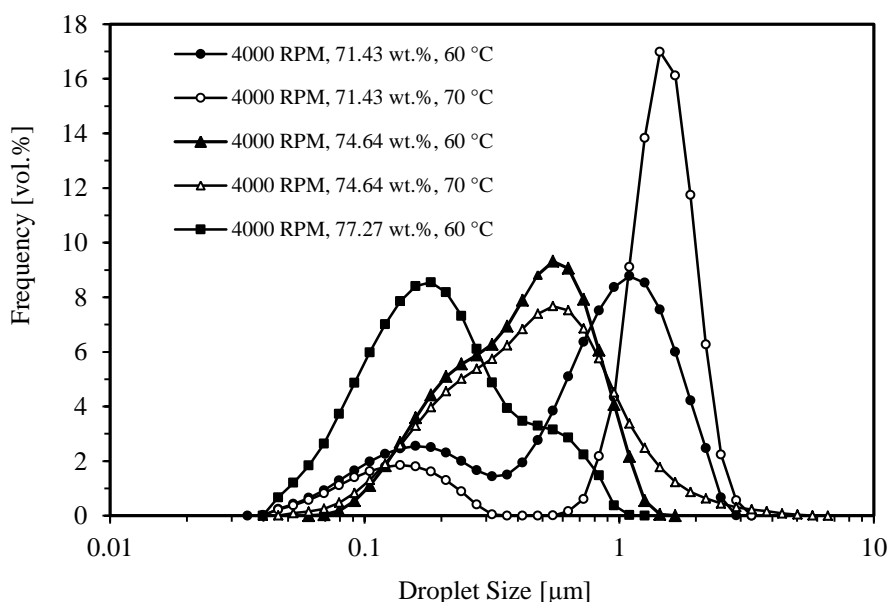


Figure 6.4: Droplet distributions of O/W dispersions, comprising PJ and SLES of varying quantities, processed on the Formax™ Platform as per methods described in Figure 6.3.

Finally, a key finding of studies indicated the importance of minimum mixing temperature as all experiments performed at temperatures below 60°C failed to emulsify. This finding is likely to be a result of PJ melting point; as a material containing multiple length hydrocarbons it exhibits a melting point range between 38.3-60°C (Technical document 8).

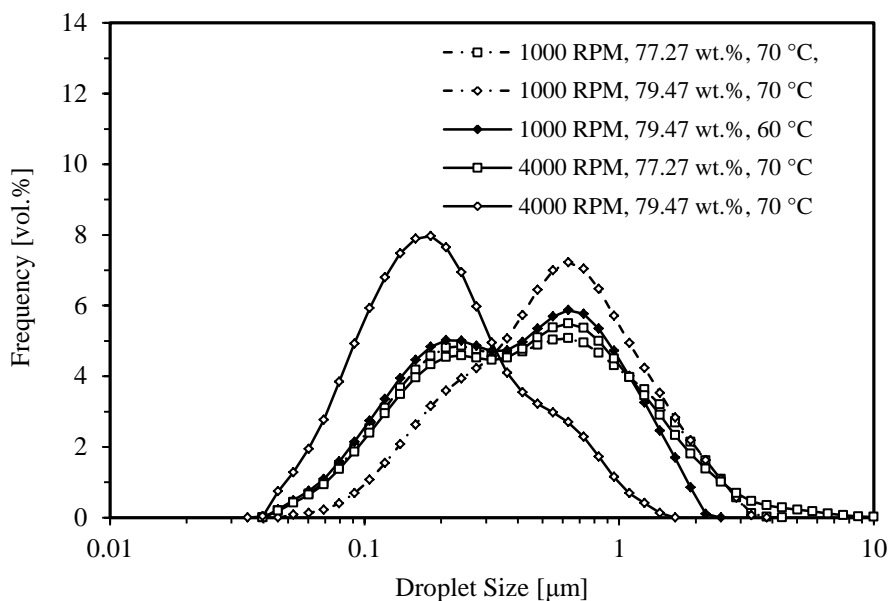


Figure 6.5: Droplet distributions of O/W dispersions, comprising PJ and SLES of varying quantities, processed on the Formax™ Platform as per methods described in Figure 6.3.

6.3.2 FDM Studies

The experiments reported in this section aim to validate the findings from the Formax™ studies, described in section 6.3.1.

The experimental results of Formax™ studies provide support to the experimental findings described in Chapter 5 (section 5.3.1, section 5.3.2 and section 5.3.4) which indicated that efficient emulsification of emulsions comprising of PJ:SLES ratios of 10:1. These findings were attributed to an improved stress transfer by reduced droplet spacing, as well as increased surfactant concentration. While the Formax Platform™ provides a systematic method for melt emulsification, the approach to emulsion formation should consider the scale at which the emulsions are produced.

In some instances, methods required the use of both 25wt.% and 70wt.% SLES solutions to achieve the required PJ:SLES mass ratio, the relative quantities of each ingredient were determined by Equations 6.1 and 6.2.

$$M_{s,LC} = \frac{M(1-f_d)(C_T - C_H)}{(C_L - C_H)} \quad (6.1)$$

$$M_{s,HC} = \frac{M(1-f_d)(C_T - C_L)}{(C_H - C_L)} \quad (6.2)$$

Where $M_{s,LC}$ is the mass of low concentration surfactant, $M_{s,HC}$ is the mass of high concentration surfactant, M is the total emulsion mass, f_d is the mass fraction of dispersed phase, C_T is the target concentration, C_H is the high surfactant concentration and C_L is the low surfactant concentration. Further, the distribution of formed emulsions within the mixing apparatus is described in the Appendix (section AX4.3).

During emulsification, the emulsions were subject to high shear and therefore, a level of viscous heating. In order to determine the impact of viscous heating, experiments were performed to compare the experiment executed without temperature control (analogous to adiabatic operation) against an experiment with forced temperature control (analogous to isothermal operation). Experiments were performed at 6000 RPM. In the forced temperature control experiment, emulsification was temporarily halted to allow the emulsion to return to 65.0°C. At this point, emulsification recommenced for the pre-determined duration. The experiment without temperature control corresponded to the highest temperature rise over the course of the experiment. Samples were collected at similar times to within both studies. Results, described in the Appendix (section AX4.4) indicated little difference in droplet diameter between results.

The strategy was extended to the FDM, which was tested as per methods described in section 6.2.4. The equipment design is provided in Chapter 4 (section 4.7) and a full data-set for studies reported here may be found in Appendix (section AX4.5). Samples were collected periodically and measured using methods described in Chapter 4 (section 4.2.2 and section 4.2.4).

Figure 6.6 presents results describing the change in d_{43} with mixing duration for emulsions, comprising PJ/SLES solutions of set PJ/SLES weight ratios. Generally,

the results indicate a diminishing reduction in d_{43} with mixing duration. These findings support results described in Figure 6.19, as the droplets asymptote towards a maximum droplet diameter (Tcholokova et al., 2004). The surfactants present in the aqueous phase are held above the CMC at 0.3wt.% and the maximum droplet size is determined by the energy dissipation rates delivered to the system (Vankova et al., 2007).

Results described in Figure 6.6 indicate improved droplet break-up for emulsions with reduced PJ/SLES mass ratios, which is likely to be a result of increased availability of the surfactant for stabilisation of the created interface. Considering results of PJ/SLES mass ratios of 8.33:1, increased oil fraction leads to a reduction in d_{43} .

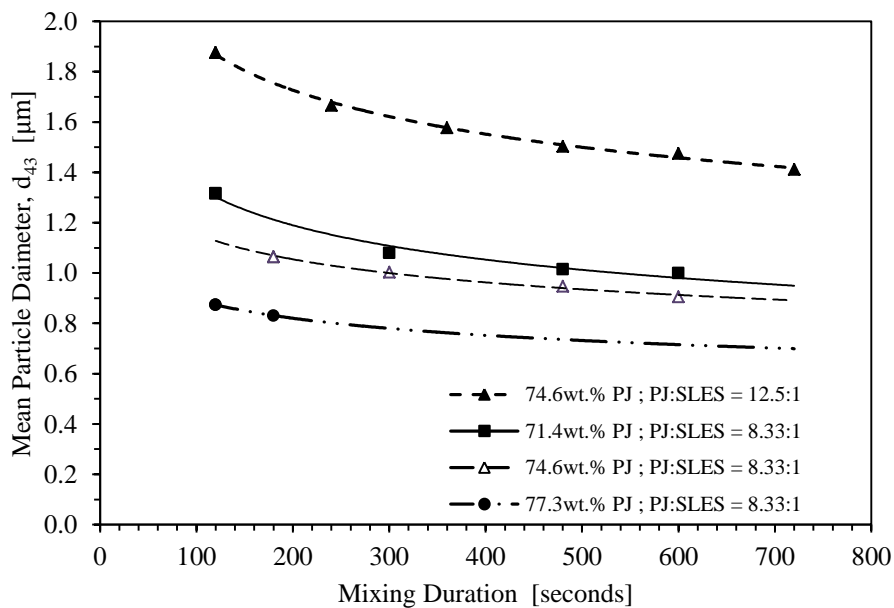


Figure 6.6: Graph describing the effect of mixing duration on mean droplet diameter (d_{43}) for dispersions, comprising PJ/SLES compositions of set O/S ratios, formed by melt emulsification, processed for varying mixer durations at 6000 RPM on the FDM apparatus. The lines of fit indicate the trajectory of the results.

This supports the findings described in section 6.3.1, for emulsions formed on the Formax™ platform, comprising of compositions of set PJ/SLES mass ratios of 10:1.

Despite a constant relative quantity of PJ and SLES, droplet break-up is improved with increased PJ fraction. As described in the Formax™ experimental studies in section 6.3.1, increased dispersed phase fraction reduced the spatial positioning of droplets and increased the concentration of surfactant in the system. As with previous studies described in section 6.3.1, droplet break-up improved with increased oil fraction. Furthermore, the results of studies described in Chapter 5 (section 5.3.1) indicated similar efficient surfactant use for processed SFSO/Pluronic compositions, comprising of set SFSO/Pluronic ratios of 10:1.

6.3.3 CDDM Studies

Building on experiments reported in section 6.3.1 and 6.3.2, the viscosity matching strategy for emulsification of PJ/SLES compositions was extended to emulsification on the Laboratory-scale CDDM.

Operation and design of the CDDM is described in Chapter 4 (section 4.6.2) and the experimental methods applied in studies are outlined in section 6.2.5. As described in section 6.2.5, experimental studies involved the processing of coarse emulsion pre-mixes, which were prepared offline as per methods described in Chapter 4, (section 4.5.1). Samples were collected periodically and measured using methods described in Chapter 4 (section 4.2.2 and section 4.2.4).

Experiments were performed at a 0mm CDDM position, which describes a mixer geometry of near overlap of axially displaced lands. The geometry is discussed in more detail in Chapter 4 (section 4.6). It was found in Chapter 5 (section 5.3.1) that the mixing regime could be manipulated by decreasing the axial displacement of lands positioned on confronting surfaces, which alters the dominant shear type during emulsification. Studies described in this chapter centre on investigating strategies for efficient emulsification, which is considered by reductions in d_{43} and increasing the surface stabilised per mass of surfactant.

The effect of PJ:SLES mass ratio on droplet size distribution for dispersions comprising PJ:SLES ratios of 15:1 and 20:1 is displayed in Figure 6.7. Emulsions

were processed at rotational speed (N) of 10000 RPM and a throughput (Q) of 243 \pm 18 kg/hr. Results indicate a decrease in droplet diameter with increasing PJ at set PJ:SLES mass ratios. These results support findings described in Figure 6.4 and Figure 6.5, for emulsions with compositions comprising of PJ:SLES mass ratios of 10:1, which were processed on the Formax™. They also support results reported in Figure 6.6, for emulsions comprising of PJ:SLES mass ratios of 8.33:1 and 12.5:1, processed on the FDM. The effect is attributed to more efficient emulsification through increased stress transfer to the system with higher PJ fraction and SLES concentrations.

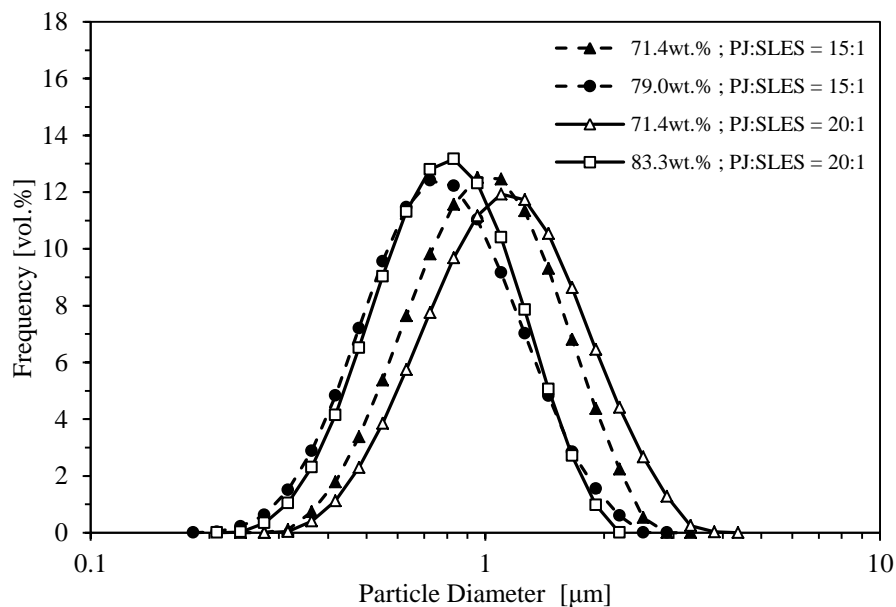


Figure 6.7: Graph describing the impact of PJ fraction on droplet size distributions of emulsions, comprising PJ/SLES compositions of set PJ:SLES ratio (15:1 vs. 20:1), post-processed through the CDDM in a 0mm geometry at static and dynamic conditions at N of 10000 RPM and at Q of 243 \pm 18 kg/hr. The lines of fit indicate the trajectory of the results.

6.3.4 Efficiency Analysis - Viscosity Matching Strategy (Set O:S Ratio)

The efficiency function, described in Chapter 3 (section 3.2.3) was applied to a number of the results described in section 6.3.1, section 6.3.2 and section 6.3.3. The

results of analysis are displayed in Figure 6.8. The efficiency generally increases with increased dispersed phase fraction. This suggested more efficient emulsification, which can be attributed to increased stress transfer by decreasing the proximity of the dispersed phase droplets and by increasing the surfactant concentration, leading to an increased continuous phase viscosity. However, some insight is gained in comparing results of emulsions formed on the CDDM apparatus. Efficiency analysis indicates more efficient emulsification for formed emulsions comprising PJ:SLES ratios of 20:1 and 15:1 of equivalent dispersed fractions, despite the former relating to higher SLES amounts. This will be explored in more detail in section 6.4. The Formax™ produced emulsions of the highest efficiencies, however were processed at significantly lower Q (50 g/hr).

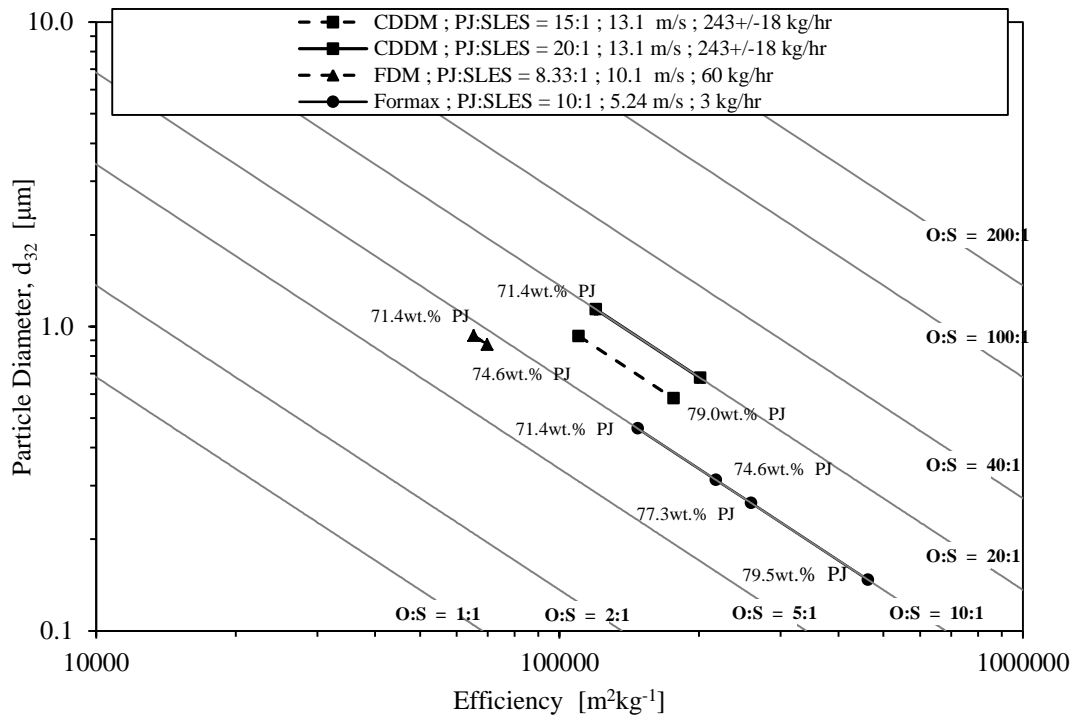


Figure 6.8: Efficiency Graph describing dispersions, comprising PJ/SLES compositions of set PJ:SLES mass ratio (8.33:1, 10:1, 15:1, 20:1), and processed on the Formax Platform (70°C), the FDM and Laboratory-scale CDDM at similar tip speeds and varying Q . The lines of fit indicate the trajectory of the results.

6.4 Results and Discussion - Surface Stabilisation Strategies

These sections reports investigations on “surface stabilisation strategies,” for efficient manufacture of a model O/W system, comprising PJ dispersed in SLES solution and SFSO dispersed in Pluronic solution.

The strategy described here, initially proposed in Chapter 3 (section 3.3.5) aims to improve the efficiency of emulsification by altering the concentration of surfactant solutions used during manufacture.

Subsequent studies on PJ/SLES compositions centred solely on emulsification in cavity-design mixers, which are high shear rotor-stator mixers comprising of confronting surfaces with cavities embedded on each surface. The strategy was tested via FDM, for emulsification of PJ/SLES compositions and via Laboratory-scale CDDM System, for emulsification of PJ/SLES and SFSO/Pluronic compositions. In the studies considered here, the fraction of dispersed phase was set and the ratio of dispersed phase to surfactant was altered.

6.4.1 FDM Studies

The strategy was applied in experimental studies on the FDM, as per methods described in section 6.2.4.

The FDM equipment design has been detailed in Chapter 4 (section 4.7) and a full data-set for studies reported in the current section may be found in the Appendix (section AX4.6). Samples were collected periodically and measured using methods described in Chapter 4 (section 4.2.2 and 4.2.4). In some instances, methods required the use of both 25wt.% and 70wt.% SLES solutions to achieve the required PJ:SLES mass ratio. The relative quantities of each ingredient were determined by equations 6.1 and 6.2.

The FDM is a type of conically shaped cavity-design mixer comprising an internal rotor encased within an outer stator. The FDM's design and operation is outlined in Chapter 4 (section 4.2.5).

The impact of SLES solution concentration on emulsification in the FDM was studied at set PJ fraction (74.6wt%). The emulsion composition was selected so that the formulation was highly concentrated in order to exploit benefits of efficient emulsification observed in previous experiments. However, the PJ fraction was maintained at a sufficiently low level to ensure that all surfactant concentrations could be processed effectively. This is in contrast to emulsions formed at a set mass ratio of O:S, where the increase in SLES concentration occurs alongside an increase in oil fraction, leading to an increased interfacial area at set domain size. Increasing the SLES concentration at fixed PJ fractions not only decreases the weight ratio of oil to surfactant but also changes the aggregate behaviour of the surfactant.

Figure 6.9 describes the change in d_{43} with mixing duration for emulsions processed at different SLES solution concentrations. Emulsions comprising low SLES solution concentrations (9.82wt.%) lead to the largest change in droplet diameter with mixing. However, emulsions comprising high SLES solution concentrations (28.2wt.%) tend to approach a minimum size earlier than low SLES concentrations. The decrease in droplet diameter is perhaps better presented in Figure 6.10, which describes the change in d_{43} with SLES concentration, for emulsions processed for different mixing durations. The results indicate reduced but diminishing d_{43} with increasing SLES solution concentration. This is likely to be due to increased availability of surfactant on surface creation, leading to improved stabilisation of dispersed droplets. Further, the decrease in droplet size between 30 and 120 seconds is far more significant than achieved for processing times between 120 seconds and 480 seconds, indicating that most of the droplet break-up occurs within the first 120 seconds of emulsification. This may be due to depletion of available surfactant with processing, analogous effects described in multiple-pass studies, described in Chapter 5 (section 5.3.2).

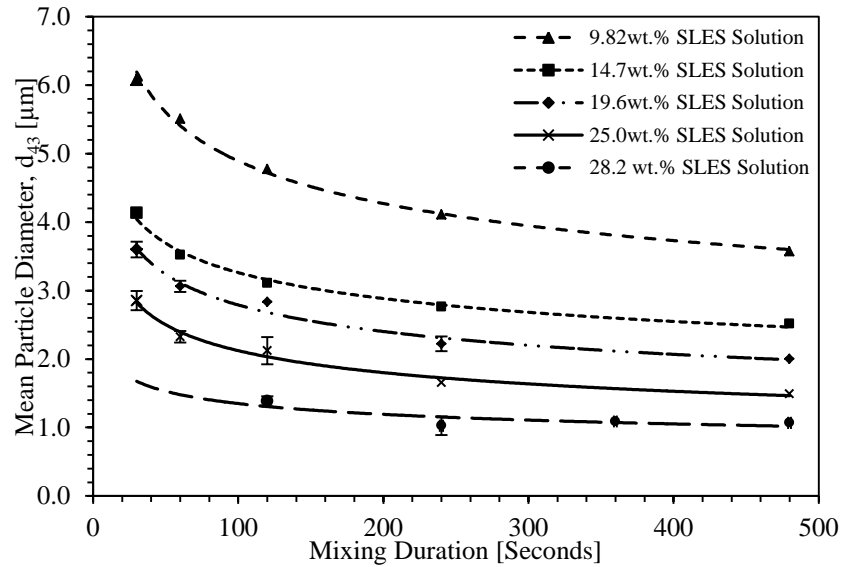


Figure 6.9: Graph describing the effect of mixing duration on mean droplet diameter (d_{43}) for dispersions comprising 74.6wt.% PJ and SLES solutions of varying concentration, formed by melt emulsification and processed for varying mixer durations, at N of 6000 RPM on the FDM apparatus. The lines of fit indicate the trajectory of the results.

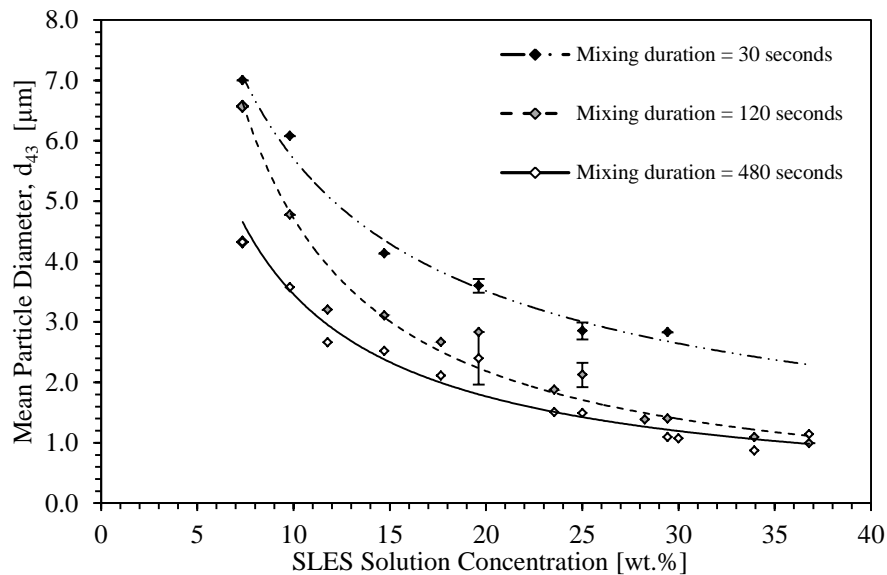


Figure 6.10: Graph describing the change in mean droplet diameter (d_{43}) with mixing duration, for dispersions comprising 74.6wt.% PJ and SLES solutions of varying concentration, formed by melt emulsification and processed for varying mixer durations at 6000 RPM on the FDM apparatus. The lines of fit indicate the trajectory of the results.

Further insight is gained by analysing the change in A_d with SLES solution concentration, for emulsions processed at increasing mixer durations. The results are described in Figure 6.11, as expected; the A_d increases with increasing SLES solution concentration. Interestingly, the rate of change of A_d with concentration increases as the concentration exceeds 21% by weight, indicating improved stress transfer for emulsions comprising ~21wt.% SLES solution. The effect is extenuated with increased mixing duration, therefore indicating improved benefits in further processing of emulsions comprising concentrated SLES solutions.

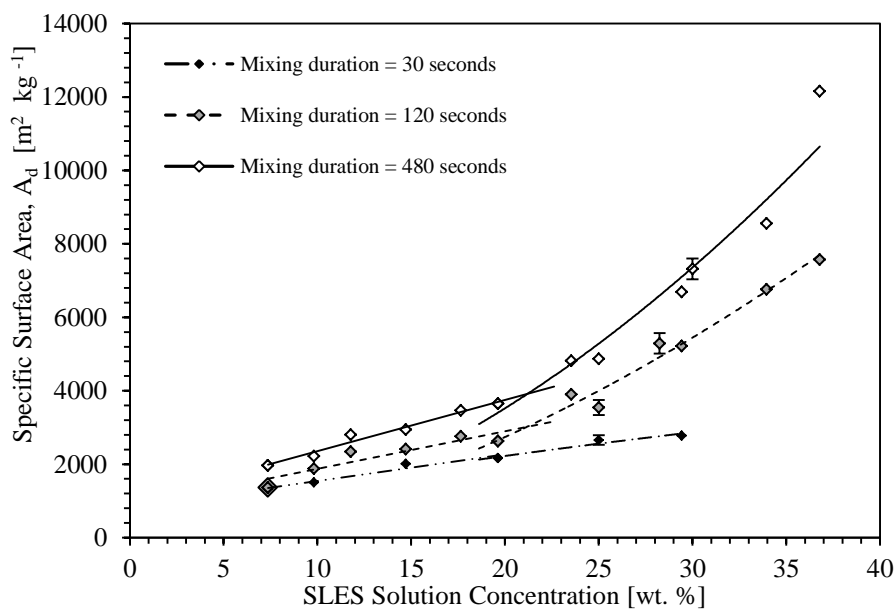


Figure 6.11: Graph describing the change in specific surface area (A_d) with mixing duration, for dispersions comprising 74.6wt.% PJ and SLES solutions of varying concentration, formed by melt emulsification and processed for varying mixer durations, at N of 6000 RPM on the FDM apparatus. The lines of fit indicate the trajectory of the results.

These results are unexpected and were not observed in previous experiments. It was expected that the A_d would be greater for emulsions with higher SLES concentration. However, the emulsification efficiency should consider how efficiently the surfactant is used. For the “surfactant-rich,” emulsions processed in these studies, it was essential that the efficiency function was considered at set PJ fraction.

Figure 6.12 displays the efficiency function with SLES concentration for emulsions, comprising 74.6wt.% PJ and SLES solutions of varying concentration, processed for mixer durations of 60 seconds and 240 seconds. Emulsions processed for 240 seconds indicated a minimum initial SLES solution concentration of around 21wt.%, which is similar to the point where a change in gradient in specific surface area is found in Figure 6.11. The latter finding, which created emulsions with the highest interfacial area, is in line with results found in the viscosity matching strategies, where increasing oil fractions at set O:S led to higher efficiencies (Figure 6.8). Further, emulsions processed for longer periods (i.e. 240 seconds) indicated benefits of efficient surfactant use for emulsions processed for longer mixing durations, similar to results observed in Figure 6.11.

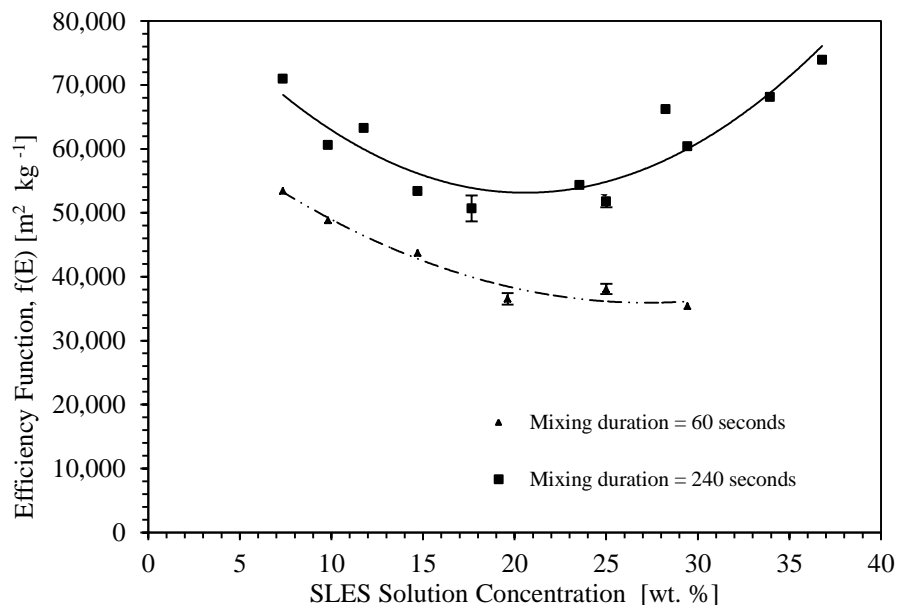


Figure 6.12: Graph describing the change in efficiency function ($f(E)$) with SLES solution concentration, for dispersions comprising 74.6wt.% PJ and SLES solutions of varying concentration, formed by melt emulsification and processed for varying mixer durations, at N of 6000 RPM on the FDM apparatus. The lines of fit indicate the trajectory of the results.

While efficient emulsification was observed for emulsions processed at high concentration, efficient formation of large diameter emulsions was not observed

previously. Table 6.1 provides details of viscosity measurements performed at 65+/-1°C for PJ and SLES solutions, measured on the HAAKE™ Rheostress Rotational Rheometer (Thermo-scientific, United States).

Table 6.1: Table describing the apparent viscosities of PJ, SLES solutions and SLES/Water/Glycerol mixtures, measured at 65+/-1°C using the Rheostress Rheometer. Further information is provided on the viscosity ratio between dispersed and continuous phases, which decreases with increasing SLES solution concentration.

Material	Equivalent Water Fraction (74.6wt.% PJ)	Viscosity @ 65°C (cP)	Viscosity Ratio @ 65°C
Petroleum Jelly	0wt.%	16.71 +/- 0.03	-
7.36wt.% SLES Solution	23.49wt.%	0.89	18.88
9.81wt.% SLES Solution	22.87wt.%	1.02	16.38
14.7wt.% SLES Solution	21.63wt.%	1.58	10.58
19.6wt.% SLES Solution	20.38wt.%	2.33	7.17
23.3wt.% SLES Solution	19.44wt.%	4.46	3.74
25.0wt.% SLES Solution	19.02wt.%	7.72	2.16
27.3wt.% SLES Solution	18.44wt.%	24.92	0.67
29.5wt.% SLES Solution	17.88wt.%	98.00	0.17
50% of 20wt.% SLES Solution, 50% of Glycerol	40wt.%	4.84	3.45

Analysis of the results for fixed oil fraction (74.6wt.% PJ), described in Figure 6.12, shows that the efficiency decreased between SLES solution concentrations of 7.36-19.6wt.% and efficiency increased between SLES solution concentrations of 19.6-29.5wt.%. Considering the viscosity ratios of PJ and SLES solutions, described in Table 6.1 and, with reference to the Grace Curve (Grace, 1982) the apparent viscosity ratios of SLES solutions below 19.6wt.% are above 5:1, which describes the limit where simple shear no longer impacts on the critical capillary number. While the FDM does not completely describe simple shear, the mixer comprises a static surface opposing a rotating surface which may be analogous to this method for droplet break-up. Therefore, for a low SLES concentration system, the ability of the mixer to deliver stress and create surface may be lowered. This is supported by a reduced efficiency observed between SLES solution concentrations of 7.36-19.6

wt.%, which may be attributed to an increased droplet capillary pressure. However, it is noted that the system corresponds to a HIPE. The studies reported by Jansen et al. (2001) indicate a relationship between viscosity ratio and critical capillary number for simple shear, where the viscosity of the continuous phase is considered as the emulsion viscosity. Despite this, an increase in the surfactant viscosity may contribute to droplet break-up.

The effect of viscosity ratio was studied in the following way; experiments were performed to match the viscosity of a 23.3wt.% SLES solution with a aqueous mix, comprising 50wt.% glycerol and 50wt.% of 20wt.% SLES solution. Emulsions comprised of a PJ fractions of 74.6wt.% and were processed on the FDM apparatus. The results of experiment are outlined in Figure 6.13.

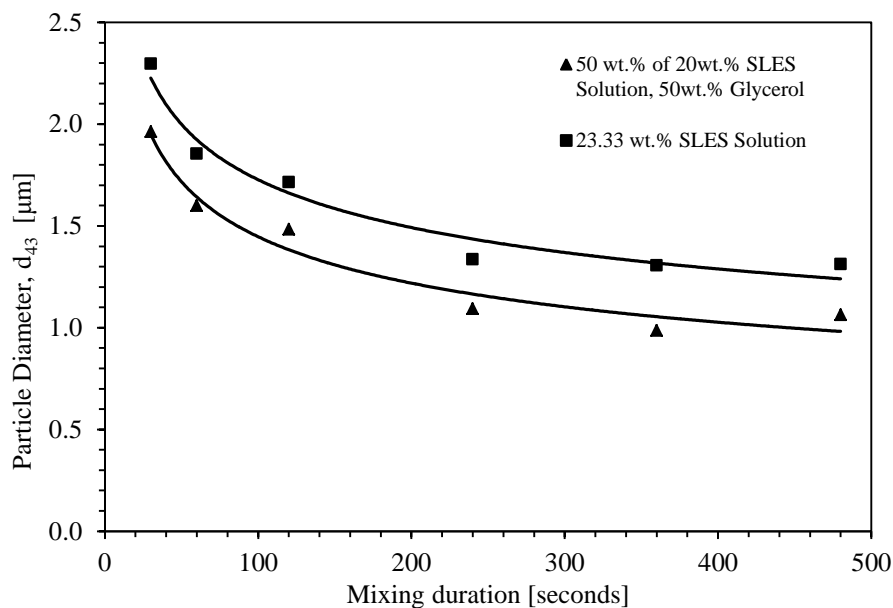


Figure 6.13: Graph showing the change in mean droplet diameter (d_{43}) with mixing duration for emulsion, comprising PJ dispersed in 23.3wt.% SLES solution and PJ dispersed in a glycerol/SLES mix similar in viscosity to 23.3wt.% SLES solution. Emulsions were formed by melt emulsification, at 6000 RPM on the FDM. The lines of fit indicate the trajectory of the results.

The results showed that the presence of glycerol significantly improves droplet break-up with processing time. This may be due to several reasons, firstly a more substantial reduction in continuous phase viscosity on processing emulsions comprising of a 23.3wt.% SLES solution versus systems with glycerol present. Secondly, the presence of glycerol may have lowered the surface tension of the system. As described by Tcholakova et al. (2004), for systems with surfactant concentrations above the CMC, the maximum droplet diameter is determined by the energy input, in the form of shear stress, to the system. Therefore, if the mixer is able to deliver greater stress to the system, the consequence may be increased droplet dispersion.

6.4.2 CDDM Studies

FDM studies on the surface stabilisation strategy, described in section 6.4.1, were extended for emulsification on the Laboratory-scale CDDM.

The effect of concentration is described in Figure 6.14, which shows 71.4wt.% Petrolatum in 12.5wt.% and 25.0wt.% SLES solutions, processed at N of 10000 RPM at low Q (55.7 \pm 7.0kg/hr) and high Q (123 \pm 2 kg/hr). As expected, increased concentration leads to improved droplet break-up, due to increased availability of surfactant on surface creation. Further, the results showed some benefit from processing at higher Q and thus extension. Figure 6.14b describes results for 78.9wt.% PJ and 12.5wt.%, 25.0wt.% and 37.5wt.% SLES solutions, processed at 10000 RPM at low Q (51.9 \pm 4.9 kg/hr) and high Q (228 \pm 3 kg/hr). The particle size distributions of processed emulsions indicate decreasing size distribution with increasing SLES concentration. Again, this is attributed to increased availability of surfactant on droplet disruption. The effects of processing on emulsions droplet size distribution are similar at low and high Q .

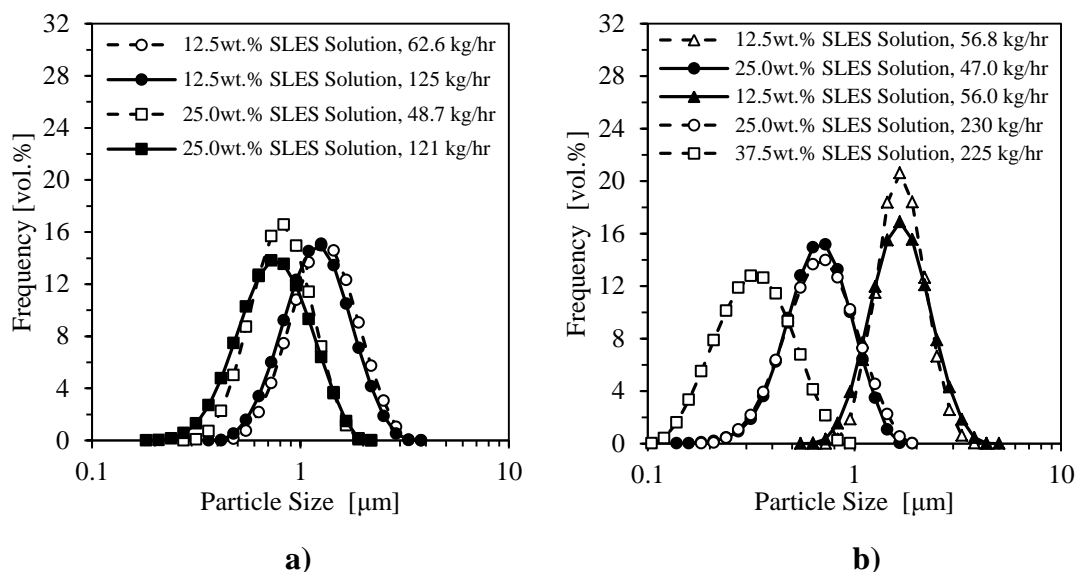


Figure 6.14: Graph describing the impact of dispersed mass fraction on droplet size distribution of PJ/SLES emulsions, comprising PJ dispersed in SLES solutions of 12.5wt.% and 25.0wt.% concentration, post-processed through the CDDM in a 0mm geometry at static and dynamic conditions at Q of **a)** 55.7 \pm 7.0 kg/hr and 123 \pm 2 kg/hr and **b)** 51.9 \pm 4.9 kg/hr and 228 \pm 3 kg/hr.

Effect of SLES/Glycerol Compositions

Emulsification strategies incorporating glycerol/SLES aqueous phases were studied. This approach was developed during the FDM studies, described in section 6.4.1 and shown in Figure 6.13, where the effect of continuous phase viscosity was tested for emulsions comprising of PJ dispersed in 23.3wt.% SLES solution and PJ dispersed in a glycerol/SLES solution mixture. The results indicated more effective emulsification for compositions containing glycerol, despite both systems comprising similar continuous phase viscosities.

For emulsification studies performed on the Laboratory-scale CDDM, pre-mixes of equal PJ fraction (79.0wt.%) and equal PJ:SLES mass ratios (30:1) were created. However, compositions without glycerol, comprised of PJ dispersed in 12.5wt.% SLES solution, and compositions with glycerol systems, comprised of PJ dispersed in a glycerol/SLES mixture of equal parts of 25wt.% SLES solution and glycerol. The results of experiment, as summarised in Figure 6.15 a) and Figure 6.15 b),

compared emulsion d_{43} and A_d for PJ/SLES and PJ/SLES/glycerol compositions processed at low Q (59.4+/-4.0kg/hr) and high Q (254kg/hr) and various mixer speeds (0-15000 RPM), respectively.

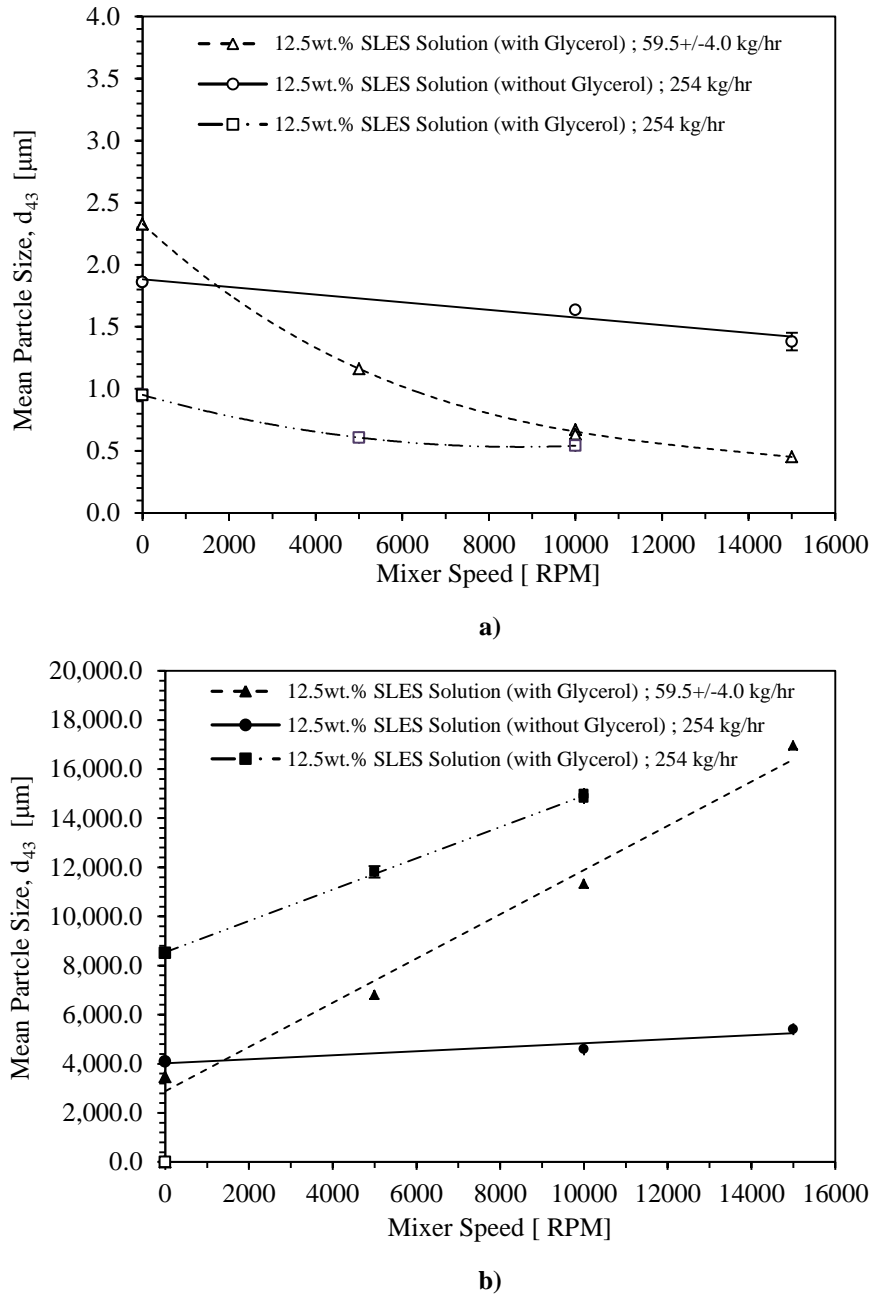


Figure 6.15: Graph describing the impact of mixer speed on **a)** mean particle size (d_{43}) and **b)** specific surface area (A_d) for PJ/SLES emulsions comprising PJ dispersed in SLES solution and PJ dispersed in a SLES/Glycerol solution, at PJ:SLES mass ratios of 30:1, post-processed on the Laboratory-scale CDDM at a 0mm position at various mixer speeds, at low Q (59.4+/-4.0kg/hr) and high Q (254kg/hr). The lines of fit indicate the trajectory of the results.

The results showed that processed emulsions containing glycerol have significantly reduced droplet diameters. Furthermore, this effect is extenuated by increased Q and therefore, extensional shear. Surprisingly, A_d shows a near linear correlation with rotational speed for all compositions studied.

Effect of Continuous Phase Surfactant Concentration

In experiments described within the current section outline the comparison of the emulsification of PJ/SLES compositions and SFSO/Pluronic composition are compared. Both systems comprise of viscous continuous phases.

Figure 6.16 describes the effect of N on d_{43} and A_d for emulsions, comprising of 80.0wt.% SFSO in 23.3wt.% Pluronic solution and a 79.0wt.% PJ fraction stabilised in 25.0% SLES solution. Considering results describing 80.0wt.% SFSO emulsions, results indicated a reduction in d_{43} with increased mixer speed.

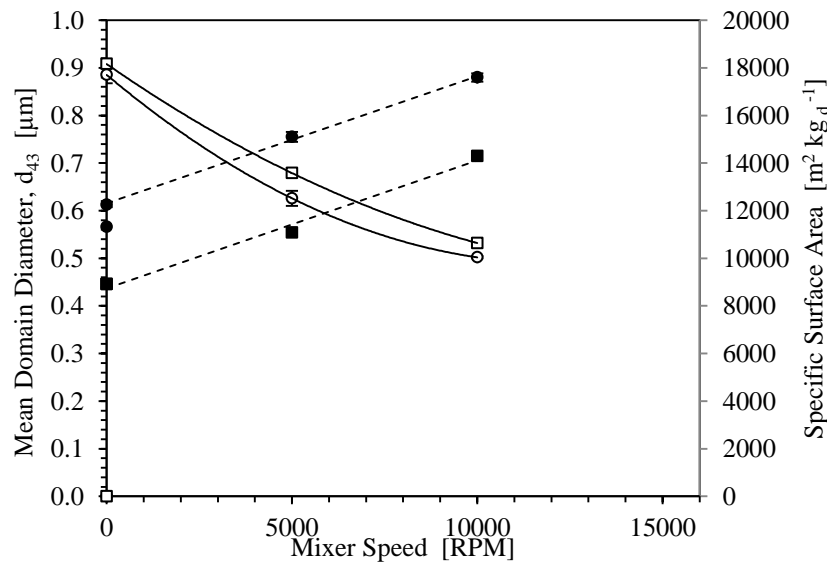


Figure 6.16: Graph describing the impact of mixer speed on mean domain size (d_{43}) and specific surface area (A_d) of emulsions, comprising SFSO in 23.3wt.% Pluronic solution and PJ in 25.0wt.% dispersed in SLES solution, post-processed on the CDDM at a 0mm position at mixer speeds of 0, 5000 and 10000 RPM and Q of 210 +/- 16 kg/hr (SFSO/Pluronic) and 236 +/- 13 kg/hr (PJ/SLES). The lines of fit indicate the trajectory of the results.

Unexpectedly, a near linear increase in A_d was observed with mixer speed. Similar results are found between analysed formulations. The results described here are analogous to experimental studies incorporating SLES/glycerol compositions, where an increase in continuous phase viscosity resulted in emulsions formed with significantly lower d_{43} and significantly higher A_d . The difference in the results may be due to variations in viscosity ratio between dispersed and continuous phases of the studied systems, as described in Table 6.2.

Table 6.2: Table describing the apparent viscosities of 25.0wt.% SLES solution, measured at 65+/-1°C and Pluronic solutions, measured at 20+/-1°C. Further, results describing the apparent viscosity ratios of PJ/25.0wt.% SLES solutions, measured at 65+/-1°C and SFSO/23.3wt.% Pluronic Solutions, measured at 20+/-1°C.

25.0wt.% SLES Solution at 65+/-1°C	7.72 cP
23.3wt.% Pluronic F68 at 20+/-1°C	83.33 +/- 11 cP
Viscosity ratio – PJ / 25.0wt.% SLES solution at 65+/-1°C	2.10
Viscosity ratio – SFSO / 23.3wt.% Pluronic solution at 20+/-1°C	0.62

6.4.3 Efficiency Analysis – Surface Stabilisation Strategies

The efficiency function was applied to a number of the results described in section 6.4.1 and section 6.4.2. These results are displayed in Figure 6.17.

The results generally show a transition in efficiency with surfactant concentration. For FDM studies, results indicate that emulsions of low concentration are high in efficiency, which decreases with increasing SLES concentrations. However, the droplet size generally decreases with increasing SLES concentration from 7.36wt.% to 19.6wt.% (Figure 6.11). The decrease in efficiency is attributed to an increase in capillary pressure, as formed droplets get smaller, higher levels of shear is required to deform them. At set processing the surface created may not be reflective of the amount of surfactant in the system. However, considering results for low Q (7.5kg/hr), emulsions are processed for longer and observe a higher efficiency when SLES solution concentrations were between 19.6-36.8wt.%. The increase in efficiency is attributed to the build in viscosity of the continuous phase which, it is proposed, leads to improved stress transfer. A more effective droplet disruption

increases the surface available for stabilisation by surfactants therefore, promoting more efficient emulsification. However, this does not occur at high Q and Figure 6.12 indicates that the effect is time dependent, which may be due to the time taken for the surfactant to form aggregate phases. Similar results are observed for emulsions processed on the CDDM (section 6.4.2), which showed an increase in efficiency with increased surfactant concentration.

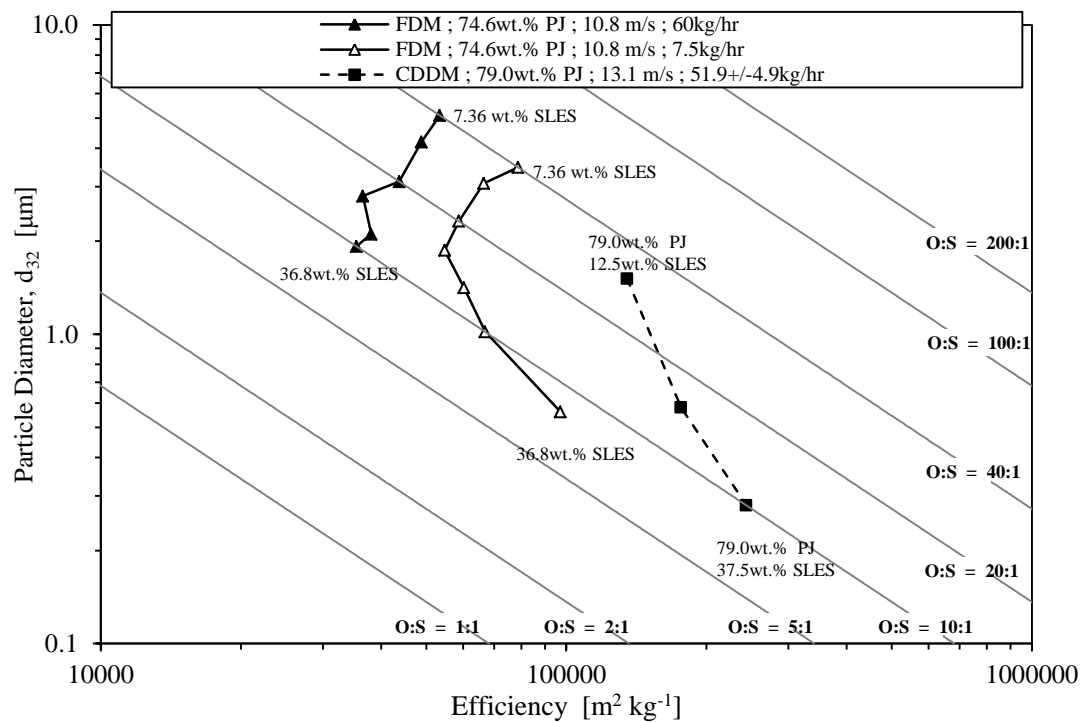


Figure 6.17: Efficiency Graph describing dispersions, comprising PJ/SLES compositions of set PJ fraction and varying SLES concentration, processed on the FDM and Laboratory-scale CDDM at similar tip speeds and varying Q . The lines of fit indicate the trajectory of the results.

6.4.4 Further Discussion of Results

It is known that surfactants are required in monomer form to stabilise an interface. It is also apparent that surfactant solutions would comprise a varied structure of SLES in solution, comprising of proportions. This point is summarised well by Patist et al. (2002), who makes the following two statements:

"The efficiency of interfacial coverage with emulsifiers, when the interfacial area is increased by drop deformation and break-up during dispersion processing strongly depends on the adsorption kinetics of emulsifier molecules at the interface."

"The emulsifier adsorption has to be considered in the context of four different steps: Emulsifier de-micellation in the bulk fluid (1), diffusive/convective transport to the interface (2), interfacial adsorption (3) and structural changes (4)."

Stabilising a created interfacial surface requires surfactants in a monomer form. Therefore, for a system comprising of high surfactant concentrations, this may require dissolution of surfactant aggregates to a monomer form, which may be rate limiting. On the other hand, studies by Tcholakova et al. (2004) indicated that for systems with surfactant concentrations below the CMC, the final droplet size was dominated by amount of surfactant available. However, for solutions above the CMC, the maximum droplet diameter was determined by the energy input to the system and a minimum surface coverage. Therefore, it is proposed that if the energy to the system does not increase significantly, the efficiency of emulsification will decrease. A model used to describe the efficiency of emulsification is outlined in Figure 6.18 and the below text (i.e. bullet points).

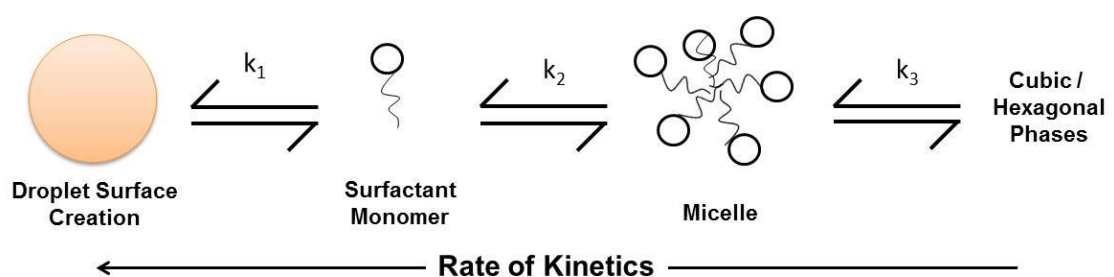


Figure 6.18: Image describing the kinetics for stabilisation of created interfaces, for surfactants held in aggregate form.

- Low surfactant concentration (0% to 5%) = high proportion of monomer phase, low stress transfer, low kinetics rate.
= large droplet size, high surfactant efficiency.
- Medium surfactant concentration (5% to ~15%)
= medium monomer phase proportion, low stress transfer, low/medium kinetics rate.
= medium droplet size, low emulsification efficiency.
- High surfactant concentration (~15% to 25%)
= low monomer phase proportion, medium stress transfer, medium kinetics rate.
= small droplet size, medium emulsification efficiency.
- Very high surfactant concentration (>25%)
= very low monomer phase proportion, high stress transfer, high kinetics rate.
= very small droplet size, high emulsification efficiency.

6.5 Results and Discussion - HIPE strategy

These sections report investigations on HIPE strategies for efficient manufacture of a model O/W systems, comprising PJ dispersed in SLES solution and SF50 dispersed in Pluronic solution.

The strategy described here was initially proposed in Chapter 3 (section 3.3.6) and aims to improve the efficiency of emulsification by raising the dispersed phase fraction at a set surfactant concentration. Further, experimental findings described in Chapter 5 (section 5.3.1, section 5.3.2 and section 5.3.3) indicated opportunities for efficient emulsion manufacture for emulsions comprising of concentrated surfactant solution.

6.5.1 FDM Studies

The strategy was applied in experimental studies on the FDM, as per methods described in section 6.2.3.

The equipment design was provided in Chapter 4 (section 4.7). A full data-set for studies reported in the present section may be found in the Appendix (section AX4.7). Samples were collected periodically and measured using methods described in Chapter 4 (section 4.2.2 and section 4.2.4).

Figure 6.19 presents d_{43} as a function of mixing duration at various phase volumes. Results describing emulsions stabilised with 25.0wt.% SLES solution indicate significantly improved droplet break-up with increasing oil fraction. On comparison, the results of emulsions dispersed 30wt.% SLES solution indicate a diminished reduction in d_{43} with increasing oil fraction. Furthermore, the change in droplet diameter with mixing duration appears to be significant, indicating that formed emulsions are approaching maximum stable droplet diameters sooner than emulsions formed with 25.0wt.% SLES solution.

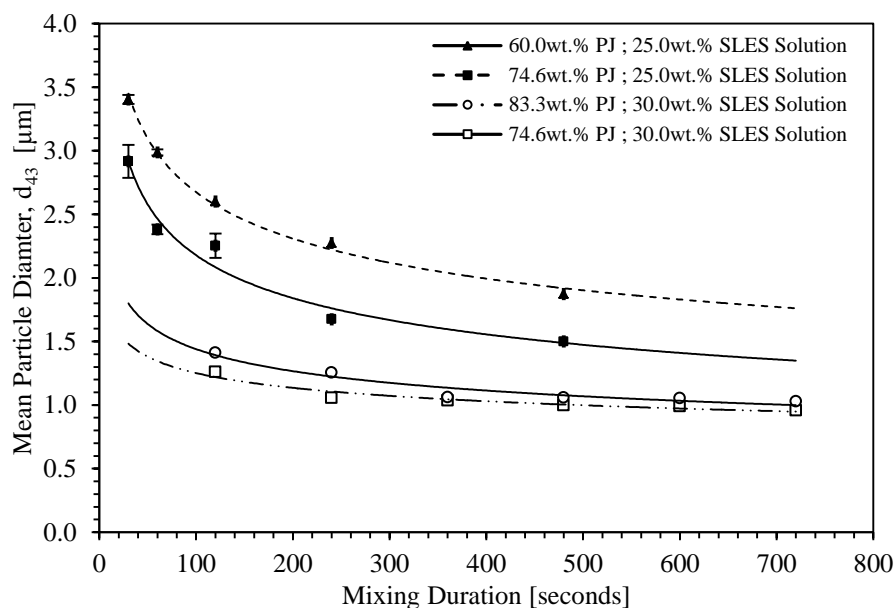


Figure 6.19: Graph describing the effect of mixing duration on mean droplet diameter (d_{43}) for dispersions, comprising various compositions of PJ dispersed in 25.0wt.% and 30.0wt.% SLES solutions, formed by melt emulsification, processed for varying mixer durations at N of 6000 RPM, on the FDM apparatus. The lines of fit indicate the trajectory of the results.

Similar findings are apparent for results describing d_{43} against PJ fraction at set mixing durations, stabilised with 25wt.% and 30wt.% SLES solutions (Figure 6.20). For all surfactant solutions studies, d_{43} generally decreases with increasing PJ fraction. Interestingly, emulsions stabilised with 30wt.% SLES solution, processed for 480 seconds, indicate very similar final sizes for all PJ fractions studied. These results indicate that the d_{43} of formed emulsions changes significantly with PJ fraction in 25wt.% SLES solutions, whereas for emulsions comprising 30wt.% SLES solutions, droplet break-up is strongly affected by SLES concentration. In addition to analysis of d_{43} , the specific surface area (A_d) of the formed emulsion is of interest, as a measure of emulsion effectiveness.

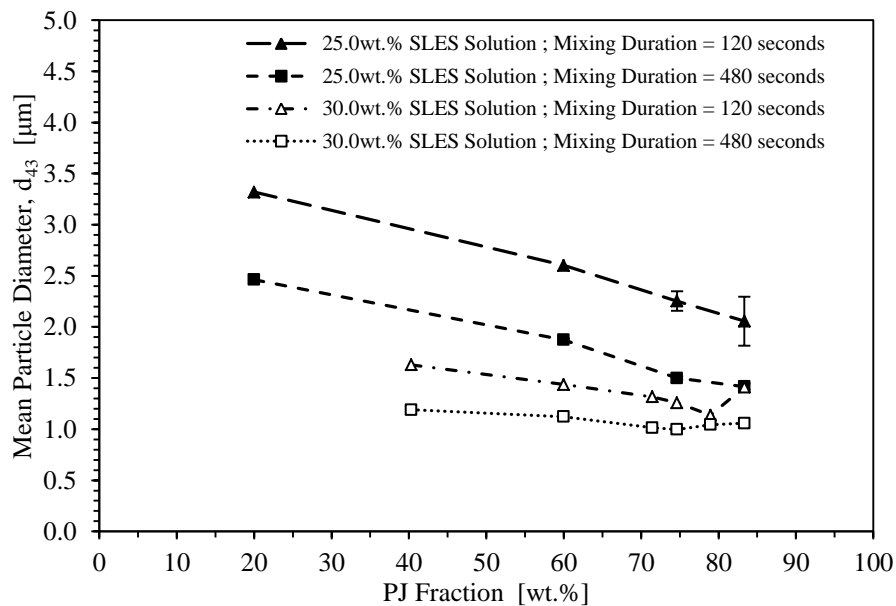


Figure 6.20: Graph describing the effect of PJ fraction on mean droplet diameter, (d_{43}) for dispersions, comprising various compositions of PJ dispersed in 25.0wt.% and 30.0wt.% SLES solutions, formed by melt emulsification, processed for varying mixer durations at 6000 RPM on the FDM apparatus. The lines of fit indicate the trajectory of the results.

Figure 6.21 describes the impact of PJ mass fraction on A_d for emulsions processed for 120 and 480 seconds. The results seem consistent with previous findings and indicate that the A_d for emulsions stabilised in 30wt.% SLES solution, processed for

480 seconds, does not change significantly across oil fractions. For emulsions formed in 25.0wt.% SLES solutions, the PJ fraction impacts significantly on d_{43} .

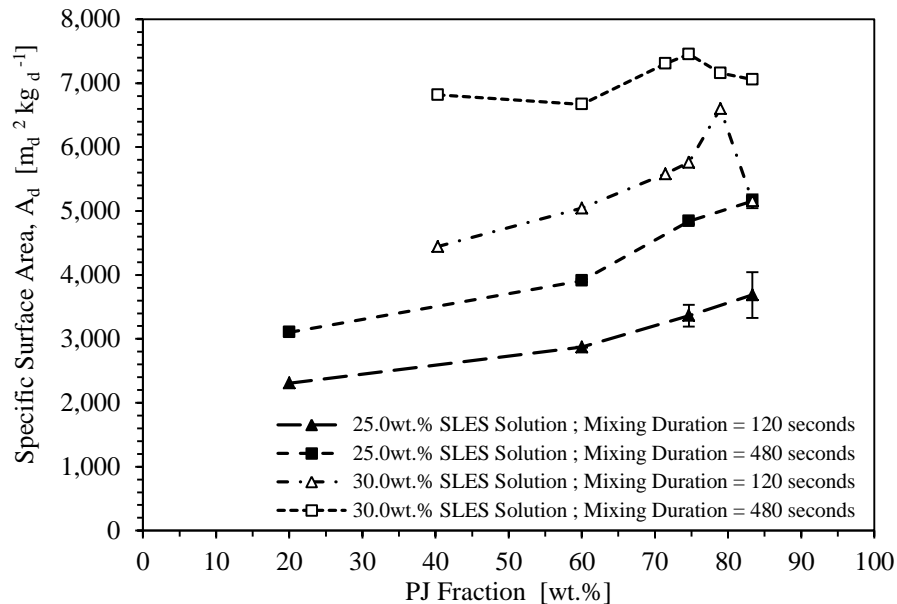


Figure 6.21: Graph describing the effect of PJ fraction on specific surface area (A_d) for dispersions, comprising various compositions of PJ dispersed in 25.0wt.% and 30.0wt.% SLES solutions, formed by melt emulsification, processed for varying mixer durations at 6000 RPM on the FDM apparatus. The lines of fit indicate the trajectory of the results.

6.5.2 CDDM Studies

FDM studies on the HIPE strategies, described in section 6.5.1, were extended for emulsification on the Laboratory-scale CDDM.

Operation and design of the CDDM is described in Chapter 4 (section 4.6.2) and the experimental methods used in the current studies are described in section 6.2.5, where studies involved the processing of coarse emulsion pre-mixes, which were prepared offline as per methods described in Chapter 4 (section 4.5.1). Samples were collected periodically and measured using methods described in Chapter 4 (section 4.2.2 and section 4.2.4).

Figure 6.22 show the effect of phase volume on droplet size distribution for emulsions, comprising a 12.5wt.% SLES solution, processed at low Q (61.7+/-1.7 kg/hr) and high Q (254+/-8 kg/hr) at static mode (0 RPM) and dynamic mode (10000 RPM). The lowest droplet distributions were achieved for experiments performed at low volume fractions, which was contrary to results achieved on the FDM (Figure 6.20). Despite this, this result was expected as the PJ:SLES mass ratio was lowest at low phase volumes. Therefore, the availability of surfactant at the O/W interface was higher. Comparing the static and dynamic results, Figure 6.22a) indicated a significant difference in d_{43} between static and dynamic operations. However, at high Q (Figure 6.22b) the difference is apparent. These results may indicate benefits of increased extensional shear in the system, which may promote droplet break-up.

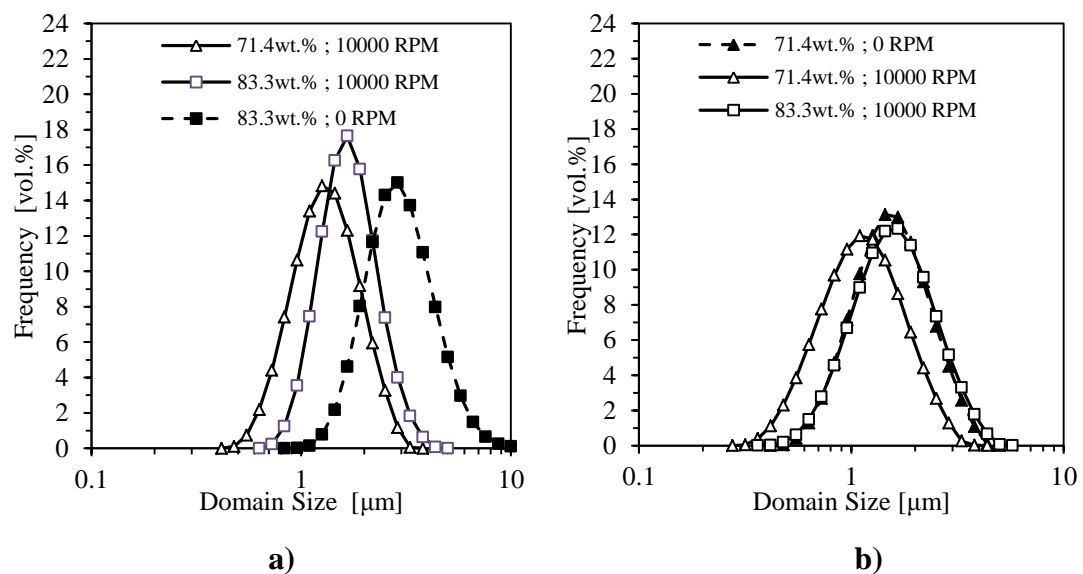


Figure 6.22: Graph describing the effect of dispersed mass fraction on droplet size distribution of PJ/SLES dispersions, comprising PJ and a 12.5 wt.% SLES solution, post-processed through the CDDM in a 0mm geometry at static and dynamic conditions at Q of **a)** 61.7+/-1.7 kg/hr and **b)** 254+/-8 kg/hr.

In comparison, Figure 6.23 shows the effect of PJ fraction on droplet size distribution emulsions, comprising PJ dispersed in a 25.0wt.% SLES solution, processed at low Q (62.5+/-0.9 kg/hr) and high Q (250+/-4 kg/hr) in static and dynamic mode (10000 RPM). In this instance, the results of experiment show very similar sizes between low and high PJ fractions (71.4wt.% vs. 83.3wt.% fractions).

Findings are similar to results reported in FDM studies (see section 6.4.1) which indicated that droplet break-up was dominated by high SLES concentrations. These findings support the previous results in that low Q results in significantly different size distributions between static and dynamic operation. However, for high PJ fractions the size distributions are similar.

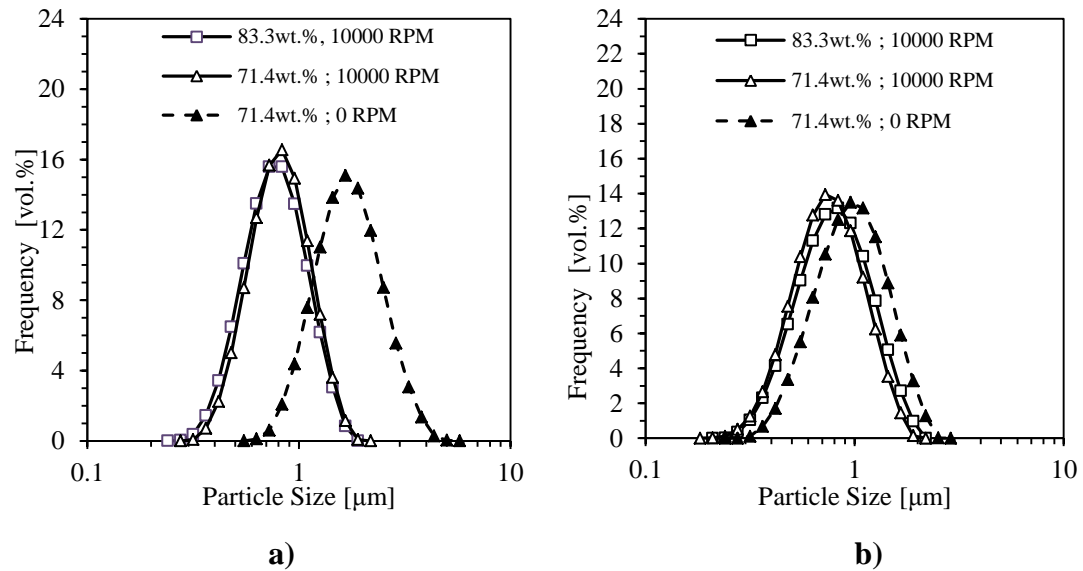


Figure 6.23: Graph describing the impact of dispersed mass fraction on droplet size distribution of PJ/SLES dispersions, comprising PJ and a 12.5wt.% SLES solution, post-processed through the CDDM in a 0mm geometry at static and dynamic conditions at Q of **a)** 62.5 \pm 0.9 kg/hr and **b)** 250 \pm 4 kg/hr.

Effect of SFSO Fraction and Processing

The effect of SFSO fraction was studied for SFSO/Pluronic emulsions, post-processed on the Laboratory-scale CDDM. Results are described in Figure 6.24 and show the impact of SFSO fraction on d_{43} for emulsions, comprising SFSO and 23.3wt.% Pluronic solution, processed in static and dynamic modes (10000 RPM) at low Q (55.0 \pm 3.5 kg/hr) and high Q (206 \pm 9 kg/hr).

Results described in Figure 6.24 a) indicate that emulsions exhibiting the lowest d_{43} values are formed for emulsions comprising of low SFSO fractions. These findings contradict results found during FDM studies (section 6.5.1, Figure 6.20). However,

they are expected as the SFSO:Pluronic mass ratio increases the availability of emulsifier at the extended interface. Further, the difference in dynamic against static results is very different, as found in PJ/SLES studies, described in Figure 6.14.

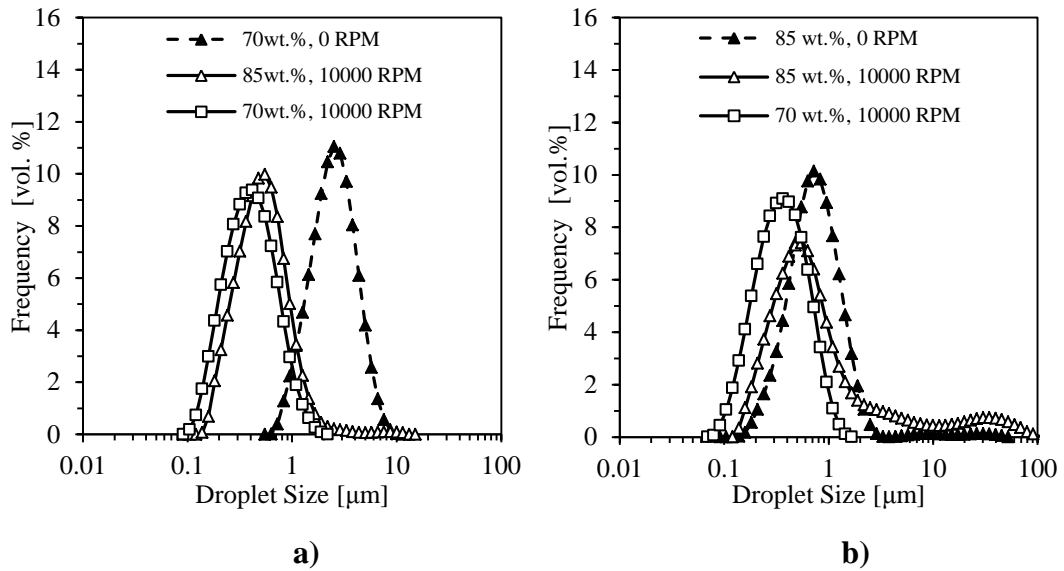


Figure 6.24: Graph describing the effect of dispersed mass fraction on droplet size distribution of formed emulsions, comprising SFSO and 23.3wt.% Pluronic solution, post-processed through the CDDM in a 0mm geometry at static and dynamic conditions at Q of **a)** 55.0+/-3.5 kg/hr and **b)** 206+/-9 kg/hr.

Furthermore, Figure 6.24b indicates that emulsions comprising the lowest d_{43} values are formed at low SFSO fractions. Interestingly, emulsions comprising 85.0wt% and processed dynamically result in emulsions with wide droplet span. This was investigated by comparing emulsions, comprising 80.0wt.% SFSO dispersed in 23.3wt.% (Figure 6.25 a)) and 85.0wt.% SFSO dispersed in 23.3wt.% (Figure 6.25 b)). Results indicated that the 80.0wt.% emulsions are far more uniform than 85.0wt.% processed at high Q (196+/-2 kg/hr; 221+/-6 kg/hr) and N (0 RPM; 5000 RPM; 10000 RPM). This may show signs of emulsion instability, which is enhanced with increased in mixer speed (see Figure 6.24 b)).

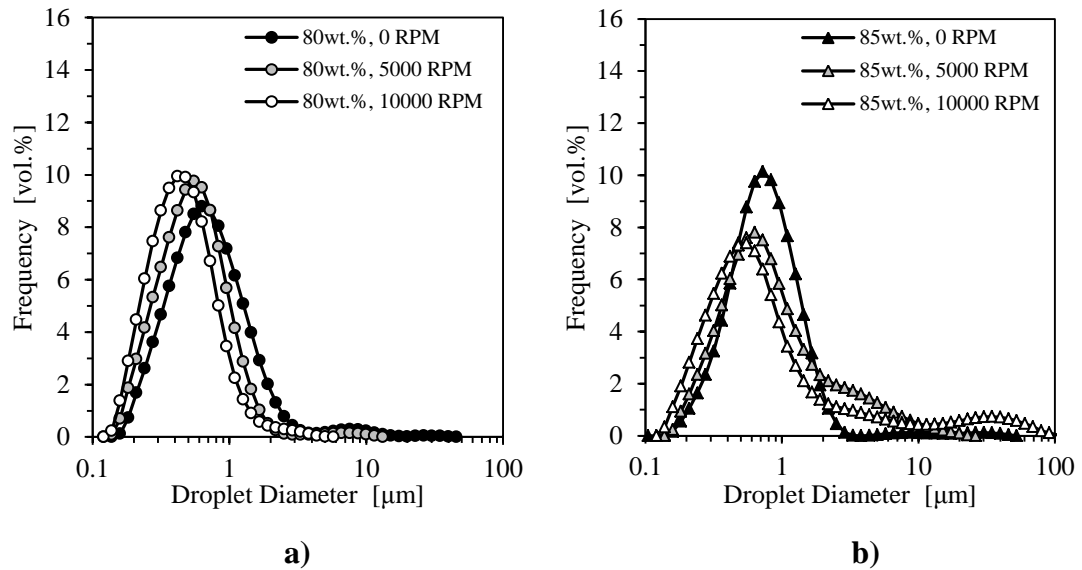


Figure 6.25: Graph describing the impact of processing on droplet size distribution of emulsions, comprising 80wt.% and 85wt.% SFSO dispersed 23.3wt.% Pluronic solution, post-processed through the CDDM in a 0mm geometry at mixer speeds of 0, 5000 and 1000 RPM at Q of **a)** 196 \pm 2 kg/hr and **b)** 221 \pm 6 kg/hr.

The effect of dispersed phase fraction on A_d is described in Figure 6.26, which shows the results of emulsions, comprising SFSO dispersed in 23.3 wt.% Pluronic and PJ dispersed in 25.0 wt.% SLES, processed at 10000 RPM at low Q (SFSO/Pluronic = 51.9 \pm 4.1kg/hr; PJ/SLES = 55.3 \pm 8.1kg/hr) and high Q (SFSO/Pluronic = 206 \pm 9kg/hr; PJ/SLES = 240 \pm 14kg/hr). The results indicated that the lowest d_{43} was observed for either emulsions formed at low dispersed phase fractions and processed at high Q , or for emulsions comprising high dispersed phase fractions and processed at low Q . These results indicated that the formulation may favour a particular shear type, though for emulsions comprising PJ/SLES the results are less apparent. Further study is recommended with the aim of investigating shear type on formulation.

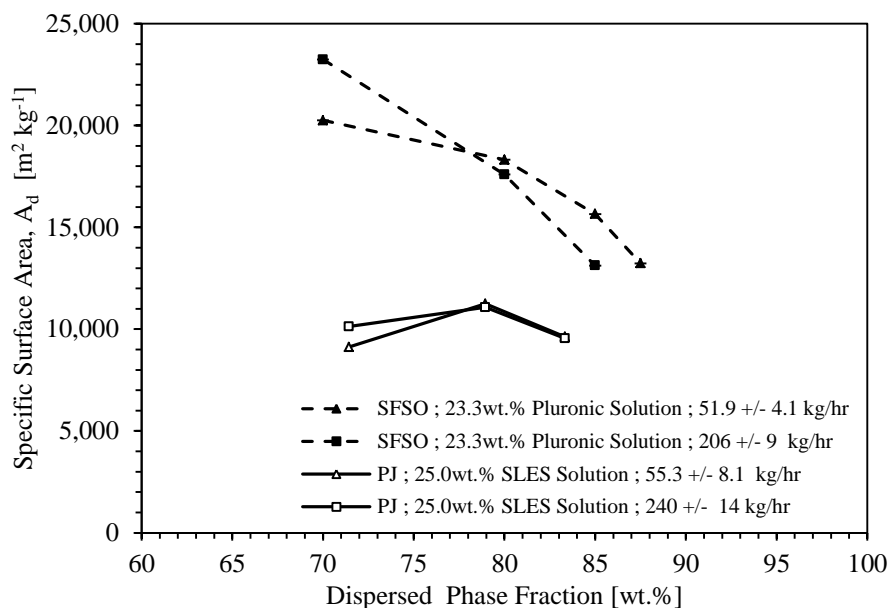


Figure 6.26: Specific surface area against oil fraction for SFSO/Pluronic emulsions and PJ/SLES dispersions processed at 210+/-16kg/hr at 10000 RPM at various mixer speeds in a 0mm CDDM mixer position. The lines of fit indicate the trajectory of the results.

6.5.3 Efficiency Analysis – HIPE Strategy

The efficiency function was applied to a number of the results, which are described in sections 6.5.1 and 6.5.2 and displayed in Figure 6.27. The results showed that efficiency generally increased at increasing dispersed phase fraction. Considering the FDM results (section 6.5.1), raising the surfactant concentration lead to more efficient emulsification which supported the findings described in section 6.4.1 and was attributed to increased stress transfer by viscosity matching. Further, the efficiency increased for longer mixing durations (60kg/hr vs. 7.5kg/hr), which was expected as the shear duration was extended. Results describing Laboratory-scale CDDM studies indicate improved efficiency with increasing dispersed phase fraction (PJ/SLES = 71.4-83.3wt.%; SFSO/Pluronic = 70.0-87.5wt.%), which is demonstrated for both PJ/SLES and SFSO/Pluronic compositions. Furthermore, when considering results of SFSO/Pluronic compositions, there appeared to be a transition in efficiency between SFSO/Pluronic compositions processed at low Q (51.9+/-4.1 kg/hr) and high Q (206+/-9 kg/hr) at similar tip speeds (13.1 m/s), where

low Q favours emulsions processed at high SF/SO fraction and high Q favours emulsions processed at low SF/SO fractions, indicative of results described in Figure 6.26.

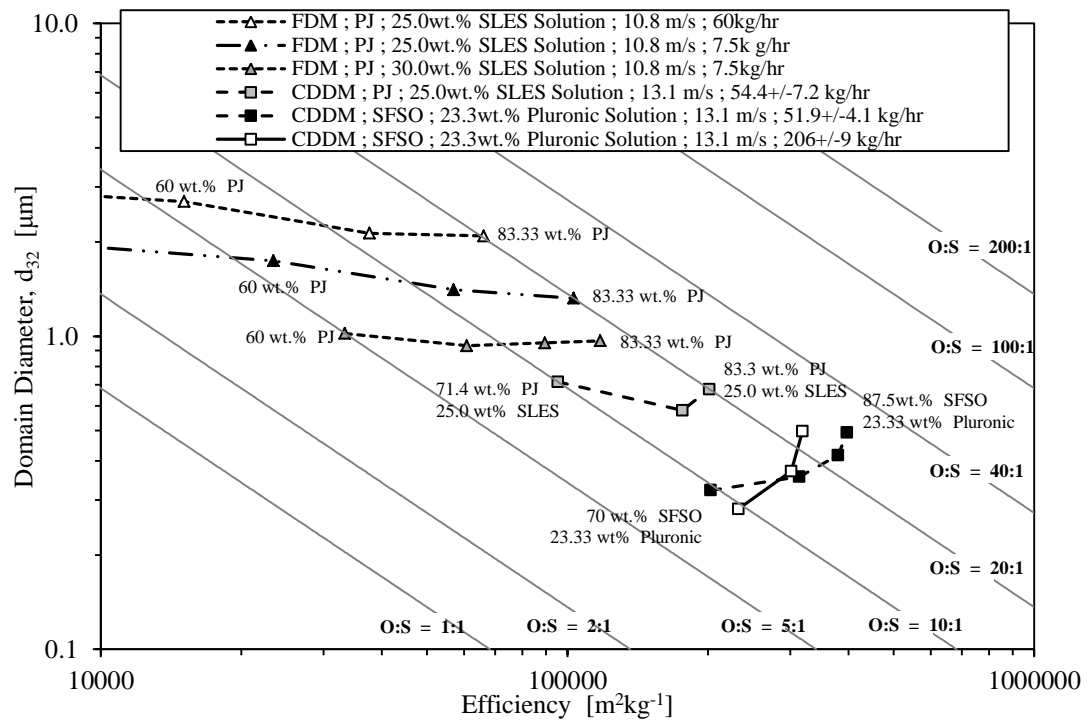


Figure 6.27: Efficiency Graph describing dispersions, comprising PJ/SLES compositions of set SLES concentration (25.0wt.% and 30.0wt.% solution), and SF/SO/Pluronic compositions of set Pluronic concentration (23.3wt.%) processed on the FDM and Laboratory-scale CDDM at varying tip speeds and Q . The lines of fit indicate the trajectory of the results.

6.5.4 Further Discussion of Results

Many of the models described in the literature relate to low oil fraction systems, with a relatively large distance between adjacent droplets. Therefore, interactions between droplets are minimal. Whilst solidified on the end user, particle sizes observed here are reflective of the droplet sizes observed at 60°C. Tcholakova et al. (2011) describes a model for droplet break-up of HIPEs, where it is proposed that emulsions with a narrow span of small droplets are formed by capillary break-up. This supports the findings of Jansen et al. (2001) who determined that the critical capillary number

(i.e. viscous stress transfer to the system) was dependent on the emulsion viscosity and thus the surrounding droplets.

Another consideration may be the relative spacing between domains during emulsification. Literature lists the maximum packing fraction of emulsions comprising of monodisperse droplets as 74.0vol.% and droplets deform to polyhedral shapes above this fraction. Furthermore, steric repulsion between droplets due to ionic surfactants positioned on the droplet surface may further increase deformation. For simplicity, we may assume that a system comprises monodisperse droplets exhibiting a cubic form; as such the relative spacing of droplets is described in Figure 6.28. Equation 6.3 describes the relative spacing of droplets in cubic form.

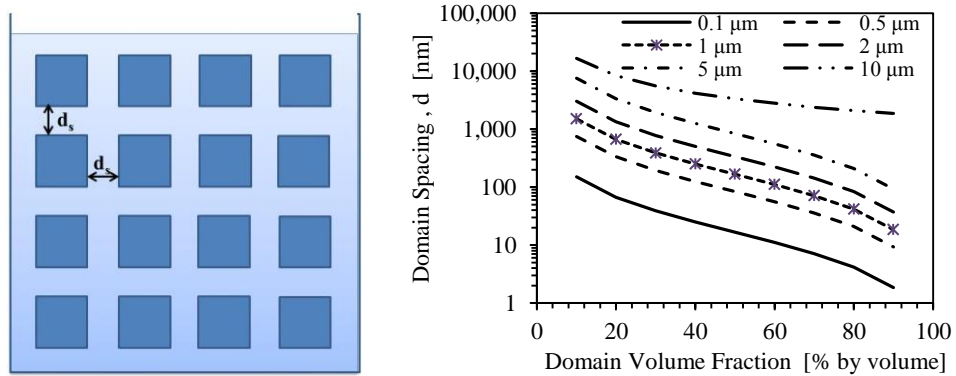


Figure 6.28: Model of domain spacing vs. domain volume fraction for various droplet diameters. Droplet spacing decreases with increasing phase volume and smaller droplet diameters.

$$\delta_d = \frac{(1-\phi)d}{\phi} \quad (6.3)$$

Where δ_d is the domain spacing, ϕ is the domain fraction and d is the droplet diameter. The model illustrates two points; firstly, that the spacing of domains decreases with increasing fraction, as expected. Secondly, the relative spacing of emulsion droplets further decreases the reduced droplet diameter. One might suggest that in the former instance, a reduced droplet distance could improve the efficiency

with which the surface is stabilised as the spatial positioning of the surfactant relative to the interface is reduced. The latter observation is important when considering the model described by Tcholakova et al. (2011), where the domain spacing and droplet sizes are proportional and therefore, the break-up mechanism described may continue as the droplet size reduces.

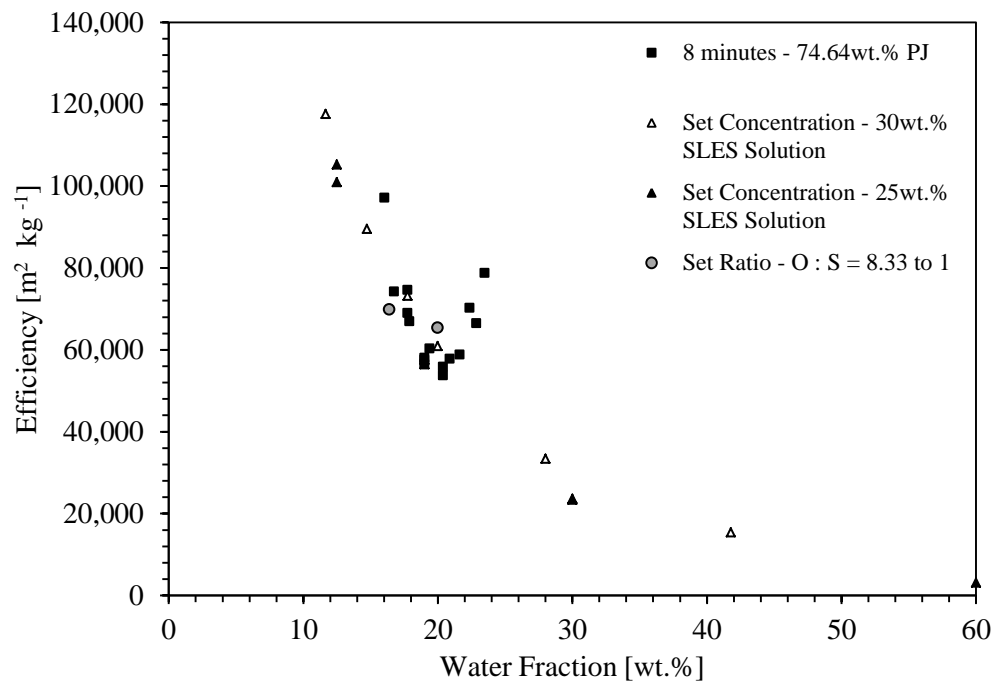


Figure 6.29: Graph displaying efficiency versus water fraction for emulsions processed for 480 seconds at set SLES solution concentration (25.0% and 30.0% by weight), set PJ mass fraction and set PJ:SLES mass ratios (8.33 to 1).

Figure 6.30 describes collated results for FDM experimental studies described in sections 6.3.2, 6.4.1 and 6.5.1. Support for experimental data is found by analysing findings outlined in results presented Tcholakova et. al. (2011). In these experiments, Hexadecane, Mineral Oil 25 and Mineral Oil 130 were emulsified in a 10wt.% Lutensol A8 (C₁₃EO₈) solution using a rotor-stator device. Assuming a temperature of 25°C, the densities of Hexadecane and mineral oil used was 771 kg/m³ and 838 kg/m³, respectively (Technical document 9; Technical document 10). Due to limited available information on surfactant solution densities, a water continuous phase at 25°C, comprising a density of 997 kg/m³ was chosen (Technical document 11).

Further, the results disclosed by Welch et al. (2006) describe 100cst Silicone Oil stabilised with SLES, where the properties of the oil are provided in Technical document 12. Figure 6.31 describes the efficiency results for data obtained by studies of Tcholakova et al. (2011) and Welch et al. (2006) which indicate similar trends of increasing efficiency with dispersed phase fraction.

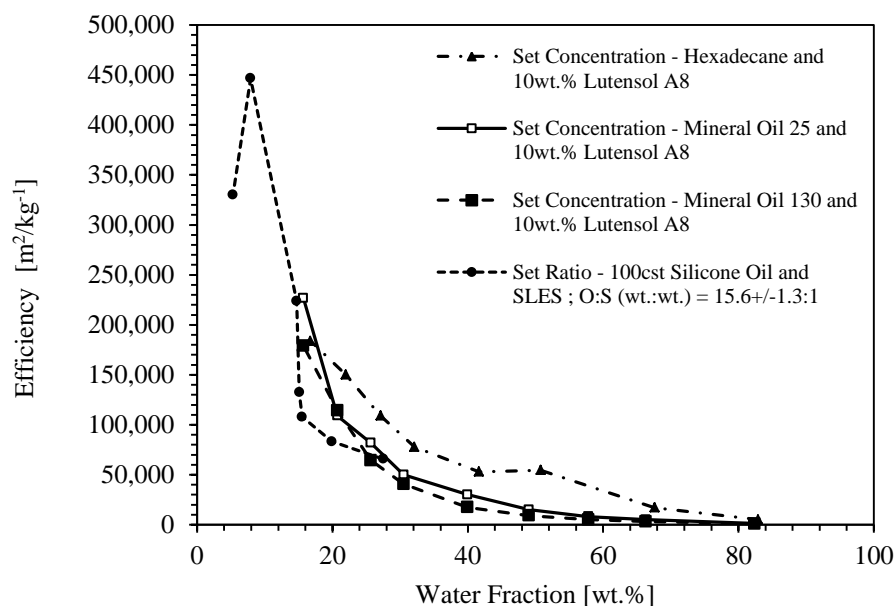


Figure 6.30: Graph displaying efficiency vs water fraction for results described by Tcholakova et al. (2011), for emulsions formed via rotor-stator apparatus, comprising Hexadecane, Mineral Oil 25 and Mineral Oil 130 stabilised with 10wt.% Lutensol, and results described by Welch (2006) for emulsions formed via rotor-stator apparatus, comprising 100cst Silicone Oil and SLES at mass ratios of 15.6+/-1.3 to 1. The lines of fit indicate the trajectory of the results.

6.6 Conclusions and Further Work

6.6.1 Viscosity Matching Strategies

- Viscosity matching strategies were investigated for efficient emulsification on the Formax™, the FDM and the CDDM apparatus for a model O/W system, stabilised by an anionic surfactant. Increasing continuous phase

viscosity through increased surfactant concentration improved droplet break-up and efficient surfactant use.

- The strategy was dependent on the properties of surfactant aggregate phases; for SLES solutions, this formed highly viscous lamellar and hexagonal phases in solution. Further studies may consider other surfactants with similar and varied aggregate phase behaviour for efficient emulsion manufacture.

6.6.2 Surface Stabilisation Strategies

- Surface stabilisation strategies were studied on the FDM and CDDM apparatus for emulsification of a model O/W system, stabilised with anionic surfactant. Studies considered emulsions of fixed oil fraction and varying surfactant concentration. For FDM studies, droplet break-up improved with increasing surfactant concentration and efficient surfactant use was found for compositions comprising low and high surfactant solution. Additionally, results indicated that efficient surfactant use at high concentrations were time dependent.
- Further benefits in droplet-breakup and surfactant use were found by replacing surfactant solutions with glycerol, which increased the continuous phase viscosity. For CDDM studies, efficient emulsification was achieved by increasing surfactant concentration and introducing glycerol ingredients in place of surfactant solution.
- Additional studies may consider the surface tension of SLES solution and SLES/glycerol compositions which may have determined the differences between emulsions formed by opposing methods. Further, the surfactant type could be altered to determine whether efficient emulsification was formulation dependent.

6.6.3 HIPE Strategy

- HIPES processing strategies were investigated for efficient manufacture of model O/W emulsions, stabilised with synthetic anionic and non-ionic

surfactants. Droplet diameter varied with oil fraction but increased the efficiency of surfactant use for both systems. A transition in dominant shear type was observed for both systems, providing some indication that elongation may favour low oil fractions and rotation may favour high oil fractions.

- Future work may investigate the dominant shear type further and may consider emulsions comprising more viscous dispersed phases.

Chapter 7: Key Outcomes and Opportunities

The research described in this thesis considers strategies for efficient manufacture of model O/W systems in Cavity-design mixers. The approach to studies centred on process design, which is directed to fulfilling a chosen objective, such as a formation of a material of a desired composition or microstructure, the lowest output of out-of-specification product, the minimum number of processing stages and the optimum usage of raw materials. A number key outcomes and potential opportunities are discussed here.

7.1 Development of New Experimental Tool

Studies reported in Chapters 5 and 6 have investigated emulsion manufacture of model systems in the CDDM. Investigations on the impact of emulsion composition, mixer geometry and processing methods provide a number of processing insights that may be exploited for product manufacture and in applications including encapsulation, flow chemistry and emulsion templating. Further work may extend investigations to other formulations. It is noted that efficient emulsion manufacture is mixer specific, where a particular equipment design favours stress transfer in materials with certain physicochemical properties (and vice versa). Further studies are needed to fully evaluate the manufacturing efficiencies of the CDDM technologies in comparison to other mixers. However, there are indications that the apparatus may offer low energy emulsification routes. Further, the mixer design may be altered to provide more characterisation of material rheology for shear sensitive systems, by alternating the measured material via cavity transfer (a limitation of rheometers described in section 2.3.2). This presents opportunities for insight on mixing properties.

7.2 *Emulsification Efficiency Function*

A parameter was developed to determine the efficiency of surfactant use in stabilising created interface during emulsification. The approach provides a simple and effective means for comparing process strategies, offering opportunities for more rapid innovation of a wide range of emulsion systems that are more effective or more efficient. However, the approach should consider the energy used in emulsion formation, this was outside the scope of the current thesis study. Additionally, the function could be improved by incorporating a surface coverage term, which would allow comparison of oils stabilised with different surfactants.

7.3 *In-line Emulsification*

The strategies outlined in Chapter 5, section 5.3.3 have demonstrated that highly concentrated emulsions may be formed inline via a series of CDDMs which eliminates the need for batch manufacture. This approach offers opportunities for process intensification, leading to low footprint product manufacture and energy efficient processing. Further investigations should consider whether the method may be applied in a single CDDM and whether the approach can be employed for other inline mixers. Additionally, further studies may investigate scale-up of the strategy to industrial-scale throughputs.

7.4 *HIPE Processing*

The strategies described in Chapter 6, section 6.3 and 6.5, have demonstrated manufacture of model emulsions via HIPE processing in cavity-design mixers. Furthermore, results indicate that the approach promotes effective surfactant use in these mixers. This offers opportunities to explore new process space for emulsions for low footprint manufacture of novel emulsions that are more efficient or more effective. Studies have focussed on the manufacture of O/W emulsions; further work may investigate whether the manufacture of W/O type emulsions offers similar benefits. Further, there are opportunities to develop methods incorporating phase inversion or spontaneous emulsification, described in Chapter 2 (section 2.2.2).

7.5 *Efficient Emulsification via Viscoelasticity?*

Further work may consider approaches that manipulate emulsion viscoelasticity as a means for improving stress transfer in emulsions. As described in Chapter 2 (section 2.3.2) materials exhibiting viscoelastic properties offer increased responsiveness to applied shear compared to fluids of low viscoelasticity. Concentrated emulsions are known to exhibit viscoelastic properties, further, the surfactant properties may be altered to obtain viscoelastic responses. This is an extension of the work described by Mason and Bibette (1996, 1997), who attributed mono-disperse emulsion formation to the viscoelastic properties of the continuous phase.

7.6 *Commercial Significance*

At the time of writing the current thesis, a number of reported studies had received commercial interest. This includes the results of experiments described in Chapter 5, which have formed a key part of a collaborative project on “Manufacturing Innovation for Resource Efficient Structuring Liquids” between the Unilever, CDDMtec and the University of Liverpool, funded by the technology strategy board. More specifically, studies on in-line emulsification strategies, reported in Chapter 5 (section 5.3.3, section 5.3.4 and section 5.3.5) offers opportunities for process intensive emulsion manufacture. Therefore, results reported on the continuous manufacture of emulsion via the CDDM apparatus have received commercial interest. Additionally, results reported in Chapter 6 (section 6.4) offer opportunities for the manufacture of more effective products (larger domain area) or milder products (low surfactant amounts). Results disclosed in this section have also received commercial interest.

Appendix

AX1: Bibliography

Acosta, E. (2009) “Bioavailability of nanoparticles in nutrient and nutraceutical delivery,” *Current Opinion in Colloid & Interface Science*, 14(1), pp. 3–15

Akay G., Irving G.N., Kowalski A.J., Machin D. (1996). *Process for the Production of Liquid Compositions*. WO 1996020270 A1

Albert L.S. (1950). *Process for Making Floating Soap*. US2525081 A

Anton, N. and Vandamme, T. F. (2009) “The universality of low-energy nano-emulsification,” *International Journal of Pharmaceutics*, 377(1-2), pp. 142–147

Anton, N. and Vandamme, T. F. (2011) “Nano-emulsions and Micro-emulsions: Clarifications of the Critical Differences,” *Pharmaceutical Research*, 28(5), pp. 978–985

Asztalos, M. L., Heller, M. M., Lee, E. S. and Koo, J. (2013) “The impact of emollients on phototherapy: A review,” *Journal of the American Academy of Dermatology*, 68(5), pp. 817–824

Atiemo-Obeng V.A. and Calabrese R.V. (2004) *Rotor–Stator Mixing Devices*. In: Paul, E.L., Atiemo-Obeng, V.A., Kresta, S.M. (Eds.), *Handbook of Industrial Mixing*. John Wiley & Sons, Inc. Chapter 8

Aveyard R., Binks B.P., Lawless T., Mead J. (1985) “Interfacial Tension Minima in Oil+Water+Surfactant Systems: Effect of Salt and Temperature in Systems

Containing Non-ionic Surfactants,” *Journal of the Chemical Society, Faraday Transactions 1: Physical Chemistry in Condensed Phases*, 81(9), pp. 2155-2168

Bancroft W.D. (1913) “The Theory of Emulsification, V,” *Journal of Physical Chemistry*, 17(1), pp. 501–519

Barnes, H. A. and Hutton, J. F. (1989) *An Introduction to Rheology*. Edited by K. Walters. 1st edn. Amsterdam: Distributors for the U.S. and Canada, Elsevier Science Pub. Co.

Batchelor G.K. (1951) “Pressure fluctuations in isotropic turbulence,” *Mathematical Proceedings of the Cambridge Philosophical Society*, 47(2), pp. 359-374

Beck H.G. (1957). *Method of and apparatus for homogenizing plastic or plasticizable materials*. US2813302

Bentley and Leal (1986a) “A computer-controlled four-roll mill for investigations of particle and drop dynamics in two-dimensional linear shear flows,” *Journal of Fluid Mechanics*, vol. 167, pp. 219-240

Bentley, B. J. and Leal, L. G. (1986) “An experimental investigation of drop deformation and breakup in steady, two-dimensional linear flows,” *Journal of Fluid Mechanics*, 167(1), pp. 241-283

Bodor J., Erdl M., Mayer K., Vermaat K. (1999). *Process for preparing a spread*. WO 1999049738 A1

Bongers P.M.M., Santos Ribeiro H., Irving G.N., Egan M.J. (2012) *Method for Production of an Emulsion*. WO2012089474 A1

Brown C.J. (2001). *Dynamic Mixer*. EP1331988B1

Brown C.J., Irving G.N., Kowalski A.J. (2010a). *Mixing Apparatus Of The cddm- and/Or ctm-Type, and Its Use*. WO2010091983 A1

Brown C. J., Irving G.N., Kowalski A.J. (2010b). *Distributive and Dispersive Mixing Apparatus of the CDDM-Type, and its use*. WO2010089322 A1

Brown D.A.R., Jones P.N., and Middleton J.C. (2004) *Part A: Measuring Tools and Techniques for Mixing and Flow Visualization Studies*. In: Paul, E.L., Atiemo-Obeng, V.A., Kresta, S.M. (Eds.), *Handbook of Industrial Mixing*. John Wiley & Sons, Inc. Chapter 4

Cain F.W., De Wit J. (1994). *Low shear inversion process and products thereof*. EP0399580 B1

Calabrese R.V., Chang T.P.K., Dang P.T. (1986) “Droplet Breakup in Turbulent Stirred-Tank Contactors. Part I: Effect of Dispersed-Phase Viscosity,” *AIChE Journal*, 32 (4), pp. 657-666

Calabrese R.V., Wang C.Y., Bryner N.P. (1986) “Droplet Breakup in Turbulent Stirred-Tank Contactors. Part III: Correlations for Mean Size and Droplet Size Distribution,” *AIChE Journal*, 32(4), pp. 677-681

Chen, H. T. and Middleman, S. (1967) “Drop size distribution in agitated liquid-liquid systems,” *AIChE Journal*, 13(5), pp. 989–995

Chesters (1991) “The Modelling of Coalescence Processes in Fluid-Liquid Dispersions: A review of Current Understanding,” *Chemical Engineering Research and Design*, 69(4), pp. 259-270

Clark T.A., Edwards R.B., Irving G.N. (1986a). *Detergent Processing*. EP 0090647 B1

Clark T.A., Edwards R.B., Irving G.N. (1986b). *Detergent Processing*. EP 0090648 B1

Clark T.A., Edwards R.B., Irving G.N. (1986c). *Detergent Bar Processing*. EP 0090649 B1

Clark T.A., Edwards R.B., Irving G.N. (1986d). *Detergent Bar Processing*. EP0090644 B1

Clark T.A., Edwards R.B., Irving G.N., 1986e. *Detergent bar processing*. EP 0090646 B1

Clay P.H. (1940) "The mechanism of emulsion formation in turbulent flow. 1. Experimental Part," *Proceedings of the Royal Academy of Sciences of Amsterdam*, 43(1), pp. 852-865

Cooke M., Naughton J. and Kowalski A.J. (2008) "A Simple Measurement Method for Determining the Constants for the Prediction of Turbulent Power in a Silverson MS 150/250 In-Line Rotor Stator Mixer," *Sixth International Symposium on Mixing in Industrial Process Industries- ISMIP VI*, pp. 1-3

Cooke, M., Rodgers, T. L. and Kowalski, A. J. (2011) "Power consumption characteristics of an in-line silverson high shear mixer," *AIChE Journal*, 58(6), pp. 1683–1692

Das, A. K. and Ghosh, P. K. (1990) "Concentrated emulsions. Investigation of polydispersity and droplet distortion and their effect on volume fraction and interfacial area," *Langmuir*, 6(11), pp. 1668–1675

Davies, J. (1985) "Drop sizes of emulsions related to turbulent energy dissipation rates," *Chemical Engineering Science*, 40(5), pp. 839–842

Davies, J. (1987) "A physical interpretation of drop sizes in homogenizers and agitated tanks, including the dispersion of viscous oils," *Chemical Engineering Science*, 42(7), pp. 1671–1676

Delgado A.V., Gonzalez-Cabllero F., Hunter R.j., Koopal L.K., Lyklema J. (2007) "Measurement and Interpretation of Electrokinetic Phenomena," *Journal of Colloid and Interface Science*, 309(2), pp. 194–224

Derkach S.R. (2009) "Rheology of Emulsions," *Advances in Colloids and Interface Science*, 151(1-2), pp. 1-23

Dukhin S.S., Sjöblom J.J., and Sæther Ø. (2005) *An Experimental and Theoretical Approach to the Dynamic Behavior of Emulsions*. In: Sjöblom, J., Sjöblom, S. (Eds.), *Emulsions and Emulsion Stability*, Second Edition (Surfactant Science). Boca Raton: Taylor & Francis, Chapter 1

Egan M.J., Irving G.N., Bongers P.M.M. (2013). *Method for production of structured liquid and structured liquid*. WO2013092118 A1

Einstein A. (1906) "A new determination of molecular dimensions," *Annalen der Physik*, 17(6), pp. 132–148

Fasina O.O., Colley Z. (2008) "Viscosity and Specific Heat Capacity of Vegetable Oils," *International Journal of Food Properties*, 11(4), pp. 738-746

Fischer, P. and Windhab, E. J. (2011) "Rheology of food materials," *Current Opinion in Colloid & Interface Science*, 16(1), pp. 36–40

Gale G.M. (1983). *Extruder Mixer*. EP0048590A1

Gaulin A. (1904). *Process of treating milk or similar liquids*. US753792 A. Filed: 27/04/1903, Published: 01/03/1904

Goodwin, J. W. and Hughes, R. W. (2008) *Rheology for chemists: an introduction*. 2nd edn. Cambridge, UK: Royal Society of Chemistry

Grace H.P. (1982) "Dispersion Phenomena in High Viscosity Immiscible Fluid Systems and Application of Static Mixers as Dispersion Devices in Such Systems," *Chemical Engineering Communications*, 14(3-6), pp. 225-277

Graves S.M., Mason T.G. (2008) "Transmission of visible and ultraviolet light through charge-stabilized nanoemulsions," *Journal of Physical Chemistry C*, vol. 112(33), pp. 12669 – 12676

Griffin W.C. (1949) "Classification of Surface-Active Agents by 'HLB'," *Journal of Cosmetic Science*, 1(5), pp. 311-326

Grosse C, Delgado A.V. (2010) "Dielectric dispersion in aqueous colloidal systems," *Current Opinion in Colloid & Interface Science*, 15(3), pp. 145–159

Golemanov K., Tcholakova S., Denkov N.D., Ananthapadmanabhan K.P., Lips A. (2008) "Break-up of Bubbles and Drops in Steadily Sheared Foams and Concentrated Emulsions," *Physical Review E*, 78(5), pp. 051405-1-051405-12

Gupta, R. K. (2001) *Non-Newtonian Fluid Behaviour*. In: *Non-Newtonian flow in the process industries: Fundamentals and engineering applications* by R.P. Chhabra and J.F. Richardson, 1st Edition, 1999, Butterworth-Heinemann, Oxford, UK

Hadamard, J. S. (1911) "Mouvement permanent lent d'une sphere liquide et visqueuse dans un liquide visqueux," *Comptes rendus de l'Académie des Sciences*, 152, pp. 1735-1738

Hait, S. K. and Moulik, S. P. (2001) "Determination of critical micelle concentration (CMC) of nonionic surfactants by donor-acceptor interaction with iodine and correlation of CMC with hydrophile-lipophile balance and other parameters of the surfactants," *Journal of Surfactants and Detergents*, 4(3), pp. 303–309

Hall, S., Cooke, M., El-Hamouz, A. and Kowalski, A. (2011) “Droplet break-up by in-line Silverson rotor–stator mixer,” *Chemical Engineering Science*, 66(10), pp. 2068–2079

Harnby, N., Edwards, M. F. and Nienow, A. W. (1997) *Introduction to Mixing Problems. In: Mixing in the Process Industries: Second Edition*, 2nd Edition, Oxford: Butterworth-Heinemann, Chapter 1

Hatanaka J1, Kimura Y, Lai-Fu Z, Onoue S, Yamada S. (2008) “Physicochemical and pharmacokinetic characterization of water-soluble Coenzyme Q10 formulations,” *International Journal of Pharmaceutics*, 363(1-2), pp. 112-117

Hinch, E. J. and Acrivos, A. (1980) “Long slender drops in a simple shear flow,” *Journal of Fluid Mechanics*, 98(2), pp. 305-328

Hindmarch R.S., Gale G.M. (1982) “Applications of the Cavity Transfer Mixer to Rubber Extrusion,” *Elastomerics*, 114(8), pp. 20-25

Hindmarch R.S., Gale G.M. (1983) “How to Achieved Quality Polymer Blends by a New Extrusion Technique,” *Materials and Design*, 56(2), pp. 344-356

Hindmarsh R.S., 1987. “The Cavity Transfer Mixer: A Blender for All Seasons,” *Materials and Design*, 8(6), pp. 331-339

Hinze, J. O. (1955) “Fundamentals of the hydrodynamic mechanism of splitting in dispersion processes,” *AIChE Journal*, 1(3), pp. 289–295

House of Commons (2004) “Government Response to the Committee's Fifth Report, Session 2003–04, Too little too late?” *Government Investment in Nanotechnology*

Huddleston E. (1988). *Mixing Apparatus Employing a Cavity Transfer Mixer*. US 4750842 A. Filed: 22/07/1987, Published: 14/07/1988

IUPAC (2014) Compendium of Chemical Terminology, 2nd ed. (the "Gold Book"). Compiled by A. D. McNaught and A. Wilkinson. Blackwell Scientific Publications, Oxford (1997). XML on-line corrected version: <http://goldbook.iupac.org> (2006-) created by M. Nic, J. Jirat, B. Kosata; updates compiled by A. Jenkins.

Janssen J.J.M., Boon A., Agterof W.G.M. (1994) "Droplet Break-up in Simple Shear Flow in the Presence of Emulsifiers," *Colloids and Surfaces A: Physicochemical and Engineering Aspects*, 91, pp. 141-148

Jansen K. M. B., Agterof W. G. M., Mellema J. (2001) "Droplet breakup in concentrated emulsions," *Journal of Rheology*, 45(1), pp. 227-236

Kabanov, A. V., Lemieux, P., Vinogradov, S. and Alakhov, V. (2002) "Pluronic® block copolymers: novel functional molecules for gene therapy," *Advanced Drug Delivery Reviews*, 54(2), pp. 223–233

Kabalnov, A. S. and Shchukin, E. D. (1992) "Ostwald ripening theory: applications to fluorocarbon emulsion stability," *Advances in Colloid and Interface Science*, 38, pp. 69–97

Kahlweit M., Busse G., Faulhaber B., Jen J. (1996) "Shape Changes of Globules in Nonionic Microemulsions," *Journal of Physical Chemistry*, 100(36), pp. 14991-14994

Karbstein, H. and Schubert, H. (1995) "Developments in the continuous mechanical production of oil-in-water macro-emulsions," *Chemical Engineering and Processing: Process Intensification*, 34(3), pp. 205–211

Kaszuba, M., Corbett, J., Watson, F. M. and Jones, A. (2010) "High-concentration zeta potential measurements using light-scattering techniques," *Philosophical Transactions of the Royal Society A: Mathematical, Physical and Engineering Sciences*, 368(1927), pp. 4439–4451

Kippax P. (2005a) “Issues in the appraisal of laser diffraction particle sizing techniques,” *Pharmaceutical Technology Europe*, vol. 17(1), pp. 32-39

Kippax P. (2005b) “Measuring particle size: Using modern laser diffraction techniques,” *Paint and Coatings Industry*, 21(8), pp. 42-47

Kolmogorov, A.N. (1941a) “The local structure of turbulence in incompressible viscous fluid for very large Reynolds numbers,” *Proceedings of the USSR Academy of Sciences*, 30, pp. 299–303

Kolmogorov, A.N. (1941b) “Dissipation of Energy in Locally Isotropic Turbulence,” *Proceedings of the USSR Academy of Sciences*, 32(1), pp. 15-17

Kolmogorov, A. N. (1949) “On the breakage of drops in a turbulent flow,” *Proceedings of the USSR Academy of Sciences*, 66, pp. 825–828

Kowalski, A. J. (2009) “An expression for the power consumption of in-line rotor-stator devices,” *Chemical Engineering and Processing: Process Intensification*, 48(1), pp. 581–585

Kresta S.M., Brodkey R.S. (2004) *Turbulence in Mixing Applications*. In: Paul, E.L., Atiemo-Obeng, V.A., Kresta, S.M. (Eds.), *Handbook of Industrial Mixing*. New York, John Wiley & Sons, Inc., Chapter 16

Krishnan, J. M., Deshpande, A. P. and Kumar, P. B. S. (eds.) (2010). *Rheology of Complex Fluids*. Edited by Springer Science + Business Media

Leal-Calderon, F., Schmitt, V., Bibette, J. and Leal-Calderon, O. (2007) *Emulsion Science: Basic Principles*. 2nd edn. New York, NY: Springer-Verlag New York

Leng D.E., Calabrese R.V., (2004) Immiscible Liquid–Liquid Systems. In: Paul, E.L., Atiemo-Obeng, V.A., Kresta, S.M. (Eds.), *Handbook of Industrial Mixing*. John Wiley & Sons, Inc. Chapter 12

Liu, Y. and Friberg, S. E. (2009) “Role of liquid crystal in the emulsification of a gel emulsion with high internal phase fraction,” *Journal of Colloid and Interface Science*, 340(2), pp. 261–268

Mabille C., Schmitt V., Gorria Ph., Leal-Calderon F., Faye V., Deminière B., Bibette J. (2000) “Rheological and Shearing Conditions for the Preparation of Monodisperse Emulsions,” *Langmuir*, 16(2), pp. 422-429

Mabille, C., Leal-Calderon, F., Bibette, J. and Schmitt, V. (2003) “Monodisperse fragmentation in emulsions: Mechanisms and kinetics,” *Europhysics Letters (EPL)*, 61(5), pp. 708–714

Malkin, A. I., Ya, A. and Malkin (1994) *Rheology Fundamentals*. Toronto-Scarborough, Ont.: ChemTec Pub.

Marshall A. (1947). *Process and apparatus for continuously processing and extruding plasticizing materials*. US2640033 A

Mason, T. (1999) “New fundamental concepts in emulsion rheology,” *Current Opinion in Colloid & Interface Science*, 4(3), pp. 231–238

Mason, T. G. and Bibette, J. (1996) “Emulsification in Viscoelastic Media,” *Physical Review Letters*, 77(16), pp. 3481–3484

Mason, T. G. and Bibette, J. (1997) “Shear Rupturing of Droplets in Complex Fluids,” *Langmuir*, 13(17), pp. 4600–4613

Mason T.G., Wilking J.N., Meleson K., Chang C.B., Graves S.M. (2006) “Nanoemulsions: Formation, Structure and Physical Properties,” *Journal of Physics: Condensed Matter*, 18(41), pp. R635-R666.

McClements D.J. (2009) *Food Emulsions: Principles, Practices and Techniques*. CRC Press, Florida

McClements D.J. (2011) “Edible nanoemulsions: Fabrication, properties, and functional performance,” *Soft Matter*, 7(6), pp. 2297-2316

McManamey, W. (1979) “Sauter mean and maximum drop diameters of liquid-liquid dispersions in turbulent agitated vessels at low dispersed phase hold-up,” *Chemical Engineering Science*, 34(3), pp. 432–434

Mie G. (1908). “Beiträge zur Optik trüber Medien,” *Annalen der Physik*, 330(3), pp. 337-445

Mitchell, D. J. and Ninham, B. W. (1981) “Micelles, vesicles and microemulsions,” *Journal of the Chemical Society, Faraday Transactions 2*, 77(4), pp. 601-629

Morrison D.S. (1996) “Petrolatum: A Useful Classic. *Cosmetics and Toiletries Magazine*,” vol. 111, pp. 59-69

Muschiolik, G. (2007) “Multiple emulsions for food use,” *Current Opinion in Colloid & Interface Science*, 12(4-5), pp. 213–220

Mugele, R. A. and Evans, H. D. (1951) “Droplet Size Distribution in Sprays,” *Industrial & Engineering Chemistry*, 43(6), pp. 1317–1324

Niedzwiedz, K., Buggisch, H. and Willenbacher, N. (2010) “Extensional rheology of concentrated emulsions as probed by capillary breakup elongational rheometry (CaBER),” *Rheologica Acta*, 49(11-12), pp. 1103–1116

Oldroyd, J. G. (1955) “The Effect of Interfacial Stabilizing Films on the Elastic and Viscous Properties of Emulsions,” *Proceedings of the Royal Society A: Mathematical, Physical and Engineering Sciences*, 232(1191), pp. 567–577

Pal, R. (2001) "Novel viscosity equations for emulsions of two immiscible liquids," *Journal of Rheology*, 45(2), p. 509-520

Patist A., Kanicky J.R., Shukla P.K., Shah D.O. (2002) "Importance of micellar kinetics in relation to technological processes," *Journal of Colloid and Interface Science*, 245(1), pp. 1-15

Piela K., Janssen J.J.M., Bongers P. (2012) "Power Consumption of a Rotor-stator Mixer with Cavities," 14th European Conference on Mixing, Warszawa, pp. 377-382

Princen H. (1983) "Rheology of Foams and Highly Concentrated Emulsions I: Elastic Properties and Yield Stress of a Cylindrical Model System," *Journal of Colloid and Interface Science*, 91(1), pp. 160-175.

Princen H.M (1986) "Osmotic Pressure of Foams and Highly Concentrated Emulsions 1: Theoretical Considerations," *Langmuir*, 2(4), pp. 519-524

Princen H.M and Kiss A.D (1986) "Rheology of Foams and Highly Concentrated Emulsions III: Static Shear Modulus," *Journal of Colloid and Interface Science*, 112(2), pp. 427-437

Pope, S. B. (2000) *Turbulent flows*. 5th edn. Cambridge: Cambridge University Press

Raikar, N. B., Bhatia S. B., Malone M. F., McClements D. J. and Henson M. A. (2011) "Predicting the Effect of Pressure on the Drop Size Distributions of Homogenized Emulsions," *Industrial Engineering and Chemistry Research*, vol. 50(10), pp. 6089-6100

Rayleigh (1879) "On the Capillary Phenomena of Jets," *Proceedings of the Royal Society of London*, 29(196-199), pp. 71-97

Rele A.S., Mohile R. B. (2003) "Effect of mineral oil, sunflower oil, and coconut oil on prevention of hair damage," *Journal of Cosmetic Science*, vol. 54, pp. 175-192

Renk P. (1981). *Mixing Apparatus*. US4128342 A

Reynolds O. (1895) "On the dynamical theory of incompressible viscous fluids and the determination of the criterion," *Philosophical Transactions of the Royal Society of London. A*, 186, pp. 123-164

Rivera A.C.P., Bongers P.M.M., Egan M.J., Irving G.N., Kowalski A.J. (2012). *Mixing Apparatus and Method for Mixing Fluids*. WO 2012065824 A1

Rosen, M. J. (2004) *Surfactants and Interfacial Phenomena*. 3rd edn. United States: Wiley-Interscience

Rowe, R. C., Sheskey, P. J. and Owen, S. C. (2006) *Handbook of Pharmaceutical Excipients for CD-ROM/Book Package*. 5th edn. London: American Pharmaceutical Association

Rumscheidt F.D., Mason S.G. (1962) "Break-up of Stationary Liquid Threads," *Journal of Colloid Science*, vol. 17(3), pp. 260-269

Rybczynski, W. (1911) "Über die fortschreitende Bewegung einer flüssigen Kugel in einem zähen Medium," *Bulletin of the Academy of Sciences Krakow, A.*, pp. 40-46

Salager, J-L., Forgiarini A., Márquez L., Peña A., Pizzino A., Rodriguez M.P., Rondón-González M. (2004) "Using emulsion inversion in industrial processes," *Advances in Colloid and Interface Science*, vol. 108-109, pp. 259-272

Salager, J-L. (2005) *Emulsion Phase Inversion Phenomena*. In: Sjöblom, J., Sjöblom, S. (Eds.), *Emulsions and Emulsion Stability, Second Edition (Surfactant Science)*. Boca Raton: Taylor & Francis, Chapter 4

Sanders N.H. (2001) *Improvements in confectionery manufacture*. EP 1133239 A1

Shah R.K., Shum H.C., Rowat A.C., Lee D., Agresti J.J., Utada A.S., Chu L-Y., Kim J-W., Fernandez-Nieves A., Martinez C.J., Weitz D.A. (2008) "Designer emulsions using microfluidics," *Materials Today*, 11(4), pp. 18–27

Shinnar, R. (1961) "On the behaviour of liquid dispersions in mixing vessels," *Journal of Fluid Mechanics*, 10(02), pp. 259-275

Shinoda, K. and Saito, H. (1969) "The Stability of O/W type emulsions as functions of temperature and the HLB of emulsifiers: The emulsification by PIT-method," *Journal of Colloid and Interface Science*, 30(2), pp. 258–263

Shinoda, K. and Kunieda, H. (1973) "Conditions to produce so-called microemulsions: Factors to increase the mutual solubility of oil and water by solubilizer," *Journal of Colloid and Interface Science*, 42(2), pp. 381–387

Sonneville-Aubrun O., Simonnet J.T., L'Alloret F. (2004) "Nano-emulsions: a new vehicle for skincare products," *Advances in Colloid and Interface Science*, 108-109, pp. 145-149

Spencer, R. and Wiley, R. (1951) "The mixing of very viscous liquids," *Journal of Colloid Science*, 6(2), pp. 133–145

Stokes, G. G, 1851. "On the Effect of the Internal Friction of Fluids on the Motion of Pendulums. *Cambridge Philosophical Transactions*, 9, pp. 8-106

Tadros T., Izquierdo P., Esquena J., Solans C. (2004) “Formation and Stability of Nano-emulsions,” *Advances in Colloid and Interface Science*, 108-109, pp. 303-318

Talegaonkar, S., Mustafa, G., Akhter, S. and Iqbal, Z. I. (2010) “Design and Development of Oral Oil-in-Water Nanoemulsion Formulation Bearing Atorvastatin: In Vitro Assessment,” *Journal of Dispersion Science and Technology*, 31(5), pp. 690–701

Tal-Figiel, B. (2007) “The Formation of Stable W/O, O/W, W/O/W Cosmetic Emulsions in an Ultrasonic Field,” *Chemical Engineering Research and Design*, 85(5), pp. 730–734

Tal-Figiel, B. and Figiel, W. (2008) “Micro- and Nanoemulsions in Cosmetic and Pharmaceutical Products,” *Journal of Dispersion Science and Technology*, 29(4), pp. 611–616

Taylor, G. I. (1932) “The Viscosity of a Fluid Containing Small Drops of Another Fluid,” *Proceedings of the Royal Society A: Mathematical, Physical and Engineering Sciences*, 138(834), pp. 41–48

Taylor, G. I. (1934) “The Formation of Emulsions in Definable Fields of Flow,” *Proceedings of the Royal Society A: Mathematical, Physical and Engineering Sciences*, 146(858), pp. 501–523

Taylor G.I. (1935) “Statistical Theory of Turbulence,” *Proceedings of the Royal Society of London. Series A, Mathematical and Physical Sciences*, 151(873), pp. 421-444

Taylor J.M. (2002) *New Dimensions for Manufacturing A UK Strategy for Nanotechnology*. (Submitted on behalf of the UK Advisory Group on Nanotechnology Applications to Lord Sainsbury, Minister for Science and Innovation)

Tcholakova, S., Denkov, N. D. and Danner, T. (2004) “Role of Surfactant Type and Concentration for the Mean Drop Size during Emulsification in Turbulent Flow,” *Langmuir*, 20(18), pp. 7444–7458

Tcholakova, S., Lesov, I., Golemanov, K., Denkov, N. D., Judat, S., Engel, R. and Danner, T. (2011) “Efficient Emulsification of Viscous Oils at High Drop Volume Fraction,” *Langmuir*, 27(24), pp. 14783–14796

Technical document 1: Rawle A. (1993) “Basic Principles of Particle Size Analysis.” (accessed 22/02/2011, www.malvern.co.uk)

Technical document 2: Determination of the particle absorption for laser diffraction size calculations – www.malvern.co.uk (accessed 23/02/2011)

Technical document 3: Brookfield Engineering Laboratories Inc. (2003) Brookfield DV-II+ Pro Programmable Viscometer Operating Instructions. Manual Number M/03-65-C0508W, accessed 09/04/2014

Technical document 4: Brookfield Engineering Laboratories, Inc. More Solutions to Sticky Problems – A Guide to Getting More From Your Brookfield

Technical document 5: Thermofisher Scientific (2012) Data Sheet – IKA EUROSTAR power control-viscosity P1 Overhead Mixer, accessed (09/04/2014) http://www.thermofisher.com.au/Uploads/file/Scientific/Laboratory-Equipment-Furniture/Small-Equipment/IKA/Data_Sheet_EUROSTAR_power_control-visc_P1%5B1%5D.pdf

Technical document 6: Thermofischer Scientific (2012) Data-sheet - IKA T50 Basic Ultra Turrax Overhead Mixer (accessed 10/04/2014 - http://www.thermofisher.com.au/Uploads/file/Scientific/Laboratory-Equipment-Furniture/Small-Equipment/IKA/Data_Sheet_T_50_basic_ULTRA-TURRAX_%5B1%5D.pdf)

Technical document 7: Inoxpa pamphlet - supplier of SLES dilution systems
www.inoxpa.com/file/13778.html (Extracted 02/06/2011)

Technical document 8: Sonneborne G2212 Petrolatum MSDS - received with material, accessed 09/07/2012

Technical document 9: Accessed 09/10/2015. Material Safety Datasheet for Hexadecane - https://www.sigmaaldrich.com/content/dam/sigma-aldrich/docs/Sigma/Product_Information_Sheet/2/h0255pis.pdf

Technical document 10: Accessed 09/10/2015. Material Safety Datasheet for Mineral oil - <http://www.sigmaaldrich.com/MSDS/MSDS/DisplayMSDSPage.do?country=GB&language=en&productNumber=330779&brand=SIAL&PageToGoToURL=http%3A%2F%2Fwww.sigmaaldrich.com%2Fcatalog%2Fproduct%2Fsial%2F330779%3Flang%3Den>

Technical document 11: Access 09/10/2015: Material Safety Datasheet for Water. <http://www.sigmaaldrich.com/catalog/product/sial/denwat?lang=en®ion=GB>

Technical document 12: Accessed 28/08/2014: XIAMETER® PMX-200 Silicone Fluid, 50-1,000 CS – Properties Sheet

Technical document 13: Accessed 09/10/2015: Dow Corning 200 - 10,000 CST Silicone Fluid Safety Data Sheet. <http://www.dowcorning.com/DataFiles/09027701823e8f05.pdf>

Technical document 14: Accessed 09/10/2015: Dow Corning 200 - 60,000 CST Silicone Fluid Safety Data Sheet. <http://www.dowcorning.com/DataFiles/09027701823ee86a.pdf>

Thomson W. (1871) “On the equilibrium of vapour at a curved surface of liquid,” *Philosophical Magazine*, 42(282), pp. 448-452

Todd, D. B. (2004) *Mixing of Highly Viscous Fluids, Polymers, and Pastes*, in *Handbook of Industrial Mixing: Science and Practice* (eds E. L. Paul, V. A. Atiemo-Obeng and S. M. Kresta), John Wiley & Sons, Inc., Hoboken, NJ, USA, Chapter 16

Tomotika S. (1935) "On the Instability of a Cylindrical Thread of Viscous Liquid Surrounded by Another Viscous Liquid," *Proceedings of the Royal Society of London. Series A, Mathematical and Physical Sciences*, 150(870), pp. 322-337

Vankova N., Tcholakova S., Denkov N.D., Ivanov N.D., Vuchev V.D., Danner T. (2007) "Emulsification in Turbulent Flow 1. Mean and Maximum Drop Diameters in Inertial and Viscous Regimes," *Journal of Colloid and Interface Science*, 312(2), pp. 363-380

Vishnupad M., Ramirez J.E., Deppert T.M. (1990). *Water Rinsable Petroleum Jelly Compositions*. US4980084

Wang C.Y., Calabrese R.V. (1986) "Droplet Breakup in Turbulent Stirred-Tank Contactors Part II: Relative Influence of Viscosity and Interfacial Tension," *AIChE Journal*, 32(4), pp. 667-676

Wang C., Manas-zloczower I. (1994) "Flow Field Analysis of a Cavity Transfer Mixer," *Polymer Engineering and Science*, 34(15), pp. 1224-1230

Watson D.J., Mackley M.R. (2002) "The rheology of aqueous emulsions prepared by direct emulsification and phase inversion from a high viscosity alkyd resin," *Colloids and Surfaces A: Physicochemical and Engineering Aspects*, 196(2-3), pp. 121-134

Welch C.F., Rose G.D., Malotky D., Eckersley S.T. (2006) "Rheology of High Internal Phase Emulsions," *Langmuir*, 22(4), pp. 1544-1550

Wesdorp L.H., Struik M. (1988). *Edible fat product and a process for preparing such product*. EP 0264149 A1

Winsor P.A. 1948 “Hydrotropy, solubilisation and related Emulsification processes,” Part I. Transactions of the Faraday Society, vol. 44, pp. 376-398

Yang Z.-Z, Zhao D.-L., 2000. “Preparation of bisphenol A epoxy resin waterborne dispersions by the phase inversion emulsification technique,” Chinese Journal of Polymer Science, 18(1), pp. 33-38

AX2: Chapter 4 Supporting Information**AX2.1: Domain Size Analysis Protocol**

Equipment Type and Measurement Settings – Laser Diffraction	
Equipment Type	
Dispersion Unit Type / Speed Setting	Hydro SM
Measurement Settings	
Dispersion Unit Speed Setting	1280 RPM
Measurement Cycles per Aliquot	3
Measurement Delay	5 seconds
Measurement Time / Background Time	12 seconds / 12 seconds
Measurement Snaps / Background Snaps	12000 / 12000
Obscuration on Measurement	0% to 13%
Laser power on Measurement	78% to 82%

AX2.2: Glass-bead Standards Size Measurement on Mastersizer 2000

Measured sample	d₃₂ (µm)
Listed particle standard size	0.200
Sample 1	0.196
Sample 2	0.216
Sample 3	0.212
Sample 4	0.214
Analysis	
Sample mean size (µm)	0.210
Sample SE (µm)	0.004
Percent SE (%)	1.891
Sample SD (µm)	0.008
Percent SD (%)	3.781
% Error from particle standard	+4.750

Table a)

Measured sample	d₅₀ (µm)
Listed particle standard size	4.520
Sample 1	4.799
Sample 2	4.619
Sample 3	4.871
Analysis	
Sample mean size (µm)	4.763
Sample SE (µm)	0.061
Percent SE (%)	1.285
Sample SD (µm)	0.106
Percent SD (%)	2.225
% Error from particle standard	+5.376

Table b)

AX2.3: Determination of PJ RI for Domain Size Measurement

Sample Number	Formulation	Refractive Index	Absorption	Residual	D ₃₂ (µm)	D ₄₃ (µm)
Set Concentration						
120718RB03	20wt.% PJ, 25wt.% SLES	1.485	0.001	0.616	2.95	3.307
120719RB24	83.33wt.% PJ, 25wt.% SLES	1.489	0.002	0.384	1.821	2.01
120719RB20-4	83.33 wt.% PJ, 25 wt.% SLES	1.485	0.004	1.052	1.296	1.387
120719RB04-2	60wt.% PJ, 25wt.% SLES	1.502	0.005	1.502	2.122	2.280
120719RB29-2	60.00 wt.% PJ, 25 wt.% SLES	1.500	0.005	1.164	2.085	2.236
Set Phase Volume						
120126RB01	74.64wt.% PJ, O : S = 16.7 : 1	1.490	0.005	0.259	2.524	2.724
120126RB10	74.64wt.% PJ, O : S = 12.5 : 1	1.468	0.001	1.451	1.400	1.492
120126RB16-2	74.64wt.% PJ, O : S = 10.4 : 1	1.502	0.002	1.480	0.986	1.050
120126RB19	74.64wt.% PJ, O : S = 8.7:1	1.496	0.001	1.232	1.041	1.111
120718RB03-2	20 wt.% PJ, 25wt.% SLES	1.491	0.001	0.629	2.976	3.280
120719RB08-1	74.64wt.% PJ, O : S = 10 : 1	1.500	0.002	1.067	2.179	2.359
120722RB26-1	74.64wt.% PJ, 25wt.% SLES	1.490	0.003	0.366	2.484	2.723
120803RB03-1	74.64wt.% PJ, 25wt.% SLES	1.483	0.004	1.166	1.299	1.390
120131RB14-2	74.64wt.% PJ, O : S = 8.0:1	1.540	0.001	1.200	0.794	0.874
120131RB07-3	74.64wt.% PJ, O : S = 9.8:1	1.491	0.003	0.979	1.371	1.464
120719RB15-1	74.64wt.% PJ, 25wt.% SLES	1.476	0.003	1.120	1.402	1.498
120722RB03-1	74.64wt.% PJ, 7.358wt.% SLES	1.479	0.001	0.649	5.180	6.502
120722RB09-1	74.64wt.% PJ, 14.72 wt.% SLES	1.490	0.002	0.741	2.588	2.788
120722RB14-3	74.64wt.% PJ, 19.621 wt.% SLES	1.495	0.002	0.946	2.148	2.306
120722RB18-3	74.64wt.% PJ, 25.00 wt.% SLES	1.469	0.001	0.839	1.686	1.816
120722RB28-1	74.64wt.% PJ, 25 wt.% SLES	1.469	0.001	0.885	1.683	1.814
120722RB25-1	74.64wt.% PJ, 19.62 wt.% SLES	1.490	0.001	0.656	1.833	1.961
120722RB28-2	74.64wt.% PJ, 25 wt.% SLES	1.466	0.002	0.970	1.683	1.814
Set Ratio						
110720RB06	74.6 wt.% PJ, O : S = 8.33 : 1	1.519	0.001	0.75	1.201	1.28
110726RB04	66.7 wt.% PJ, O : S = 8.33 : 1	1.494	0.004	0.625	1.325	1.41
120720RB05	71.4 wt.% PJ, O : S = 8.33 : 1	1.516	0.001	1.059	0.946	1.00
Average Results:		1.49	0.003			

AX2.4: Measurement of Dow Corning 200 Standard, 10000 cSt silicone oil on Brookfield™ DV-II+ Pro Programmable Viscometer at 25°C

Measured viscosity (cP)	Mean viscosity (cP)	Silicone oil standard viscosity (cP)	SE (cP)	SE (%)	SD (cP)	SE (%)	% difference from standard
10715	10797	9710	58	0.539	82	0.76	+11.19
10879							

*Properties of the 10000 cSt Silicone Oil standard were extracted from Technical document 13.

AX2.5: Measurement of Dow Corning 200 Standard, 60000 cSt silicone oil on Brookfield™ DV-II+ Pro Programmable Viscometer at 25°C

Measured viscosity at	Mean viscosity at	Silicone oil standard viscosity at 25°C (cP)	SE (cP)	SE (%)	SD (cP)	SE (%)	% difference from standard
58786	59342	58800	316	0.532	547	0.92	+0.922
59155							
60086							

*Properties of the 60000 cSt Silicone Oil standard were extracted from Technical document 14.

AX2.6: Repeat Measurements of PJ/SLES (Table 1), SFSO/NS samples (Table 2) and SFSO/Pluronic (Table 3) on the Malvern™ Mastersizer 2000

Repeat measurements - PJ/SLES samples	Domain size		Repeat measurements - SFSO/NS samples	Domain size	
	d ₃₂ (µm)	d ₄₃ (µm)		d ₃₂ (µm)	d ₄₃ (µm)
Sample 1	1.789	2.182	Sample 1	43.235	51.196
Sample 2	1.808	2.276	Sample 2	41.526	48.055
Sample 3	1.849	2.909	Sample 3	43.443	49.466
Sample 4	1.778	2.181	Sample 4	41.616	49.718
Sample 5	1.749	2.139	Sample 5	42.560	49.098
Sample 6	1.804	2.242	Sample 6	31.887	45.948
Sample 7	1.752	2.141	Sample 7	43.943	50.250
Sample 8	1.816	2.304	Sample 8	45.588	51.499
Sample 9	1.801	2.210	Sample 9	41.539	48.875
Sample 10	1.790	2.225	Sample 10	42.174	49.939
Analysis			Analysis		
Sample mean size (µm)	1.794	2.281	Sample mean size (µm)	41.751	49.404
Sample SE (µm)	0.009	0.068	Sample SE (µm)	1.11	0.48
Sample SE (%)	0.497	2.987	Sample SE (%)	2.65	0.97
Sample SD (µm)	0.028	0.215	Sample SD	3.505	1.511
Sample SD (%)	1.571	9.446	Sample SD (%)	8.395	3.059

Table a)

Table b)


Repeat measurements - SFSO/Pluronic samples	Domain size	
	d ₃₂ (µm)	d ₄₃ (µm)
Sample 1	2.950	4.960
Sample 2	3.031	5.037
Sample 3	3.061	5.319
Analysis		
Sample mean size (µm)	3.014	5.105
Sample SE (µm)	0.001	0.008
Sample SE (%)	0.023	0.148
Sample SD (µm)	0.002	0.024
Sample SD (%)	0.073	0.466

Table c)


AX2.7: Repeat measurements of SFSO/NS samples on Brookfield™*DV-II+ Pro Programmable Viscometer at 20+/-1 °C*

Measured viscosity (cP)	Mean viscosity (cP)	SE (cP)	SE (%)	SD (cP)	SD (%)
37102	40162	1124	2.798	3554	8.848
33313					
46002					
40057					
39109					
39284					
45944					
39794					
40189					
40821					


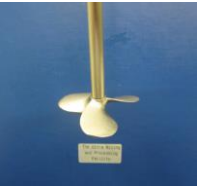


AX2.8: Images and Design Criteria of Overhead Mixers**Design Criteria: Overhead Stirrer - IKA EUROSTAR power control-visc P1**

	Motor Power (W) of Input / Output	153 / 134
	Power Output Max at Stirrer Shaft	126
	Speed Display	LCD
	Speed Range (RPM)	50 - 2000
	Maximum Viscosity (cP)	70000
	Speed Control Type	Stepless Drive
	Dimensions (mm) (W x H x D)	80 x 253 x 190

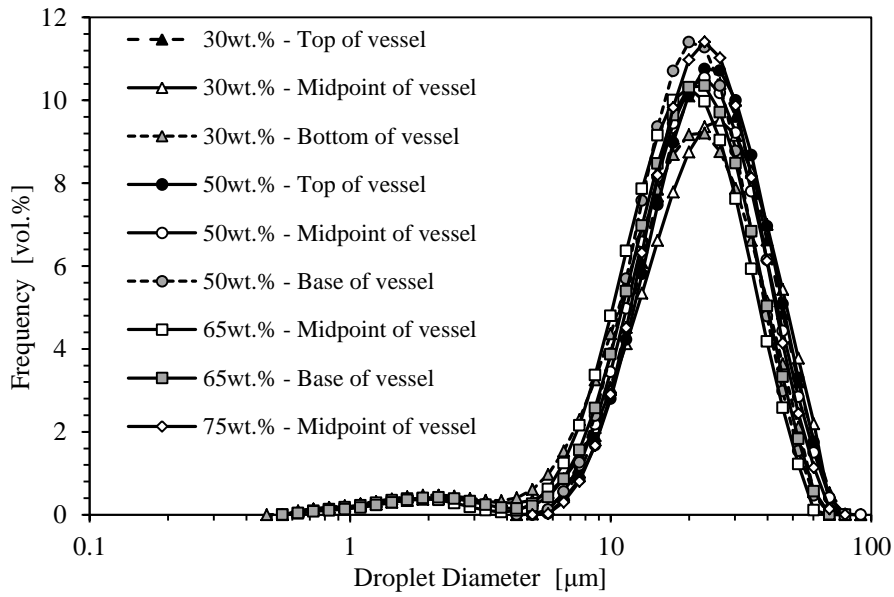
Design Criteria: IKA T 50 basic ULTRA-TURRAX®

	Motor Power (W) of Input / Output	1100 / 700
	Speed Display	scale
	Speed Range (RPM)	500 - 10000
	Maximum Viscosity	5000
	Speed Control Type	Stepless Drive
	Dimensions (mm) (W x H x D)	125 x 367 x 120
	Batch Volume (l): Maximum / Minimum	30 / 0.25

AX2.9: Images and Design Criteria of Overhead Mixing Attachments

Design Criteria: Overhead Mixers	Shaft Length	Head Diameter	Blade Length	Head Height	Blade Width
4-Blade Paddle 	530 mm +/- 0.5 mm	109.6 mm +/- 0.02 mm	41.18 mm +/- 0.02 mm	13.74 mm +/- 0.02 mm	14.34 mm +/- 0.02 mm
3-Blade Propeller 	390 mm +/- 0.5 mm	53.14 mm +/- 0.02 mm	25.92 mm +/- 0.02 mm	10.70 mm +/- 0.02 mm	19.52 mm +/- 0.02 mm
Jiffy Mixer 	315 mm +/- 0.5 mm	65.20 mm +/- 0.5 mm	65.80 mm +/- 0.02 mm	59.02 mm +/- 0.02 mm	19.72 +/- 0.02 mm
5-Blade Toothed 	340 mm +/- 0.5 mm	29.55 mm +/- 0.02 mm	9.68 mm +/- 0.02 mm	11.38 mm +/- 0.02 mm	8.04 mm +/- 0.02 mm

AX2.10: Coarse pre-mix size distributions – SFSO/Pluronic



AX2.11: Coarse pre-mix size distribution – Table a) SFSO/Pluronic and Table b) SFSO/NS

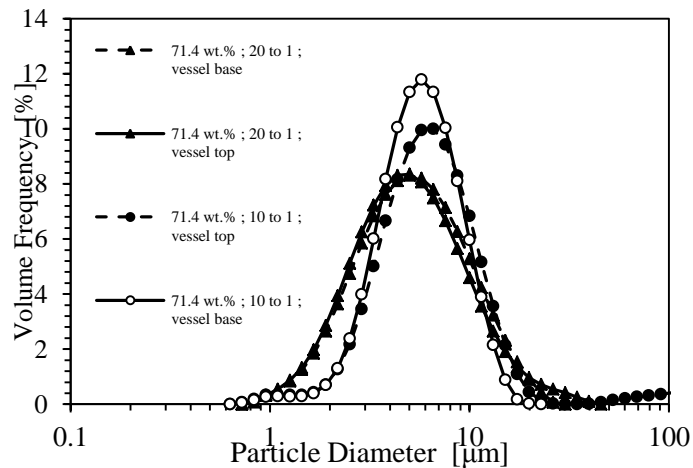
Vessel Position	Domain size	
	d ₃₂ (μm)	d ₄₃ (μm)
Top-middle	11.021	20.074
Middle-middle	11.971	19.275
Bottom-middle	12.726	20.676
Analysis		
Mean domain size (μm)	11.91	20.01
SE (μm)	0.285	0.234
Percent SE (%)	2.39	1.17
SD (μm)	0.70	0.57
Percent SD (%)	5.859	2.868

Table a)

Vessel Position	Domain size	
	d ₃₂ (μm)	d ₄₃ (μm)
Top-middle	34.365	40.452
Top-right	35.921	43.250
Middle-left	36.445	44.37
Middle-middle	37.297	44.574
Middle-right	34.174	42.153
Back-middle	41.128	47.675
Analysis		
Mean domain size (μm)	36.56	43.75
SE (μm)	0.95	0.92
Percent SE (%)	2.59	2.09
SD (μm)	2.32	2.24
Percent SD (%)	6.351	5.124

Table b)

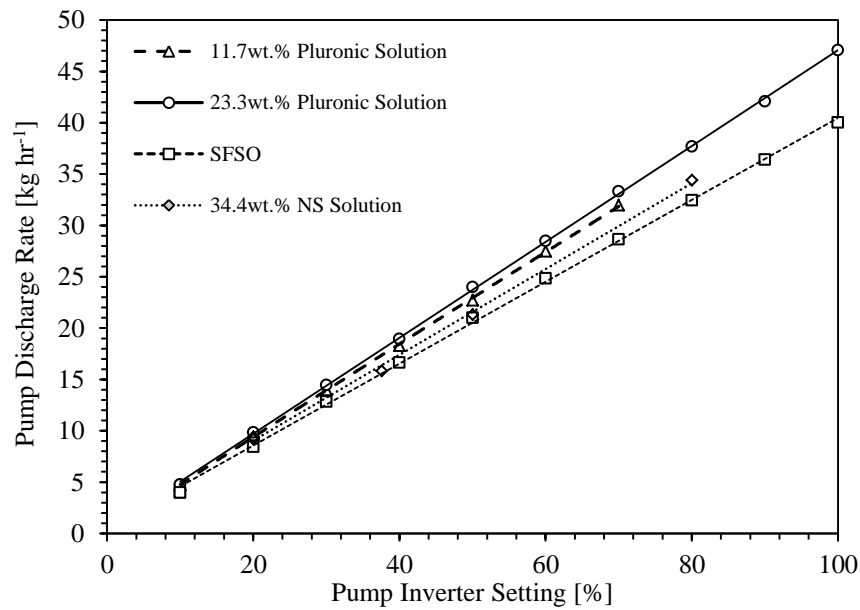
AX2.12: Coarse pre-mix size distributions – PJ/SLES



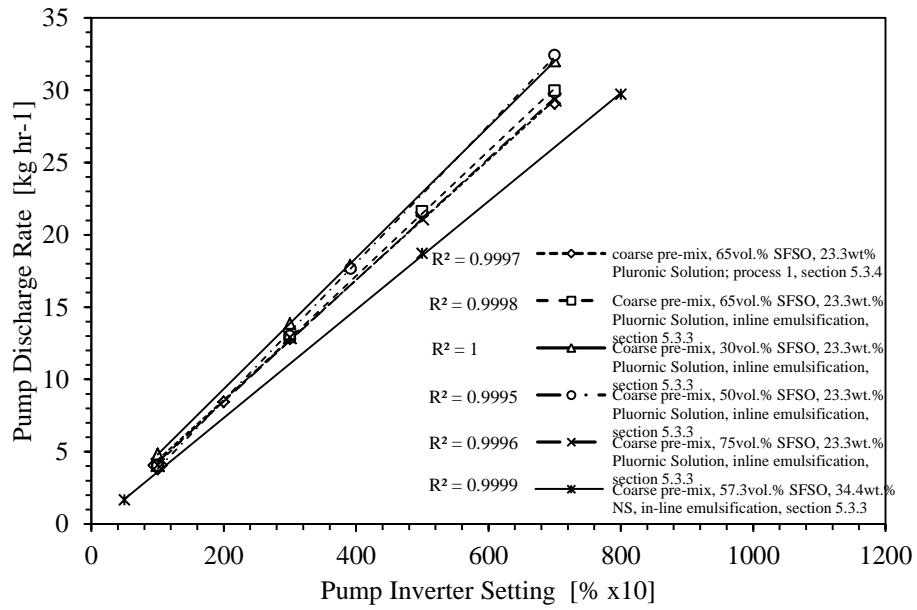
AX2.13: Course pre-mix size distribution - 83.33wt.% PJ /SLES, PJ:SLES = 20:1

Vessel Position	Domain size	
	d ₃₂ (μm)	d ₄₃ (μm)
Top-middle	4.169	6.169
Top-right	3.726	5.090
Middle-middle	3.702	4.966
Middle-right	4.296	6.127
Middle-left	4.070	5.582
Back-middle	4.038	5.319
Analysis		
Mean domain size (μm)	4.00	5.54
SE (μm)	0.089	0.192
Percent SE (%)	2.23	3.46
SD (μm)	0.22	0.47
Percent SD (%)	5.462	8.472

AX2.14: PCP Discharge Calibration Curves – SFSO and Surfactant Solutions



AX2.15: PCP Discharge Calibration Curves – Pre-mixes

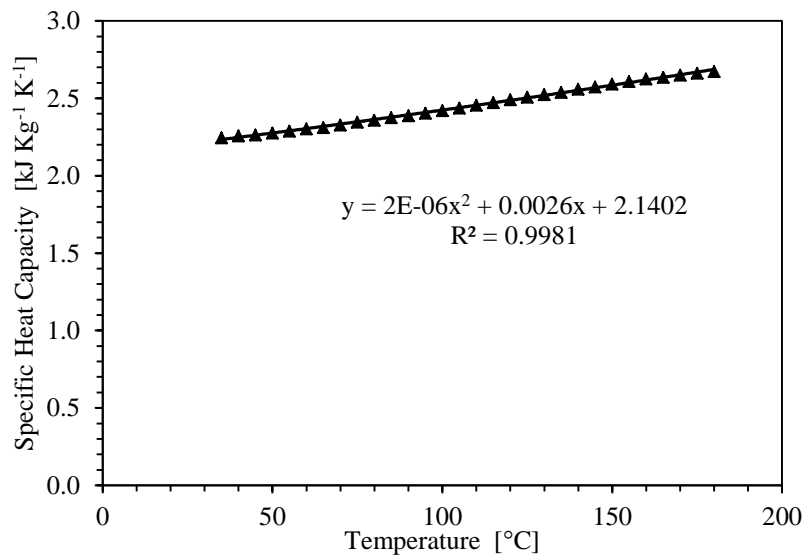


AX3: Chapter 5 Supporting Information

AX3.1: Results of Chapter 5, section 5.3.1

Mixer Position	Oil [wt%]	O / S [wt./wt.]	Throughput [kg/hr]	Rotational Speed [RPM]	d ₃₂ [µm]	d ₄₃ [µm]	d ₁₀ [µm]	d ₅₀ [µm]	d ₉₀ [µm]	Span
-0.25mm	50	10	CONTROL		10.11	14.97	5.91	13.61	26.34	1.50
	50	10	69.62	10000	1.40	3.39	0.98	2.84	6.57	1.97
+0.25mm	50	10	CONTROL		10.11	14.97	5.91	13.61	26.34	1.50
	50	10	69.62	10000	1.71	3.14	1.05	2.72	5.93	1.80
+0.75mm	50	10	CONTROL		9.02	13.02	5.32	11.43	23.26	1.57
	50	10	69.62	10000	2.21	3.46	1.14	2.99	6.52	1.80
+1.75mm	50	10	CONTROL		9.70	12.90	5.675	11.32	22.46	1.482
	50	10	69.62	10000	1.97	3.31	1.081	2.884	6.234	1.787
	50	10	69.62	10000	1.95	3.37	1.065	2.883	6.438	1.864
+2.75mm	50	10	CONTROL		8.38	10.58	4.93	9.54	17.84	1.35
	50	10	69.62	10000	1.86	3.31	1.00	2.83	6.29	1.87

Mixer Position	Oil [wt%]	O / S [wt./wt.]	Throughput [kg/hr]	Rotational Speed [RPM]	d ₃₂ [μm]	d ₄₃ [μm]	d ₁₀ [μm]	d ₅₀ [μm]	d ₉₀ [μm]	Span	T _{in} (°C)	T _{out} (°C)
+0.25mm	70	10	CONTROL		12.27	19.28	8.77	17.75	32.53	1.34	N/A	
	70	10	65.97	0	4.57	8.13	2.34	6.11	17.07	2.41	15.1	17.7
	70	10	66.66	5000	0.56	1.01	0.24	0.91	1.98	1.92	14.9	25.1
	70	10	85.55	10000	0.29	0.47	0.14	0.37	0.95	2.16	15.0	37.7
	70	10	119.91	0	2.42	3.72	1.31	2.86	7.31	2.10	15.1	19.0
	70	10	116.82	5000	0.62	0.95	0.30	0.84	1.75	1.73	14.9	21.6
+0.75mm	70	10	CONTROL		10.32	15.30	6.44	13.73	26.68	1.48	N/A	
	70	10	63.22	0	5.51	9.90	3.14	7.81	18.54	1.97	15.1	17.7
	70	10	64.25	5000	0.60	1.25	0.24	1.16	2.47	1.92	14.9	24.1
	70	10	64.25	10000	0.35	0.57	0.18	0.45	1.15	2.16	14.9	37.7
	70	10	123.69	0	4.86	7.83	2.80	6.52	14.68	1.82	15.1	18.3
	70	10	123.69	5000	0.62	1.56	0.22	1.47	3.05	1.93	14.9	21.2
	70	10	129.19	10000	0.43	0.72	0.20	0.63	1.37	1.86	14.9	29.1
	70	10	266.28	0	2.95	4.08	1.71	3.51	7.01	1.51	15.1	18.0
	70	10	253.57	5000	0.98	1.81	0.43	1.65	3.38	1.79	14.9	19.6
	70	10	275.6	10000	0.46	0.77	0.21	0.70	1.45	1.76	15.0	22.8
	70	10	270.06	0	3.06	4.23	1.79	3.76	7.45	1.50	15.1	17.9
	70	10	257.01	0	3.53	5.22	2.03	4.37	9.54	1.72	15.1	17.9
	70	10	64.6	10000	0.35	0.55	0.18	0.44	1.10	2.08	15.0	37.9
	70	10	64.6	10000	0.35	0.56	0.17	0.45	1.13	2.15	15.0	38.2
+1.75mm	70	10	CONTROL		9.07	14.63	5.48	13.00	26.48	1.62	N/A	
	70	10	62.88	0	6.34	10.01	3.52	8.48	18.99	1.83	15.0	17.1
	70	10	61.50	5000	0.52	1.17	0.21	1.06	2.38	2.05	14.8	23.4
	70	10	62.88	10000	0.33	0.55	0.16	0.43	1.12	2.23	14.9	37.1
	70	10	121.63	0	6.99	11.46	3.95	9.74	21.78	1.83	15.0	18.0
	70	10	128.50	5000	0.74	2.02	0.27	1.91	3.87	1.89	14.8	20.3
	70	10	120.94	10000	0.35	0.69	0.16	0.58	1.40	2.13	14.9	28.1
	70	10	287.93	0	4.47	7.00	2.53	6.01	13.05	1.75	15.0	17.8
	70	10	288.62	5	1.21	2.49	0.51	2.30	4.62	1.79	14.8	18.9
	70	10	290.34	10000	0.66	1.04	0.30	0.97	1.85	1.58	14.9	21.6
	70	10	286.21	0	3.99	6.12	2.40	5.43	11.00	1.58	15.1	17.8
	70	10	275.56	0	4.99	7.96	2.82	6.83	15.00	1.78	15.1	17.5
	70	10	74.90	10000	0.40	0.62	0.20	0.52	1.22	1.98	14.9	34.6
	70	10	66.31	10000	0.37	0.58	0.19	0.47	1.14	2.05	14.9	37.3
+2.75mm	70	10	CONTROL		11.71	15.57	7.42	14.19	25.93	1.31	N/A	
	70	10	63.91	5000	0.63	1.44	0.24	1.34	2.84	1.95	21.2	27.9
	70	10	65.63	10000	0.37	0.59	0.18	0.47	1.19	2.16	21.2	37.6
	70	10	127.13	0	6.51	10.26	3.55	8.82	19.26	1.78	21.3	21.3
	70	10	127.13	5000	0.71	1.89	0.25	1.78	3.66	1.91	21.1	24.6
	70	10	127.13	10000	0.53	0.80	0.26	0.73	1.45	1.64	21.1	31.6
	70	10	264.57	0	5.40	8.02	3.08	7.03	14.59	1.64	21.0	21.3
	70	10	280.37	5000	1.17	2.65	0.51	2.47	4.82	1.74	21.0	23.2
	70	10	261.13	10000	0.48	0.96	0.21	0.91	1.78	1.72	21.0	26.3
	70	10	65.63	0	6.18	9.13	3.59	8.27	16.15	1.52	21.2	21.7
	70	10	CONTROL		9.12	12.39	5.44	11.10	21.36	1.44	N/A	
	70	10	84.52	10000	0.37	0.66	0.18	0.53	1.27	2.06	15.6	32.8
	70	10	84.87	10000	0.39	0.64	0.19	0.54	1.26	1.98	15.6	32.2
	70	10	85.55	10000	0.40	0.66	0.19	0.55	1.28	1.98	15.6	32.9

AX3.2: Specific Heat Capacity (C_p) of Sunflower Oil (Fasina, Colley, 2008)**AX3.3: Results of experiments in section 5.3.2**

Mixer Geometry	SFSO Fraction [vol.%]	Pluronic Conc. [wt.%]	Throughput [kg/hr]	Rotational Speed [RPM]	d_{32} [μ m]	d_{43} [μ m]	d_{10} [μ m]	d_{50} [μ m]	d_{90} [μ m]	Span
0mm	65.0	11.7	36.0	0	1.52	4.82	1.11	3.51	10.59	2.70
		11.7	35.7	6000	2.30	3.48	1.24	2.93	6.38	1.76
		11.7	36.5	6000	2.35	3.60	1.27	3.08	6.76	1.78
		11.7	35.8	12000	1.63	2.36	0.96	2.12	4.16	1.51
		11.7	36.7	12000	1.72	2.42	1.03	2.18	4.21	1.46
		11.7	36.4	15000	1.26	1.94	0.78	1.76	3.40	1.49
0mm	79.5	11.7	35.7	15000	1.47	2.06	0.90	1.88	3.54	1.41
		11.7	35.7	6000	2.32	3.23	1.27	2.78	5.92	1.67
		11.7	35.9	12000	1.52	1.87	0.93	1.69	3.11	1.29
0mm	65.0	11.7	35.3	15000	1.44	1.62	0.98	1.55	2.36	0.89
		23.3	35.0	6000	0.52	0.75	0.27	0.62	1.43	1.87
		11.7	36.1	15000	0.46	0.56	0.27	0.52	0.90	1.20
		11.7	35.5	12000	0.44	0.56	0.25	0.50	0.95	1.39
		11.7	35.5	6000	0.51	0.72	0.27	0.61	1.35	1.78
		11.7	34.4	6000	0.50	0.71	0.26	0.60	1.33	1.79

Mixer Geometry	SFSO Fraction [vol.%]	Pluronic Conc. [wt.%]	Flowrate [kg/hr]	Mixing Speed [RPM]	D ₃₂ [μm]	d ₄₃ [μm]	d ₁₀ [μm]	d ₅₀ [μm]	d ₉₀ [μm]	Span
1.35mm	65	23.3	COARSE PRE-MIX		11.97	19.28	8.46	17.61	33.01	1.40
	65	23.3			12.73	20.68	9.02	18.97	35.32	1.39
	65.0	23.3	4.2	6000	0.41	0.55	0.22	0.49	0.99	1.58
	65.0	23.3	13.5	6000	0.83	1.28	0.41	1.14	2.34	1.69
	65.0	23.3	22.6	6000	1.05	1.72	0.52	1.47	3.31	1.89
	65.0	23.3	31.3	6000	1.47	2.14	0.77	1.79	4.03	1.82
	65.0	23.33	COARSE PRE-MIX		1.54	3.03	0.87	2.26	6.32	2.41
	65.0	23.3	3.4	6000	0.55	0.76	0.29	0.67	1.37	1.62
	65.0	23.3	12.8	6000	0.77	1.12	0.39	1.02	1.99	1.57
	65.0	23.3	21.3	6000	0.79	1.17	0.41	1.06	2.09	1.59
	65.0	23.3	29.1	6000	0.82	1.21	0.42	1.10	2.22	1.65
	65.0	23.3	8.4	6000	0.64	0.93	0.33	0.84	1.68	1.62
	65.0	23.3	4.4	6000	0.54	0.75	0.29	0.66	1.33	1.57
	65.0	23.3	4.4	6000	0.54	0.75	0.29	0.66	1.34	1.59
	65.0	23.3	4.4	6000	0.53	0.75	0.28	0.66	1.36	1.64
			COARSE PRE-MIX		0.74	1.09	0.39	0.92	1.94	1.69
	65.0	23.3	5.0	6000	0.47	0.63	0.26	0.55	1.12	1.55
	65.0	23.3	10.3	6000	0.67	0.91	0.37	0.79	1.64	1.61
	65.0	23.3	17.2	6000	0.68	0.99	0.36	0.85	1.76	1.63
	65.0	23.3	28.8	6000	0.62	0.89	0.32	0.79	1.60	1.61
65.0	23.3	19.2	6000	0.58	0.81	0.31	0.72	1.44	1.57	
0mm	65.0		COARSE PRE-MIX			10.34	14.90	6.47	13.54	25.71
	65.0	23.3	35.0	6000	0.52	0.75	0.27	0.62	1.43	1.87
	65.0	23.3	35.5	6000	0.51	0.72	0.27	0.61	1.35	1.78
	65.0	23.3	34.4	6000	0.50	0.71	0.26	0.60	1.33	1.79
	65.0	23.3	18.0	6000	0.59	0.76	0.34	0.68	1.30	1.41
	65.0	23.3	18.8	6000	0.61	0.73	0.38	0.68	1.14	1.11
	65.0	23.3	19.0	6000	0.55	0.63	0.36	0.60	0.94	0.96
	65.0	23.3	17.9	6000	0.59	0.91	0.39	0.84	1.54	1.38
65.0	23.3	67.4	6000	0.33	0.55	0.16	0.42	1.14	2.32	

AX3.4: Further results of experiments in section 5.3.2

Mixer Geometry	SFSO Fraction [vol.%]	Pluronic Conc. [wt.%]	Flowrate [kg/hr]	Mixing Speed [RPM]	Pass #	d ₃₂ [μm]	d ₄₃ [μm]	d ₁₀ [μm]	d ₅₀ [μm]	d ₉₀ [μm]	Span
0mm	65.0	11.7	CONTROL		0	21.68	24.90	14.28	23.31	37.75	1.01
	65.0	11.7	17.35	6000	1	2.85	4.21	1.61	3.71	7.60	1.61
	65.0	11.7	17.50	6000	2	1.91	2.70	1.11	2.42	4.73	1.50
	65.0	11.7	17.46	6000	3	1.72	2.38	1.02	2.16	4.10	1.43
0mm	65.0	23.3	CONTROL		0	9.78	19.22	6.83	17.72	34.16	1.54
	65.0	23.3				7.74	15.91	3.92	13.99	30.70	1.92
	65.0	23.3				10.84	20.68	8.30	19.03	36.22	1.47
	65.0	23.3	17.31	6000	1	1.01	1.64	0.53	1.43	3.06	1.77
	65.0	23.3	17.31	6000		1.11	1.70	0.62	1.44	3.03	1.68
	65.0	23.3	17.31	6000		1.07	1.69	0.56	1.46	3.14	1.77
	65.0	23.3	17.12	6000	2	0.73	1.05	0.37	0.96	1.87	1.57
	65.0	23.3	17.12	6000		0.72	1.05	0.36	0.96	1.86	1.57
	65.0	23.3	17.12	6000		0.68	1.04	0.33	0.96	1.86	1.59
	65.0	23.3	17.12	6000	3	0.62	0.87	0.32	0.79	1.55	1.56
65.0	23.3	17.12	6000	0.63		0.87	0.33	0.79	1.53	1.52	
65.0	23.3	17.12	6000	0.62		0.87	0.32	0.79	1.55	1.56	
1.35mm	65.0	23.3	CONTROL		0	10.34	14.90	6.47	13.54	25.71	1.42
	65.0	23.3	17.33	6000	1	0.59	0.76	0.34	0.68	1.30	1.41
	65.0	23.3	17.94	6000		0.59	0.91	0.39	0.84	1.54	1.38
	65.0	23.3	17.90	6000		0.63	0.92	0.41	0.85	1.55	1.34
	65.0	23.3	17.77	6000	2	0.65	0.93	0.42	0.86	1.55	1.32
	65.0	23.3	17.04	6000		0.58	0.73	0.34	0.67	1.20	1.29
65.0	23.3	17.05	6000	3	0.48	0.59	0.28	0.55	0.97	1.26	

AX3.5: Results of Experiments in section 5.3.3 – Direct Formation

Final SFSO [wt%]	Pluronic Solution [wt.%]	Q [kg/hr]	N [RPM]	d ₃₂ [µm]	d ₄₃ [µm]	d ₁₀ [µm]	d ₅₀ [µm]	d ₉₀ [µm]	Span	
30.0	23.3	18+/-1.8	3000	9.13	25.90	4.57	19.73	57.00	2.66	
30.0	23.3		6000	2.37	6.85	1.44	4.82	15.14	2.84	
30.0	23.3		6000	3.02	5.82	1.36	4.56	12.33	2.41	
30.0	23.3		6000	2.38	6.77	1.29	4.74	15.56	3.01	
40.0	23.3		3000	6.93	17.64	3.27	13.44	38.73	2.64	
40.0	23.3		6000	2.24	4.98	1.14	3.49	10.95	2.81	
50.0	23.3		3000	5.05	12.95	2.30	9.62	28.82	2.76	
50.0	23.3		6000	1.28	2.89	0.63	2.29	6.00	2.35	
60.0	23.3		3000	3.86	8.91	1.74	6.56	19.82	2.76	
60.0	23.3		3000	4.25	9.66	1.89	7.53	20.94	2.53	
60.0	23.3		3000	4.40	9.79	1.95	7.53	21.28	2.57	
60.0	23.3		6000	1.35	2.57	0.66	1.98	5.11	2.25	
70.0	23.3		3000	DESTABILISED						
70.0	23.3		6000	DESTABILISED						
65.0	23.3		3000	4.24	9.68	1.84	7.74	20.59	2.42	
65.0	23.3		6000	1.19	2.05	0.64	1.62	4.12	2.15	
67.5	23.3		3000	DESTABILISED						
67.5	23.3		6000	1.24	2.38	0.61	1.65	4.95	2.63	
67.5	23.3		6000	1.36	3.09	0.66	1.90	6.92	3.30	
67.5	23.3		6000	1.49	2.54	0.72	1.87	5.09	2.33	
67.5	23.3	7200	0.83	1.40	0.41	1.15	2.77	2.06		
67.5	23.3	7200	0.85	1.39	0.42	1.15	2.72	1.99		
Final SFSO [wt%]	Pluronic Solution [wt.%]	Q [kg/hr]	N [RPM]	d ₃₂ [µm]	d ₄₃ [µm]	d ₁₀ [µm]	d ₅₀ [µm]	d ₉₀ [µm]	Span	
30.0	23.3	36+/-3.6	3000	10.80	26.48	5.74	22.37	53.64	2.14	
30.0	23.3		6000	4.79	11.12	2.20	8.39	24.51	2.66	
40.0	23.3		3000	8.84	20.37	4.28	18.45	39.57	1.91	
40.0	23.3		6000	3.69	8.65	1.67	6.24	19.44	2.85	
50.0	23.3		3000	7.22	19.41	3.24	15.45	41.93	2.50	
50.0	23.3		6000	2.70	6.87	1.40	5.04	15.24	2.75	
60.0	23.3		3000	7.07	19.06	3.09	15.47	40.81	2.44	
60.0	23.3		6000	2.25	4.49	1.00	3.44	9.72	2.54	
65.0	23.3		3000	6.34	15.38	2.79	12.64	32.39	2.34	
65.0	23.3		6000	1.86	4.61	0.94	3.62	9.85	2.46	
70.0	23.3		6000	DESTABILISED						
70.0	23.3		7200	DESTABILISED						
70.0	23.3		8400	DESTABILISED						
67.5	23.3		8400	DESTABILISED						
65.0	23.3		6000	2.29	5.10	1.03	4.03	10.87	2.44	
65.0	23.3		7200	1.71	2.97	0.81	2.39	6.03	2.18	
65.0	23.3		8400	DESTABILISED						
65.0	23.3		8400	1.48	2.76	0.71	2.06	5.84	2.49	

Final SFSO [wt%]	Pluronic Solution [wt.%]	Q [kg/hr]	N [RPM]	d ₃₂ [μm]	d ₄₃ [μm]	d ₁₀ [μm]	d ₅₀ [μm]	d ₉₀ [μm]	Span	
30.0	11.7	18+/-1.8	3000	DESTABILISED						
30.0	11.7		6000	DESTABILISED						
40.0	11.7		3000	DESTABILISED						
40.0	11.7		6000	10.48	23.02	5.88	18.09	46.95	2.27	
50.0	11.7		3000	18.00	38.38	11.62	32.94	73.93	1.89	
50.0	11.7		6000	7.57	15.22	3.84	11.94	31.74	2.34	
60.0	11.7		3000	15.38	35.56	8.94	30.63	70.09	2.00	
60.0	11.7		6000	5.88	11.41	3.01	8.85	23.73	2.34	
60.0	11.7		6000	6.23	11.95	3.18	9.26	24.93	2.35	
60.0	11.7		6000	5.67	11.85	2.80	9.08	25.15	2.46	
65.0	11.7		3000	10.86	22.32	5.38	21.38	40.50	1.64	
65.0	11.7		6000	3.71	7.02	1.87	5.44	14.46	2.32	
70.0	11.7		3000	DESTABILISED						
70.0	11.7		6000	DESTABILISED						
70.0	11.7		7200	DESTABILISED						
70.0	11.7		8400	2.09	3.09	1.15	2.51	5.64	1.79	
70.0	11.7		9600	1.76	2.92	0.93	2.22	5.07	1.87	
67.5	11.7		3000	DESTABILISED						
67.5	11.7		6000	3.03	5.05	1.56	3.93	10.41	2.25	
67.5	11.7		6000	3.71	7.40	1.84	5.05	15.84	2.77	
67.5	11.7		6000	3.64	6.87	1.84	4.86	14.96	2.70	
67.5	11.7		8400	DESTABILISED						
Final SFSO [wt%]	Pluronic Solution [wt.%]		Q [kg/hr]	N [RPM]	d ₃₂ [μm]	d ₄₃ [μm]	d ₁₀ [μm]	d ₅₀ [μm]	d ₉₀ [μm]	Span
30.0	11.7		36+/-3.6	3000	DESTABILISED					
30.0	11.7	6000		15.80	33.64	11.05	29.68	62.76	1.74	
40.0	11.7	3000		20.52	50.16	16.01	45.54	91.67	1.66	
40.0	11.7	6000		11.14	25.17	6.56	21.74	49.39	1.97	
50.0	11.7	3000		23.83	50.55	15.91	44.67	94.47	1.76	
50.0	11.7	6000		10.15	22.88	5.60	18.88	46.49	2.17	
60.0	11.7	3000		DESTABILISED						
60.0	11.7	6000		8.52	18.44	4.25	15.25	37.74	2.20	
65.0	11.7	3000		15.70	35.76	9.90	31.74	67.86	1.83	
65.0	11.7	6000		6.80	14.61	3.31	12.09	29.92	2.20	
70.0	11.7	3000		DESTABILISED						
70.0	11.7	6000		5.50	11.31	2.50	9.20	23.66	2.30	
67.5	11.7	3000		16.61	37.16	10.17	32.98	70.67	1.83	
67.5	11.7	6000		5.53	11.98	2.57	9.48	25.38	2.41	
67.5	11.7	6000		5.92	12.60	2.72	10.06	26.64	2.38	
67.5	11.7	6000		5.73	12.27	2.86	10.03	25.14	2.22	

AX3.6: Results of Experiments in section 5.3.3 – Concentrating Methods

Initial Oil Fraction [vol.%]	Final Oil Fraction [vol.%]	Pluronic Conc. [wt.%]	Q [kg/hr]	N [RPM]	d ₃₂ [μm]	d ₄₃ [μm]	d ₁₀ [μm]	d ₅₀ [μm]	d ₉₀ [μm]	Span
75.0	30.0	23.3	COARSE PRE-MIX		11.02	20.07	7.45	18.22	35.92	1.56
75.0	30.0	23.3	COARSE PRE-MIX		12.86	23.45	9.02	21.50	41.38	1.51
75.0	30.0	23.3	COARSE PRE-MIX		18.91	23.89	11.14	21.56	40.19	1.35
75.0	50.0	23.3	COARSE PRE-MIX		19.38	24.22	11.50	22.02	40.30	1.31
75.0	50.0	23.3	COARSE PRE-MIX		18.30	23.13	10.79	20.78	39.00	1.36
75.0	50.0	23.3	COARSE PRE-MIX		17.24	21.12	10.49	19.25	34.49	1.25
75.0	65.0	23.3	COARSE PRE-MIX		11.97	19.28	8.46	17.61	33.01	1.40
75.0	65.0	23.3	COARSE PRE-MIX		12.73	20.68	9.02	18.97	35.32	1.39
0.0	75.0	23.3	COARSE PRE-MIX		18.81	23.08	11.42	21.06	37.73	1.25

Initial SFISO Fraction [vol.%]	Final SFISO Fraction [vol.%]	Pluronic Solution Conc. [wt.%]	Throughput [kg/hr]	Mixing Speed [RPM]	d ₃₂ [µm]	d ₄₃ [µm]	d ₁₀ [µm]	d ₅₀ [µm]	d ₉₀ [µm]	Span
30.0	30.0	23.3	18+/-1.8	6000	1.97	3.54	1.01	3.03	6.85	1.93
30.0	50.0	23.3	18+/-1.8	6000	1.46	2.85	0.72	2.28	5.61	2.15
30.0	65.0	23.3	18+/-1.8	6000	0.88	1.75	0.42	1.44	3.52	2.15
30.0	70.0	23.3	18+/-1.8	6000	DESTABILISED					
30.0	65.0	23.3	18+/-1.8	6000	0.89	1.43	0.44	1.20	2.79	1.96
30.0	67.5	23.3	18+/-1.8	6000	0.88	1.41	0.44	1.19	2.74	1.94
50.0	50.0	23.3	18+/-1.8	6000	1.50	2.89	0.77	2.29	5.45	2.04
50.0	60.0	23.3	18+/-1.8	6000	1.26	2.18	0.63	1.84	4.15	1.91
50.0	70.0	23.3	18+/-1.8	6000	0.85	1.34	0.43	1.16	2.53	1.80
50.0	75.0	23.3	18+/-1.8	6000	0.77	1.17	0.39	0.98	2.26	1.92
50.0	77.5	23.3	18+/-1.8	6000	DESTABILISED					
65.0	70.0	23.3	18+/-1.8	6000	0.565	0.794	0.300	0.684	1.445	1.675
65.0	75.0	23.3	18+/-1.8	6000	0.611	0.852	0.334	0.724	1.508	1.622
65.0	80.0	23.3	18+/-1.8	6000	DESTABILISED					
65.0	77.5	23.3	18+/-1.8	6000	DESTABILISED					
65.0	77.5	23.3	18+/-1.8	6000	DESTABILISED					
65.0	77.5	23.3	18+/-1.8	6000	DESTABILISED					
65.0	65.0	23.3	18+/-1.8	6000	0.578	0.794	0.308	0.707	1.417	1.568
75.0	75.0	23.3	18+/-1.8	6000	0.96	1.50	0.48	1.27	2.89	1.91
75.0	80.0	23.3	18+/-1.8	6000	0.72	1.05	0.38	0.88	1.89	1.72
75.0	82.5	23.3	18+/-1.8	6000	0.68	0.98	0.36	0.84	1.82	1.73
75.0	85.0	23.3	18+/-1.8	6000	DESTABILISED					
75.0	83.8	23.3	18+/-1.8	6000	0.83	1.23	0.44	1.03	2.33	1.83
75.0	85.0	23.3	18+/-1.8	6000	DESTABILISED					
75.0	85.0	23.3	18+/-1.8	6000	DESTABILISED					

AX3.7: Results of experiments in section 5.3.4

Stage	Initial SFISO Fraction [vol%]	Final SFISO Fraction [vol.%]	Throughput [kg/hr]	d ₃₂ [µm]	d ₄₃ [µm]	d ₁₀ [µm]	d ₅₀ [µm]	d ₉₀ [µm]	Span
1	65	65	18.1	1.54	3.03	0.87	2.26	6.32	2.41
2	65	75	17.2	0.76	1.10	0.41	0.95	1.91	1.58
3	65	65	-	0.74	1.09	0.39	0.92	1.94	1.69

Stage	Initial SFISO Fraction [vol.%]	Final SFISO Fraction [vol.%]	Flowrate [kg/hr]	d ₃₂ [µm]	d ₄₃ [µm]	d ₁₀ [µm]	d ₅₀ [µm]	d ₉₀ [µm]	Span
0	65.0	65.0	-	9.78	19.22	6.83	17.72	34.16	1.54
	65.0	65.0	-	7.74	15.91	3.92	13.99	30.70	1.92
	65.0	65.0	-	10.84	20.68	8.30	19.03	36.22	1.47
1	65.0	65.0	17.32	1.01	1.64	0.53	1.43	3.06	1.77
	65.0	65.0	17.32	1.11	1.70	0.62	1.44	3.03	1.68
	65.0	65.0	17.32	1.07	1.69	0.56	1.46	3.14	1.77
2	65.0	65.0	17.34	0.73	1.05	0.37	0.96	1.87	1.57

AX3.8: Results of experiments in 5.3.5*AX3.8.1 Single Pass*

Mixer Geometry	SFSO Fraction [wt.%]	NS Conc. [wt.%]	Q [kg/hr]	N [RPM]	Viscosity [cP]	d ₃₂ [µm]	d ₄₃ [µm]	d ₁₀ [µm]	d ₅₀ [µm]	d ₉₀ [µm]	Span
0mm	65.0	34.4	CONTROL		135	13.18	28.62	11.65	26.86	49.23	1.40
	65.0		34.63	13200	3987	6.54	8.61	3.71	7.62	15.08	1.49
	65.0		33.98	15000	4333	5.88	7.43	3.50	6.59	12.64	1.39
	65.0		33.69	10800	6003	5.62	6.94	3.40	6.24	11.57	1.31
	65.0		34.73	15000	3526	7.22	9.25	4.21	8.24	15.85	1.41
	65.0		34.17	15000	3840	6.03	7.56	3.63	6.72	12.54	1.33
	67.5		CONTROL		1373	25.84	32.16	15.54	28.94	53.53	1.31
	67.5		31.81	10800	5750	7.57	9.74	4.40	8.72	16.63	1.40
	67.5		35.62	15000	13076	3.99	5.86	2.51	5.28	10.22	1.46
	67.5		35.42	15000	11231	2.98	4.38	1.79	3.93	7.70	1.50
	72.5		CONTROL		2099	31.92	36.25	21.30	34.15	54.13	0.96
	72.5			10800	28115	4.35	6.49	2.62	5.72	11.66	1.58
	72.5		33.79	15000	36766	4.09	6.26	2.42	5.48	11.41	1.64
	72.5		33.91	15000	40090	2.62	4.30	1.45	3.70	8.08	1.79
	77.5		CONTROL		5083	21.77	26.99	12.99	24.63	44.69	1.29
	77.5		33.49	10800	70970	3.98	5.92	2.35	5.08	10.65	1.63
	77.5		38.47	13200	79000	4.31	5.43	2.59	4.79	9.22	1.39
	77.5		33.65	13200	80816	3.73	5.06	2.17	4.62	8.68	1.41
	77.5		33.28	15000	88007	3.16	3.81	1.96	3.46	6.19	1.22

Mixer Geometry	SFSO Fraction [wt.%]	NS Conc. [wt.%]	Q [kg/hr]	N [RPM]	Viscosity [cP]	d ₃₂ [µm]	d ₄₃ [µm]	d ₁₀ [µm]	d ₅₀ [µm]	d ₉₀ [µm]	Span
1.35mm	67.5	34.4	CONTROL		1529.76	13.75	32.25	10.84	29.85	57.51	1.563
	67.5	34.4	35.18	15000	2654.55	6.31	8.29	3.63	7.21	14.58	1.518
	67.5	34.4	33.45	15000	7910.18	5.41	7.70	3.13	6.71	13.90	1.605
0mm	67.5	34.4			5083	21.77	26.99	12.99	24.63	44.69	1.287
	67.5	34.4	35.62	15000	13076	3.99	5.86	2.51	5.28	10.22	1.459
	67.5	34.4	30.08	15000	11954	3.95	5.82	2.32	5.14	10.45	1.583

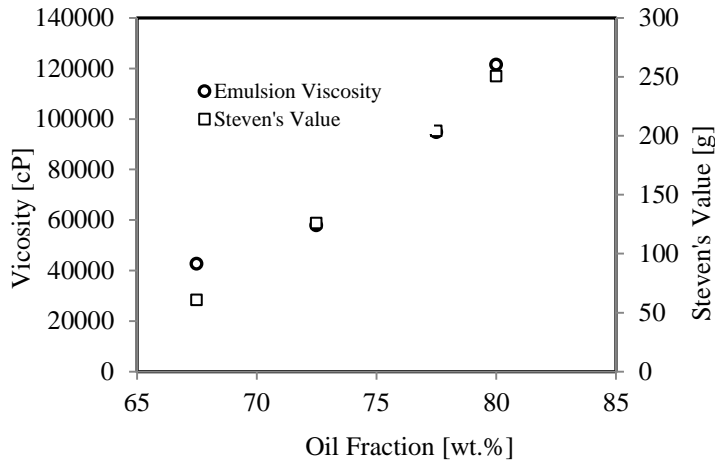
AX3.8.2 In-line Emulsification

Mixer Geometry	Initial SFSO Fraction [wt.%]	Final SFSO Fraction [wt.%]	NS Conc. [wt.%]	Q [kg/hr]	N [RPM]	Viscosity [cP]	d ₃₂ [µm]	d ₄₃ [µm]	d ₁₀ [µm]	d ₅₀ [µm]	d ₉₀ [µm]	Span
1.35mm	0	27.69	34.4	32.59	6000	EMULSION DESTABILISED						
1.35mm	0	47.18	34.4	32.55	6000	EMULSION DESTABILISED						
1.35mm	0	57.27	34.4	31.31	6000	EMULSION DESTABILISED						
1.35mm	0	67.58	34.4	31.56	6000	EMULSION DESTABILISED						
1.35mm	0	62.39	34.4	30.82	6000	EMULSION DESTABILISED						
1.35mm	0	57.27	34.4		13200	8079	5.96	8.26	3.29	7.18	14.96	1.62
1.35mm	0	57.27	34.4	29.57	15000	10176	4.84	7.00	2.82	6.13	12.62	1.60
1.35mm	0	62.39	34.4	32.24	8400	EMULSION DESTABILISED						
1.35mm	0	62.39	34.4	31.46	10800	EMULSION DESTABILISED						
1.35mm	0	62.39	34.4	34.36	13200	EMULSION DESTABILISED						
1.35mm	0	62.39	34.4	32.81	15000	EMULSION DESTABILISED						
1.35mm	0	57.27	34.4	31.05	10800	2938.73	9.21	12.93	5.09	11.17	23.45	1.64

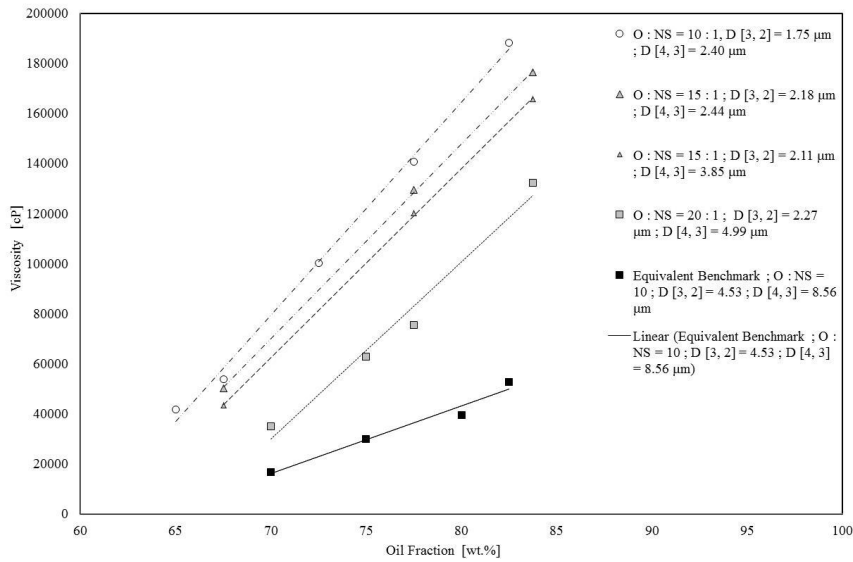
Mixer Geometry	Initial SF50 Fraction [wt.%]	Final SF50 Fraction [wt.%]	NS Conc. [wt.%]	Q [kg/hr]	N [RPM]	Viscosity [cP]	d ₃₂ [µm]	d ₄₃ [µm]	d ₁₀ [µm]	d ₅₀ [µm]	d ₉₀ [µm]	Span
1.35mm	60	60	34.4	33.98	10800	4031	7.07	9.22	4.08	8.20	15.93	1.45
1.35mm	60	65	34.4	34.39	10800	6308	6.98	9.21	3.99	8.09	16.15	1.50
1.35mm	60	70	34.4	33.87	10800	19518	5.63	8.38	3.28	7.28	15.31	1.65
1.35mm	60	75	34.4	33.65	10800	32821	5.15	7.82	2.99	6.74	14.43	1.70
1.35mm	60	80	34.4	34.16	10800	EMULSION DESTABILISED						
1.35mm	60	77.5	34.4	34.13	10800	EMULSION DESTABILISED						
1.35mm	60	65	34.4	34.05	13200	10749	5.08	7.76	2.95	6.61	14.45	1.74
1.35mm	60	77.5	34.4	33.93	13200	33219	4.83	8.64	2.63	5.95	18.68	2.70
1.35mm	60	77.5	34.4	33.38	15000	79681	3.53	5.41	1.91	4.48	10.38	1.89
1.35mm	60	65	34.4	34.19	15000	14492	4.81	7.12	2.81	6.11	13.09	1.69
1.35mm	60	67.5	34.4	33.67	15000	25186	4.44	6.43	2.61	5.66	11.54	1.58
1.35mm	60	67.5	34.4	34.25	15000	17419	4.75	7.29	2.74	6.17	13.63	1.77
1.35mm	60	67.5	34.4	34.48	10800	8873	5.67	8.72	3.24	7.35	16.40	1.79
1.35mm	60	72.5	34.4	33.96	10800	32071	5.39	8.12	3.15	7.02	14.90	1.67
1.35mm	60	72.5	34.4	34.04	13200	43934	4.58	6.94	2.55	5.84	13.05	1.80
1.35mm	60	72.5	34.4	34.29	15000	59595	4.18	6.23	2.46	5.37	11.38	1.66
1.35mm	60	80	34.4	34.01	13200	EMULSION DESTABILISED						
1.35mm	60	80	34.4	33.98	15000	EMULSION DESTABILISED						
1.35mm	60	80	34.4	33.59	13200	EMULSION DESTABILISED						
1.35mm	60	80	34.4	33.76	15000	EMULSION DESTABILISED						

AX3.9: Additional data describing SFSO/NS microstructure.

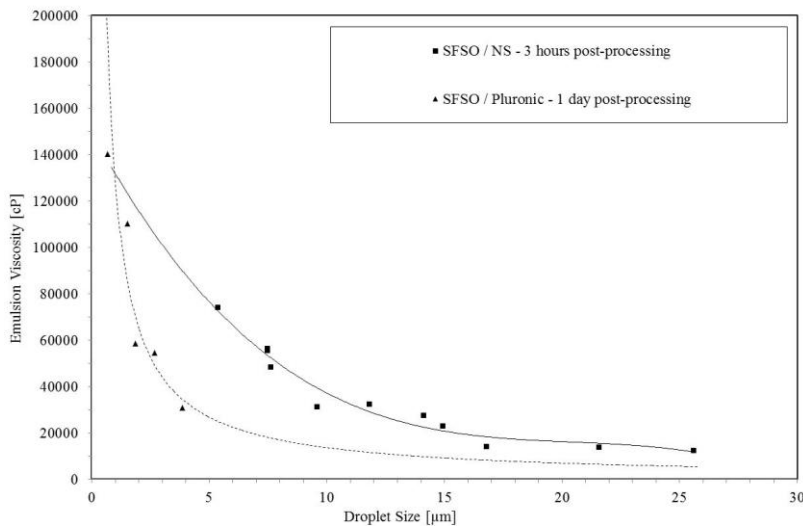
AX3.9.1: SFSO/NS Composition; $d_{43} = 2.26 \pm 0.13 \mu\text{m}$; $T = 22 \pm 1^\circ\text{C}$

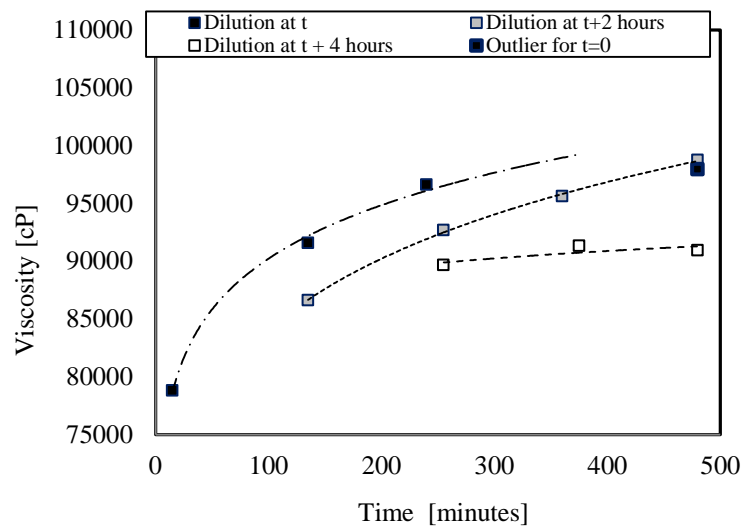


AX3.9.2: Viscosity with dilution; SFSO/NS compositions



AX3.9.3: Viscosity vs. d_{43} for SFSO/NS and SFSO/Pluronic compositions (20:1)



AX3.9.4: Dilution time, 80wt.% SFSO and NS; $d_{32} = 0.99\mu\text{m}$; $d_{43} = 2.11\mu\text{m}$;**SFSO:NS = 20:1**

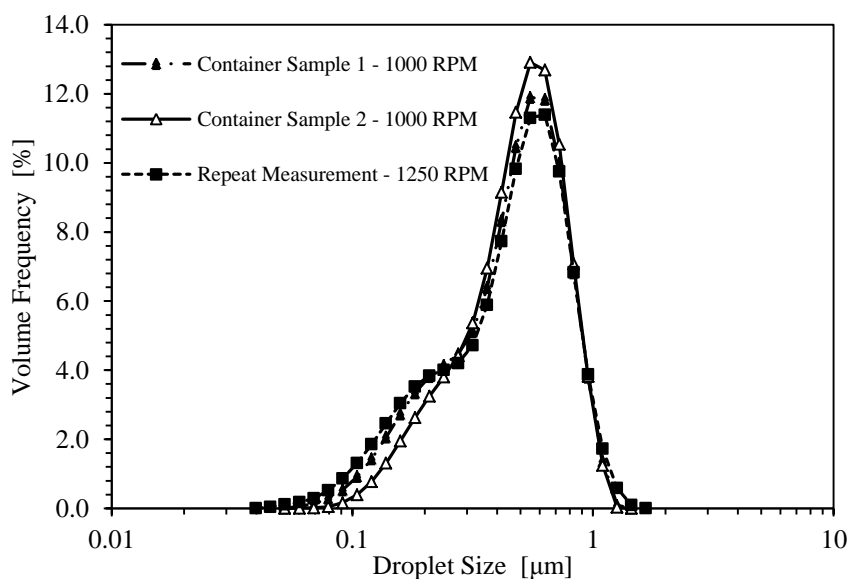
AX4: Chapter 6 Supporting Information

AX4.1: Results of Experiments in 6.3.1 – Formax™ Studies

N [RPM]	Final Mass Fraction [wt.%]	PJ:SLES [wt.:wt.]	Temperature °C	d ₃₂ [μm]	d ₄₃ [μm]	d ₁₀ [μm]	d ₅₀ [μm]	d ₉₀ [μm]	Span
4000	71.43	10	60	0.34	0.81	0.12	0.78	1.55	1.83
4000	74.64	10	60	0.31	0.44	0.16	0.40	0.77	1.52
4000	71.43	10	70	0.46	1.22	0.14	1.30	1.88	1.34
4000	74.64	10	70	0.31	0.54	0.15	0.43	1.02	2.02
4000	77.27	10	70	0.26	0.64	0.12	0.42	1.37	3.00

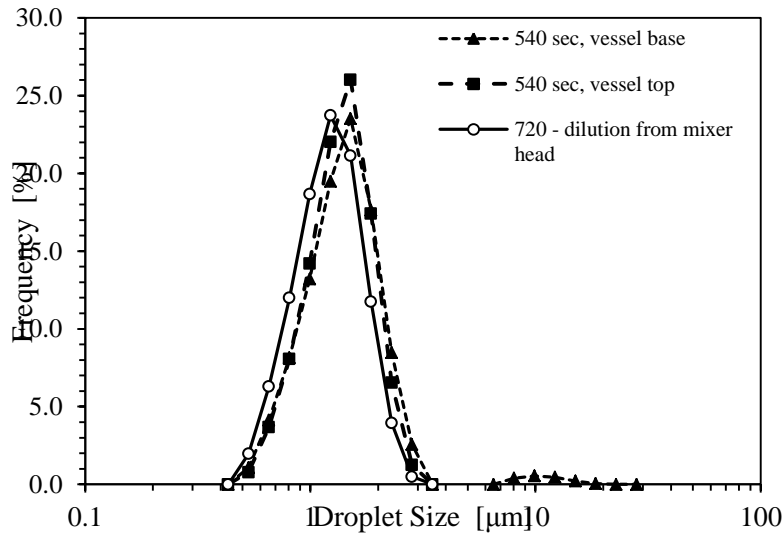
N [RPM]	Final Mass Fraction [wt.%]	PJ:SLES [wt.:wt.]	Temperature °C	d ₃₂ [μm]	d ₄₃ [μm]	d ₁₀ [μm]	d ₅₀ [μm]	d ₉₀ [μm]	Span
1000	79.47	10	60	0.24	0.49	0.11	0.37	1.04	2.52
1000	77.27	10	70	0.26	0.58	0.11	0.39	1.34	3.11
1000	79.47	10	70	0.36	0.66	0.17	0.52	1.35	2.26
4000	77.27	10	70	0.26	0.64	0.12	0.42	1.37	3.00
4000	79.47	10	70	0.15	0.25	0.08	0.18	0.53	2.53

AX4.2: Variation of Droplet Size in Formax™ Mixing Vessel

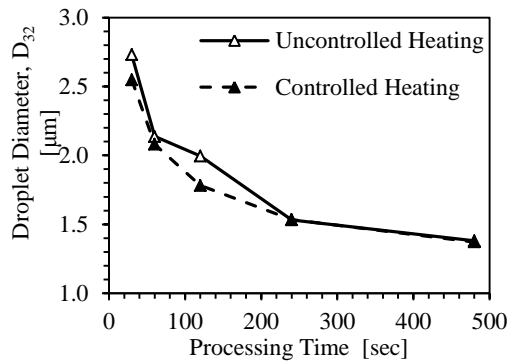


Nd [RPM]	Final Mass Fraction [wt.%]	PJ:SLES [wt.:wt.]	Temperature °C	d ₃₂ [μm]	d ₄₃ [μm]	d ₁₀ [μm]	d ₅₀ [μm]	d ₉₀ [μm]	Span
1000	79.47	10	70	0.34	0.46	0.17	0.45	0.75	1.28
1000	79.47	10	70	0.37	0.48	0.21	0.47	0.75	1.16
1000	79.47	10	70	0.31	0.46	0.15	0.45	0.77	1.36

AX4.3: Distribution of PJ/SLES in FDM vessel



AX4.4: Uncontrolled Heating (~adiabatic) vs. Controlled Heating (~isothermal) of PJ/SLES composition, 1kg, 6000RPM



Uncontrolled Heating		Controlled Heating	
Time (minutes)	D ₃₂ (µm)	Time (minutes)	D ₃₂ (µm)
30.00	2.730	30.00	2.548
60.00	2.137	60.00	2.080
120.00	1.995	120.00	1.782
240.00	1.533	240.00	1.534
480.00	1.380	480.00	1.372

AX4.5: Results of Experiments in 6.3.2 – FDM Studies

PJ [wt%]	PJ/SLES [wt./wt.]	Mixing Time [sec]	N [RPM]	d ₃₂ [µm]	d ₄₃ [µm]	d ₁₀ [µm]	d ₅₀ [µm]	d ₉₀ [µm]	Span
71.4	8.33	120	6000	1.22	1.32	0.89	1.27	1.80	0.71
71.4	8.33	300	6000	0.99	1.08	0.71	1.04	1.51	0.77
71.4	8.33	480	6000	0.93	1.02	0.66	0.98	1.42	0.77
71.4	8.33	600	6000	0.92	1.00	0.66	0.97	1.39	0.76
74.6	8.33	180	6000	0.99	1.07	0.72	1.03	1.45	0.71
74.6	8.33	300	6000	0.94	1.00	0.70	0.98	1.35	0.67
74.6	8.33	480	6000	0.87	0.95	0.62	0.92	1.32	0.76
74.6	8.33	600	6000	0.83	0.91	0.59	0.87	1.26	0.77

AX4.6: Results of Experiments in 6.4.1 – FDM Studies

PJ [wt%]	PJ/SLES [wt./wt.]	Mixing Time [sec]	N [RPM]	d ₃₂ [μm]	d ₄₃ [μm]	d ₁₀ [μm]	d ₅₀ [μm]	d ₉₀ [μm]	Span
74.6	40	30	6000	5.18	7.00	3.16	6.28	11.95	1.40
74.6	40	60	6000	5.10	6.71	3.19	6.12	11.22	1.31
74.6	40	120	6000	5.00	6.57	3.13	5.99	10.96	1.31
74.6	40	240	6000	3.84	5.04	2.41	4.66	8.30	1.26
74.6	40	480	6000	3.46	4.32	2.17	4.02	6.93	1.18
74.6	30	30	6000	4.54	6.08	2.82	5.56	10.22	1.33
74.6	30	60	6000	4.19	5.51	2.64	5.07	9.11	1.28
74.6	30	120	6000	3.63	4.78	2.25	4.42	7.89	1.28
74.6	30	240	6000	3.38	4.11	2.13	3.82	6.53	1.15
74.6	30	480	6000	3.08	3.57	2.02	3.32	5.49	1.04
74.6	20	30	6000	3.39	4.13	2.12	3.82	6.63	1.18
74.6	20	60	6000	3.12	3.52	2.12	3.31	5.22	0.94
74.6	20	120	6000	2.83	3.11	2.01	2.95	4.42	0.82
74.6	20	240	6000	2.55	2.76	1.86	2.64	3.83	0.75
74.6	20	480	6000	2.32	2.52	1.68	2.41	3.50	0.76
74.6	17	120	6000	2.47	2.67	1.81	2.56	3.67	0.73
74.6	17	240	6000	2.17	2.33	1.59	2.24	3.18	0.71
74.6	17	360	6000	2.00	2.16	1.45	2.08	2.98	0.74
74.6	17	480	6000	1.97	2.11	1.45	2.04	2.87	0.70
74.6	17	600	6000	1.78	1.91	1.30	1.84	2.59	0.70

PJ [wt%]	PJ/SLES [wt./wt.]	Mixing Time [sec]	N [RPM]	d ₃₂ [μm]	d ₄₃ [μm]	d ₁₀ [μm]	d ₅₀ [μm]	d ₉₀ [μm]	Span
74.6	15	30	6000	3.19	3.71	2.08	3.45	5.73	1.06
74.6	15	30	6000	3.10	3.49	2.12	3.28	5.15	0.92
74.6	15	60	6000	2.87	3.14	2.04	2.99	4.45	0.81
74.6	15	60	6000	2.73	2.98	1.96	2.84	4.19	0.78
74.6	15	120	6000	2.64	2.87	1.92	2.74	3.98	0.75
74.6	15	120	6000	2.54	2.80	1.79	2.65	4.01	0.84
74.6	15	240	6000	2.14	2.33	1.53	2.23	3.26	0.78
74.6	15	240	6000	1.98	2.11	1.46	2.04	2.87	0.69
74.6	15	480	6000	1.90	2.04	1.40	1.97	2.77	0.69
74.6	15	480	6000	1.83	1.96	1.35	1.90	2.65	0.69
74.6	13	120	6000	1.75	1.88	1.29	1.81	2.55	0.70
74.6	13	240	6000	1.57	1.67	1.17	1.62	2.22	0.65
74.6	13	360	6000	1.49	1.58	1.12	1.53	2.10	0.64
74.6	13	480	6000	1.41	1.50	1.06	1.46	2.01	0.65
74.6	13	600	6000	1.39	1.48	1.05	1.44	1.97	0.64
74.6	13	720	6000	1.33	1.41	0.99	1.38	1.88	0.64
74.6	12	30	6000	2.51	2.79	1.74	2.64	4.04	0.88
74.6	12	30	6000	2.73	3.05	1.88	2.87	4.45	0.89
74.6	12	30	6000	2.48	2.72	1.76	2.59	3.87	0.81
74.6	12	60	6000	2.17	2.42	1.48	2.29	3.54	0.90
74.6	12	60	6000	2.10	2.34	1.44	2.22	3.42	0.89
74.6	12	60	6000	2.06	2.21	1.51	2.13	3.02	0.71
74.6	12	120	6000	2.13	2.35	1.50	2.23	3.35	0.83
74.6	12	120	6000	1.93	2.16	1.33	2.04	3.16	0.90
74.6	12	120	6000	1.74	1.86	1.29	1.80	2.52	0.68
74.6	12	240	6000	1.59	1.70	1.17	1.64	2.30	0.69
74.6	12	240	6000	1.55	1.65	1.14	1.60	2.24	0.69
74.6	12	240	6000	1.52	1.61	1.14	1.56	2.15	0.65
74.6	12	480	6000	1.40	1.49	1.04	1.44	1.99	0.66
74.6	12	480	6000	1.42	1.52	1.06	1.47	2.04	0.67
74.6	12	480	6000	1.38	1.47	1.04	1.43	1.97	0.65

PJ [wt%]	PJ/SLES [wt./wt.]	Mixing Time [sec]	N [RPM]	d ₃₂ [μm]	d ₄₃ [μm]	d ₁₀ [μm]	d ₅₀ [μm]	d ₉₀ [μm]	Span
74.6	10	120	6000	1.23	1.31	0.91	1.27	1.76	0.67
74.6	10	120	6000	1.36	1.45	1.01	1.41	1.96	0.68
74.6	10	240	6000	1.07	1.16	0.78	1.12	1.60	0.73
74.6	10	240	6000	0.58	0.89	0.36	0.85	1.50	1.34
74.6	10	360	6000	0.98	1.07	0.70	1.04	1.49	0.76
74.6	10	360	6000	1.01	1.10	0.72	1.07	1.54	0.77
74.6	10	480	6000	0.97	1.05	0.70	1.01	1.43	0.72
74.6	10	480	6000	0.90	1.09	0.69	1.06	1.55	0.81
74.6	10	30	6000	2.46	2.83	1.63	2.62	4.31	1.03
74.6	10	60	6000	1.93	2.13	1.34	2.03	3.08	0.86
74.6	10	120	6000	1.31	1.40	0.97	1.36	1.88	0.67
74.6	10	240	6000	1.13	1.20	0.84	1.17	1.61	0.66
74.6	10	480	6000	1.02	1.09	0.75	1.06	1.49	0.69
74.6	9	120	6000	1.01	1.09	0.73	1.05	1.49	0.72
74.6	9	240	6000	0.87	0.95	0.61	0.92	1.33	0.79
74.6	9	360	6000	0.82	0.90	0.58	0.87	1.27	0.80
74.6	9	480	6000	0.80	0.87	0.57	0.84	1.21	0.77
74.6	9	600	6000	0.79	0.86	0.55	0.83	1.22	0.79
74.6	9	720	6000	0.75	0.83	0.53	0.80	1.17	0.80
74.6	8	120	6000	0.90	0.99	0.63	0.95	1.41	0.82
74.6	8	240	6000	0.74	0.85	0.48	0.80	1.27	0.98
74.6	8	360	6000	0.68	0.76	0.47	0.72	1.10	0.87
74.6	8	480	6000	0.56	0.64	0.38	0.61	0.95	0.95
74.6	8	600	6000	0.58	0.66	0.38	0.63	0.98	0.96
74.6	8	720	6000	0.59	0.66	0.41	0.63	0.96	0.88

AX4.7: Results of Experiments in 6.5.1 – FDM Studies

Data - Set Concentration - 25wt.% SLES Solution									
PJ [wt%]	PJ/SLES [wt./wt.]	Mixing Time [sec]	N [RPM]	d ₃₂ [μm]	d ₄₃ [μm]	d ₁₀ [μm]	d ₅₀ [μm]	d ₉₀ [μm]	Span
20.0	1.0	30	6000	3.47	4.13	2.21	3.82	6.49	1.12
20.0	1.0	60	6000	3.23	3.79	2.09	3.52	5.89	1.08
20.0	1.0	120	6000	2.96	3.32	2.03	3.12	4.89	0.92
20.0	1.0	240	6000	2.67	2.95	1.86	2.79	4.26	0.86
20.0	1.0	480	6000	2.20	2.46	1.49	2.33	3.63	0.92
60.0	6.0	30	6000	3.02	3.44	2.04	3.22	5.15	0.97
60.0	6.0	30	6000	2.92	3.37	1.92	3.15	5.14	1.02
60.0	6.0	60	6000	2.71	3.01	1.89	2.85	4.36	0.87
60.0	6.0	60	6000	2.68	2.96	1.87	2.81	4.27	0.85
60.0	6.0	120	6000	2.38	2.61	1.68	2.48	3.70	0.81
60.0	6.0	120	6000	2.37	2.60	1.69	2.48	3.66	0.79
60.0	6.0	240	6000	2.07	2.29	1.44	2.18	3.30	0.85
60.0	6.0	240	6000	2.08	2.26	1.49	2.17	3.15	0.77
60.0	6.0	480	6000	1.75	1.89	1.28	1.83	2.57	0.71
60.0	6.0	480	6000	1.73	1.86	1.27	1.80	2.53	0.70

Data - Set Concentration - 25wt.% SLES Solution									
PJ [wt%]	PJ/SLES [wt./wt.]	Mixing Time [sec]	N [RPM]	d ₃₂ [μm]	d ₄₃ [μm]	d ₁₀ [μm]	d ₅₀ [μm]	d ₉₀ [μm]	Span
74.6	11.8	30	6000	2.51	2.79	1.74	2.64	4.04	0.88
74.6	11.8	30	6000	2.73	3.05	1.88	2.87	4.45	0.89
74.6	11.8	60	6000	2.17	2.42	1.48	2.29	3.54	0.90
74.6	11.8	60	6000	2.10	2.34	1.44	2.22	3.42	0.89
74.6	11.8	120	6000	2.13	2.35	1.50	2.23	3.35	0.83
74.6	11.8	120	6000	1.93	2.16	1.33	2.04	3.16	0.90
74.6	11.8	240	6000	1.59	1.70	1.17	1.64	2.30	0.69
74.6	11.8	240	6000	1.55	1.65	1.14	1.60	2.24	0.69
74.6	11.8	480	6000	1.40	1.49	1.04	1.44	1.99	0.66
74.6	11.8	480	6000	1.42	1.52	1.06	1.47	2.04	0.67
83.3	20.0	30	6000	2.54	2.81	1.77	2.66	4.04	0.85
83.3	20.0	60	6000	1.84	1.99	1.33	1.91	2.74	0.74
83.3	20.0	120	6000	1.69	1.82	1.23	1.75	2.50	0.73
83.3	20.0	240	6000	1.45	1.55	1.07	1.50	2.09	0.68
83.3	20.0	480	6000	1.30	1.39	0.96	1.35	1.86	0.67
83.3	20.0	30	6000	2.83	3.18	1.94	2.99	4.67	0.92
83.3	20.0	60	6000	2.35	2.62	1.62	2.48	3.84	0.90
83.3	20.0	120	6000	2.05	2.30	1.39	2.16	3.39	0.93
83.3	20.0	240	6000	1.81	1.98	1.27	1.89	2.81	0.81
83.3	20.0	480	6000	1.35	1.45	1.00	1.40	1.96	0.68

Data - Set Concentration - 30wt.%									
PJ [wt%]	PJ/SLES [wt./wt.]	Mixing Time [sec]	N [RPM]	d ₃₂ [μm]	d ₄₃ [μm]	d ₁₀ [μm]	d ₅₀ [μm]	d ₉₀ [μm]	
40.3	2.3	120	6000	1.53	1.63	1.15	1.58	2.17	
40.3	2.3	240	6000	1.38	1.47	1.04	1.43	1.97	
40.3	2.3	360	6000	1.34	1.43	1.00	1.40	1.93	
40.3	2.3	480	6000	1.00	1.19	0.70	1.15	1.76	
40.3	2.3	600	6000	1.05	1.26	0.74	1.21	1.87	
40.3	2.3	720	6000	0.96	1.11	0.65	1.07	1.64	
60.0	5.0	120	6000	1.35	1.44	1.01	1.40	1.92	
60.0	5.0	240	6000	1.19	1.28	0.89	1.24	1.72	
60.0	5.0	360	6000	1.17	1.24	0.87	1.21	1.66	
60.0	5.0	480	6000	1.02	1.12	0.72	1.08	1.59	
60.0	5.0	600	6000	0.98	1.07	0.69	1.04	1.50	
60.0	5.0	720	6000	0.92	1.01	0.64	0.98	1.42	
71.4	8.3	120	6000	2.04	10.96	1.07	1.85	33.92	
71.4	8.3	240	6000	1.22	1.32	0.89	1.27	1.80	
71.4	8.3	360	6000	0.99	1.08	0.71	1.04	1.51	
71.4	8.3	480	6000	0.93	1.02	0.66	0.98	1.42	
71.4	8.3	600	6000	0.92	1.00	0.66	0.97	1.39	

Data - Set Concentration - 30wt.%								
PJ [wt%]	PJ/SLES [wt./wt.]	Mixing Time [sec]	N [RPM]	d ₃₂ [μm]	d ₄₃ [μm]	d ₁₀ [μm]	d ₅₀ [μm]	d ₉₀ [μm]
74.6	9.8	120	6000	1.23	1.31	0.91	1.27	1.76
74.6	9.8	120	6000	1.18	1.26	0.89	1.23	1.68
74.6	9.8	240	6000	1.07	1.16	0.78	1.12	1.60
74.6	9.8	240	6000	0.98	1.06	0.71	1.02	1.45
74.6	9.8	360	6000	0.98	1.07	0.70	1.04	1.49
74.6	9.8	360	6000	0.95	1.04	0.68	1.00	1.44
74.6	9.8	480	6000	0.97	1.05	0.70	1.01	1.43
74.6	9.8	480	6000	0.91	1.00	0.65	0.97	1.40
74.6	9.8	600	6000	0.92	1.00	0.65	0.97	1.40
74.6	9.8	600	6000	0.92	0.99	0.68	0.96	1.34
74.6	9.8	720	6000	0.89	0.97	0.62	0.94	1.36
74.6	9.8	720	6000	0.88	0.96	0.63	0.93	1.34
78.9	12.5	120	6000	1.03	1.14	0.72	1.09	1.61
78.9	12.5	240	6000	1.03	1.14	0.72	1.09	1.61
78.9	12.5	360	6000	1.00	1.09	0.71	1.05	1.51
78.9	12.5	480	6000	0.95	1.04	0.67	1.01	1.47
78.9	12.5	600	6000	0.91	1.00	0.63	0.96	1.43
78.9	12.5	720	6000	0.93	1.00	0.68	0.97	1.36
83.3	16.7	120	6000	1.32	1.41	0.98	1.37	1.90
83.3	16.7	240	6000	1.15	1.25	0.83	1.21	1.74
83.3	16.7	360	6000	0.96	1.06	0.67	1.02	1.52
83.3	16.7	480	6000	0.97	1.06	0.68	1.02	1.49
83.3	16.7	600	6000	0.96	1.05	0.67	1.01	1.49
83.3	16.7	720	6000	0.93	1.03	0.65	0.99	1.47